



land surface
temperature
cci



CCI Land Surface Temperature

Product Validation and Intercomparison Report (PVIR)

WP4 – DEL4.1

Ref.: LST-CCI-D4.1-PVIR

Date: 23-Jun-2023

Organisation: Consortium LST_CCI



UNIVERSITY OF
LEICESTER



National Centre for
Earth Observation
NATURAL ENVIRONMENT RESEARCH COUNCIL



University of
Reading



IPMA



Karlsruhe Institute of Technology



Met Office
Hadley Centre



UNIVERSITAT
DE VALÈNCIA



Met Office
Hadley Centre



DMI
Danish Meteorological Institute



LUXEMBOURG
INSTITUTE OF SCIENCE
AND TECHNOLOGY

LIST



 land surface temperature cci	Product Validation Plan (PVP) <i>WP4 – DEL4.1</i>	Ref.: LST-CCI-D4.1-PVIR Version: 3.1 Date: 23-Jun-2023 Page: i
--	---	---

Signatures

	Name	Organisation	Signature
Written by	Lluís Pérez-Planells	KIT	
	Maria Martin	KIT	
Reviewed by	Darren Ghent	ULeic	
Approved by			
Authorized by			

Change log

Version	Date	Changes
1.0	3-Jun-2020	First version
2.0	23-Mar-2022	Time span of validated and intercompared datasets is increased. New sites are included.
3.0	6-Apr-2023	New satellite data sets, i.e. AVHRMA, GOES16 and HMWR_8, are included in the insitu validation.
3.1	23-Jun-2023	Data in Tables 5 and 6 were updated.




 land surface temperature cci	Product Validation Plan (PVP) <i>WP4 – DEL4.1</i>	Ref.: LST-CCI-D4.1-PVIR Version: 3.1 Date: 23-Jun-2023 Page: ii
--	---	--

Table of Content

0. EXECUTIVE SUMMARY	1
1. INTRODUCTION	3
1.1. Purpose and Scope	3
1.2. Structure of the Document	6
1.3. Applicable Documents	7
1.4. Reference Documents	7
1.5. Glossary	8
2. SATELLITE DATA SETS	10
2.1. LST_cci Satellite Data Sets	10
2.2. External Satellite Data Sets	12
3. DESCRIPTION AND ANALYSIS OF IN SITU VALIDATION RESULTS	13
3.1. Overview of Results	13
3.2. Results for different stations	24
3.2.1. Results over ARM Station	24
3.2.2. Results over Copernicus LAW Stations	25
3.2.3. Results over Heihe Stations	26
3.2.4. Results over KIT Stations	29
3.2.5. Results over SURFRAD stations	33
3.3. In Situ Uncertainty Validation	39
3.3.1. Overview	39
3.3.2. Results for ATSR_2 and ATSR_3 data sets	40
3.3.3. Results for AVHRMA data set	42
3.3.4. Results for GOES12, GOES13 and GOES16 data sets	43
3.3.5. Results for MODISA and MODIST data sets	44
3.3.6. Results for MTSAT2 and HMWR_8 data sets	46
3.3.7. Results for SEVIR 1 – 4 data sets	48
3.3.8. Results for SLSTRA and SLSTRB data sets	50
3.3.9. Results for the SSMI13 and SSMI17 data sets	52
4. DESCRIPTION AND ANALYSIS OF INTERCOMPARISON RESULTS	54
4.1. Overview of Results	54
4.2. Results for different Continents	59
4.2.1. Results over Africa	59
4.2.2. Results over Antarctica	64
4.2.3. Results over Asia	66
4.2.4. Results over Australia	70
4.2.5. Results over Europe	74
4.2.6. Results over North America	78
4.2.7. Results over South America	83
5. CONCLUSIONS	89
6. RECOMMENDATIONS FOR THE NEXT PROCESSING CYCLE	91
7. APPENDIX	92
7.1. Africa	92

 land surface temperature cci	Product Validation Plan (PVP) <i>WP4 – DEL4.1</i>	Ref.: LST-CCI-D4.1-PVIR Version: 3.1 Date: 23-Jun-2023 Page: iii
--	---	---

7.2. Antarctica	110
7.3. Asia	114
7.4. Australia	119
7.5. Europe	124
7.6. North America	142
7.7. South America	147

 land surface temperature cci	Product Validation Plan (PVP) <i>WP4 – DEL4.1</i>	Ref.: LST-CCI-D4.1-PVIR Version: 3.1 Date: 23-Jun-2023 Page: iv
--	---	--

List of Figures

Figure 1: Overview over the biases of all validated satellite LST data sets against all stations, for night-time (upper plot) and daytime (lower plot) data. The matched time of the satellite data sets varies, depending on data availability, as indicated in Table 7. The red span marks the bias range of ± 2 K. ---- 13

Figure 2: Overview over the RSTD of all validated satellite LST data sets against all stations, for night-time (upper plot) and daytime (lower plot) data. -----14

Figure 3: Number of averaged data points over all validated satellite LST data sets and stations, for night-time (upper plot) and daytime (lower plot) data. -----16

Figure 4: Monthly mean biases (satellite LST - station LST) over SGP___ station. The upper plot represents night-time and the lower daytime data. The red span is the area where the bias is in a ± 2 K range. ----24

Figure 5: Monthly mean biases (satellite LST – station LST) over KIT_F_ station. The upper plot represents night-time and the lower daytime data. The red span is the area where the bias is in a ± 2 K range. ----25

Figure 6: Monthly mean biases (satellite LST - station LST) over BGB___ station. The upper plot represents night-time and the lower daytime data. The red span is the area where the bias is in a ± 2 K range. ----26

Figure 7: Monthly mean biases (satellite LST - station LST) over DMN___ station. The upper plot represents night-time and the lower daytime data. The red span is the area where the bias is in a ± 2 K range. ----27

Figure 8: Monthly mean biases (satellite LST - station LST) over HZZ___ station. The upper plot represents night-time and the lower daytime data. The red span is the area where the bias is in a ± 2 K range. ----28

Figure 9: Monthly mean biases (satellite LST – station LST) over DAH_T_ station. The upper plot represents night-time and the lower daytime data. The red span is the area where the bias is in a ± 2 K range. ----29

Figure 10: Monthly mean biases (satellite LST – station LST) over EVO___ station. The upper plot represents night-time and the lower daytime data. The red span is the area where the bias is in a ± 2 K range. ----30

Figure 11: Monthly mean biases (satellite LST – station LST) over GBB_W_ station. The upper plot represents night-time and the lower daytime data. The red span is the area where the bias is in a ± 2 K range.-----31

Figure 12: Monthly mean biases (satellite LST – station LST) over KAL_R_ (upper) and KAL_H_ (lower) stations. The upper plot represents night-time and the lower daytime data. The red span is the area where the bias is in a ± 2 K range. -----32

Figure 13: Monthly mean biases (satellite LST – station LST) over BND___ station. The upper plot represents night-time and the lower daytime data. The red span is the area where the bias is in a ± 2 K range.-----33

Figure 14: Monthly mean biases (satellite LST – station LST) over DRA___ station. The upper plot represents night-time and the lower daytime data. The red span is the area where the bias is in a ± 2 K range. ----34

Figure 15: Monthly mean biases (satellite LST – station LST) over GCM___ station. The upper plot represents night-time and the lower daytime data. The red span is the area where the bias is in a ± 2 K range.-----35

Figure 16: Monthly mean night-time biases (satellite LST – station LST) over FPK___ station. The red span is the area where the bias is in a ± 2 K range.-----36

Figure 17: Monthly mean biases (satellite LST – station LST) over PSU___ station. The upper plot represents night-time and the lower daytime data. The red span is the area where the bias is in a ± 2 K range. ----37


 land surface temperature cci	Product Validation Plan (PVP) <i>WP4 – DEL4.1</i>	Ref.: LST-CCI-D4.1-PVIR Version: 3.1 Date: 23-Jun-2023 Page: v
--	---	---

Figure 18: Monthly mean biases (satellite LST – station LST) over TBL___ station. The upper plot represents night-time and the lower daytime data. The red span is the area where the bias is in a ± 2 K range. -----38

Figure 19: RSTD of the bias (satellite LST – in situ LST) vs total uncertainty for ATSR_2 and ATSR_3 data sets over GCM___ (upper plot) and TBL___ (lower plot) station. The total uncertainty is divided into bins of 0.1 K. The right axis displays the number of data points per bin.-----41

Figure 20: RSTD of the bias (satellite LST – in situ LST) vs total uncertainty for AVHRMA data set over PSU___ (upper plot) and FPK___ (lower plot) station. The total uncertainty is divided into bins of 0.1 K. The right axis displays the number of data points per bin. -----43

Figure 21: RSTD of the bias (satellite LST – in situ LST) vs total uncertainty for GOES12, GOES13 and GOES16 data sets over FPK___ station. The total uncertainty is divided into bins of 0.1 K. The right axis displays the number of data points per bin. -----44

Figure 22: RSTD of the bias (satellite LST – in situ LST) vs total uncertainty for MODISA and MODIST data sets over SGP___ (upper plot), KAL_H_ (lower plot) station. The total uncertainty is divided into bins of 0.1 K. The right axis displays the number of data points per bin.-----45

Figure 23: RSTD of the bias (satellite LST – in situ LST) vs total uncertainty for MTSAT2 data set over DMN___ (upper plot) and HZZ___ (lower plot) station. The total uncertainty is divided into bins of 0.1 K. The right axis displays the number of data points per bin.-----47

Figure 24: RSTD of the bias (satellite LST – in situ LST) vs total uncertainty for SEVIR1-4 data sets over GBB_W_ (upper plot) and EVO___ (lower plot) station. The total uncertainty is divided into bins of 0.1 K. The right axis displays the number of data points per bin.-----49

Figure 25: RSTD of the bias (satellite LST – in situ LST) vs total uncertainty for SLSTRA and SLSTRB data sets over KAL_H_ (upper plot) and GCM___ (lower plot) station. The total uncertainty is divided into bins of 0.1 K. The right axis displays the number of data points per bin.-----51

Figure 26: RSTD of the bias (satellite LST – in situ LST) vs total uncertainty for SSMI13 and SSMI17 data sets over BND___ (upper plot) and GBB_W_ (lower plot) station. The total uncertainty is divided into bins of 0.1 K. The right axis displays the number of data points per bin. -----53

Figure 27: Overview of the daytime differences over the four seasons for all nine intercompared satellite-satellite pairs. The red span marks the difference range of ± 2 K.-----55

Figure 28: Overview of the night-time differences over the four seasons for all nine intercompared satellite-satellite pairs. The red span marks the difference range of ± 2 K. -----56

Figure 29: Monthly time series for all investigated satellite – satellite data sets over Africa for the time span 2008 - 2010. Red stars represent the daytime data, blue dots the night-time data, the green stars and dots on the right axis display the averaged pixel numbers for daytime and night-time, respectively. ----60

Figure 30: Monthly time series for the investigated satellite – satellite data sets over Africa for the time span 2018 - 2020. Red stars represent the daytime data, blue dots the night-time data, the green stars and dots on the right axis display the averaged pixel numbers for daytime and night-time, respectively. ----60

Figure 31: Number of seasonal night-time averaged data points per pixel for ATSR_3-SEVIR2 differences over Africa-----61

Figure 32: Seasonal differences between ATSR3-SEVIR2 LST data for different satze*sign(sataz) values of ATSR_3; red stars represent the daytime data, blue dots the night-time data, and the green stars and dots on the right axis display the averaged pixel numbers for daytime and night-time data, respectively-----62


 land surface temperature cci	Product Validation Plan (PVP) <i>WP4 – DEL4.1</i>	Ref.: LST-CCI-D4.1-PVIR Version: 3.1 Date: 23-Jun-2023 Page: vi
--	---	--

Figure 33: Seasonal differences between MODIST and SEVIR2 LST data for different satze*sign(sataz) of MODIST; red stars represent the daytime data, blue dots the night-time data, and the green stars and dots on the right axis display the averaged pixel numbers for daytime and night-time data, respectively-----63

Figure 34: Seasonal differences between SLSTRA and SEVIR4 LST data for different satze*sign(sataz) of SLSTRA; red stars represent the daytime data, blue dots the night-time data, and the green stars and dots on the right axis display the averaged pixel numbers for daytime and night-time data, respectively-----63

Figure 35: Monthly time series for all investigated satellite – satellite data sets over Antarctica. Red stars represent the daytime data, blue dots the night-time data, the green stars and dots on the right axis display the averaged pixel numbers for daytime and night-time, respectively. -----64

Figure 36: Number of seasonal night-time averaged data points per pixel for ATSR_3-MOD11T differences over Antarctica -----65

Figure 37: Seasonal LST differences between MODIST and ATSOP_ LST data for different satze*sign(sataz) of MODIST; red stars represent the daytime data, blue dots the night-time data, and the green stars and dots on the right axis display the averaged pixel numbers for daytime and night-time data, respectively66

Figure 38: Monthly time series for all investigated satellite – satellite data sets over Asia. Red stars represent the daytime data, blue dots the night-time data, the green stars and dots on the right axis display the averaged pixel numbers for daytime and night-time, respectively. -----67

Figure 39: Number of seasonal daytime averaged data points per pixel for ATSR_3-MOD11T data over Asia -----68

Figure 40: Seasonal daytime differences for different land cover classes for ATSR3-MODIST over Asia; the bars are the median differences, red points the RSTD and the green points on the right axis show the number of averaged data points -----69

Figure 41: Seasonal LST differences between MODIST and ATSOP_ LST data for different satze*sign(sataz) of MODIST; red stars represent the daytime data, blue dots the night-time data, and the green stars and dots on the right axis display the averaged pixel numbers for daytime and night-time data, respectively69

Figure 42: Monthly time series for all investigated satellite – satellite data sets over Australia. Red stars represent the daytime data, blue dots the night-time data, the green stars and dots on the right axis display the averaged pixel numbers for daytime and night-time, respectively. -----70

Figure 43: Seasonal distribution of the number of daytime (upper) and night-time (lower) averaged data points per pixel for ATSR_3-MOD11T data over Australia-----71

Figure 44: Seasonal daytime differences for different elevation classes for ATSR3-MODIST over Australia; blue bars are the median differences, red points the RSTD and the green points on the right axis show the number of averaged data points -----72

Figure 45: Seasonal daytime differences for different land cover classes for ATSR_3-MOD11T over Australia; the bars are the median differences, red points the RSTD and the green points on the right axis show the number of averaged data points-----73

Figure 46: Seasonal LST differences between ATSR_3 and MODIST LST data for different satze*sign(sataz) of ATSR_3; red stars represent the daytime data, blue dots the night-time data, and the green stars and dots on the right axis display the averaged pixel numbers for daytime and night-time data, respectively74

Figure 47: Monthly time series for all investigated satellite – satellite data sets over Europe from 2008 - 10. Red stars represent the daytime data, blue dots the night-time data, the green stars and dots on the right axis display the averaged pixel numbers for daytime and night-time, respectively.-----75


 land surface temperature cci	Product Validation Plan (PVP) <i>WP4 – DEL4.1</i>	Ref.: LST-CCI-D4.1-PVIR Version: 3.1 Date: 23-Jun-2023 Page: vii
--	---	---

Figure 48: Monthly time series for the investigated satellite – satellite data sets over Europe from 2018 - 2020. Red stars represent the daytime data, blue dots the night-time data, the green stars and dots on the right axis display the averaged pixel numbers for daytime and night-time, respectively.-----75

Figure 49: Number of seasonal daytime averaged data points per pixel for MODIST-SEVIR2 (upper plot) and MODIST-ATSOP_ (lower plot) data over Europe -----76

Figure 50: Seasonal daytime differences for different land cover classes for MODISA-SEVIR2 over Europe; the bars are the median differences, red points the RSTD and the green points on the right axis show the number of averaged data points -----77

Figure 51: Seasonal LST differences between MODISA -SEVIR2 LST data for different satze*sign(sataz) of MODISA; red stars represent the daytime data, blue dots the night-time data, and the green stars and dots on the right axis display the averaged pixel numbers for daytime and night-time data, respectively-----78

Figure 52: Monthly time series for all investigated satellite – satellite data sets over North America. Red stars represent the daytime data, blue dots the night-time data, the green stars and dots on the right axis display the averaged pixel numbers for daytime and night-time, respectively. -----79

Figure 53: Number of seasonal daytime (upper) and night-time (lower) averaged data points per pixel for ATSR_3-MODIST data over North America-----80

Figure 54: Seasonal daytime differences for different elevation classes for ATSR_3-MODIST over North America; blue bars are the median differences, red points the RSTD and the green points on the right axis show the number of averaged data points-----81

Figure 55: Seasonal daytime differences for different land cover classes for ATSR_3-MOD11T over North America; the bars are the median differences, red points the RSTD and the green points on the right axis show the number of averaged data points-----82

Figure 56: Seasonal LST differences between ATSR_3 and MODIST LST data for different satze*sign(sataz) of MODIST; red stars represent the daytime data, blue dots the night-time data, and the green stars and dots on the right axis display the averaged pixel numbers for daytime and night-time data, respectively83

Figure 57: Monthly time series for all investigated satellite – satellite data sets over South America. Red stars represent the daytime data, blue dots the night-time data, the green stars and dots on the right axis display the averaged pixel numbers for daytime and night-time, respectively. -----84

Figure 58: Number of seasonal daytime averaged data points per pixel for ATSR_3-MODIST data over South America-----85

Figure 59: Seasonal daytime differences for different elevation classes for ATSR_3-MOD11T over South America; blue bars are the median differences, red points the RSTD and the green points on the right axis show the number of averaged data points-----86

Figure 60: Seasonal daytime differences for different land cover classes for ATSR_3-MODIST over South America; the bars are the median differences, red points the RSTD and the green points on the right axis show the number of averaged data points-----87

Figure 61: Seasonal LST differences between ATSR_3 and MODIST LST data for different satze*sign(sataz) of ATSR_3; red stars represent the daytime data, blue dots the night-time data, and the green stars and dots on the right axis display the averaged pixel numbers for daytime and night-time data, respectively88

Figure 62: Seasonal mean differences of LST_satellite 1 – LST_satellite 2 in K; left row displays night-time and right row daytime data. Upper plots are for MOD11A-SEVIR2, middle plots for MODISA-SEVIR2, and lower plots for MOD11T-SEVIR2.-----92


 land surface temperature cci	Product Validation Plan (PVP) <i>WP4 – DEL4.1</i>	Ref.: LST-CCI-D4.1-PVIR Version: 3.1 Date: 23-Jun-2023 Page: viii
--	---	--

Figure 63: Seasonal mean differences of LST_satellite 1 – LST_satellite 2 in K; left row displays night-time and right row daytime data. Upper plots are for MODIST-SEVIR2, middle plots for ATSOP_-SEVIR2, and lower plots for ATSR_3-SEVIR2.-----93

Figure 64: Seasonal mean differences of LST_satellite 1 – LST_satellite 2 in K; left row displays night-time and right row daytime data. Upper plots are for ATSR_3-MOD11T, middle plots for ATSR_3-MODIST, and lower plots for MODIST-ATSOP_-.-----94

Figure 65: Seasonal mean differences of LST_satellite 1 – LST_satellite 2 in K; left row displays night-time and right row daytime data. Upper plots are for SLSTRA-SEVIR4, middle plots for SLSTRB-SEVIR4, for the years 2018 - 2020.-----95

Figure 66: Number of seasonal averaged data points per pixel; left row displays night-time and right row daytime data. Upper plots are for MOD11A-SEVIR2, middle plots for MODISA-SEVIR2, and lower plots for MOD11T-SEVIR2.-----96

Figure 67: Number of seasonal averaged data points per pixel; left row displays night-time and right row daytime data. Upper plots are for MODIST-SEVIR2, middle plots for ATSOP_-SEVIR2, and lower plots for ATSR_3-SEVIR2.-----97

Figure 68: Number of seasonal averaged data points per pixel; left row displays night-time and right row daytime data. Upper plots are for ATSR_3-MOD11T, middle plots for ATSR_3-MODIST, and lower plots for MODIST-ATSOP_-.-----98

Figure 69: Number of seasonal averaged data points per pixel; left row displays night-time and right row daytime data. Upper plots are for SLSTRA-SEVIR4, middle plots for SLSTRB-SEVIR4, for the years 2018 - 2020. -----99

Figure 70: Seasonal differences for different elevation classes; blue bars are the median differences, red points the RSTD and the green points on the right axis show the number of averaged data points Left row displays night-time and right row daytime data. Upper plots are for MOD11A-SEVIR2, middle plots for MODISA-SEVIR2, and lower plots for MOD11T-SEVIR2. ----- 100


Figure 71: Seasonal differences for different elevation classes; blue bars are the median differences, red points the RSTD and the green points on the right axis show the number of averaged data points Left row displays night-time and right row daytime data. Upper plots are for MODIST-SEVIR2, middle plots for ATSOP_-SEVIR2, and lower plots for ATSR_3-SEVIR2. ----- 101

Figure 72: Seasonal differences for different elevation classes; blue bars are the median differences, red points the RSTD and the green points on the right axis show the number of averaged data points Left row displays night-time and right row daytime data. Upper plots are for ATSR_3-MOD11T, middle plots for ATSR_3-MODIST, and lower plots for MODIST-ATSOP_-. ----- 102

Figure 73: Seasonal differences for different elevation classes; blue bars are the median differences, red points the RSTD and the green points on the right axis show the number of averaged data points Left row displays night-time and right row daytime data. Upper plots are for SLSTRA-SEVIR4, middle plots for SLSTRB-SEVIR4, for the years 2018 - 2020. ----- 103

Figure 74: Seasonal differences for different land cover classes; coloured bars are the differences, red points the RSTD and the green points on the right axis show the number of averaged data points. Left row displays night-time and right row daytime data. Upper plots are for MOD11A-SEVIR2, middle plots for MODISA-SEVIR2, and lower plots for MOD11T-SEVIR2. ----- 104

Figure 75: Seasonal differences for different land cover classes; coloured bars are the differences, red points the RSTD and the green points on the right axis show the number of averaged data points. Left row

 land surface temperature cci	Product Validation Plan (PVP) <i>WP4 – DEL4.1</i>	Ref.: LST-CCI-D4.1-PVIR Version: 3.1 Date: 23-Jun-2023 Page: ix
--	---	--

displays night-time and right row daytime data. Upper plots are for MODIST-SEVIR2, middle plots for ATSR_3-SEVIR2, and lower plots for ATSR_3-SEVIR2. ----- 105

Figure 76: Seasonal differences for different land cover classes; coloured bars are the differences, red points the RSTD and the green points on the right axis show the number of averaged data points. Left row displays night-time and right row daytime data. Upper plots are for ATSR_3-MOD11T, middle plots for ATSR_3-MODIST, and lower plots for MODIST-ATSR_3. ----- 106

Figure 77: Seasonal differences for different land cover classes; coloured bars are the differences, red points the RSTD and the green points on the right axis show the number of averaged data points. Left row displays night-time and right row daytime data. Upper plots are for SLSTRA-SEVIR4, middle plots for SLSTB-SEVIR4, for the years 2018 – 2020. ----- 107

Figure 78: Seasonal differences versus $\text{satze} * \text{sign}(\text{sataz})$ of satellite_1; red stars represent the daytime data, blue dots the night-time data, and the green stars and dots on the right axis display the averaged pixel numbers for daytime and night-time data. Upper left plot displays MOD11A-SEVIR2, upper right MODISA-SEVIR2, middle left MOD11T-SEVIR2, middle right MODIST-SEVIR2, lower left ATSR_3-SEVIR2, and lower right ATSR_3-SEVIR2. ----- 108

Figure 79: Seasonal differences versus $\text{satze} * \text{sign}(\text{sataz})$ of satellite_1; red stars represent the daytime data, blue dots the night-time data, and the green stars and dots on the right axis display the averaged pixel numbers for daytime and night-time data. Upper left plot displays ATSR_3-MOD11T, upper right ATSR_3-MODIST, middle left MODIST-ATSR_3, lower left SLSTRA-SEVIR4, lower right SLSTRB-SEVIR4. 109

Figure 80: Seasonal mean differences of $\text{LST}_{\text{satellite 1}} - \text{LST}_{\text{satellite 2}}$ in K; two upmost plots are for ATSR_3-MOD11T, two middle plots for ATSR_3-MODIST, and two lowest plots for MODIST-ATSR_3, each time for night-time and daytime data, respectively. ----- 110

Figure 81: Number of seasonal averaged data points per pixel; two upmost plots are for ATSR_3-MOD11T, two middle plots for ATSR_3-MODIST, and two lowest plots for MODIST-ATSR_3. Each time for night-time and daytime data, respectively. ----- 111

Figure 82: Seasonal differences for different elevation classes; blue bars are the median differences, red points the RSTD and the green points on the right axis show the number of averaged data points Left row displays night-time and right row daytime data. Upper plots are for ATSR_3-MOD11T, middle plots for ATSR_3-MODIST, and lower plots for MODIST-ATSR_3. ----- 112

Figure 83: Seasonal differences versus $\text{satze} * \text{sign}(\text{sataz})$ of satellite_1; red stars represent the daytime data, blue dots the night-time data, and the green stars and dots on the right axis display the averaged pixel numbers for daytime and night-time data. Upper left plot displays ATSR_3-MOD11T, upper right ATSR_3-MODIST, lower left MODIST-ATSR_3. ----- 113

Figure 84: Seasonal mean differences of $\text{LST}_{\text{satellite 1}} - \text{LST}_{\text{satellite 2}}$ in K; left row displays night-time and right row daytime data. Upper plots are for ATSR_3-MOD11T, middle plots for ATSR_3-MODIST, and lower plots for MODIST-ATSR_3. ----- 114

Figure 85: Number of seasonal averaged data points per pixel; left row displays night-time and right row daytime data. Upper plots are for ATSR_3-MOD11T, middle plots for ATSR_3-MODIST, and lower plots for MODIST-ATSR_3. ----- 115

Figure 86: Seasonal differences for different elevation classes; blue bars are the median differences, red points the RSTD and the green points on the right axis show the number of averaged data points Left row displays night-time and right row daytime data. Upper plots are for ATSR_3-MOD11T, middle plots for ATSR_3-MODIST, and lower plots for MODIST-ATSR_3. ----- 116


 land surface temperature cci	Product Validation Plan (PVP) <i>WP4 – DEL4.1</i>	Ref.: LST-CCI-D4.1-PVIR Version: 3.1 Date: 23-Jun-2023 Page: x
--	---	---

Figure 87: Seasonal differences for different land cover classes; coloured bars are the differences, red points the RSTD and the green points on the right axis show the number of averaged data points. Left row displays night-time and right row daytime data. Upper plots are for ATSR_3-MOD11T, middle plots for ATSR_3-MODIST, and lower plots for MODIST-ATSOP_. ----- 117

Figure 88: Seasonal differences versus $\text{satze} * \text{sign}(\text{sataz})$ of satellite_1; red stars represent the daytime data, blue dots the night-time data, and the green stars and dots on the right axis display the averaged pixel numbers for daytime and night-time data. Upper left plot displays ATSR_3-MOD11T, upper right ATSR_3-MODIST, lower left MODIST-ATSOP_.----- 118

Figure 89: Seasonal mean differences of LST_satellite 1 – LST_satellite 2 in K; left row displays night-time and right row daytime data. Upper plots are for ATSR_3-MOD11T, middle plots for ATSR_3-MODIST, and lower plots for MODIST-ATSOP_.----- 119

Figure 90: Number of seasonal averaged data points per pixel; left row displays night-time and right row daytime data. Upper plots are for ATSR_3-MOD11T, middle plots for ATSR_3-MODIST, and lower plots for MODIST-ATSOP_.----- 120

Figure 91: Seasonal differences for different elevation classes; blue bars are the median differences, red points the RSTD and the green points on the right axis show the number of averaged data points Left row displays night-time and right row daytime data. Upper plots are for ATSR_3-MOD11T, middle plots for ATSR_3-MODIST, and lower plots for MODIST-ATSOP_. ----- 121

Figure 92: Seasonal differences for different land cover classes; coloured bars are the differences, red points the RSTD and the green points on the right axis show the number of averaged data points. Left row displays night-time and right row daytime data. Upper plots are for ATSR_3-MOD11T, middle plots for ATSR_3-MODIST, and lower plots for MODIST-ATSOP_. ----- 122

Figure 93: Seasonal differences versus $\text{satze} * \text{sign}(\text{sataz})$ of satellite_1; red stars represent the daytime data, blue dots the night-time data, and the green stars and dots on the right axis display the averaged pixel numbers for daytime and night-time data. Upper left plot displays ATSR_3-MOD11T, upper right ATSR_3-MODIST, lower left MODIST-ATSOP_.----- 123

Figure 94: Seasonal mean differences of LST_satellite 1 – LST_satellite 2 in K; left row displays night-time and right row daytime data. Upper plots are for MOD11A-SEVIR2, middle plots for MODISA-SEVIR2, and lower plots for MOD11T-SEVIR2.----- 124

Figure 95: Seasonal mean differences of LST_satellite 1 – LST_satellite 2 in K; left row displays night-time and right row daytime data. Upper plots are for MODIST-SEVIR2, middle plots for ATSOP_-SEVIR2, and lower plots for ATSR_3-SEVIR2.----- 125

Figure 96: Seasonal mean differences of LST_satellite 1 – LST_satellite 2 in K; left row displays night-time and right row daytime data. Upper plots are for ATSR_3-MOD11T, middle plots for ATSR_3-MODIST, and lower plots for MODIST-ATSOP_.----- 126

Figure 97: Seasonal mean differences of LST_satellite 1 – LST_satellite 2 in K; left row displays night-time and right row daytime data. Upper plots are for SLSTRA-SEVIR4, middle plots for SLSTB-SEVIR4, for the years 2018 - 2020.----- 127

Figure 98: Number of seasonal averaged data points per pixel; left row displays night-time and right row daytime data. Upper plots are for MOD11A-SEVIR2, middle plots for MODISA-SEVIR2, and lower plots for MOD11T-SEVIR2.----- 128


 land surface temperature cci	Product Validation Plan (PVP) <i>WP4 – DEL4.1</i>	Ref.: LST-CCI-D4.1-PVIR Version: 3.1 Date: 23-Jun-2023 Page: xi
--	---	--

Figure 99: Number of seasonal averaged data points per pixel; left row displays night-time and right row daytime data. Upper plots are for MODIST-SEVIR2, middle plots for ATSOP_-SEVIR2, and lower plots for ATSR_3-SEVIR2.----- 129

Figure 100: Number of seasonal averaged data points per pixel; left row displays night-time and right row daytime data. Upper plots are for ATSR_3-MOD11T, middle plots for ATSR_3-MODIST, and lower plots for MODIST-ATSOP_-.----- 130

Figure 101: Number of seasonal averaged data points per pixel; left row displays night-time and right row daytime data. Upper plots are for SLSTRA-SEVIR4, middle plots for SLSTRB-SEVIR4, for the years 2018 - 2020. ----- 131

Figure 102: Seasonal differences for different elevation classes; blue bars are the median differences, red points the RSTD and the green points on the right axis show the number of averaged data points Left row displays night-time and right row daytime data. Upper plots are for MOD11A-SEVIR2, middle plots for MODISA-SEVIR2, and lower plots for MOD11T-SEVIR2. ----- 132

Figure 103: Seasonal differences for different elevation classes; blue bars are the median differences, red points the RSTD and the green points on the right axis show the number of averaged data points Left row displays night-time and right row daytime data. Upper plots are for MODIST-SEVIR2, middle plots for ATSOP_-SEVIR2, and lower plots for ATSR_3-SEVIR2. ----- 133

Figure 104: Seasonal differences for different elevation classes; blue bars are the median differences, red points the RSTD and the green points on the right axis show the number of averaged data points Left row displays night-time and right row daytime data. Upper plots are for ATSR_3-MOD11T, middle plots for ATSR_3-MODIST, and lower plots for MODIST-ATSOP_-. ----- 134

Figure 105: Seasonal differences for different elevation classes; blue bars are the median differences, red points the RSTD and the green points on the right axis show the number of averaged data points Left row displays night-time and right row daytime data. Upper plots are for SLSTRA-SEVIR4, middle plots for SLSTRB-SEVIR4, for the years 2018 - 2020. ----- 135


Figure 106: Seasonal differences for different land cover classes; coloured bars are the differences, red points the RSTD and the green points on the right axis show the number of averaged data points. Left row displays night-time and right row daytime data. Upper plots are for MOD11A-SEVIR2, middle plots for MODISA-SEVIR2, and lower plots for MOD11T-SEVIR2. ----- 136

Figure 107: Seasonal differences for different land cover classes; coloured bars are the differences, red points the RSTD and the green points on the right axis show the number of averaged data points. Left row displays night-time and right row daytime data. Upper plots are for MODIST-SEVIR2, middle plots for ATSOP_-SEVIR2, and lower plots for ATSR_3-SEVIR2. ----- 137

Figure 108: Seasonal differences for different land cover classes; coloured bars are the differences, red points the RSTD and the green points on the right axis show the number of averaged data points. Left row displays night-time and right row daytime data. Upper plots are for ATSR_3-MOD11T, middle plots for ATSR_3-MODIST, and lower plots for MODIST-ATSOP_-. ----- 138

Figure 109: Seasonal differences for different land cover classes; coloured bars are the differences, red points the RSTD and the green points on the right axis show the number of averaged data points. Left row displays night-time and right row daytime data. Upper plots are for SLSTRA-SEVIR4, middle plots for SLSTRB-SEVIR4, for the years 2018 - 2020. ----- 139

Figure 110: Seasonal differences versus $\text{satze} * \text{sign}(\text{sataz})$ of satellite_1 ; red stars represent the daytime data, blue dots the night-time data, and the green stars and dots on the right axis display the averaged pixel numbers for daytime and night-time data. Upper left plot displays MOD11A-SEVIR2, upper right

 land surface temperature cci	Product Validation Plan (PVP) <i>WP4 – DEL4.1</i>	Ref.: LST-CCI-D4.1-PVIR Version: 3.1 Date: 23-Jun-2023 Page: xii
--	---	---

MODISA-SEVIR2, middle left MOD11T-SEVIR2, middle right MODIST-SEVIR2, lower left ATSR_3-SEVIR2, and lower right ATSR_3-SEVIR2. ----- 140

Figure 111: Seasonal differences versus $\text{satze} * \text{sign}(\text{sataz})$ of satellite_1; red stars represent the daytime data, blue dots the night-time data, and the green stars and dots on the right axis display the averaged pixel numbers for daytime and night-time data. Upper left plot displays ATSR_3-MOD11T, upper right ATSR_3-MODIST, lower left MODIST-ATSR_3, lower right SLSTRA-SEVIR4, lower right SLSTRB-SEVIR4. - 141

Figure 112: Seasonal mean differences of $\text{LST}_{\text{satellite 1}} - \text{LST}_{\text{satellite 2}}$ in K; left row displays night-time and right row daytime data. Upper plots are for ATSR_3-MOD11T, middle plots for ATSR_3-MODIST, and lower plots for MODIST-ATSR_3. ----- 142

Figure 113: Number of seasonal averaged data points per pixel; left row displays night-time and right row daytime data. Upper plots are for ATSR_3-MOD11T, middle plots for ATSR_3-MODIST, and lower plots for MODIST-ATSR_3. ----- 143

Figure 114: Seasonal differences for different elevation classes; blue bars are the median differences, red points the RSTD and the green points on the right axis show the number of averaged data points Left row displays night-time and right row daytime data. Upper plots are for ATSR_3-MOD11T, middle plots for ATSR_3-MODIST, and lower plots for MODIST-ATSR_3. ----- 144

Figure 115: Seasonal differences for different land cover classes; coloured bars are the differences, red points the RSTD and the green points on the right axis show the number of averaged data points. Left row displays night-time and right row daytime data. Upper plots are for ATSR_3-MOD11T, middle plots for ATSR_3-MODIST, and lower plots for MODIST-ATSR_3. ----- 145

Figure 116: Seasonal differences versus $\text{satze} * \text{sign}(\text{sataz})$ of satellite_1; red stars represent the daytime data, blue dots the night-time data, and the green stars and dots on the right axis display the averaged pixel numbers for daytime and night-time data. Upper left plot displays ATSR_3-MOD11T, upper right ATSR_3-MODIST, lower left MODIST-ATSR_3. ----- 146


Figure 117: Seasonal mean differences of $\text{LST}_{\text{satellite 1}} - \text{LST}_{\text{satellite 2}}$ in K; left row displays night-time and right row daytime data. Upper plots are for ATSR_3-MOD11T, middle plots for ATSR_3-MODIST, and lower plots for MODIST-ATSR_3. ----- 147

Figure 118: Number of seasonal averaged data points per pixel; left row displays night-time and right row daytime data. Upper plots are for ATSR_3-MOD11T, middle plots for ATSR_3-MODIST, and lower plots for MODIST-ATSR_3. ----- 148

Figure 119: Seasonal differences for different elevation classes; blue bars are the median differences, red points the RSTD and the green points on the right axis show the number of averaged data points Left row displays night-time and right row daytime data. Upper plots are for ATSR_3-MOD11T, middle plots for ATSR_3-MODIST, and lower plots for MODIST-ATSR_3. ----- 149


Figure 120: Seasonal differences for different land cover classes; coloured bars are the differences, red points the RSTD and the green points on the right axis show the number of averaged data points. Left row displays night-time and right row daytime data. Upper plots are for ATSR_3-MOD11T, middle plots for ATSR_3-MODIST, and lower plots for MODIST-ATSR_3. ----- 150

Figure 121: Seasonal differences versus $\text{satze} * \text{sign}(\text{sataz})$ of satellite_1; red stars represent the daytime data, blue dots the night-time data, and the green stars and dots on the right axis display the averaged pixel numbers for daytime and night-time data. Upper left plot displays ATSR_3-MOD11T, upper right ATSR_3-MODIST, lower left MODIST-ATSR_3. ----- 151

 land surface temperature cci	Product Validation Plan (PVP) <i>WP4 – DEL4.1</i>	Ref.: LST-CCI-D4.1-PVIR Version: 3.1 Date: 23-Jun-2023 Page: xiii
--	---	--

List of Tables

Table 1: Overview of the used in situ stations. -----	4
Table 2: Summary of the satellite – satellite data pairs used in the intercomparisons. -----	6
Table 3: Median night-time bias and RSTD in K for the analysed time period. -----	17
Table 4: Median daytime bias and RSTD in K for the analysed time period. -----	19
Table 5: Percentage (%) of night-time datapoints with the required accuracy ($ \text{satellite LST} - \text{station LST} < 1 \text{ K}$). -----	21
Table 6: Percentage (%) of daytime datapoints with the required accuracy ($ \text{satellite LST} - \text{station LST} < 1 \text{ K}$). -----	22
Table 7: Analysed years for the validation of satellite LST data sets over in situ stations -----	23
Table 8: Overview of seasonal results of the median differences of the analysed satellite -satellite pairs over the continents Africa and Europe, where data from all satellite - satellite pairs are available. Results are presented in terms of difference (diff) and RSTD-----	56
Table 9: Overview of seasonal results of the median differences of the analysed satellite -satellite pairs over the continents where only LEO – LEO matches are available -----	57

 land surface temperature cci	Product Validation Plan (PVP) <i>WP4 – DEL4.1</i>	Ref.: LST-CCI-D4.1-PVIR Version: 3.1 Date: 23-Jun-2023 Page: 1
--	---	---

0. Executive Summary


Within the land surface temperature (LST) Climate Change Initiative project (LST_cci), which is part of the European Space Agency (ESA) Climate Change Initiative (CCI), a set of LST products from major satellites is developed. These LST data sets can be used for various applications within climate science.

For users to understand these data sets well and take them up, information on their quality is crucial. This is achieved within the project by validation of the developed data sets by an independent validation team, which ensures impartial results of the validation analysis.

This documents reports the results and interpretations of the validations carried out within LST_cci, which are split in two parts. First is the more straightforward approach of validating the satellite data sets against in situ point measurements, and second is the intercomparison of the data sets with third party data sets which are used as reference. This gives additional insights in the quality of the developed data. The results are presented in terms of bias for the in situ validation, difference for the intercomparisons, and accuracy and robust standard deviation for both with reference to the LST_cci requirements.

For the in situ validation, 16 infrared LST_cci products, for sensors Aqua-MODIS, Terra-MODIS, GOES-12, GOES-13, GOES-16, MTSAT-2, Himawari 8, SEVIRI (MSG1-4), MetOp-A AVHRR, ATSR-2, AATSR, SLSTR-A, and SLSTR-B and two microwave LST_cci products, from sensors SSMI-13 and SSMI-17, are validated against in situ data from 16 globally distributed stations. The LST_cci products from these sensors are henceforth identified by six character codes: MODISA (for Aqua-MODIS), MODIST (for Terra-MODIS), MTSAT2 (for MTSAT-2), HMWR_8 (for Himawari 8), GOES12 (for GOES-12), GOES13 (for GOES-13), GOES16 (for GOES-16), SEVIR1-SEVIR4 (SEVIRI), AVHRMA (for MetOpA-AVHRR), ATSR_2 (for ATSR-2), ATSR_3 (for AATSR), SLSTRA (for SLSTR-A), SLSTRB (for SLSTR-B), SSMI13 (for SSMI-13) and SSMI17 (for SSMI-17). The stations utilised are from the KIT network, SURFRAD network, Copernicus LAW network, ARM network and Heihe network. The validation time period ranges from 1995 – 2020.

The results of the in situ validation show that in general the accuracies of the LST_cci products are better at night than during the day, which is entirely as expected. MODISA, MODIST, ATSR_2 and ATSR_3 generally have biases $< \pm 2$ K. The latest V3.00 of the data sets show a marked improvement on the V1.00 data sets validated in V1.00 of this document. The significant negative bias for SLSTRA V1.00 has been reduced in V3.00. The results are similar for SLSTRB. The bias of SEVIR1 - 4 is $< \pm 2.5$ K over all validated stations, with the exception of one station that experiences a strong seasonal cycle. The biases of GOES12, GOES13 and GOES16 are also low. The results of MTSAT2 vary depending on the station, which might be due to the varying heterogeneity of the different in situ stations. The biases for AVHRMA are generally low, especially at night. High RSTDs were however observed at some stations. The AVHRMA cloud mask is at an early maturity level and is expected to improve in future versions of the AVHRMA data set. The HMWR_8 data set showed similar biases to MTSAT2 dataset at Heihe sites but displayed lower RSTDs. The microwave data sets tend to have higher positive biases compared with the other data sets, however they do view a larger area than the infrared data sets and thus incorporate more heterogeneities around the stations. Large differences can be found between the biases of LST_cci products with respect to in situ observations at certain single stations, showing that the performance of different data sets varies with the


 land surface temperature cci	Product Validation Plan (PVP) <i>WP4 – DEL4.1</i>	Ref.: LST-CCI-D4.1-PVIR Version: 3.1 Date: 23-Jun-2023 Page: 2
--	---	---

land cover type and elevation over which it is evaluated. The uncertainty validation showed that depending on station and data set, the total uncertainty often matches the robust standard deviation of the bias. Larger deviations are caused by more heterogeneous surrounding of the in situ station, an over- or underestimation of the in situ uncertainty or wrong estimation of the satellite emissivity uncertainty. For the MW data, a further assessment of the spatial uncertainty is needed in the next project phase.

Intercomparisons of satellite - satellite data pairs are a valuable asset to in situ validation results, especially as not all land covers types and regions are covered by in situ stations. For this project, 11 satellite - satellite pairs were globally matched and intercompared, which are namely MOD11A-SEVIR2, MODISA-SEVIR2, ATSOP_-SEVIR2, ATSR_3-SEVIR2, MOD11T-SEVIR2, MODIST-SEVIR2, ATSR_3-MOD11T, ATSR_3-MODIST, MODIST-ATSOP_, SLSTRA-SEVIR4, and SLSTRB-SEVIR4. In these cases, the LST_cci products are identified by their six character codes as described above, MOD11A is the operational Aqua-MODIS LST product, MOD11T is the operational Terra-MODIS LST product, and ATSOP_ is the operational AATSR LST product. All intercomparisons were performed for the years 2008 – 2010 over different continents, which varied due to the data availability of the data sets, with the exception of SLSTRA-SEVIR4 and SLSTRB-SEVIR4, which were analysed for the years 2018 - 2020. All 11 data pairs could be analysed over Africa and Europe. A monthly time series was analysed for all pairs, and additionally the dependence of the differences on elevation, land cover, and satellite angles was investigated.

The results show that higher positive differences were found for ATSR_3-MOD11T than for ATSR_3-MODIST. MOD11T-SEVIR2 and MOD11A-SEVIR2 have higher differences than MODIST-SEVIR2 and MODISA-SEVIR2. ATSOP_-SEVIR2 displays a strong seasonal cycle during the day, which is considerably reduced for ATSR_3-SEVIR2. MODIST-ATSOP_ has high differences, especially during the night. SLSTRA-SEVIR4 and SLSTRB-SEVIR4 have differences mainly within ± 2 K. The variability between the data pairs varies across the different continents, it is larger over Africa during night, over Europe during day, and in general higher over Asia and South America than over the other continents.

It can be concluded that the LEO IR data sets are showing good performance against in situ data, which has improved for the latest V3.00 compared with previous versions. The higher biases are for AVHRMA, particularly during the day, but this is the first release of this data set, and improvements are expected in future releases. Furthermore, ATSR_3 and MODIST are well correlated. The intercomparison analysis revealed that all LEO IR LST_cci products are more comparable with the LST_cci SEVIRI product than the corresponding operational products. While these results about the performances of the products are encouraging, further improvements can still be made to single products or over single regions. Therefore, recommendations for efforts for possible improvements are provided to the algorithm developments teams at the end of the document.

 land surface temperature cci	Product Validation Plan (PVP) <i>WP4 – DEL4.1</i>	Ref.: LST-CCI-D4.1-PVIR Version: 3.1 Date: 23-Jun-2023 Page: 3
--	---	---

1. Introduction

1.1. Purpose and Scope

Several satellite LST products are developed within the land surface temperature (LST) Climate Change Initiative project (LST_cci), which is part of the European Space Agency (ESA) Climate Change Initiative (CCI). These data sets can be used for a large variety of applications in different fields of climate science.

For ensuring that the users understand these data sets in the best possible way, it is important that information about their quality is available. This can also help to promote the uptake of LST data sets and possible users are informed about differences between the single produced data sets, their global performance as well as their performance over different landscapes and in different regions.

The quality of the data sets is investigated within LST_cci through their validation by an independent validation team. This procedure ensures that the validation results and their interpretations are gained impartial from the producers of the data sets. In this document, the results of the first validation round are presented. The theoretical background for the validation is described separately in the Product Validation Plan (PVP) [AD-1], which informs in detail about the investigated satellite LST data sets (which are also described in [AD-2]), the used in situ stations and reference data sets for validation, the validation methodology, as well as the used harmonized data formats for storing the data.

There are two different validation approaches used. The first one is the in situ validation, which is the most straight forward approach, where satellite LST data are directly compared to in situ point measurements over several globally distributed stations. For this version of the report, 18 LST_cci satellite data sets were validated, which are identified by a 6-character code. They are namely ATSR_2 (for ATSR-2), ATSR_3 (for AATSR), AVHRMA (for MetopA-AVHRR), GOES12, GOES13 and GOES16 (for GOES), HMWR_8 (for Himawari8-AHI), MODISA (for Aqua-MODIS), MODIST (for Terra-MODIS), MTSAT2 (for MTSAT), SEVIR1, SEVIR2, SEVIR3, SEVIR4 (for SEVIRI), SLSTRA (for SLSTR-A), SLSTRB (for SLSTR-B), SSMI13 (for SSMI-13), and SSMI17 (for SSMI-17). They are analysed over 16 in situ stations belonging to different networks: KIT network, SURFRAD network, ARM network, Copernicus LAW, and the Heihe network. An overview over the single stations, their locations and surfaces can be found in Table 1. This set of stations is distributed over different climatic zones, land covers, elevations and regions worldwide, as detailed in [AD-1]. The validation time period differs depending on the availability of in situ and satellite data, ranging from 1995 to 2020. Note, only one Copernicus LAW station is included here as the other four stations (Svartberget, Hyttiala, Puechabon and Robson Creek) did not start operations until the end of 2021. These will all be included in the next version of the report.


 land surface temperature cci	Product Validation Plan (PVP) <i>WP4 – DEL4.1</i>	Ref.: LST-CCI-D4.1-PVIR Version: 3.1 Date: 23-Jun-2023 Page: 4
--	---	---

Table 1: Overview of the used in situ stations.

Code	Network	Name	Latitude	Longitude	Elevation	Surface type	Temporal availability
SGP____	ARM	Southern Great Plains Facility, Oklahoma	36.605° N	97.485° W	318 m	rural (mixture of grassland pasture / wheat fields/ bare soil [RD-20])	2003 – now
KIT_F_	Copernicus LAW	KIT Forest, Eggenstein-Leopoldshafen, Germany	49.09139	8.424819	308 m	Deciduous / mixed forest	2020 - now
EVO____	KIT	Evora, Portugal	38.540244	-8.003368	230 m	Savannas, woody savanna; 32% tree, 68% grass	2010 – now
DAH_T_	KIT	Dahra tree mast, Senegal	15.402336	-15.432744	90 m	Grassland; 96% grass, 4% tree	2010 – 2017
GBB_W_	KIT	Gobabeb wind tower, Namibia	-23.550956	15.05138	406 m	Bare ground; 75% gravel, 25% dry grass	2010 – now
KAL_R_	KIT	Rust mijn Ziel (RMZ) Farm, Kalahari, Namibia	-23.010532	18.352897	1450 m	Shrub land; 85% grass / soil, 15% tree	2010 - 2011
KAL_H_	KIT	Farm Heimat, Kalahari, Namibia	-22.932827	17.992137	1380 m	Shrub land; 37% tree / bush, 63% grass	2011 – 2018
BND____	SURFRAD	Bondville, Illinois	40.05155	-88.37325	230 m	Grassland	1995 - now
TBL____	SURFRAD	Table Mountain, Boulder, Colorado	40.12557	-105.23775	1689 m	Sparse grassland	1995 - now

DRA__	SURFRAD	Desert Rock, Nevada	36.62320	-116.01962	1007 m	Arid shrub land	1998 - now
FPK__	SURFRAD	Fort Peck, Montana	48.30798	-105.10177	634 m	Grassland	1995 - now
GCM__	SURFRAD	Goodwin Creek, Mississippi	34.2547	-89.8729	98 m	Grassland	1995 - now
PSU__	SURFRAD	Penn. State Univ., Pennsylvania	40.72033	-77.93100	376 m	Cropland	1998 - now
BGB__	Heihe Integrated Observatory Network	Heihe River Basin, China	38,899	100,282	1562 m	Desert	2013 - 15
DMN__	Heihe Integrated Observatory Network	Heihe River Basin, China	38,86	100,37	1556 m	Maize fields	2013 - now
HZZ__	Heihe Integrated Observatory Network	Heihe River Basin, China	38,746	100,29	1731 m	Desert	2013 - now

In spite of the global distribution of the in situ stations, they do not cover all important land covers and regions perfectly. Therefore, supplementary satellite – satellite intercomparisons are carried out between LST_cci data sets and operational LST products over different continents. The relative algorithm performances of the LST_cci data products over different regions worldwide can be investigated with these intercomparisons. For this report, intercomparisons were carried out for the years 2008 – 2010 for nine satellite-satellite pairs, and for the years 2018 – 2020 for two satellite-satellite pairs, which are summarized in Table 2. All LEO satellite data sets developed in LST_cci that span the years 2008 – 2010 (ENVISAT AATSR, AQUA MODIS, and TERRA MODIS) as well as the operational products of those three data sets are compared against MSG_SEVIRI. The two remaining LEO LST_cci satellite data sets (SLSTR-A, SLSTR-B) that started operating after that time period are validated against MSG_SEVIRI for 2018 – 2020. As MSG_SEVIRI is a geostationary satellite that has no global coverage, they are analysed over the continents Africa and Europe only. Additionally, ATSR_3 and MODIS are intercompared against each other, as they have a similar local overpass time. For comparability, ATSR_3 and MODIS are also compared against the operational data product of the other satellite product. Namely, these three remaining data pairs ENVISAT_AATSR vs TERRA_MOD11, ENVISAT_AATSR vs TERRA_MODIS, and TERRA_MODIS vs ENVISAT_ATSOP. They are also analysed over Antarctica, Asia, Australia, North America and South America.


 land surface temperature cci	Product Validation Plan (PVP) <i>WP4 – DEL4.1</i>	Ref.: LST-CCI-D4.1-PVIR Version: 3.1 Date: 23-Jun-2023 Page: 6
--	---	---

Table 2: Summary of the satellite – satellite data pairs used in the intercomparisons.


Sat 1 Full name	Sat 1 6 char code	Sat 1 Data set producer	Sat 2 Full name	Sat 2 6 char code	Sat 2 Data set producer	analysed time period
AQUA MODIS (operational product)	MOD11A	NASA	MSG-2 SEVIRI	SEVIR2	LST_cci	2008 - 10
AQUA MODIS	MODISA	LST_cci	MSG-2 SEVIRI	SEVIR2	LST_cci	2008 - 10
ENVISAT AATSR (operational product)	ATSOP_	ESA	MSG-2 SEVIRI	SEVIR2	LST_cci	2008 - 10
ENVISAT AATSR	ATSR_3	LST_cci	MSG-2 SEVIRI	SEVIR2	LST_cci	2008 - 10
ENVISAT AATSR	ATSR_3	LST_cci	TERRA MODIS (operational product)	MOD11T	NASA	2008 - 10
ENVISAT AATSR	ATSR_3	LST_cci	TERRA MODIS	MODIST	LST_cci	2008 - 10
TERRA MODIS (operational product)	MOD11T	NASA	MSG-2 SEVIRI	SEVIR2	LST_cci	2008 - 10
TERRA MODIS	MODIST	LST_cci	ENVISAT AATSR (operational product)	ATSOP_	ESA	2008 - 10
TERRA MODIS	MODIST	LST_cci	MSG-2 SEVIRI	SEVIR2	LST_cci	2008 - 10
SENTINEL-3A	SLSTRA	LST_cci	MSG-4 SEVIRI	SEVIR4	LST_cci	2018 - 20
SENTINEL-3B	SLSTRB	LST_cci	MSG-4 SEVIRI	SEVIR4	LST_cci	2018 - 20

The data files used in the validation process can be categorized as four different types: in situ data files (IS_); satellite extraction data files (SE_); matched satellite – satellite (SS_); and matched satellite – in situ data files (SI_). All four classes have a common data format that is introduced in [AD-1]. In this way, the validation procedure is harmonized, and can be carried out in the same way for all data sets, which in turn makes the different validation results comparable to each other. This also ensures that the analysis software can be re-used on additional data sets throughout the project, thus making the validation process faster.

The results for the in situ validation are presented in terms of bias which is the median average of the difference of satellite LST minus in situ LST (following [RD-3]) and by the robust standard deviation (RSTD) (see e.g. [RD-4]), which is linked to the precision (median absolute deviation) introduced in [RD-3] by a constant factor of 1.48, i.e. $RSTD = 1.48 * MAD$. Higher accuracy is used as a synonym for smaller bias. For the intercomparisons the results are presented in terms of a “difference” between products, which is the difference of satellite 1 LST minus satellite 2 LST. In this case, higher accuracy relates to smaller differences. All biases and differences displayed in this report are on an axis ranging from -10 K to 10 K to make the figures easily comparable to each other.

1.2. Structure of the Document

First, a short summary of the introduced satellite data sets is given, followed by an overview of the results of the in situ validations over all satellite data sets and over all stations in Section 3.1. Next, the validation results are described for each station individually in Section 3.2. An overview of the intercomparison results is given in Section 4.1, which are then described in more detail for each continent in Section 4.2. In

 land surface temperature cci	Product Validation Plan (PVP) <i>WP4 – DEL4.1</i>	Ref.: LST-CCI-D4.1-PVIR Version: 3.1 Date: 23-Jun-2023 Page: 7
--	---	---

Section 5, conclusions on the overall results are drawn, and finally recommendations for the producer of the data sets are given in Section 6. In the Appendix (Section 7) additional figures from the intercomparisons are displayed.


1.3. Applicable Documents

Ref Id	Applicable document
AD-1	CCI LST Product Validation Plan (LST-CCI-D2.5-PVP)
AD-2	CCI LST Product Specification Document (LST-CCI-D1.2-PSD)
AD-3	CCI End-To-End ECV Uncertainty Budget (LST-CCI-D2.3-E3UB)

1.4. Reference Documents

The following is a list of reference documents with a direct bearing on the content of this report. Where referenced in the text, these are identified as RD-xx, where ‘xx’ is the number in the table below.

Ref Id	Reference document
RD-1	Martin, M.; Göttsche, F.M. ESA DUE GlobTemperature Project: Satellite LST Validation report. Technical report, ESA, 2016. http://www.globtemperature.info/index.php/public-documentation/deliverables-1
RD-2	Martin, M.; Göttsche, F.M.; Ghent, D.; Trent, T.; Dodd, E.; Pires, A.; Trigo, I.; Prigent, C.; Jimenez, C. ESA DUE GlobTemperature Project: Satellite LST Intercomparison Report. Technical report, ESA, 2016. http://www.globtemperature.info/index.php/public-documentation/deliverables-1
RD-3	Guillevic, P.; Göttsche, F.; Nickeson, J.; Hulley, G.; Ghent, D.; Yu, Y.; Trigo, I.; Hook, S.; Sobrino, J.; Remedios, J.; Román, M.; Camacho, F. Land Surface Temperature Product Validation Best Practice Protocol, Version 1.1 2018. https://lpvs.gsfc.nasa.gov/PDF/CEOS_LST_PROTOCOL_Feb2018_v1.1.0_light.pdf
RD-4	Pearson, R.K. Outliers in Process Modeling and Identification. IEEE Transactions On Control Systems Technology 2002, 10, 55–63.
RD-5	Göttsche, F.M.; Hulley, G.C. Validation of six satellite-retrieved land surface emissivity products over two land cover types in a hyper-arid region. Remote Sensing of Environment 2012, 124, 149–158.
RD-6	Wan, Z.; Dozier, J. A Generalized Split-Window Algorithm for Retrieving Land-Surface Temperature from Space. IEEE Transactions on Geoscience and Remote Sensing 1996, 34, 892–905.
RD-7	Aires, F.; Prigent, C.; Rossow, W.; Rothstein, M. A new neural network approach including first guess for retrieval of atmospheric water vapor, cloud liquid water path, surface temperature, and emissivities over land from satellite microwave observations. Journal of Geophysical Research 2001, 106, 14887–14907.


 land surface temperature cci	Product Validation Plan (PVP) <i>WP4 – DEL4.1</i>	Ref.: LST-CCI-D4.1-PVIR Version: 3.1 Date: 23-Jun-2023 Page: 8
--	---	---

Ref Id	Reference document
RD-8	Prata, F. Land surface temperature measurement from space: AATSR algorithm theoretical basis document. Technical report, CSIRO Atmospheric Research, Aspendale, Australia, 2002.
RD-9	Ghent, D. GlobTemperature Project Technical Specification Document. Technical report, ESA, 2016.
RD-10	Michel, D.; Philipona, R.; Ruckstuhl, C.; Vogt, R.; and Vuilleumier, L.. Performance and Uncertainty of CNR1 Net Radiometers during a One-Year Field Comparison, Journal of Atmospheric and Oceanic Technology, 2008, 25(3), 442-451.
RD-11	Ermida, S.L.; Trigo, I.F.; DaCamara, C.C.; Göttsche, F.M.; Olesen, F.S.; Hulley, G. Validation of remotely sensed surface temperature over an oak woodland landscape – The problem of viewing and illumination geometries. Remote Sensing of Environment 2014, 148, 16–27.
RD-12	Liu, S.M. et al, Upscaling evapotranspiration measurements from multi-site to the satellite pixel scale over heterogeneous land surfaces. Agricultural and Forest Meteorology, 2016, 230-231, 97-113.
RD-13	Xu, Z.W. et al, Intercomparison of surface energy flux measurement systems used during the HiWATER-MUSOEXE. Journal of Geophysical Research, 2013, 118, 13140-13157.
RD-14	Liu, S.M. et al, The Heihe Integrated Observatory Network: A basin-scale land surface processes observatory in China. Vadose Zone Journal, 2018, 17:180072.
RD-15	Liu, S.M. et al, A comparison of eddy-covariance and large aperture scintillometer measurements with respect to the energy balance closure problem. Hydrology and Earth System Sciences, 2011, 15(4): 1291-1306.
RD-16	Li, X. et al, Heihe Watershed Allied Telemetry Experimental Research (HiWATER): Scientific objectives and experimental design, 2013, Bull. Am. Meteorol. Soc., 94 (8), 1145–1160.

1.5. Glossary

Term	Definition
ARM	Atmospheric Radiation Measurement
ATSR	Along Track Scanning Radiometer; the ATSR series of instruments comprises ATSR-1, ATSR-2 and AATSR (ATSR_3)
CCI	Climate Change Initiative
ESA	European Space Agency
GEO	Geostationary orbit
IS	In Situ Files
IR	Infrared
KIT	Karlsruhe Institute of Technology
LCC	Land Cover Class
LCCS	ULeic / LandCover_cci hybrid biome scheme
LEO	Low Earth Orbit
LST	Land Surface Temperature

Term	Definition
LST_cci	Land Surface Temperature Climate Change Initiative
MAD	Median Absolute Deviation
MODIS	Moderate Resolution Imaging Spectroradiometer
MSG	Meteosat Second Generation
MW	Microwave
NetCDF	Network Common Data Format
PSD	Product Specification Document
PVIR	Product Validation and Intercomparison Report
PVP	Product Validation Plan
RSTD	Robust Standard Deviation
Sataz	satellite azimuth angle
Satze	satellite zenith angle
SE	Satellite Extraction Files
SEVIRI	Spinning Enhanced Visible Infra-Red Imager
SH	Southern Hemisphere
SI	Satellite – In situ match ups
SLSTR	Sea and Land Surface Temperature Radiometer
SS	Satellite – Satellite match ups
SSM/I	Special Sensor Microwave – Imager
STD	Standard Deviation
SURFRAD	Surface Radiation Budget Network
ULeic	University of Leicester

 land surface temperature cci	Product Validation Plan (PVP) <i>WP4 – DEL4.1</i>	Ref.: LST-CCI-D4.1-PVIR Version: 3.1 Date: 23-Jun-2023 Page: 10
--	---	--

2. Satellite Data Sets

The validated LST_cci satellite and reference data sets are briefly introduced here. A more complete overview of the data sets can be found in the PVP [AD-1].

2.1. LST_cci Satellite Data Sets

Along Track Scanning Radiometer - 2 (ATSR-2 / ATSR_2) and Advanced Along Track Scanning Radiometer (AATSR / ATSR_3)

The Along Track Scanning Radiometer (ATSR) series of instruments include ATSR-2 and AATSR (Advanced Along-Track Scanning Radiometer). These were launched on board European Space Agency (ESA) sun synchronous, polar orbiting satellites ERS-2 in April 1995, and Envisat (Environmental Satellite) in March 2002, respectively. The last of these instruments – AATSR – provided its final data on 8th April 2012. These ATSRs therefore provide approximately 17 years of data. The UOL algorithm is used in LST_cci for the ATSR series of LST ECV datasets. The algorithm uses a nadir-only (SW) approach with classes of coefficients for each combination of land cover-diurnal (day/night) condition.

Advanced Very High Resolution Radiometer - Meteorological Operational satellite A (AVHRRMA)

The Advanced Very High Resolution Radiometer (AVHRR/3) is on board the Meteorological Operational (MetOp) satellite constellation. MetOp-A satellite, the first of the MetOp series, was launched in 2006 and was in operation until November 2021. Thus, it provided approximately 15 years of data which are processed in LST_cci. The LST_cci AVHRR/3– MetOpA (AVHRRMA) product uses a Generalized Split Window (GSW) Algorithm to estimate LST as a combination of clear-sky brightness temperatures from 2 thermal infrared bands centred on 10.8 μm and 12.0 μm . Retrieval coefficients are categorised into classes of satellite viewing angle and water vapour. MetOp-B and MetOp-C datasets will be produced in future processing cycles.

Geostationary Operational Environmental Satellite (GOES) Imager Data (GOES12, GOES13, GOES16)

The GOES series are part of the National Ocean and Atmosphere Administration (NOAA) earth observation mission and provide coverage over the American continent. GOES-12 was launched in July 2001, GOES-13 in May 2006 and GOES-16 in November 2016. GOES-13 replaced GOES-12 as the operational satellite in April 2010, while GOES-16 replaced GOES-13 as the operational satellite in December 2018. The operational location of the satellites renamed GOES-East (GOES-E) is 75°W. The Imager onboard the GOES satellites (GOES-12 and GOES-13) does not include two channels in the thermal atmospheric window of the spectrum, only the one centred at 10.8 μm . This channel has a spatial resolution of 4 km at SSP and a 3-hourly observation frequency for the full disk. The LST_cci GOES products use the single channel (SMW) algorithm to estimate LST. Retrieval coefficients are categorised into classes of satellite viewing angle and water vapour.

 land surface temperature cci	Product Validation Plan (PVP) <i>WP4 – DEL4.1</i>	Ref.: LST-CCI-D4.1-PVIR Version: 3.1 Date: 23-Jun-2023 Page: 11
--	---	--

Multifunctional Transport Satellites (MTSAT2) and Himawari 8 (HMWR_8)

The Multifunction Transport SATellite (MTSAT) series was operated by the Japanese Meteorological Association (JMA), providing coverage over the eastern part of Asia and over Australia. MTSAT-1R was launched in February 2005 and it was located at 140°E. MTSAT-2 was launched in February 2006 and it was located at 145°E. MTSAT-2 replaced MTSAT-1R as the operational satellite in July 2010 and was in operations until December 2015. The LST_cci MTSAT products use the single channel (SMW) algorithm to estimate LST. Himawari 8 (HMWR_8) was launched in 2014 and replaced MTSAT2 in December 2015. The LST_cci HMWR_8 product uses the GSW algorithm to estimate LST as a combination of clear-sky brightness temperatures from 2 thermal infrared bands centred on 11.2 μm and 12.3 μm . For MTSAT2 and HMWR_8 algorithms, retrieval coefficients are categorised into classes of satellite viewing angle and water vapour. A Himawari 9 dataset will be produced in future processing cycles.

Moderate Resolution Imaging Spectrometer (MODIS / MODISA and MODIST)


MODIS (Moderate Resolution Imaging Spectroradiometer) instruments were launched on board two sun-synchronous, near-polar orbiting satellites Terra (EOS AM-1) launched on 18 December 1999 and Aqua (EOS PM-1) launched on 4 May 2002, respectively. Each instrument provides a pair of observations each day acquiring data in 36 spectral bands. Terra-MODIS acquires data at approximately 10:30am (local solar time) in its descending node and at approximately 10:30pm (local solar time) in its ascending node; while Aqua-MODIS observes the Earth at approximately 1:30pm (local solar time) in its ascending node; and at approximately 1:30am (local solar time) in its descending node. The LST_cci MODIS products use the GSW approach to estimate LST as a linear function of clear-sky TOA brightness temperatures from bands 31 and 32 centred on 11 μm and 12 μm , respectively. Retrieval coefficients are categorised into classes of satellite viewing angle and water vapour.

Sea and Land Surface Temperature Radiometer (SLSTR / SLSTRA and SLSTRB)

The Sea and Land Surface Temperature Radiometer (SLSTR) –which is based on the principles of AATSR – on board the Sentinel satellites 3-A and 3-B comprises a space element of Copernicus programme. This responds to the requirements for an operational and near-real-time monitoring of the Earth surface over a period of 15 to 20 years. Sentinel-3A was launched on 16th February 2016, and Sentinel-3B was launched on 25th April 2017. The UOL algorithm is used in LST_cci for the SLSTR series of LST ECV datasets. The algorithm uses a nadir-only (SW) approach with classes of coefficients for each combination of land cover-diurnal (day/night) condition.

Special Sensor Microwave / Imager (SSM/I / SSMI_13 and SSMI_17)

SSM/I sensors have been on board the Defense Meteorological Satellite Program (DMSP) polar satellites since 1987, which observe the Earth twice daily. The local times of their descending and ascending modes are early morning and late afternoon, respectively. There are up to 4 SSM/I instruments in space at the same time with similar overpassing times. A methodology has been developed to estimate LST, along with atmospheric water vapour, cloud liquid water, and surface emissivities over land, from passive microwave imagers [RD-7]. It is based on a neural network inversion, trained on a large data set of simulated

 land surface temperature cci	Product Validation Plan (PVP) <i>WP4 – DEL4.1</i>	Ref.: LST-CCI-D4.1-PVIR Version: 3.1 Date: 23-Jun-2023 Page: 12
--	---	--

radiances, using real atmospheric and surface information over the globe. LST are estimated with a spatial resolution of $0.25^\circ \times 0.25^\circ$.

Spinning Enhanced Visible and Infrared Imager (SEVIRI /SEVIR1, SEVIR2, SEVIR3, SEVIR4)

SEVIRI is the main sensor on board Meteosat Second Generation (MSG), a series of 4 geostationary satellites to be operated by EUMETSAT. SEVIRI was designed to observe the Earth disk with view zenith angles (SZA) ranging from 0° to 80° at a temporal sampling rate of 15 minutes. The first MSG satellite was launched in August 2002, and operational observations are available since January 2004. The High Resolution Visible channel provides measurements with a 1 km sampling distance at sub-satellite point (SSP); for the remaining channels the spatial resolution is 3 km at SSP. The nominal SSP is located at 0° longitude and therefore the MSG disk covers Africa, most of Europe and parts of South America. A SEVIRI LST product is produced by the Land Surface Analysis Satellite Application Facility (LSA SAF). LST is obtained by correcting top-of-atmosphere (TOA) radiances for surface emissivity, atmospheric attenuation along the path and reflection of downward radiation. The LST_cci SEVIRI products use the generalized split-window (GSW) approach to estimate LST as a linear function of clear-sky TOA brightness temperatures from bands 31 and 32 centred on $11\ \mu\text{m}$ and $12\ \mu\text{m}$, respectively. Retrieval coefficients are categorised into classes of satellite viewing angle and water vapour.

2.2. External Satellite Data Sets

NASA Operational MODIS (MYD11 and MOD11 / MOD11A and MOD11T)

The standard NASA operational MODIS LST products MOD11_L2 (Terra) and MYD11_L2 (Aqua) uses a generalized split-window algorithm to retrieve LST of clear-sky pixels from brightness temperatures. This implementation of the algorithm operates with classification-based emissivities. The retrieval coefficients are determined by interpolation on a set of multi-dimensional look-up tables; these are obtained by linear regression of the simulation data generated by radiative transfer over a broad range of surface and atmospheric conditions.

ESA Operational Advanced Along Track Scanning Radiometer (AATSR / ATSOP_)

For the standard ESA AATSR LST retrieval, only the nadir view is used. LST are retrieved with a split-window algorithm [RD-8] with 1 km resolution based on the infrared channels at $11\ \mu\text{m}$ and $12\ \mu\text{m}$ [RD-9].

3. Description and Analysis of In Situ Validation Results

3.1. Overview of Results

First, an overview of the validation results for all satellite data sets over all in situ stations is given. The biases for the investigated data sets over each station are shown in Figure 1, the robust standard deviations (RSTD) in Figure 2. The bias and RSTD is also given in Table 3 for night-time and in Table 4 for daytime data. When interpreting the results, one has to keep in mind that the time period over which the data is averaged varies between stations and satellite data sets due to their temporal and spatial availability. The matched time periods can be seen in Table 7. Additionally, the percentage of the matched data that meet the accuracy requirements, i.e. $|\text{satellite LST} - \text{station LST}| < 1 \text{ K}$, is given in Table 5 and Table 6.



Figure 1: Overview over the biases of all validated satellite LST data sets against all stations, for night-time (upper plot) and daytime (lower plot) data. The matched time of the satellite data sets varies, depending on data availability, as indicated in Table 7. The red span marks the bias range of $\pm 2 \text{ K}$.

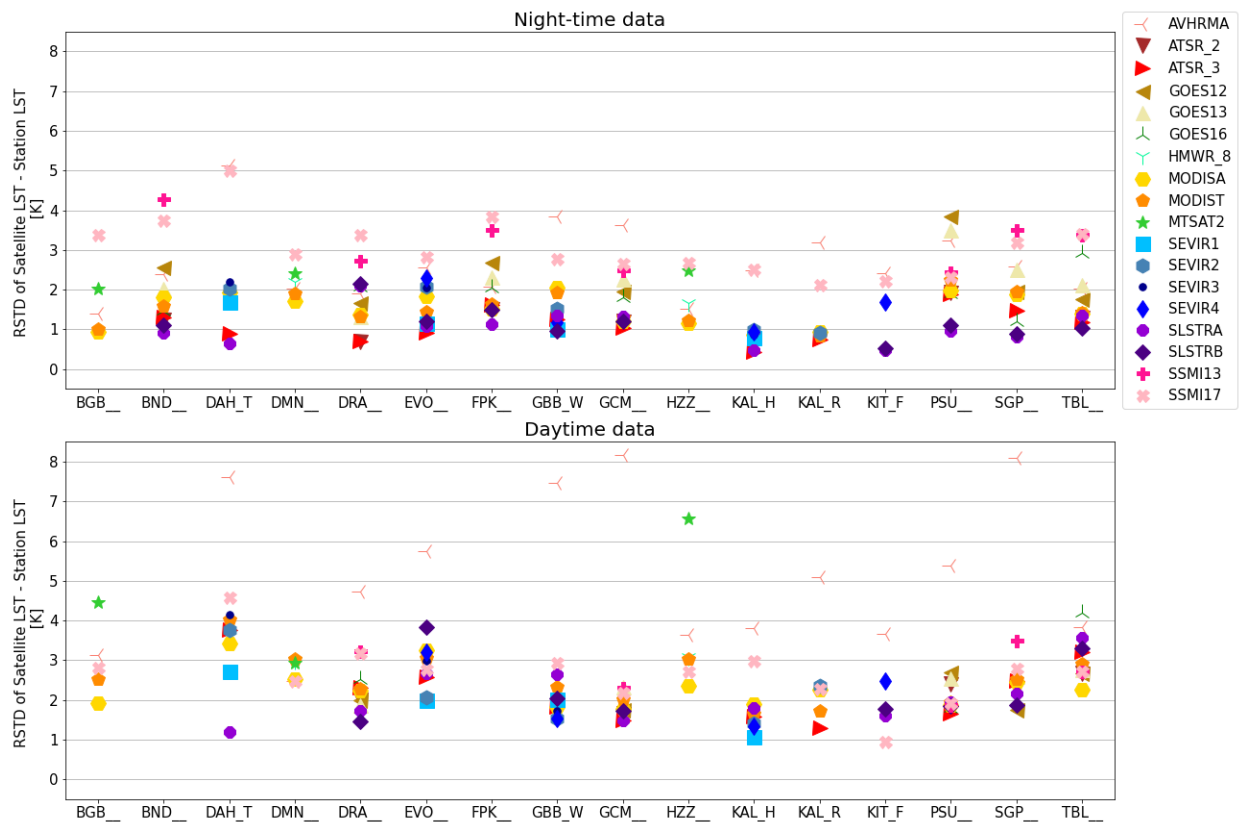



Figure 2: Overview over the RSTD of all validated satellite LST data sets against all stations, for night-time (upper plot) and daytime (lower plot) data.

In general, the night-time biases are smaller than the daytime biases and have also lower RSTDs. This is expected and mainly caused by the influence of solar radiation during daytime, which results in different surface temperatures observed by the satellite sensors at sunlit and shadowy areas. These differences are often to a lower extent reflected in the point measurements of the in situ sensors. SLSTRA had large negative biases over certain stations for V1.00 of the data set. This improved for V3.00 of the data set, where an improved cloud mask is introduced. The MW data sets SSMI13 and SSMI17 tend to have the largest positive biases over certain stations. The MW data sets sample a larger area than the IR data sets (see [AD-1]) and thus capture for most stations a more heterogeneous surface than the IR data sets. The four SEVIRI data sets (SEVIR1 – 4) are only validated over the KIT stations due to the spatial coverage of the data sets. The bias are within ± 2.5 K over all validated stations for night-time and daytime results, with the exception of DAH_T_ station during day, the reason for which is detailed below in Section 3.2.4. The GOES data sets, i.e. GOES12, GOES13 and GOES16, are validated over the SURFRAD and ARM stations only due to their spatial coverage. Their biases are mostly within ± 2.5 K, and these tend to be negative.

Furthermore, it can be seen in Figure 1 that the magnitude of the biases varies significantly between single stations and also between satellite data sets. For example, over GBB_W_, KAL_R_, KAL_H_ and DAH_T_ the MW data sets have very high biases. Very large differences between the biases for all investigated data sets are observed over DAH_T_ station and KIT_F_ station. These differences can either be caused by the different satellite algorithms, which might represent some surfaces better than others, or it is due to a

 land surface temperature cci	Product Validation Plan (PVP) <i>WP4 – DEL4.1</i>	Ref.: LST-CCI-D4.1-PVIR Version: 3.1 Date: 23-Jun-2023 Page: 15
--	---	--

different homogeneity in the area around the in situ stations, as larger surface heterogeneities are often not represented by the in situ LST measurement. The reasons for the biases vary from station to station and will be investigated in detail for each station individually below.

The results of the different RSTD over the stations (Figure 2) show that for night-time the RSTD for the MW data sets is highest. This is caused by the fact, as mentioned above, that the MW sensors observe a larger area than the IR sensors and thus views more heterogeneity around the stations. Furthermore, the SSMI sensors have a local overpass time at around 6:30 am /pm, which can be, depending on location and season, be close to local sunrise / sunset. In these cases, the discrimination between daytime and night-time data is less discernible than for the other sensors. The distinction between day and night is based on the solar elevation angle at the time of the satellite observation. For the other sensors, the RSTD is usually larger during daytime, which is due to the influence of sunlight and shadows during day. Large daytime RSTD for all data sets are found for station DAH_T_ and TBL___. Both stations are located in very heterogeneous surroundings. Increased RSTD are also found over station EVO___, which is located in an area covered with cork-oak trees, where the influence of shadows is significant during day. The AVHRMA sensor, included in the first cycle of LST_cci Phase 2, showed large RSTD at half of the sites. These large RSTDs can be related with unmasked clouds since the cloud mask for this product is still at an early maturity level.

The percentage of datapoints that meet the required accuracy is directly linked to the bias and RSTD. Thus, those matched data with low bias and RSTD showed higher percentage of accurate datapoints. Most values are between 5 and 15 %. GEO and MW datasets show the lowest quantity of accurate datapoints due to its lower spatial resolution.

The number of matched data points is shown in Figure 3. The number of matches also varies between satellite data sets and stations due to the specific time span for each data set and the spatial coverage of the data sets dependent on the width of each satellite swath. The MW data sets have in general a high number of matches, as they can retrieve LST during cloudy periods. The overflight time close to sunrise or sunset of the SSMI sensors also leads to a varying number in daytime and night-time data. There are more daytime and less night-time data points in summer, when sunset is at a later time and vice-versa during winter, when the days are shorter. This might make the statistics of the averaged biases for the time periods with fewer data points less robust.

Both MODIS data sets have many data points as they have the longest time period (see Table 7). The high number of matches of the GEO sensors (MTSAT2, SEVIR1-4, GOES12, GOES13 and GOES16) is due to the higher temporal data coverage of the geostationary data sets. The low number of SLSTRA data points over DAH_T_ station is caused by the fact that the in situ measurements at this station stopped in January 2017, whereas the SLSTRA data sets starts in mid-2016

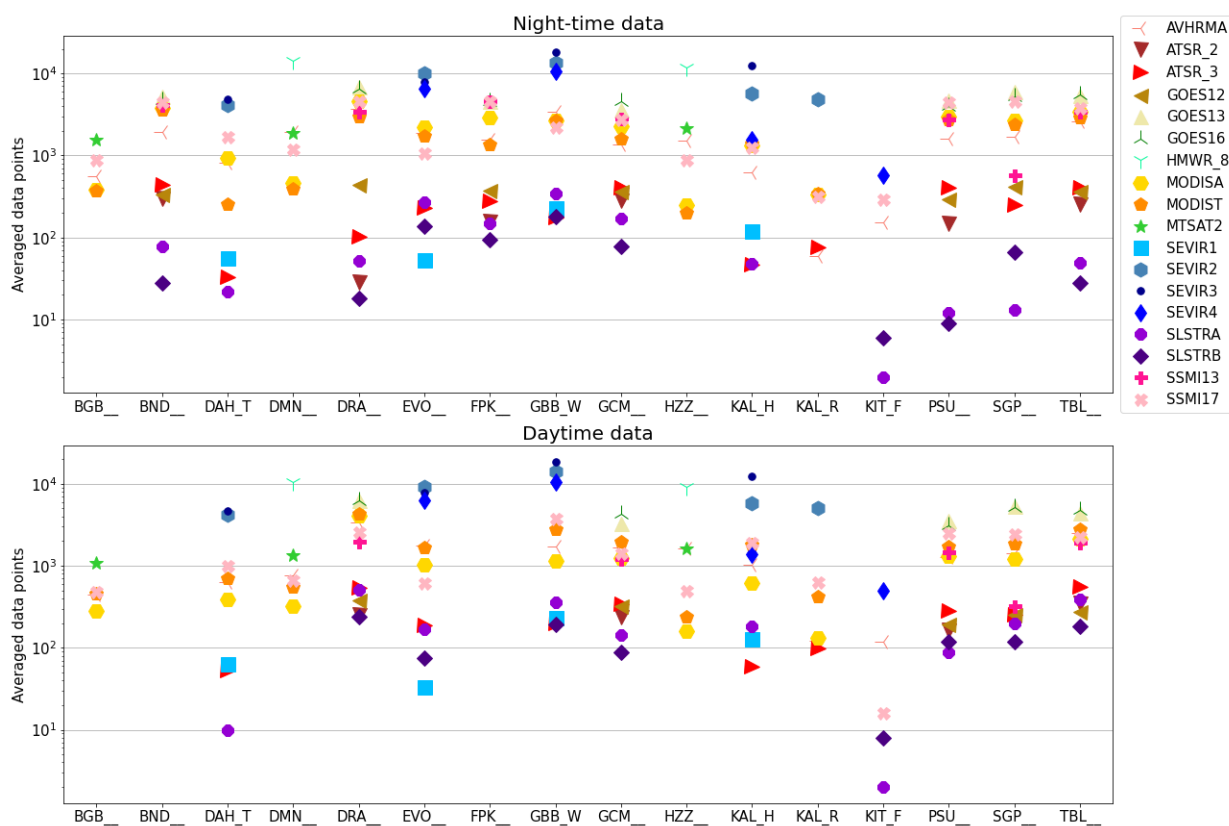


Figure 3: Number of averaged data points over all validated satellite LST data sets and stations, for night-time (upper plot) and daytime (lower plot) data.

Table 3: Median night-time bias and RSTD in K for the analysed time period.

		BGB__	BND__	DAH_T	DMN__	DRA__	EVO__	FPK__	GBB_W	GCM__	HZZ__	KAL_H_	KAL_R_	KIT_F_	PSU__	SGP__	TBL__
		-	-	-	-	-	-	-	-	-	-	-	-	-	-	-	-
AVHRMA	bias	1.26	0.48	-0.82	-0.33	0.32	0.72	0.64	3.08	0.92	0.38	1.37	-0.66	0.44	0.85	-0.24	0.08
	RSTD	1.40	2.39	5.13	2.03	1.91	2.56	2.08	3.84	3.63	1.51	2.49	3.18	2.41	3.23	2.59	2.03
ATSR_2	bias	-	-0.25	-	-	0.09	-	0.55	-	0.49	-	-	-	-	0.98	-	-0.17
	RSTD	-	1.25	-	-	0.70	-	1.51	-	1.20	-	-	-	-	1.93	-	1.29
ATSR_3	bias	-	0.81	1.32	-	0.16	0.31	0.92	0.79	0.66	-	2.07	-0.41	-	0.67	-0.96	0.00
	RSTD	-	1.31	0.89	-	0.70	0.92	1.62	1.25	1.04	-	0.43	0.75	-	1.88	1.47	1.17
GOES12	bias	-	-0.39	-	-	-2.35	-	0.19	-	1.45	-	-	-	-	0.00	-2.18	-0.70
	RSTD	-	2.56	-	-	1.66	-	2.68	-	1.96	-	-	-	-	3.85	1.96	1.76
GOES13	bias	-	0.37	-	-	-2.48	-	-1.18	-	2.34	-	-	-	-	0.48	-1.10	-0.94
	RSTD	-	2.03	-	-	1.33	-	2.31	-	2.27	-	-	-	-	3.51	2.51	2.12
GOES16	bias	-	0.12	-	-	-3.68	-	-0.99	-	2.19	-	-	-	-	0.46	-0.47	0.37
	RSTD	-	1.48	-	-	2.08	-	2.05	-	1.81	-	-	-	-	1.90	1.20	2.94
HMWR_8	bias	-	-	-	-1.44	-	-	-	-	-	-1.77	-	-	-	-	-	-
	RSTD	-	-	-	2.21	-	-	-	-	-	1.68	-	-	-	-	-	-
MODISA	bias	0.49	1.15	1.91	0.36	0.15	0.83	0.99	-0.23	0.53	1.06	1.35	0.65	-	1.21	-0.22	0.18
	RSTD	0.95	1.81	1.94	1.72	1.36	1.84	1.51	2.06	1.22	1.16	0.87	0.93	-	1.99	1.88	1.41
MODIST	bias	0.43	0.13	-0.21	0.11	0.06	0.56	0.02	-0.99	0.37	0.17	1.67	0.45	-	0.32	-1.13	0.04
	RSTD	1.02	1.60	1.66	1.91	1.32	1.45	1.65	1.94	1.29	1.24	0.86	0.83	-	2.24	1.95	1.42

MTSAT2	bias	-0.50	-	-	0.63	-	-	-	-	-	-1.39	-	-	-	-	-	-
	RSTD	2.03	-	-	2.42	-	-	-	-	-	2.49	-	-	-	-	-	-
SEVIR1	Bias	-	-	-3.28	-	-	1.31	-	-1.58	-	-	0.72	-	-	-	-	-
	RSTD	-	-	1.70	-	-	1.16	-	1.02	-	-	0.79	-	-	-	-	-
SEVIR2	Bias	-	-	-0.81	-	-	1.73	-	-0.17	-	-	0.39	-1.07	-	-	-	-
	RSTD	-	-	2.03	-	-	2.08	-	1.51	-	-	0.99	0.90	-	-	-	-
SEVIR3	bias	-	-	-1.02	-	-	1.02	-	-0.96	-	-	0.23	-	-	-	-	-
	RSTD	-	-	2.21	-	-	2.05	-	1.33	-	-	0.87	-	-	-	-	-
SEVIR4	bias	-	-	-	-	-	1.21	-	-0.29	-	-	0.71	-	0.64	-	-	-
	RSTD	-	-	-	-	-	2.28	-	1.19	-	-	0.95	-	1.69	-	-	-
SLSTRA	bias	-	0.44	-0.47	-	-0.58	-0.20	-0.02	0.09	-0.51	-	0.47	-	-1.73	1.53	-0.25	-0.55
	RSTD	-	0.92	0.66	-	2.11	1.07	1.14	1.35	1.33	-	0.49	-	0.48	0.96	0.82	1.35
SLSTRB	bias	-	0.36	-	-	-1.08	0.19	0.18	0.18	-0.44	-	-	-	-0.60	0.88	0.71	-0.46
	RSTD	-	1.10	-	-	2.15	1.22	1.50	0.96	1.19	-	-	-	0.53	1.10	0.89	1.04
SSM113	bias	-	0.80	-	-	-1.22	-	1.74	-	1.39	-	-	-	-	-0.40	1.14	-1.91
	RSTD	-	4.27	-	-	2.74	-	3.51	-	2.48	-	-	-	-	2.43	3.50	3.40
SSM117	bias	-1.27	0.52	2.93	1.29	-1.82	2.11	1.04	3.54	1.32	-2.30	4.55	3.31	-2.54	-0.50	1.76	-2.42
	RSTD	3.38	3.74	5.00	2.91	3.38	2.83	3.85	2.79	2.67	2.68	2.52	2.12	2.22	2.33	3.20	3.41

Table 4: Median daytime bias and RSTD in K for the analysed time period.

		BGB___	BND___	DAH_T___	DMN___	DRA___	EVO___	FPK___	GBB_W___	GCM___	HZZ___	KAL_H___	KAL_R___	KIT_F___	PSU___	SGP___	TBL___
AVHRMA	Bias	3.58	-	-6.56	1.05	0.94	-1.10	-	3.13	-5.88	2.83	2.09	2.48	2.00	-1.30	-3.12	0.95
	RSTD	3.13	-	7.61	2.48	4.73	5.75	-	7.47	8.17	3.64	3.80	5.10	3.66	5.40	8.10	3.83
ATSR_2	Bias	-	-	-	-	0.58	-	-	-	0.63	-	-	-	-	-0.44	-	0.33
	RSTD	-	-	-	-	2.02	-	-	-	1.65	-	-	-	-	2.42	-	2.68
ATSR_3	Bias	-	-	0.34	-	0.34	0.02	-	-0.87	0.56	-	-1.41	0.09	-	0.29	-1.82	0.41
	RSTD	-	-	3.75	-	2.30	2.56	-	1.83	1.48	-	1.57	1.29	-	1.65	2.48	3.22
GOES12	Bias	-	-	-	-	-2.71	-	-	-	-0.56	-	-	-	-	-0.61	-2.18	-2.73
	RSTD	-	-	-	-	1.99	-	-	-	1.75	-	-	-	-	2.70	1.75	2.68
GOES13	Bias	-	-	-	-	-2.04	-	-	-	-0.64	-	-	-	-	-0.72	-1.77	-2.16
	RSTD	-	-	-	-	1.88	-	-	-	2.34	-	-	-	-	2.55	2.61	2.77
GOES16	Bias	-	-	-	-	-3.65	-	-	-	-1.12	-	-	-	-	-0.39	-1.25	-3.29
	RSTD	-	-	-	-	2.52	-	-	-	1.87	-	-	-	-	1.79	1.93	4.21
HMWR_8	bias	-	-	-	0.55	-	-	-	-	-	-1.57	-	-	-	-	-	-
	RSTD	-	-	-	2.99	-	-	-	-	-	3.08	-	-	-	-	-	-
MODISA	Bias	-1.22	-	-2.63	-0.07	0.26	1.06	-	-1.13	0.26	-0.50	-1.00	2.16	-	-0.59	-2.03	-0.13
	RSTD	1.93	-	3.42	2.54	2.24	3.25	-	1.82	1.78	2.36	1.89	2.25	-	1.87	2.45	2.27
MODIST	Bias	-0.91	-	-3.38	0.73	0.13	-0.95	-	-0.88	0.35	-0.11	-0.38	1.59	-	-0.96	-2.43	-0.39
	RSTD	2.53	-	4.03	3.03	2.28	3.05	-	2.34	2.01	3.04	1.65	1.73	-	1.94	2.52	2.92
MTSAT2	Bias	-2.67	-	-	0.68	-	-	-	-	-	-3.47	-	-	-	-	-	-



	RSTD	4.46	-	-	2.94	-	-	-	-	-	6.58	-	-	-	-	-	-
SEVIR1	Bias	-	-	-5.57	-	-	0.28	-	0.03	-	-	0.22	-	-	-	-	-
	RSTD	-	-	2.73	-	-	1.99	-	2.01	-	-	1.07	-	-	-	-	-
SEVIR2	Bias	-	-	-1.25	-	-	-0.48	-	0.94	-	-	0.19	1.51	-	-	-	-
	RSTD	-	-	3.77	-	-	2.08	-	1.54	-	-	1.41	2.36	-	-	-	-
SEVIR3	Bias	-	-	-3.18	-	-	-0.22	-	0.35	-	-	-0.19	-	-	-	-	-
	RSTD	-	-	4.15	-	-	2.99	-	1.72	-	-	1.30	-	-	-	-	-
SEVIR4	bias	-	-	-	-	-	-0.92	-	0.26	-	-	-0.19	-	1.60	-	-	-
	RSTD	-	-	-	-	-	3.22	-	1.54	-	-	1.33	-	2.48	-	-	-
SLSTRA	Bias	-	-	-5.65	-	0.37	-0.50	-	-0.43	2.61	-	-2.15	-	-4.85	0.46	-1.76	0.34
	RSTD	-	-	1.19	-	1.72	2.68	-	2.64	1.48	-	1.79	-	1.62	1.96	2.17	3.57
SLSTRB	bias	-	-	-	-	0.19	0.38	-	-0.72	1.46	-	-	-	0.32	0.32	-1.95	0.01
	RSTD	-	-	-	-	1.45	3.84	-	2.05	1.73	-	-	-	1.77	1.84	1.88	3.31
SSM113	Bias	-	-	-	-	-1.17	-	-	-	0.65	-	-	-	-	-0.15	0.47	-0.82
	RSTD	-	-	-	-	3.24	-	-	-	2.30	-	-	-	-	1.88	3.48	2.73
SSM117	Bias	-1.83	-	3.88	0.10	-1.84	3.07	-	5.36	1.22	-2.54	6.05	5.12	-2.47	0.03	2.47	-1.00
	RSTD	2.81	-	4.58	2.49	3.19	2.78	-	2.94	2.19	2.73	2.98	2.28	0.96	1.93	2.79	2.73



Table 5: Percentage (%) of night-time datapoints with the required accuracy ($|satellite\ LST - station\ LST| < 1\ K$).

	BGB_	BND_	DAH_T_	DMN_	DRA_	EVO_	FPK_	GBB_W_	GCM_	HZZ_	KAL_H_	KAL_R_	KIT_F_	PSU_	SGP_	TBL_
AVHRMA	28.21	30.08	15.21	35.97	36.22	26.84	34.19	12.12	16.76	42.42	22.60	23.33	27.27	24.78	30.49	37.57
ATSR_2	-	54.36	-	-	75.86	-	45.22	-	49.65	-	-	-	-	31.29	-	53.75
ATSR_3	-	42.57	24.24	-	88.12	49.56	33.69	41.95	49.25	-	14.89	72.37	-	32.34	36.95	59.90
GOES12	-	34.63	-	-	18.71	-	22.46	-	21.55	-	-	-	-	20.21	17.83	39.56
GOES13	-	35.42	-	-	11.84	-	31.31	-	15.40	-	-	-	-	21.85	28.62	36.76
GOES16	-	48.15	-	-	10.00	-	35.42	-	14.62	-	-	-	-	33.25	57.67	29.24
HMWR_8	-	-	-	25.64	-	-	-	-	-	24.71	-	-	-	-	-	-
MODISA	55.70	25.77	14.67	43.89	53.05	31.94	32.90	31.71	50.37	33.47	31.12	56.16	-	20.36	39.03	50.30
MODIST	58.22	45.73	43.19	43.04	53.89	40.49	45.35	31.97	51.82	50.75	19.63	68.59	-	30.72	35.33	51.20
MTSAT2	41.48	-	-	29.12	-	-	-	-	-	30.48	-	-	-	-	-	-
SEVIR1	-	-	10.71	-	-	27.78	-	25.11	-	-	58.68	-	-	-	-	-
SEVIR2	-	-	36.66	-	-	22.29	-	43.19	-	-	50.94	46.74	-	-	-	-
SEVIR3	-	-	37.00	-	-	33.69	-	38.98	-	-	68.92	-	-	-	-	-
SEVIR4	-	-	-	-	-	30.43	-	53.43	-	-	50.82	-	39.83	-	-	-
SLSTRA	-	70.13	63.64	-	42.31	58.61	60.67	48.99	53.22	-	83.33	-	0.00	33.33	69.23	51.02
SLSTRB	-	60.71	-	-	22.22	52.52	51.06	67.04	52.56	-	-	-	66.67	66.67	59.70	67.86
SSMI13	-	17.35	-	-	23.99	-	16.05	-	26.38	-	-	-	-	31.92	11.86	20.39
SSMI17	24.83	21.42	13.75	23.30	20.25	17.93	18.07	11.45	26.69	21.62	7.27	13.21	18.64	31.70	17.91	18.82



Table 6: Percentage (%) of daytime datapoints with the required accuracy ($| \text{satellite LST} - \text{station LST} | < 1 \text{ K}$).

	BGB_	BND_	DAH_T_	DMN_	DRA_	EVO_	FPK_	GBB_W_	GCM_	HZZ_	KAL_H_	KAL_R_	KIT_F_	PSU_	SGP_	TBL_
AVHRMA	8.16	-	6.91	27.59	15.70	13.95	-	6.94	8.24	11.74	8.30	7.32	15.97	14.15	11.46	18.37
ATSR_2	-	-	-	-	25.20	-	-	-	34.44	-	-	-	-	34.94	-	28.33
ATSR_3	-	-	18.87	-	32.90	20.53	-	24.87	40.94	-	25.42	57.58	-	45.07	21.09	21.88
GOES12	-	-	-	-	18.80	-	-	-	45.91	-	-	-	-	31.44	20.00	15.50
GOES13	-	-	-	-	25.08	-	-	-	34.62	-	-	-	-	33.52	27.00	24.75
GOES16	-	-	-	-	11.50	-	-	-	38.03	-	-	-	-	43.98	39.26	15.17
HMWR_8	-	-	-	23.97	-	-	-	-	-	23.59	-	-	-	-	-	-
MODISA	34.98	-	11.42	28.84	34.48	21.43	-	16.19	41.14	32.70	33.06	9.02	-	40.09	22.27	35.01
MODIST	35.65	-	11.88	22.18	33.63	21.30	-	18.39	36.60	22.59	40.40	28.61	-	35.10	16.23	28.35
MTSAT2	17.37	-	-	25.00	-	-	-	-	-	12.00	-	-	-	-	-	-
SEVIR1	-	-	12.70	-	-	42.42	-	28.63	-	-	66.67	-	-	-	-	-
SEVIR2	-	-	23.47	-	-	31.52	-	24.62	-	-	42.07	31.70	-	-	-	-
SEVIR3	-	-	18.03	-	-	26.16	-	29.85	-	-	53.41	-	-	-	-	-
SEVIR4	-	-	-	-	-	23.75	-	32.36	-	-	54.66	-	25.35	-	-	-
SLSTRA	-	-	0.00	-	44.14	26.79	-	19.50	11.11	-	23.20	-	0.00	41.38	21.83	19.07
SLSTRB	-	-	-	-	46.84	14.67	-	26.04	29.55	-	-	-	50.00	43.33	23.93	24.73
SSMII13	-	-	-	-	21.17	-	-	-	33.17	-	-	-	-	40.16	12.58	28.61
SSMII17	24.07	-	13.04	30.76	20.25	13.93	-	4.43	26.61	18.38	4.60	6.86	6.25	39.79	16.61	27.70



Table 7: Analysed years for the validation of satellite LST data sets over in situ stations

	BGB___	BND___	DAH_T_	DMN___	DRA___	EVO___	FPK___	GBB_W_	GCM___	HZZ___	KAL_H_	KAL_R_	KIT_F_	PSU___	SGP___	TBL___
AVHRMA	2013 - 15	2010 - 20	2009 - 17	2013 - 20	2007 - 20	2009 - 20	2007 - 20	2009 20	2007 - 20	2013 - 20	2011 - 18	2009 - 11	2020	2007 - 20	2010 - 20	2007 - 20
ATSR_2	-	1995 - 2003	-	-	1998 - 2003	-	1995 - 2003	-	1995 - 2003	-	-	-	-	1998 - 2003	-	1995 - 2003
ATSR_3	-	2002 - 12	2009 - 12	-	2002 - 12	2009 - 12	2009 - 12	2009 - 12	2002 - 12	-	2011 - 12	2009 - 11	-	2002 - 12	2007 - 12	2002 - 12
GOES12	-	2009 - 10	-	-	2009 - 10	-	2009 - 10	-	2009 - 10	-	-	-	-	2009 - 10	2009 - 10	2009 - 10
GOES13	-	2010 - 17	-	-	2010 - 17	-	2010 - 17	-	2010 - 17	-	-	-	-	2010 - 17	2010 - 17	2010 - 17
GOES16	-	2018 - 20	-	-	2018 - 20	-	2018 - 20	-	-	-	-	-	-	2018 - 20	2018 - 20	2018-20
HMWR_8				2015 - 20						2015 - 20						
MODISA	2013 - 15	2002 - 18	2009 - 17	2013 - 15	2002 - 18	2009 - 18	2002 - 18	2009 - 18	2002 - 18	2013 - 15	2011 - 18	2009 - 11	-	2002 - 18	2007 - 18	2002 - 18
MODIST	2013 - 15	2000 - 18	2009 - 17	2013 - 15	2000 - 18	2009 - 18	2000 - 18	2009 - 18	2000 - 18	2013 - 15	2011 - 18	2009 - 11	-	2000 - 18	2007 - 18	2000 - 18
MTSAT2	2013 - 15	-	-	2013 - 15	-	-	-	-	-	2013 - 15	-	-	-	-	-	-
SEVIR1	-	-	2009 - 15	-	-	2009 - 15	-	2009 - 15	-	-	2011 - 15	2009 - 11	-	-	-	-
SEVIR2	-	-	2009 - 17	-	-	2009 - 20	-	2009 - 20	-	-	2011 - 18	2009 - 11	-	-	-	-
SEVIR3	-	-	2013 - 17	-	-	2013 - 18	-	2013 - 18	-	-	2013 - 18	2009 - 11	-	-	-	-
SEVIR4	-	-	-	-	-	2018 - 20	-	2018 - 20	-	-	2018	-	2020	-	-	-
SLSTRA	-	2016 - 20	2016 - 17		2016 - 20	2016 - 20	2016 - 20	2016 - 20	2016 - 20	-	2016 - 18	-	2020	2017 - 20	2016 - 20	2017 - 20
SLSTRB	-	2018 - 20	-	-	2018 - 20	2018 - 20	2018 - 20	2018 - 20	2018 - 20	-	-	-	2020	2018 - 20	2018 - 20	2018 - 20
SSMII13	-	1995 - 2008	-	-	1998 - 2008	-	1995 - 2008	-	1995 - 2008	-	-	-	-	1998 - 2008	2007 - 08	1995 - 2008
SSMII17	2013 - 15	2009 - 20	2009 - 17	2013 - 15	2009 - 20	2009 - 20	2009 - 20	2009 - 20	2009 - 20	2013 - 15	2011 - 18	2009 - 11	2020	2009 - 20	2009 - 20	2009 - 20

3.2. Results for different stations

The results for the in situ validation over the different stations are presented in the following, more details about the stations and the land surfaces surrounding the stations can be found in the Product Validation Plan [AD-1].

3.2.1. Results over ARM Station

Results over SGP___ (Southern Great Plains) Station



Figure 4: Monthly mean biases (satellite LST - station LST) over SGP___ station. The upper plot represents night-time and the lower daytime data. The red span is the area where the bias is in a ± 2 K range.

The night-time as well as the daytime biases for the investigated IR LST data sets (AVHRRMA, ATSR_3, GOES12, GOES13, GOES16, MODISA, MODIST, SLSTRA, and SLSTRB) and the MW LST data sets (SSMI13 and SSMI17) are displayed in Figure 4. All data sets show a seasonal cycle, which has higher amplitude during day, and is strongest for the MODIS data sets. The biases are more positive in the summer months and more negative in the winter months. This is probably caused by the phenological cycle found in the

rural area around the station, which is dominated by agricultural fields where wheat and cattle pasture is grown. This cycle leads to changing differences between the in situ and the satellite data sets. There are high absolute biases seen for the SSMI13 and SSMI17 MW data sets, which observe, as mentioned above, a larger area than the IR sensors. The differences between the MW daytime and night-time results are smaller than for the IR sensors due to the local overpass time for the SSMI sensors, as also described above.


3.2.2. Results over Copernicus LAW Stations

Copernicus LAW stations at Puechabon Forest (PUE_F_), Svartberget Forest (SVA_F_), Hyytiälä Forest (HYY_F_) and Robson Creek Forest (ROB_F_) started their operation in November 2021. Thus, they will be included in future validations.

Results over KIT_F_ (Kit Forest) station



Figure 5: Monthly mean biases (satellite LST – station LST) over KIT_F_ station. The upper plot represents night-time and the lower daytime data. The red span is the area where the bias is in a ± 2 K range.

	Product Validation Plan (PVP) <i>WP4 – DEL4.1</i>	Ref.: LST-CCI-D4.1-PVIR Version: 3.1 Date: 23-Jun-2023 Page: 26
---	---	--

This station is located in a forest close to Karlsruhe, and it started operating in July 2020. Thus, only half a year of data was analysed. The monthly biases are mainly within a ± 2 K range for the analysed IR data sets, with smaller biases during night-time. The MW night-time biases are more negative.

3.2.3. Results over Heihe Stations

Results over BGB___ (Bajitan Gobi) Station

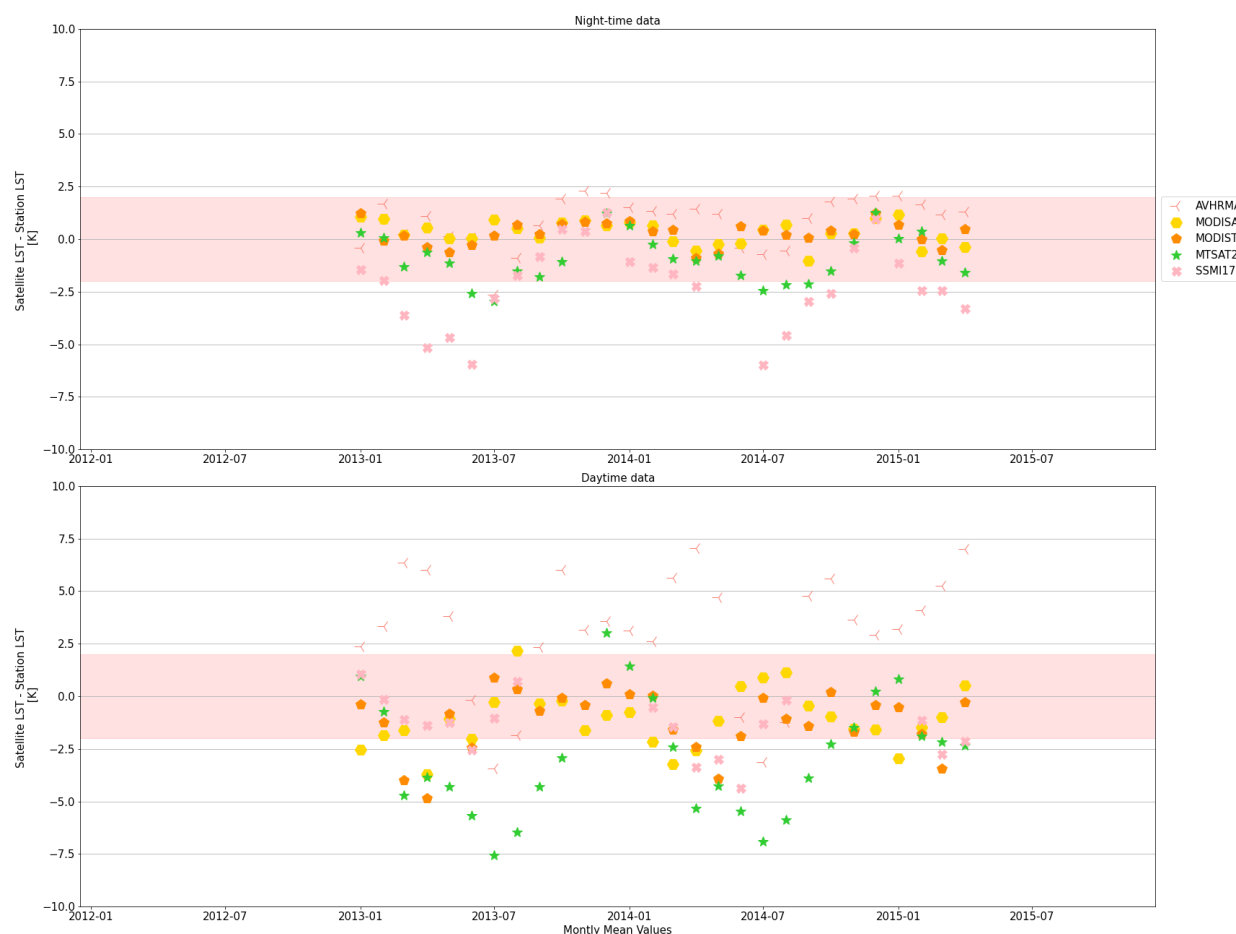


Figure 6: Monthly mean biases (satellite LST - station LST) over BGB___ station. The upper plot represents night-time and the lower daytime data. The red span is the area where the bias is in a ± 2 K range.

The results over BGB___ station show a seasonal cycle during daytime, which is strongest for MTSAT2 data, with negative biases during the summer months and smaller biases during winter. Positive biases are observed for AVHRMA during daytime. Furthermore, in the months June and July, the biases from MODISA and MODIST become positive, whereas they become increasing negative for MTSAT2. This could be a result of the differing treatment of the atmospheric correction between the data sets as MTSAT2 is limited to one thermal band. During night-time, the monthly mean values for the three IR data sets (MODISA,

MODIST, and MTSAT2) are mainly within the ± 2 K range, whereas the MW biases for SSMI17 are more negative in the summer months.

Larger differences between satellite and in situ LST are expected over all Heihe stations compared to the other stations, as here there is a higher temporal difference of 10 minutes between the LST values (compared to 3 minutes over the other stations) due to the coarser temporal coverage of the Heihe in situ data. For details on the Heihe measurement sites and set-up see [RD-12] to [RD-16].

Results over DMN___ (Daman) station



Figure 7: Monthly mean biases (satellite LST - station LST) over DMN___ station. The upper plot represents night-time and the lower daytime data. The red span is the area where the bias is in a ± 2 K range.

This station has the smallest monthly biases from the three investigated Heihe stations. However, a yearly cycle is seen in all data sets. Whereas the night-time biases are largest in winter and smallest in summer, it is the other way round for the daytime data. This station is located in a rural area with fields, where mainly maize is grown. Thus, the seasonal cycle during daytime could be due to the harvesting cycle in this agricultural area. The reason for the strong seasonal cycle during night is less clear.

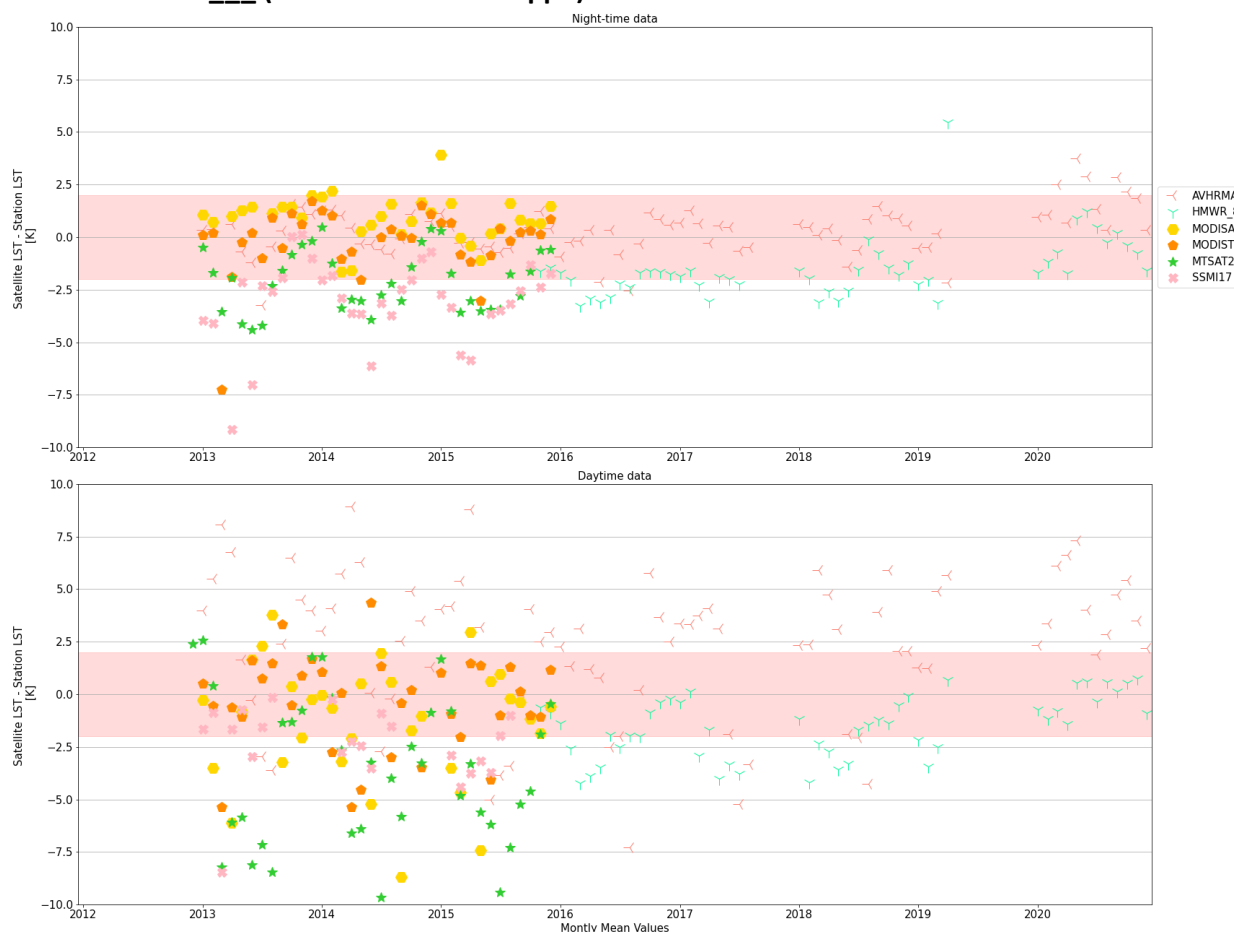
Results over HZZ___ (Huazhaizi Desert Steppe) station


Figure 8: Monthly mean biases (satellite LST - station LST) over HZZ___ station. The upper plot represents night-time and the lower daytime data. The red span is the area where the bias is in a ± 2 K range.

Over HZZ___ station, the night-time results for MODISA and MODIST are in an acceptable range. For daytime, a seasonal cycle is seen with negative biases in summer. For MTSAT2, HMWR_8 and SSMI17, a night-time seasonal cycle is seen, and is stronger than for MODIS. During daytime the seasonal cycle is more pronounced with a negative overall bias, although it is positive for AVHRMA. This station is also located in a desert area, close to a change in land cover and a more agricultural area northeast of the station. To avoid validating over pixels with this different LCC, the validation was done over a desert area SE of the station. However, also in this region a decreasing elevation is found due to a mountain range SE of the station. This might lead to different influence of shadow / sunlit measurements at the station and at the pixels used for validation, and therefore to a higher differences between satellite and in situ LST during daytime.

3.2.4. Results over KIT Stations

Results over DAH_T_ (Dahra tree mast) Station

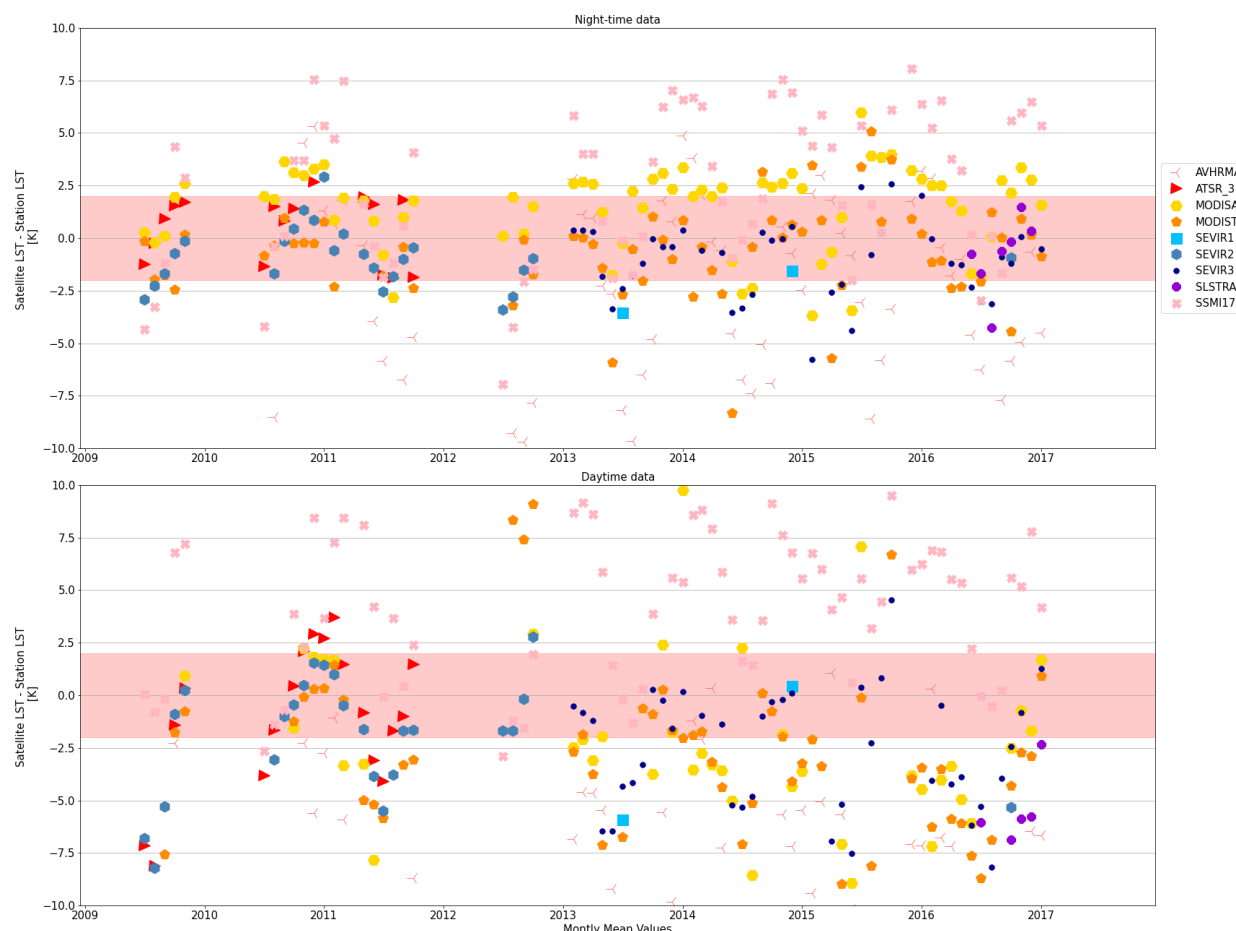


Figure 9: Monthly mean biases (satellite LST – station LST) over DAH_T_ station. The upper plot represents night-time and the lower daytime data. The red span is the area where the bias is in a ± 2 K range.

The data gaps in 2012 are due to missing in situ data at these times, and the station stopped operating in January 2017.

The strong seasonal vegetation cycle present at this station [AD-1] is reflected in the observed monthly biases. They increase in the first half of the year and decrease after that. As the rainy season lasts from June to November, the strong negative IR biases for AVHRRMA, MODIST, SEVIRx and ATSR_3 data seen during this time in summer and winter months are probably due to non-flagged cloudy data points observed in daytime and night-time results. In addition, the number of data points is reduced during the rainy seasons due to the present clouds, which makes the results during these months less robust. Also at this station, the results of the SSMI data sets are similar for daytime and night-time results with positive biases and very strong seasonality.

Results over EVO___ (Evora) Station

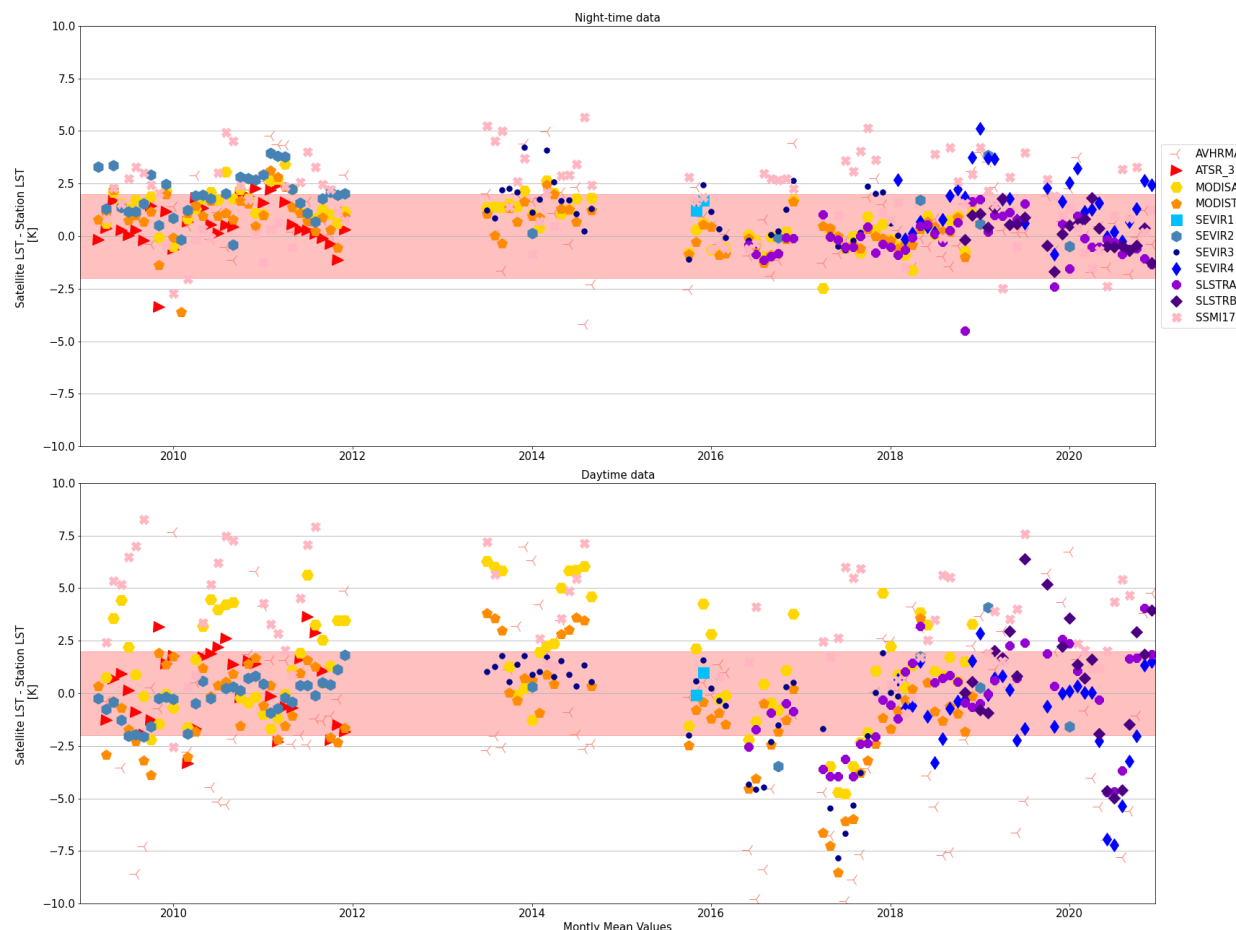


Figure 10: Monthly mean biases (satellite LST – station LST) over EVO___ station. The upper plot represents night-time and the lower daytime data. The red span is the area where the bias is in a ± 2 K range.

The night-time IR biases are mainly within ± 2 K (Figure 10), with increased values for SEVIR2 and SEVIR4. For all LEO IR daytime biases, a seasonal cycle is seen, with higher values in the summer months, which is less pronounced for the SEVIRx daytime biases. This is caused by the directional effects at this station caused by the trees around the station, resulting in an increased influence of sunlit and shaded areas in summer. The in situ data gap in 2013 is caused by the breakdown of the measurement mast due to a storm, and the gap in 2015 is due to malfunctioning of an instrument. Pronounced negative daytime values are seen for both MODIS data sets as well as for SLSTRA and SEVIR3 in the first half of 2017 and for SLSTRB and SEVIR4 in 2020. The in situ LST shows for these years a stronger seasonal cycle with high summer LST values, which is seen to a lesser extent in the satellite LST cycles. This might be caused by the large influence of shadows and sunlit areas in summer at this station. Constant endmember fractions are used over this station to estimate in situ LST, whereas it was shown before that the use of a geometrical model to estimate in situ LST improves the results [RD-11]. This should be considered for next validations of the LST_cci project.

Results over GBB_W_ (Gobabeb wind tower) Station

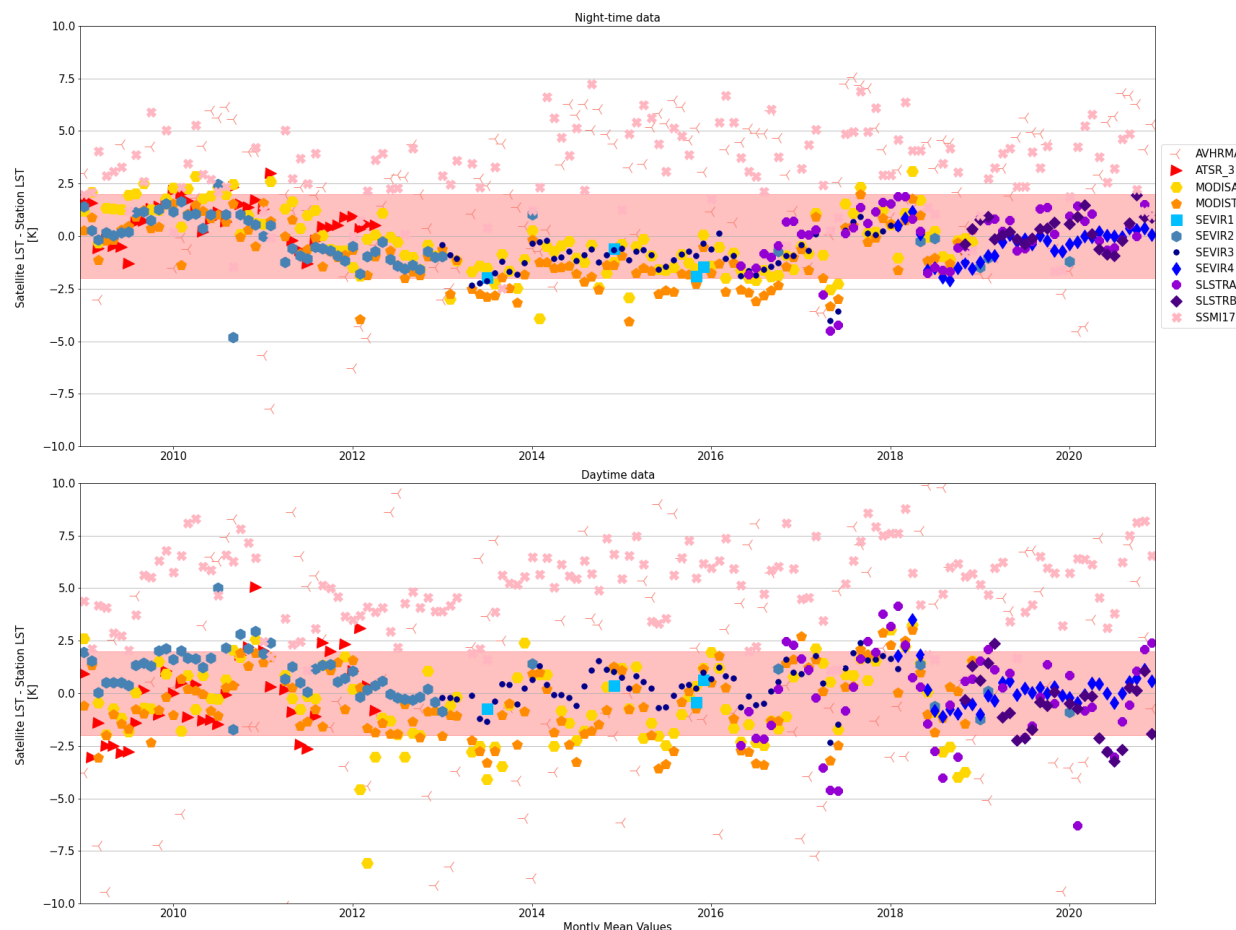


Figure 11: Monthly mean biases (satellite LST – station LST) over GBB_W_ station. The upper plot represents night-time and the lower daytime data. The red span is the area where the bias is in a ± 2 K range.

The night-time IR biases are for all sensors in an acceptable range, and also the daytime biases are mainly within ± 2 K for the LEO and GEO IR data sets. The daytime bias for ATSR_3, MODIST and MODISA were generally > 2 K for V1.00 of the data sets, but it these biases have reduced in the latest version (V3.00) of the data sets. Positive biases are observed for AVHRMA night-time data, and large standard deviations for both day and night. The station is a well-known and good characterised in situ station located in a hyper-arid and very homogeneous surrounding of the gravel-plains of the Namib Desert. The in situ LST are calculated with a constant emissivity of 0.94 [RD-5] that was determined by combining in situ measurements and laboratory emissivity spectra of soil samples. The increased biases for daytime and night-time of the SSMI MW data sets were similarly found for both old and new versions of the data set.

Results over KAL_R_ / KAL_H_ (Kalahari Farm Rust mijn Ziel / Kalahari Farm Heimat) Stations

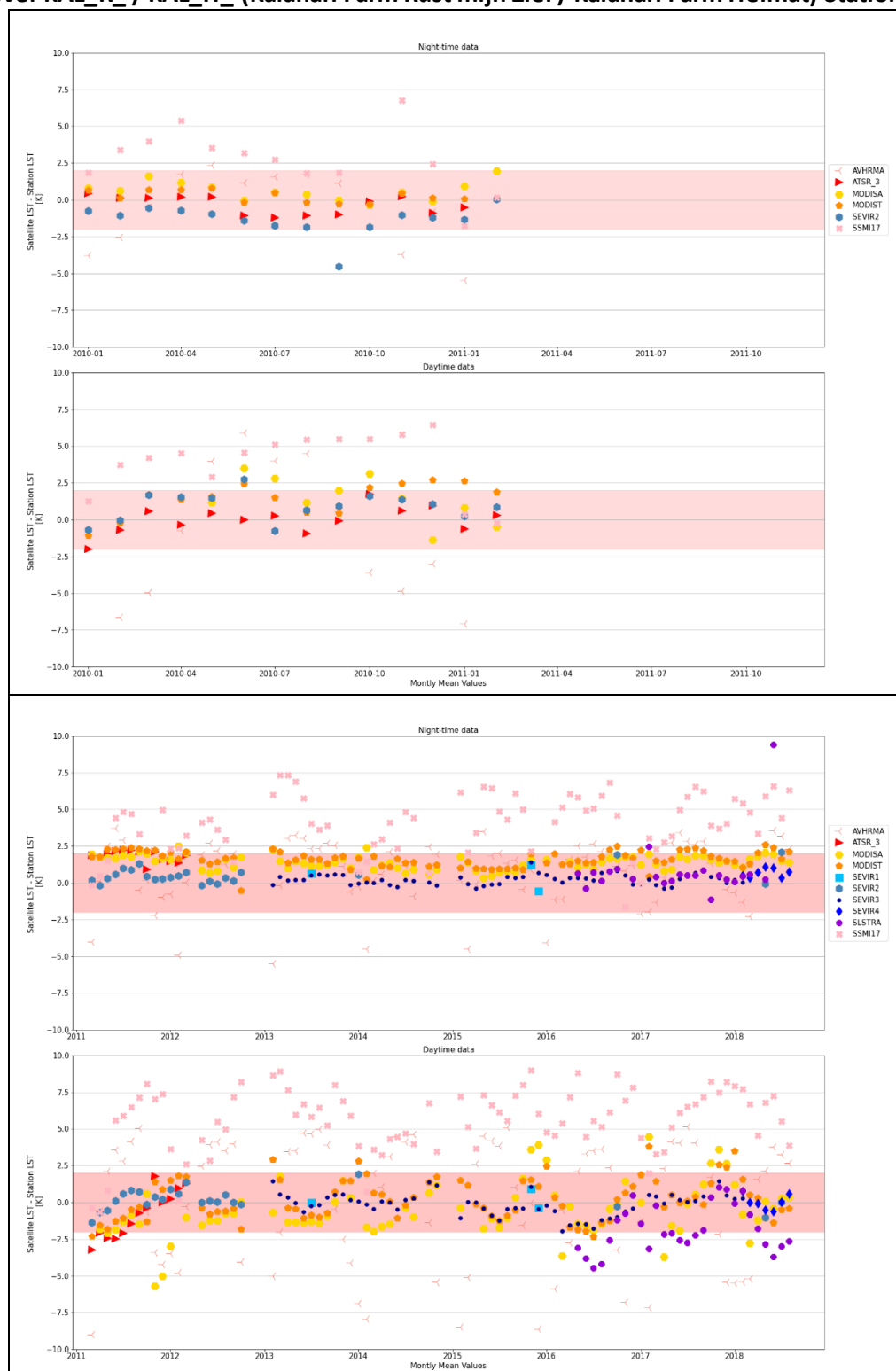



Figure 12: Monthly mean biases (satellite LST – station LST) over KAL_R_ (upper) and KAL_H_ (lower) stations. The upper plot represents night-time and the lower daytime data. The red span is the area where the bias is in a ± 2 K range.

	Product Validation Plan (PVP) <i>WP4 – DEL4.1</i>	Ref.: LST-CCI-D4.1-PVIR Version: 3.1 Date: 23-Jun-2023 Page: 33
---	---	--

The station in the Kalahari semi-desert was located at farm “Rust mijn Ziel” (KAL_R_) until February 2011 and at farm “Heimat” (KAL_H_) afterwards until 2018. KAL_H_ has more bushes and less large trees than KAL_R_, which might explain the smaller daytime IR biases at KAL_H_ station due to a lesser influence of sunlit and shaded areas. Increased night-time biases at KAL_H_ are found for the SH winter months. During winter, the number of IR data points increases as during summer there are two rainy seasons observed in the region [AD-1]. Thus, lower biases in summer might be due to a larger influence of missed clouds. Similar to the results over GBB_W_, the daytime biases for ATSR_3, MODISA and MODIST were generally > 2 K in V1.00 of the data sets and generally reduced for V3.00. The SLSTRA results are within ± 2 K at night-time, although for daytime some negative biases are found. The MW biases are similarly very high for night-time and daytime data. Large standard deviations are seen for AVHRMA data.

3.2.5. Results over SURFRAD stations

Results over BND___ (Bondville) Station

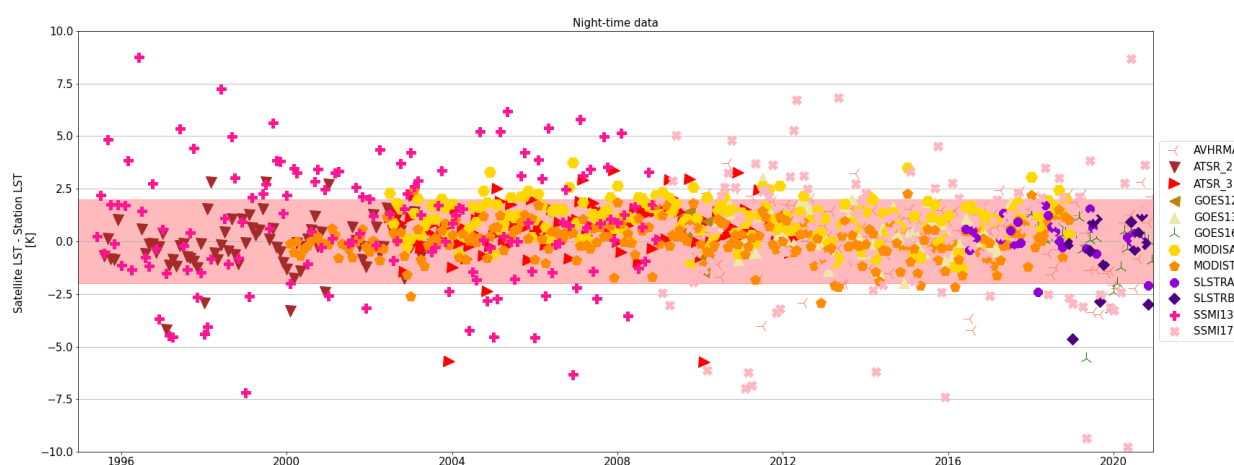


Figure 13: Monthly mean biases (satellite LST – station LST) over BND___ station. The upper plot represents night-time and the lower daytime data. The red span is the area where the bias is in a ± 2 K range.

For the IR data sets, the night-time biases are generally within ± 2 K, whereas the MW data sets have a larger spread with negative as well as positive biases. This might be caused mainly by their larger footprint above this station in a heterogeneous surrounding. A strong seasonal cycle was seen for validations over this station for daytime data within the GlobTemperature project [RD-1]. It was then concluded that this is mainly due to the harvesting cycle caused by the agricultural area around the station. Thus, the BND___ daytime data was removed for validation as the biases are mainly reflecting the missing homogeneity around the station and cannot be attributed to the quality of the satellite data sets.

Results over DRA___ (Desert Rock) Station



Figure 14: Monthly mean biases (satellite LST – station LST) over DRA___ station. The upper plot represents night-time and the lower daytime data. The red span is the area where the bias is in a ± 2 K range.


The night-time biases for the IR validation of AVHRMA, ATSR_2, ATSR_3, MODISA, MODIST, SLSTRA and SLSTRB lie for most of the months within ± 2 K. However, the daytime biases display a strong seasonal cycle, with increased biases in the summer months. This daytime bias was reduced notably for ATSR_3 for the V3.00 of the data set. Furthermore, the previous negative biases for SLSTRA seen during night-time and daytime have been removed in V3.00 due to the improved cloud mask of the data set. Positive biases are observed for AVHRMA at daytime, but with large standard deviations. As DRA___ station is located within a valley and surrounded by mountains, the seasonal cycle of the daytime biases might be due to different observed sunlit and shadowy areas throughout the year, which was already observed and described in the GlobTemperature project validation [RD-1]. For that reason, only an area of 3 km x 3 km is validated for the LEO data sets to avoid the influence of the mountains. To reduce the area, however, was not possible for GOES data sets due to their coarser spatial resolution. GOES data sets have negative biases, which are more pronounced during night-time.

Results over GCM___ (Goodwin Creek) Station



Figure 15: Monthly mean biases (satellite LST – station LST) over GCM___ station. The upper plot represents night-time and the lower daytime data. The red span is the area where the bias is in a ± 2 K range.

The area around this station consists of a heterogeneous mixture of grassland and woods. During the validation of the V1.00 LST_cci data sets, it was seen that the daytime biases were smaller than the night-time biases [RD-1]. The reason for this is probably the inhomogeneous area around the station, where the woods might stay warmer during night than the grass observed by the in situ sensor. These higher biases during night are not seen any more for V3.00 of the validation cycle. The biases are in general reduced for V3.00 of the data sets, which is especially the case for ATSR_2 during night-time and daytime, as well as for ATSR_3 during daytime. For V3.00 of the data sets, a new land cover classification system is used (ULeic / LandCover_cci (LCCS) hybrid biome map). The area around the station is now mainly classified as “croplands and grassland”, whereas it was “broadleaved / needleleaved evergreen forest” before and more pixels around the station fall in the LCCS land cover class and are used to calculate the median IR satellite LST. This change might have led to the smaller biases seen for the IR sensors. Negative biases are seen for AVHRRMA daytime data, mainly due to unmasked clouds, which also drives the large standard deviations. The SSMI biases are often within the ± 2 K range, although those sensors are viewing an even

	Product Validation Plan (PVP) <i>WP4 – DEL4.1</i>	Ref.: LST-CCI-D4.1-PVIR Version: 3.1 Date: 23-Jun-2023 Page: 36
---	---	--

larger area around the station. The GOES night-time biases are above 2 K during night-time, as are a few of the SLSTRA daytime biases.

Results over FPK____ (Fort Peck) Station



Figure 16: Monthly mean night-time biases (satellite LST – station LST) over FPK____ station. The red span is the area where the bias is in a ± 2 K range.

The night-time IR biases are well within ± 2 K most of the time. A strong yearly cycle was seen for the daytime biases, which has been observed before [RD-1]. This is probably caused by a small fence around the station to protect it from gazing bison. This could lead to a difference in the length or colour of the grass inside and outside the fence in the summer months. The in situ daytime biases might therefore not be representative for the larger area seen by the satellites, and thus, the daytime data are not considered over this station. The night-time results are mainly within the ± 2 K range for the IR data sets, a larger spread is again observed for the SSMI data sets.

Results over PSU___ (Penn. State University) Station



Figure 17: Monthly mean biases (satellite LST – station LST) over PSU___ station. The upper plot represents night-time and the lower daytime data. The red span is the area where the bias is in a ± 2 K range.

As the area around the station is very heterogeneous and consists of different land covers including populated areas, only one pixel was used for validation of the IR satellite LST data sets. The night-time data is well within ± 2 K for most IR satellite data sets. For ATSR_2 and ATSR_3 the daytime biases have reduced for V3.00 of the data sets in comparison with V1.00. For MODISA and MODIST daytime data, the biases of V3.00 have also reduced compared with V1.00. Negative biases are observed for AVHRRMA day-time data mainly due to unmasked clouds, with large standard deviations. The results of the GOES satellites are mainly within the ± 2 K range. The night-time biases of the MW sensors tend to be lower than that of the IR sensors. However, the heterogeneous area around the station is reflected stronger in the larger area observed by the MW sensors, which cannot be reduced, which influences the MW biases.


Results over TBL____ (Table Mountain) Station



Figure 18: Monthly mean biases (satellite LST – station LST) over TBL____ station. The upper plot represents night-time and the lower daytime data. The red span is the area where the bias is in a ± 2 K range.

This station is located on the edge of a mountain, and only one pixel representing the land cover around the station best was chosen to validate the IR LEO LST data sets to avoid the influence of the mountain ridge west of the station.

The biases are in a good range during night-time, but during day especially both ATSR data sets show more positive biases, which though are smaller for the V3.00 data sets than for V1.00. AVHRMA data set also show more positive biases, but large standard deviations. For the GEO satellite data sets GOES12, GOES13 and GOES16, the validated region could not be reduced and they observe a larger area than the IR LEO

 land surface temperature cci	Product Validation Plan (PVP) <i>WP4 – DEL4.1</i>	Ref.: LST-CCI-D4.1-PVIR Version: 3.1 Date: 23-Jun-2023 Page: 39
--	---	--

data sets. This might cause the larger negative biases seen for both GOES sensors during day. An even larger area is seen by the MW sensors, which might cause the strong negative outliers during the night.

3.3. In Situ Uncertainty Validation

3.3.1. Overview

The uncertainty of the in situ validation was assessed by comparing the RSTD of the in situ biases with the total uncertainty of the validation. The time period used for in situ validation was also used for the uncertainty validation. The approach presented here is described in detail in [AD-3].

In general, the total uncertainty should take into account all uncertainty components influencing the validation. It is estimated by taking the square root of the sum of the quadrature of its single elements (see [AD-3]). If all components are considered and estimated correctly, the total uncertainty should approximate the empirically determined RSTD. If the total uncertainty is lower than the RSTD, there are either uncertainty components missing or the ones considered are too low. If the total uncertainty is higher than the RSTD, one or more of the uncertainty components are too high.


The single elements of the total uncertainty are namely:

- Uncertainty of in situ LST (described in AD-1)
- Uncertainty of satellite LST (described in AD-2)
- Spatial uncertainty

This component displays the uncertainty caused by the comparison of a measurement over an area (satellite measurement) with a point measurement (in situ measurement). Depending on the homogeneity of the area surrounding the station, this uncertainty varies.

The spatial uncertainty was estimated differently for the validated data sets as follows:

- For LEO IR data sets, it is the RSTD of the LST of 5 x 5 pixels around each station (i.e. the same area as in the validation).
- For GEO IR data sets, it is the RSTD of the LST of 3 x 3 pixels around each station (as only the pixel directly above the station is taken for validation).
- For MW data sets, spatial uncertainty is not considered yet. Due to the coarser spatial resolution of the MW data sets, it is difficult to estimate spatial uncertainty at this larger spatial scale, and no applied methodologies provide currently these estimates.
- Temporal uncertainty

 land surface temperature cci	Product Validation Plan (PVP) <i>WP4 – DEL4.1</i>	Ref.: LST-CCI-D4.1-PVIR Version: 3.1 Date: 23-Jun-2023 Page: 40
--	---	--

This component reflects the difference in the acquisition time between both measurements, as LST can vary substantially with time. However, as the maximal temporal difference between in situ and satellite LST measurements is set to 3 minutes for all stations except for the Heihe stations, the temporal uncertainty component is disregarded. It should be considered in future work for the Heihe stations at least, where due to the lower sampling frequency of the in situ data a temporal difference of up to 10 min with the satellite LST measurements is allowed.

In the following, the results of the uncertainty validation are presented in separate sections for the different satellite data sets to investigate their performance. However, there are also uncertainty differences between the stations, which are independent of the satellite data sets and due to the different representativeness of the stations. This is most noticeable for the following stations:

- At BGB___ station the total uncertainty generally exceeds the RSTD. At this station, no value for in situ uncertainty was given by the data provider. Thus, a value for the in situ uncertainty of 15 W/m² was taken [RD-10] for in situ uncertainty, which might be too high.
- At EVO___ station, total uncertainty agrees well with RSTD for lower total uncertainty values but underestimates RSTD for higher total uncertainties. Very high RSTD values might be caused by an increased influence of shadowy / sunlit areas at this station, which might be not considered in the total uncertainty.
- At TBL___ station, the total uncertainties of most data sets underestimate the RSTD. This might be caused by a too low spatial uncertainty, as the station is located in a very heterogeneous surrounding.

3.3.2. Results for ATSR_2 and ATSR_3 data sets

For the ATSR_2 and ATSR_3 data sets the total uncertainty fits often well to the RSTD of the bias (see e.g. Figure 19, upper plot: Results at the GCM___ station). In this figure and in the following uncertainty plots the total uncertainty is displayed on the x-axis divided into bins of 0.1 K. On the left y-axis, the RSTD of the bias for each bin is shown as bars. On the right y-axis the number of data points per bin is displayed, represented by dots. For some displayed bins, the number of data points is very low, which can lead to a larger influence of outliers and more fluctuating RSTD values. Thus, the number of data points need to be considered when interpreting the plots.

The total uncertainty of the ATSR data sets is high (i.e. total uncertainty shifted to the right) over stations located in a more heterogeneous surrounding (see Figure 19, lower plot for TBL___ station) due to an increase in the spatial uncertainty. However, for high total uncertainties values (above 2.5 K) it still underestimated the RSTD over these stations, which might be caused by the very low number of available matches (i.e. data points).

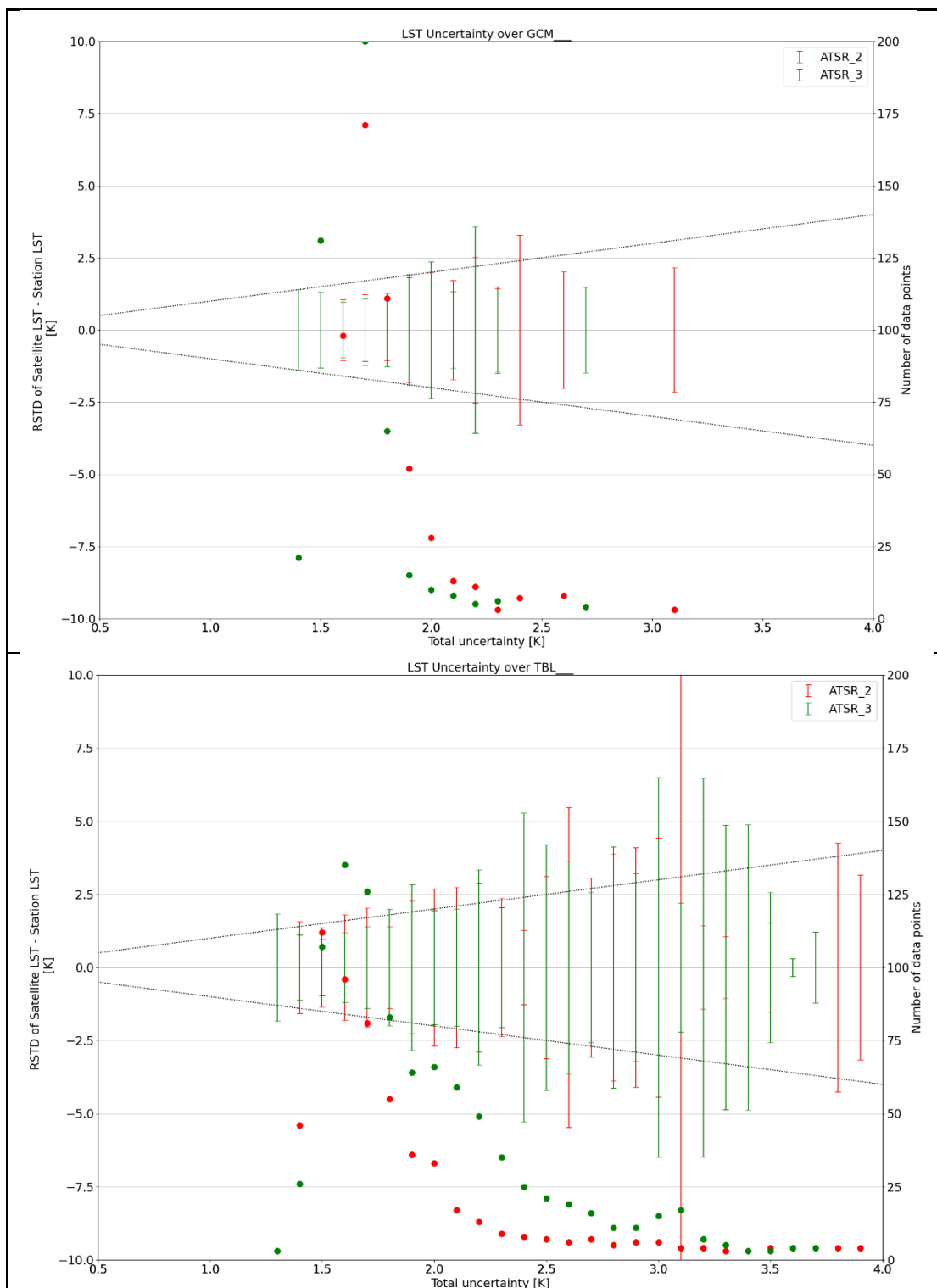
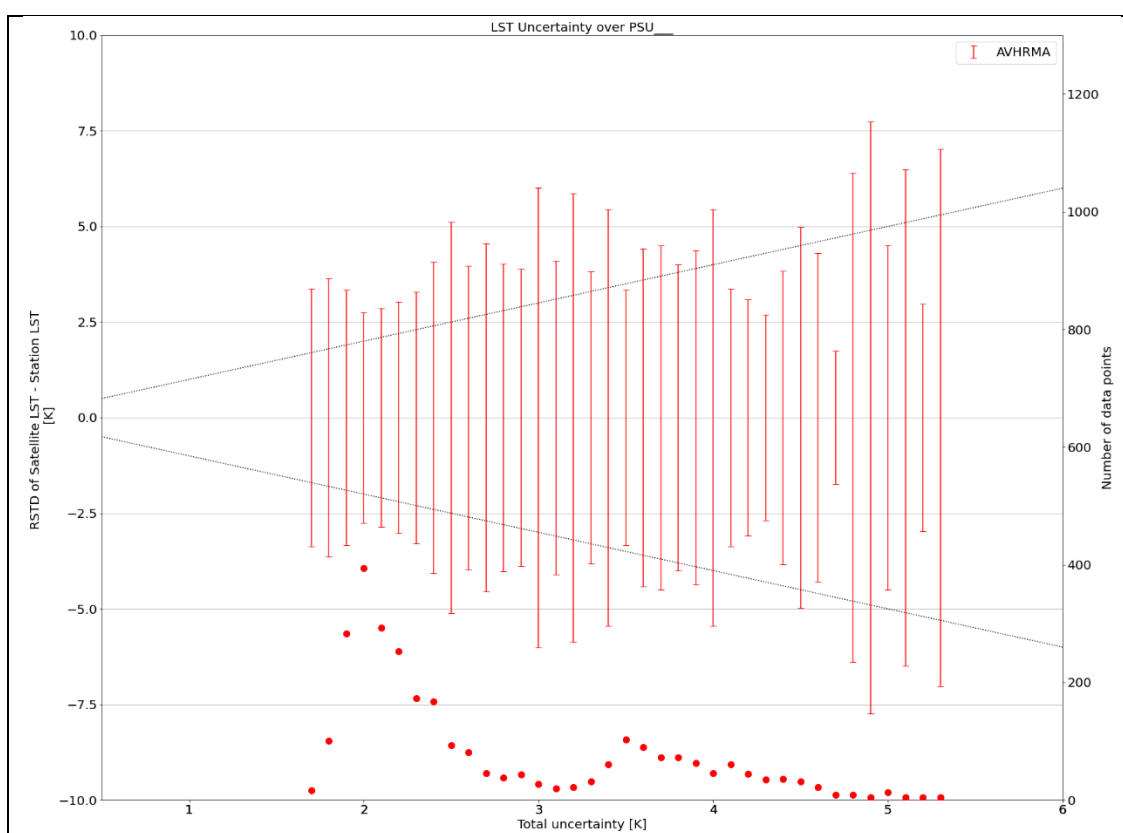


Figure 19: RSTD of the bias (satellite LST – in situ LST) vs total uncertainty for ATSR_2 and ATSR_3 data sets over GCM___ (upper plot) and TBL___ (lower plot) station. The total uncertainty is divided into bins of 0.1 K. The right axis displays the number of data points per bin.

3.3.3. Results for AVHRMA data set

For the AVHRMA data set the total uncertainty underestimates the RSTD at most sites (see e.g. Figure 20, upper plot). This underestimation is more pronounced at those sites with high RSTD caused mainly by a first version of the cloud detection algorithm which isn't as mature as for other sensors. This results in a higher proportion of unmasked clouds. Thus, the uncertainty validation of AVHRMA at those sites can be less representative. The validation at PSU____ (Figure 20, lower plot), which only uses night-time data, shows an accurate estimation of the uncertainty with respect to the RSTD. Only at Heihe sites the total uncertainty overestimates the RSTD, mainly due to the higher uncertainty of the in situ measurements.



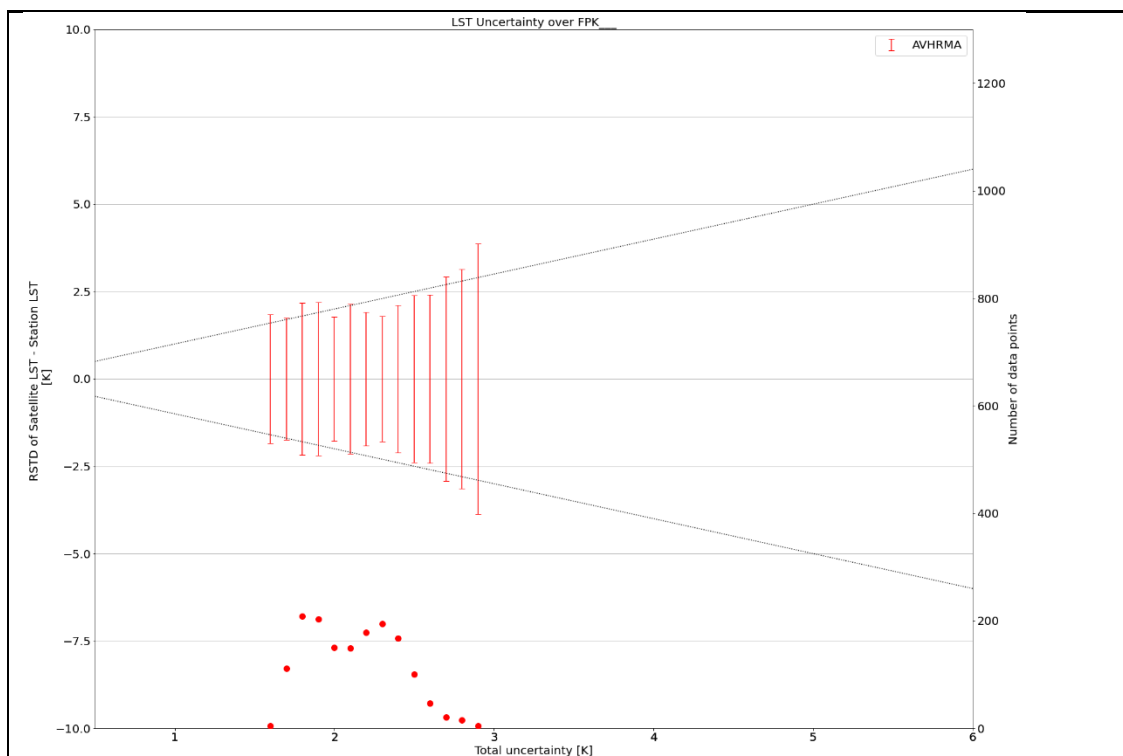


Figure 20: RSTD of the bias (satellite LST – in situ LST) vs total uncertainty for AVHRMA data set over PSU___ (upper plot) and FPK___ (lower plot) station. The total uncertainty is divided into bins of 0.1 K. The right axis displays the number of data points per bin.

3.3.4. Results for GOES12, GOES13 and GOES16 data sets

The total uncertainties for the GOES data sets tend to overestimate the RSTD (see Figure 21 for FPK___ station). This is more pronounced for GOES12 where the number of matches is lower. For GOES13 and GOES16, the agreement between total uncertainty and RSTD is good for bins with a high number of data points and decreases for a total uncertainty above ~2.5 K where the number of data points is low.

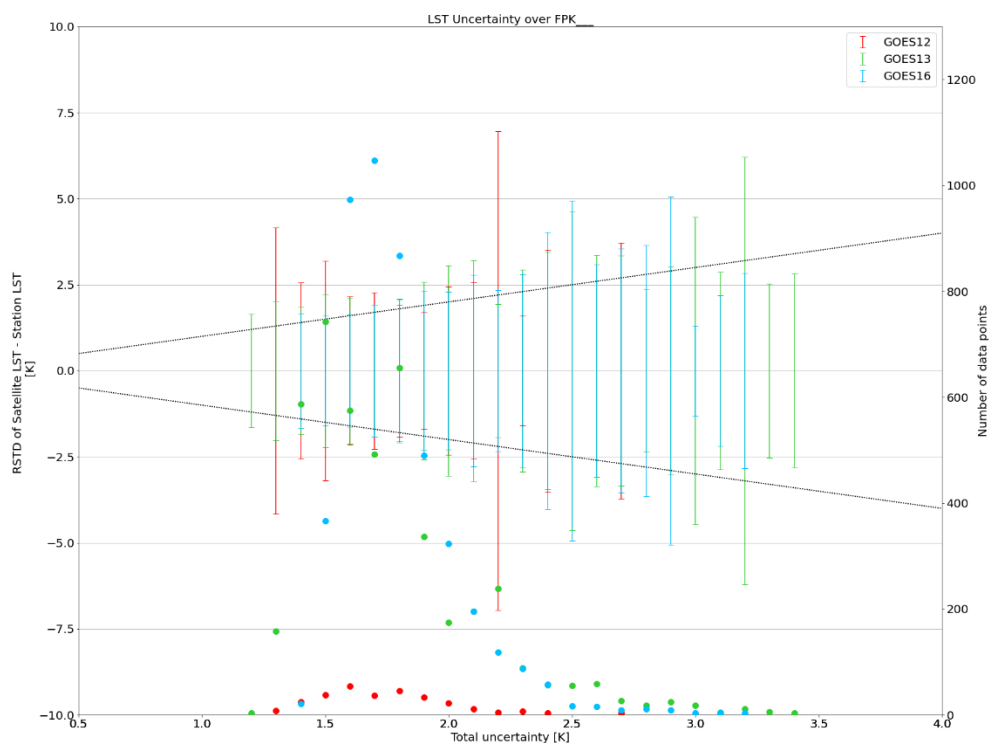


Figure 21: RSTD of the bias (satellite LST – in situ LST) vs total uncertainty for GOES12, GOES13 and GOES16 data sets over FPK___ station. The total uncertainty is divided into bins of 0.1 K. The right axis displays the number of data points per bin.

3.3.5. Results for MODISA and MODIST data sets

For these data sets, the results vary between stations, they fit very well for some stations (see e.g. Figure 22, upper plot for SGP___ station) whereas for other stations they significantly overestimate the RSTD (Figure 22, lower plot for KAL_H_ station). The reason for this could be an overestimation of the CAMEL emissivity uncertainty in the specific regions or an overestimation of the spatial matchup uncertainty at more homogeneous sites.

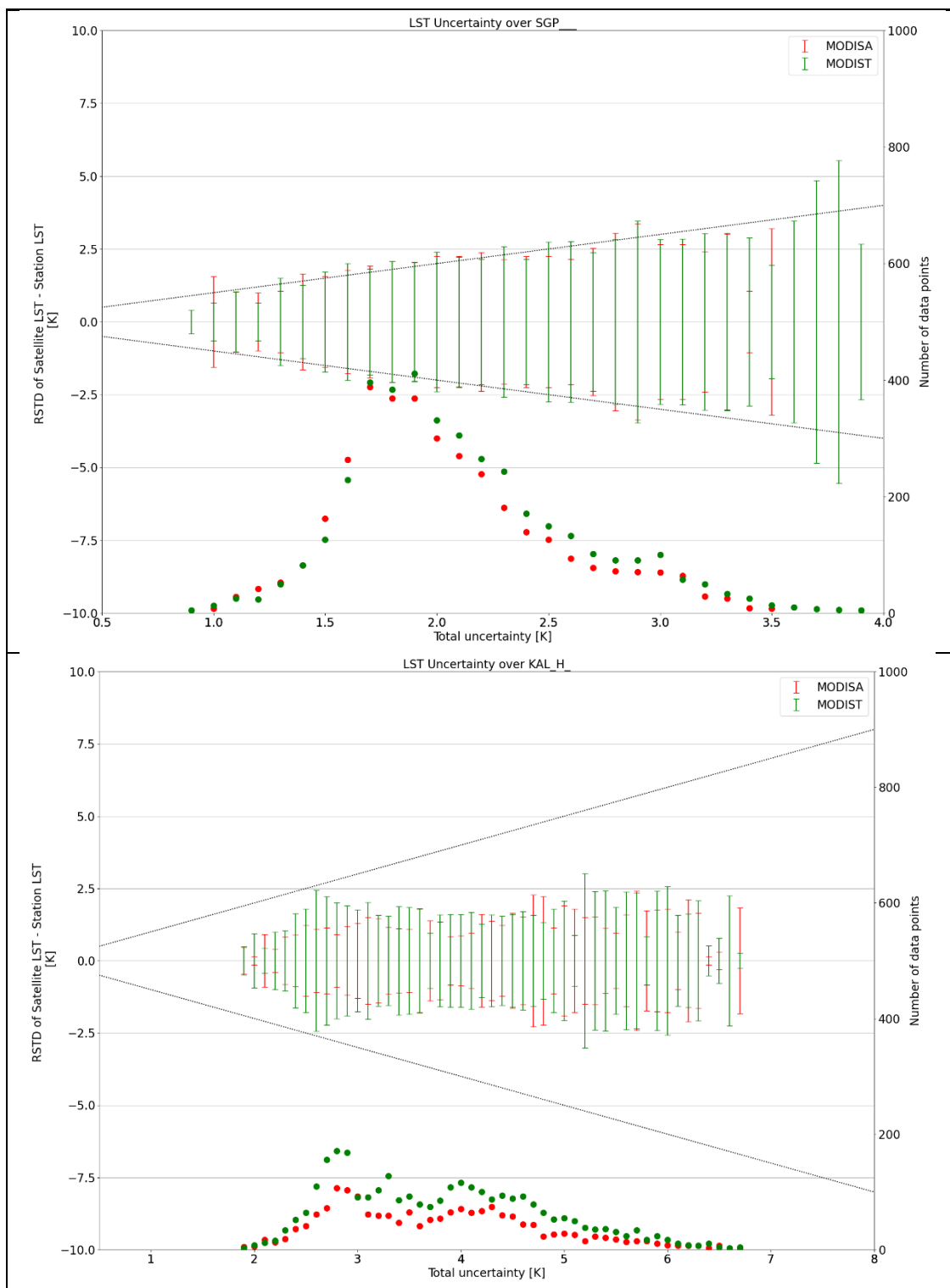



Figure 22: RSTD of the bias (satellite LST – in situ LST) vs total uncertainty for MODISA and MODIST data sets over SGP___ (upper plot), KAL_H_ (lower plot) station. The total uncertainty is divided into bins of 0.1 K. The right axis displays the number of data points per bin.

 land surface temperature cci	Product Validation Plan (PVP) <i>WP4 – DEL4.1</i>	Ref.: LST-CCI-D4.1-PVIR Version: 3.1 Date: 23-Jun-2023 Page: 46
--	---	--

3.3.6. Results for MTSAT2 and HMWR_8 data sets

The MTSAT2 data set was validated over the three Heihe stations (BGB____, DMN____, and HZZ____) for the years 2013 – 2015 and HMWR_8 data set was validated over DMN____ and HZZ____ for years 2016 – 2020. The results of the uncertainty validation for these three stations differs considerably. For the DMN____ station (Figure 23 upper plot) the total uncertainty underestimates the RSTD whereas for HZZ____ station (see Figure 23, lower plot) it overestimates the RSTD for uncertainties larger than 3.5 K. For HZZ____ station the results are less clear and vary with the number of analysed data points.

At DMN____ station, the instrumentation differs from the instrumentation at the other two stations and, thus, the estimated in situ data uncertainty differs. For the stations BGB____ and HZZ____ the considered in situ uncertainty might be too high as described above.

Furthermore, the coarser spatial resolution of the GEO data sets might lead to a less representative spatial uncertainty estimation of the actual heterogeneity around the station. Different ways of calculating spatial uncertainty should be considered and compared to minimise this influence.

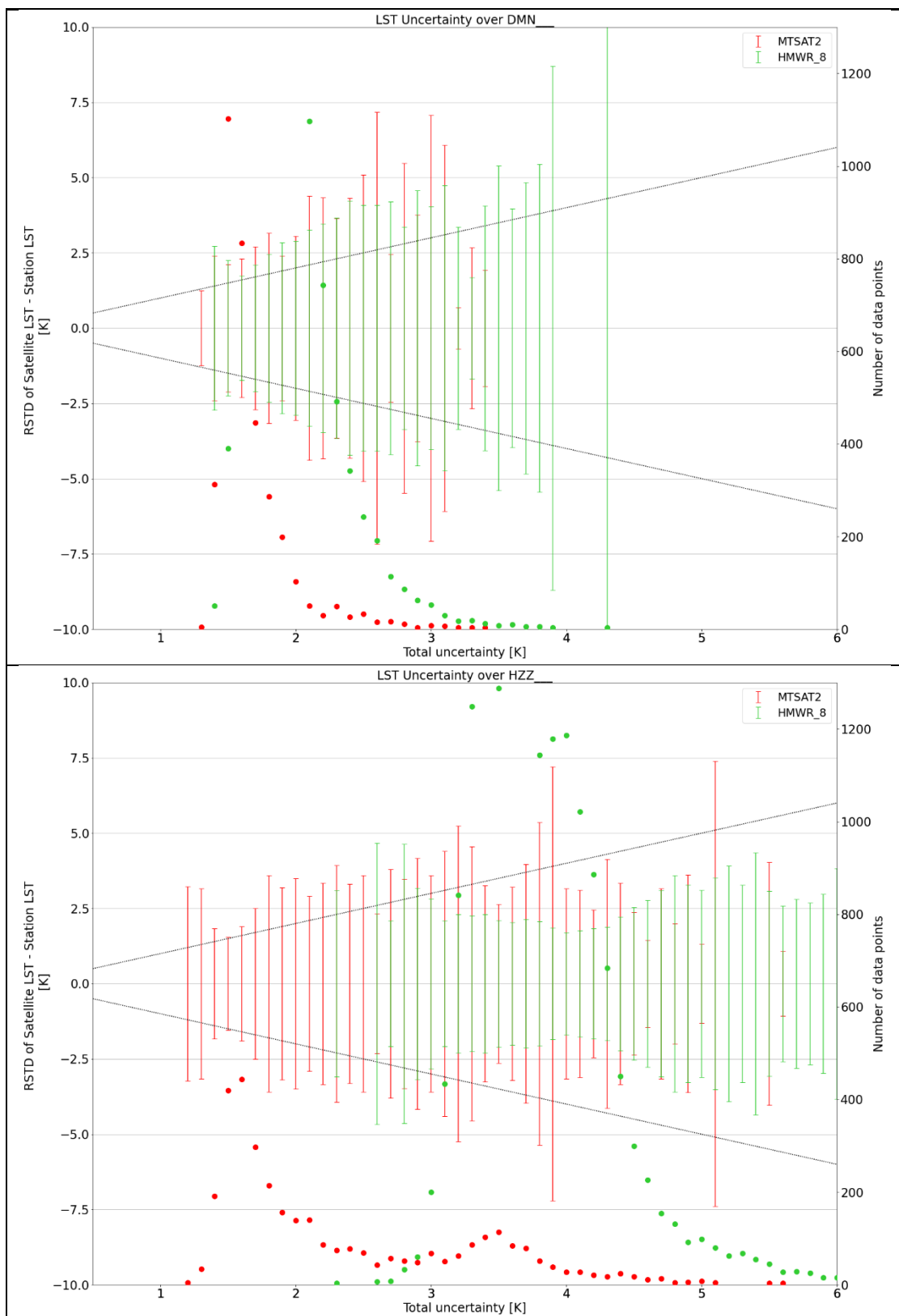



Figure 23: RSTD of the bias (satellite LST – in situ LST) vs total uncertainty for MTSAT2 data set over DMN (upper plot) and HZZ (lower plot) station. The total uncertainty is divided into bins of 0.1 K. The right axis displays the number of data points per bin.

 land surface temperature cci	Product Validation Plan (PVP) <i>WP4 – DEL4.1</i>	Ref.: LST-CCI-D4.1-PVIR Version: 3.1 Date: 23-Jun-2023 Page: 48
--	---	--

3.3.7. Results for SEVIR 1 – 4 data sets

A very large number of data points was available for these four data sets. The results over GBB_W_station (Figure 24, upper plot) show similar RSTDs for bins of total uncertainty containing most of the data points. The RSTD increases for higher total uncertainties with fewer data points, which might be caused by outliers. The results are similar over stations KAL_R_ and KIT_F_.

At KAL_H_, the total uncertainty overestimates the RSTD.

Over EVO___ station (Figure 24, lower plot), the total uncertainty underestimates the RSTD. Over this station, a strong influence of sunlit / shadowy areas is found during day, which leads to larger biases. If this influence is not represented correctly in the spatial uncertainty estimation, this might lead to the observed underestimation. Over DAH_T_ station, the total uncertainty underestimates the RSTD as well. Over this station the influence of the strong seasonal cycle including rainy seasons might not be sufficiently accounted for in the total uncertainty.

When comparing the four data sets with one another, it can be seen that SEVIR3 has the highest uncertainty range whereas SEVIR2 appears to have the best representation of the uncertainties.

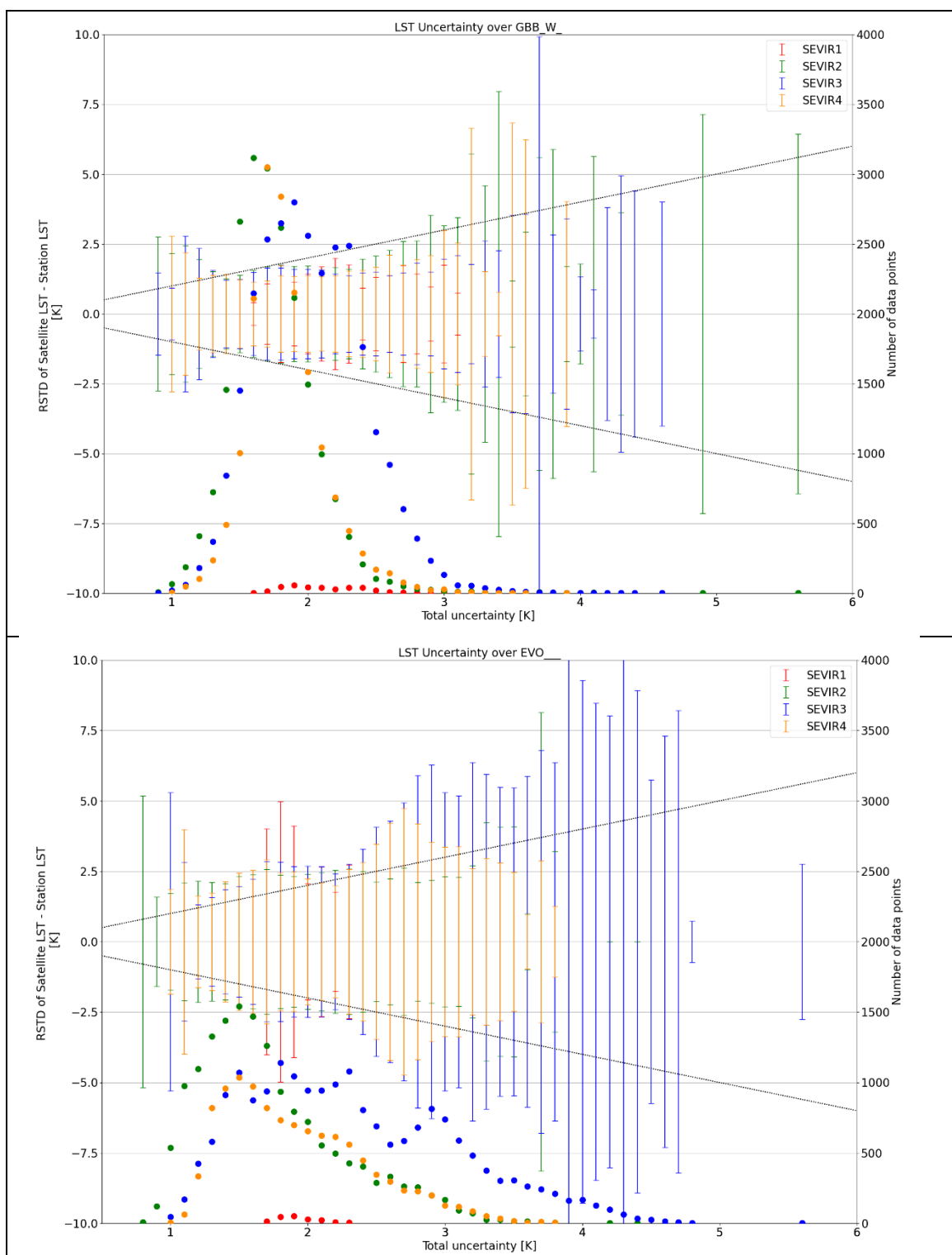



Figure 24: RSTD of the bias (satellite LST – in situ LST) vs total uncertainty for SEVIR1-4 data sets over GBB_W_ (upper plot) and EVO___ (lower plot) station. The total uncertainty is divided into bins of 0.1 K. The right axis displays the number of data points per bin.

 land surface temperature cci	Product Validation Plan (PVP) <i>WP4 – DEL4.1</i>	Ref.: LST-CCI-D4.1-PVIR Version: 3.1 Date: 23-Jun-2023 Page: 50
--	---	--

3.3.8. Results for SLSTRA and SLSTRB data sets

For the SLSTR data sets, the total uncertainty fits well with the RSTD over some stations (see e.g. Figure 25, upper plot for KAL_H_ station), whereas over other stations the total uncertainty overestimates the RSTD (see Figure 25, lower plot for GCM___ station). In contrast to the MODIS data sets, the SLSTR algorithm does not include CAMEL emissivities. Thus, the observed overestimation is more likely to be related to an overestimation of the spatial matchup component. At GCM___ station the total uncertainty is divided into two ranges (1.5 – 3 K and 4 - 6 K), which is probably caused by the difference in total uncertainty for daytime and night-time. However, the number of available data points for the SLSTR data sets is still small and more representative results are expected to be obtained during phase 2 of the project.

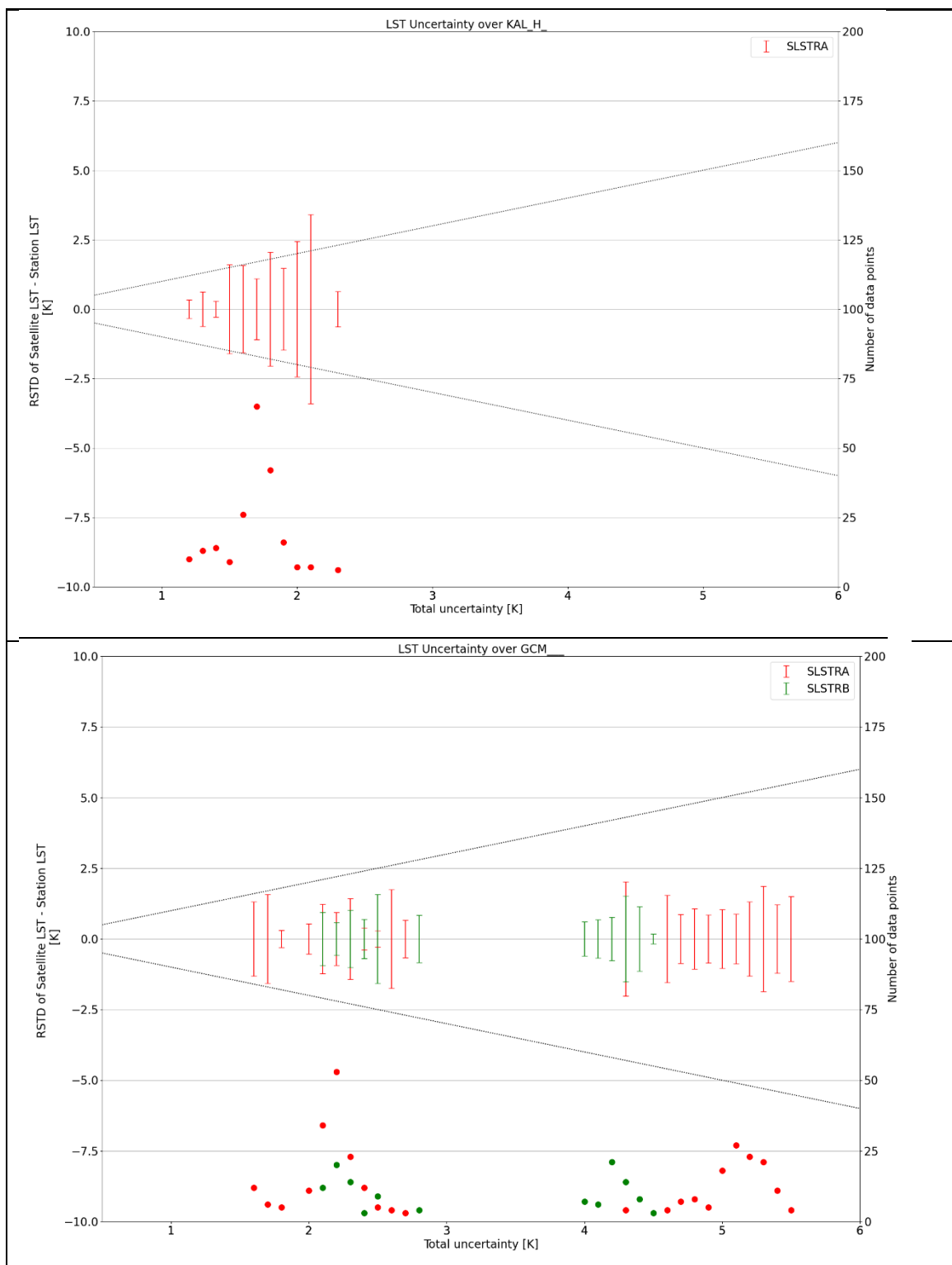



Figure 25: RSTD of the bias (satellite LST – in situ LST) vs total uncertainty for SLSTRA and SLSTRB data sets over KAL_H_ (upper plot) and GCM___ (lower plot) station. The total uncertainty is divided into bins of 0.1 K. The right axis displays the number of data points per bin.

 land surface temperature cci	Product Validation Plan (PVP) <i>WP4 – DEL4.1</i>	Ref.: LST-CCI-D4.1-PVIR Version: 3.1 Date: 23-Jun-2023 Page: 52
--	---	--

3.3.9. Results for the SSMI13 and SSMI17 data sets

For the two validated MW data sets, the total uncertainty was determined considering the in situ uncertainty and the satellite uncertainty, as no spatial uncertainty was estimated yet as mentioned above. The results for SSMI13 and SSMI17 fit well at most stations, although for some SURFRAD stations the total uncertainty overestimates the RSTD (see Figure 26, upper plot for BND____ station). For HZZ____ and BGB____ stations the total uncertainty underestimates the RSTD, probably due to the high in situ uncertainty considered for these stations.

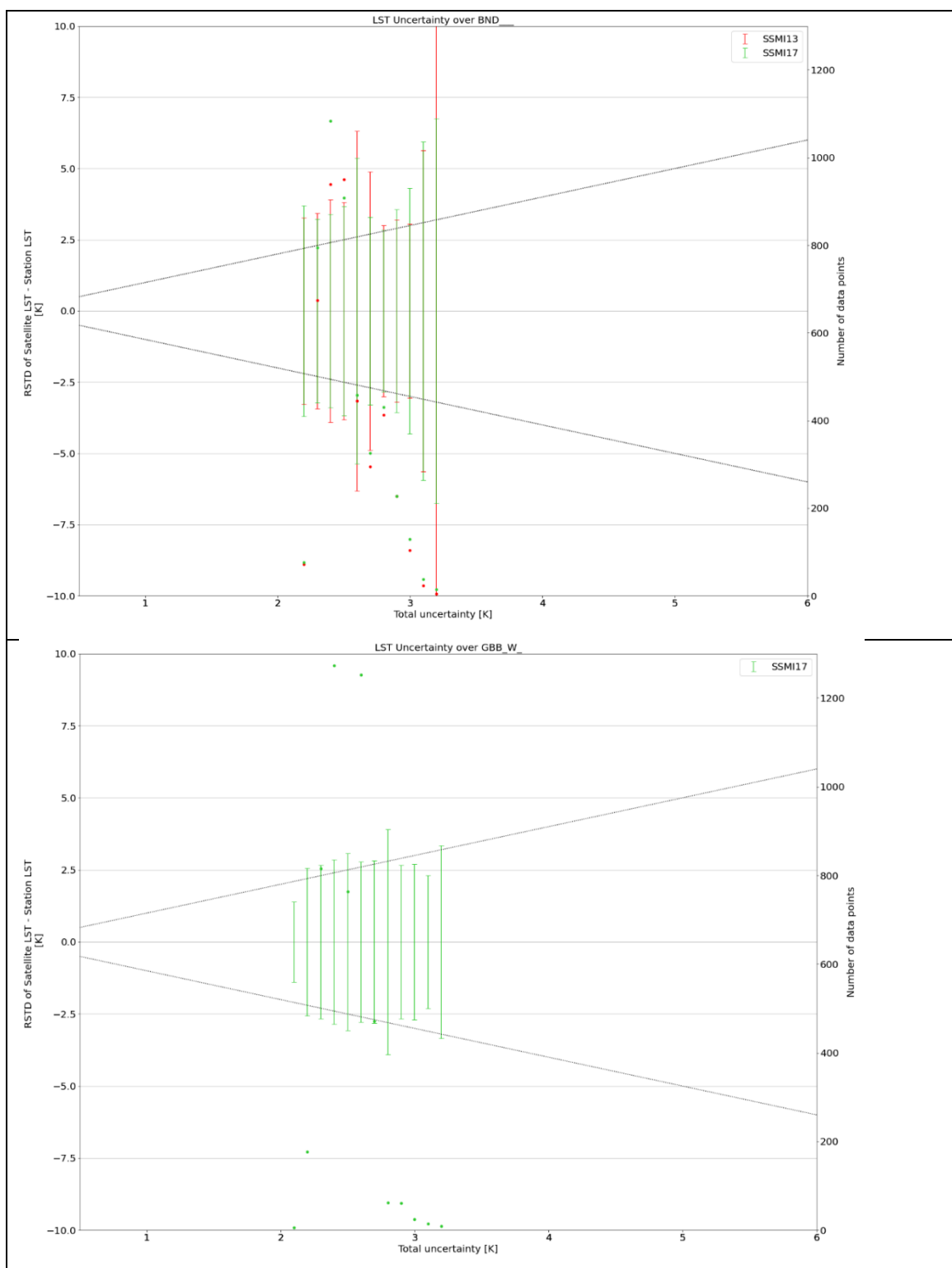



Figure 26. RSTD of the bias (satellite LST – in situ LST) vs total uncertainty for SSMI13 and SSMI17 data sets over BND___ (upper plot) and GBB_W_ (lower plot) station. The total uncertainty is divided into bins of 0.1 K. The right axis displays the number of data points per bin.

 land surface temperature cci	Product Validation Plan (PVP) <i>WP4 – DEL4.1</i>	Ref.: LST-CCI-D4.1-PVIR Version: 3.1 Date: 23-Jun-2023 Page: 54
--	---	--

4. Description and Analysis of Intercomparison Results

4.1. Overview of Results

Eleven satellite – satellite data pairs were intercompared globally, and the results were analysed for different continents for the years 2008 – 2010 or for 2018 – 2020, depending on data availability.

Eight of the satellite – satellite pairs were analysed over Africa (Afr) and Europe (Eur) only, as they were intercompared against SEVIRI data, which are not globally available. This data pairs are namely MOD11A-SEVIR2, MODISA-SEVIR2, ATSOP_-SEVIR2, ATSR_3-SEVIR2, MOD11T-SEVIR2, MODIST-SEVIR2, SLSTRA-SEVIR4, and SLSTRB-SEVIR4, where SEVIR2 / SEVIR4 are the respective LST_cci SEVIRI products, ATSOP_ the operational ESA AATSR product, MOD11A the operational NASA Aqua-MODIS LST product, and MOD11T the operational NASA Terra-MODIS LST product. Three other data pairs, where both satellite data sets have global coverage, were additionally intercompared over Antarctica (Ant), Asia (Asi), Australia (Aus), North America (NAM), and South America (SAM). These data pairs are namely ATSR_3-MOD11T, ATSR_3-MODIST, and MODIST-ATSOP_. All data pairs were temporally analysed for the time period of 2008 – 2010, except for SLSTRA-SEVIR4 and SLSTRB-SEVIR4, which were analysed for 2018 – 2020.

All analysis is divided into daytime and night-time data, based on solar elevation angle, and assessed seasonally. The seasons are named “DJF” (December, January, February) for NH winter, “MAM” (March, April, May) for NH spring, “JJA” (June, July, August) for NH summer, and “SON” (September, October, November) for NH autumn. The differences were evaluated for different metrics:

- ❖ Time series of monthly differences
- ❖ Differences for different satellite angles
- ❖ Differences for different land cover classes
- ❖ Differences for different elevation heights
- ❖ Number of averaged data points per pixel

An overview of the seasonal differences over the different continents is given in Figure 27 for daytime and in Figure 28 for night-time data. The differences are also described in Table 8 for the results over Africa and Europe, and in

Table 9 for the results over the other continents. All these data are averaged over a large time span and large regions, and many regional or temporal differences might overlie and average out each other. Thus, these results can only give a first indication about the differences between data sets but should also be considered carefully and cannot replace the more detailed analysis carried out for the single continents in the sections below. Furthermore, the two data pairs comparing SLSTR data to SEVIR4 data are analysed over a separate data period (2018 – 20) and caution must be taken if directly comparing with the results of the other data pairs.

For the daytime data, ATSR_3-MOD11T has often the highest differences, and ATSR_3-MODIST often has smaller differences close to 0K, except over South America where it has some larger negative values. Over

Africa and Europe, where all data pairs are analysed, it can be seen that MOD11A-SEVIR2 and MOD11T-SEVIR2 have more negative differences than the other data pairs, and large positive differences are found for ATSR_3-SEVIR2. This indicates that the MOD11A and MOD11T algorithms tends to have lower LST values than the LST_cci MODIS algorithm, where the differences are more positive. A larger spread between the analysed data pairs is seen for the continents Africa, Australia, and South America. In comparison to the intercomparison analysis for V1.00 of the data sets, the differences for ATSR_3-MOD11T decreased for V3.00, as well as the differences between the data pairs over Africa.

For the night-time data, again ATSR_3-MOD11T has slightly larger differences than ATSR_3-MODIST. The largest positive differences during night-time over Africa are found for MODIST-ATSR_3, although they are smaller than those found with the V1.00 intercomparisons. As ATSR_3-SEVIR2 has negative differences over Africa during night-time, both differences might be due to low ATSR_3 LST values over Africa. In general, the differences between the data pairs is larger over Africa than over Europe during night, in contrast to what is found during day. For the LEO-LEO intercomparisons over all continents, the largest differences during night-time are found over South America and over Asia. The differences over Africa and Europe for SLSTRA and SLSTRB against SEVIR4 are within the ± 2 K range.

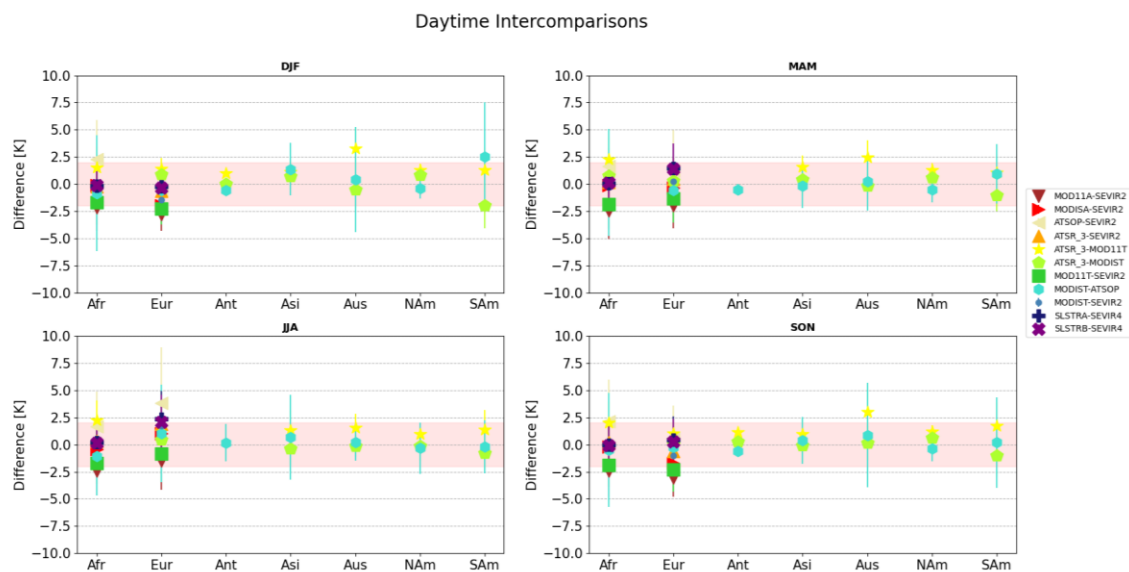


Figure 27: Overview of the daytime differences over the four seasons for all nine intercompared satellite-satellite pairs. The red span marks the difference range of ± 2 K.

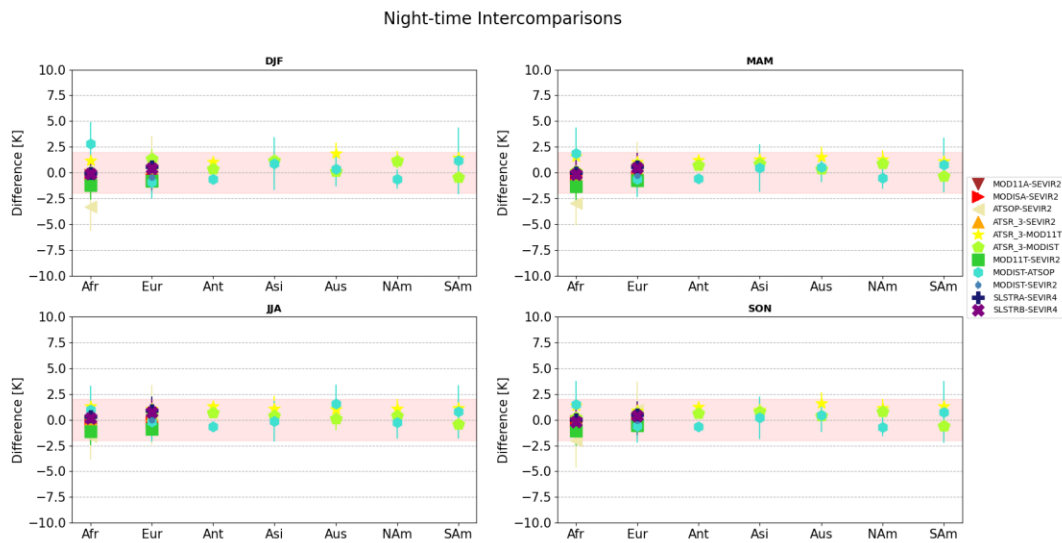



Figure 28: Overview of the night-time differences over the four seasons for all nine intercompared satellite-satellite pairs. The red span marks the difference range of ± 2 K.

Table 8: Overview of seasonal results of the median differences of the analysed satellite-satellite pairs over the continents Africa and Europe, where data from all satellite - satellite pairs are available. Results are presented in terms of difference (diff) and RSTD

Region	Product 1	Product 2		Seasonal Median (K)							
				DJF		MAM		JJA		SON	
				Day	Night	Day	Night	Day	Night	Day	Night
Africa	MOD11A	SEVIR2	diff	-2.13	-1.01	-2.46	-1.01	-2.43	-0.90	-2.43	-0.77
			RSTD	2.15	1.35	2.62	1.35	2.27	1.32	2.39	1.41
	MODISA	SEVIR2	diff	-0.12	-0.22	-0.10	-0.31	-0.43	-0.21	-0.17	-0.13
			RSTD	1.96	1.16	2.24	1.38	2.00	1.28	2.21	1.35
	ATSOP_	SEVIR2	diff	2.28	-3.34	1.62	-2.99	1.67	-1.60	2.15	-2.00
			RSTD	3.62	2.31	3.34	2.12	3.23	2.25	3.81	2.62
	ATSR_3	SEVIR2	diff	-0.20	-0.36	0.19	-0.22	0.35	0.04	0.21	-0.03
			RSTD	1.33	1.02	1.35	1.02	1.33	0.99	1.59	1.05
	ATSR_3	MOD11T	diff	1.53	1.18	2.28	1.56	2.24	1.35	2.05	1.41
			RSTD	1.90	1.41	2.03	1.42	1.84	1.30	1.88	1.17
	ATSR_3	MODIST	diff	-0.24	0.09	0.74	0.15	0.16	0.21	-0.03	0.21
			RSTD	1.90	1.13	2.58	1.45	1.84	1.30	1.91	1.29
	MOD11T	SEVIR2	diff	-1.69	-1.24	-1.86	-1.32	-1.72	-1.13	-1.86	-1.09
			RSTD	1.96	1.36	2.18	1.41	1.87	1.32	2.03	1.44
	MODIST	ATSOP_	diff	-0.84	2.83	0.14	1.87	-1.09	0.98	-0.48	1.51
			RSTD	5.32	2.09	4.92	2.51	3.57	2.30	5.26	2.28
	MODIST	SEVIR2	diff	0.06	-0.10	0.11	-0.12	0.23	-0.03	0.15	-0.01
			RSTD	2.09	1.23	2.25	1.38	1.88	1.25	2.16	1.39
	SLSTRA	SEVIR4	diff	-0.15	-0.03	0.07	0.01	0.22	0.31	-0.01	0.04
			RSTD	1.69	1.25	1.62	1.22	1.57	1.25	1.75	1.16
	SLSTRB	SEVIR4	diff	-0.12	-0.12	0.12	-0.16	0.13	0.15	-0.07	-0.18
			RSTD	1.78	1.26	1.63	1.22	1.54	1.22	1.81	1.19


 land surface temperature cci	Product Validation Plan (PVP) <i>WP4 – DEL4.1</i>	Ref.: LST-CCI-D4.1-PVIR Version: 3.1 Date: 23-Jun-2023 Page: 57
--	---	--

Europe	MOD11A	SEVIR2	diff	-2.79	-0.73	-1.97	-0.62	-1.49	-0.66	-3.04	-0.47
			RSTD	1.51	1.04	2.13	1.07	2.65	1.08	1.78	1.11
	MODISA	SEVIR2	diff	-1.96	-0.62	-0.35	-0.38	1.03	-0.22	-1.72	-0.32
			RSTD	1.41	1.19	2.22	1.10	2.65	1.01	1.73	1.20
	ATSOP_	SEVIR2	diff	-0.56	0.81	1.21	0.46	3.85	0.47	0.63	0.99
			RSTD	2.09	2.73	3.74	2.51	5.13	2.89	2.97	2.73
	ATSR_3	SEVIR2	diff	-0.64	0.52	0.50	0.28	1.91	0.44	-0.60	0.40
			RSTD	1.53	1.47	1.97	1.16	2.19	0.96	1.63	1.30
	ATSR_3	MOD11T	diff	1.43	1.29	1.47	1.08	1.59	1.08	1.06	0.91
			RSTD	0.96	0.92	1.01	0.85	1.38	0.82	1.01	0.79
	ATSR_3	MODIST	diff	0.88	1.36	0.32	0.73	0.47	0.44	0.05	0.62
			RSTD	0.89	0.90	1.11	0.93	1.17	0.76	0.96	0.87
	MOD11T	SEVIR2	diff	-2.27	-0.81	-1.35	-0.78	-0.84	-0.87	-2.31	-0.54
			RSTD	1.45	1.08	2.18	1.07	2.59	1.10	2.03	1.29
	MODIST	ATSOP_	diff	-0.57	-0.94	-0.59	-0.62	1.03	-0.21	-0.26	-0.62
			RSTD	1.29	1.54	1.88	1.75	4.51	1.93	1.82	1.59
	MODIST	SEVIR2	diff	-1.43	-0.47	0.22	-0.26	1.72	0.00	-1.00	-0.09
			RSTD	1.39	1.25	2.21	1.13	2.46	1.07	1.96	1.36
	SLSTRA	SEVIR4	diff	-0.22	0.56	1.47	0.60	2.37	0.92	0.44	0.49
			RSTD	1.70	1.33	2.27	1.35	2.55	1.32	2.18	1.28
	SLSTRB	SEVIR4	diff	-0.33	0.43	1.40	0.48	2.11	0.72	0.25	0.38
			RSTD	1.73	1.33	2.34	1.38	2.49	1.26	2.13	1.26

Table 9: Overview of seasonal results of the median differences of the analysed satellite-satellite pairs over the continents where only LEO – LEO matches are available

Region	Product 1	Product 2		Seasonal Median (K)							
				DJF		MAM		JJA		SON	
				Day	Night	Day	Night	Day	Night	Day	Night
Antarctica	ATSR_3	MOD11T	Diff	0.98	1.03	-	1.22	-	1.33	1.12	1.29
			RSTD	0.22	0.28	-	0.36	-	0.37	0.31	0.36
	ATSR_3	MODIST	Diff	-0.01	0.35		0.69		0.66	0.30	0.64
			RSTD	0.56	0.47		0.43		0.43	0.56	0.44
	MODIST	ATSOP_	Diff	-0.60	-0.61	-0.50	-0.58	0.18	-0.64	-0.61	-0.64
			RSTD	0.33	0.36	0.50	0.49	1.72	0.49	0.37	0.44
Asia	ATSR_3	MOD11T	Diff	1.09	1.10	1.56	1.29	1.32	1.07	0.95	0.96
			RSTD	1.10	0.9	1.07	1.08	1.84	1.26	1.32	0.98

	ATSR_3	MODIST	Diff	0.68	1.20	0.40	0.88	-0.38	0.38	-0.08	0.81
			RSTD	1.14	0.92	1.44	1.01	1.50	1.11	1.51	1.16
	MODIST	ATSOP_	Diff	1.36	0.89	-0.15	0.45	0.69	-0.12	0.37	0.19
			RSTD	2.43	2.56	2.08	2.30	3.88	1.97	2.15	2.06
Australia	ATSR_3	MOD11T	Diff	3.28	1.87	2.44	1.50	1.57	1.06	3.01	1.60
			RSTD	1.91	1.05	1.57	1.01	1.25	0.92	2.06	1.05
	ATSR_3	MODIST	Diff	-0.53	0.12	-0.18	0.37	-0.13	0.07	0.17	0.37
			RSTD	1.66	0.99	1.13	0.93	0.98	1.07	1.59	0.92
	MODIST	ATSOP_	Diff	0.41	0.38	0.22	0.53	0.24	1.56	0.87	0.46
			RSTD	4.85	1.70	2.64	1.47	1.72	1.88	4.82	1.65
Namerica	ATSR_3	MOD11T	Diff	1.31	1.28	1.29	1.30	0.97	1.10	1.19	1.16
			RSTD	0.56	0.85	0.65	0.86	0.70	0.95	0.61	0.89
	ATSR_3	MODIST	Diff	0.82	1.11	0.56	0.87	-0.14	0.38	0.60	0.80
			RSTD	0.59	0.71	0.99	0.79	1.36	0.96	0.79	0.87
	MODIST	ATSOP_	Diff	-0.38	-0.61	-0.50	-0.52	-0.33	-0.25	-0.34	-0.69
			RSTD	0.96	0.93	1.17	1.02	2.36	1.57	1.19	0.92
Samerica	ATSR_3	MOD11T	Diff	1.31	1.45	1.05	1.09	1.41	1.12	1.72	1.32
			RSTD	2.03	1.13	1.56	1.07	1.78	1.01	2.18	0.99
	ATSR_3	MODIST	Diff	-1.96	-0.46	-1.06	-0.37	-0.77	-0.41	-1.01	-0.59
			RSTD	2.11	1.45	1.44	1.38	1.50	1.22	1.90	1.32
	MODIST	ATSOP_	Diff	2.51	1.15	0.93	0.76	-0.18	0.78	0.19	0.75
			RSTD	5.00	3.23	2.74	2.65	2.46	2.59	4.17	3.01

 land surface temperature cci	Product Validation Plan (PVP) <i>WP4 – DEL4.1</i>	Ref.: LST-CCI-D4.1-PVIR Version: 3.1 Date: 23-Jun-2023 Page: 59
--	---	--

4.2. Results for different Continents

The results of the intercomparison analysis are displayed in the following for each continent separately. For clarity, not all analysed figures are presented in this section, however, they can all be found in the Appendix (Section 7).

4.2.1. Results over Africa

The monthly differences over the investigated time span is shown in Figure 29 for all investigated satellite – satellite pairs for the time span 2008 – 2010, and in Figure 30 for the two data pairs analysed for 2018 – 2020. The number of monthly averaged data points is also shown. The highest number of data points is found for the MODIS data sets against SEVIR2 data. MOD11A-SEVIR2 and MOD11T-SEVIR2 daytime differences are more negative than MODISA-SEVIR2 and MODIST-SEVIR2 differences, as already mentioned in Section 4.1. For MOD11A and MOD11T versus SEVIR2 also the absolute daytime differences are larger than for MODIST and MODISA against SEVIR2. ATSR_3-SEVIR2 has smaller differences than ATSR_3-MODIST and ATSR_3-MOD11T. ATSR_3-MODIST has smaller differences than ATSR_3-MOD11T, which also shows that MOD11T has lower LST values than the MODIST algorithm. ATSOP_-SEVIR2 shows the strongest seasonal cycle both for daytime and night-time data, and also the largest absolute differences, followed by MODIST – ATSOP_. For all data sets intercompared against SEVIR2, there is a strong positive outlier for night-time data in 2010/09, which must be caused by the SEVIR2 data. As yet no explanation has been found for this anomaly. SLSTRA – SEVIR4 and SLSTRB – SEVIR4 have very small differences and also no seasonal cycle, for daytime and for night-time data.

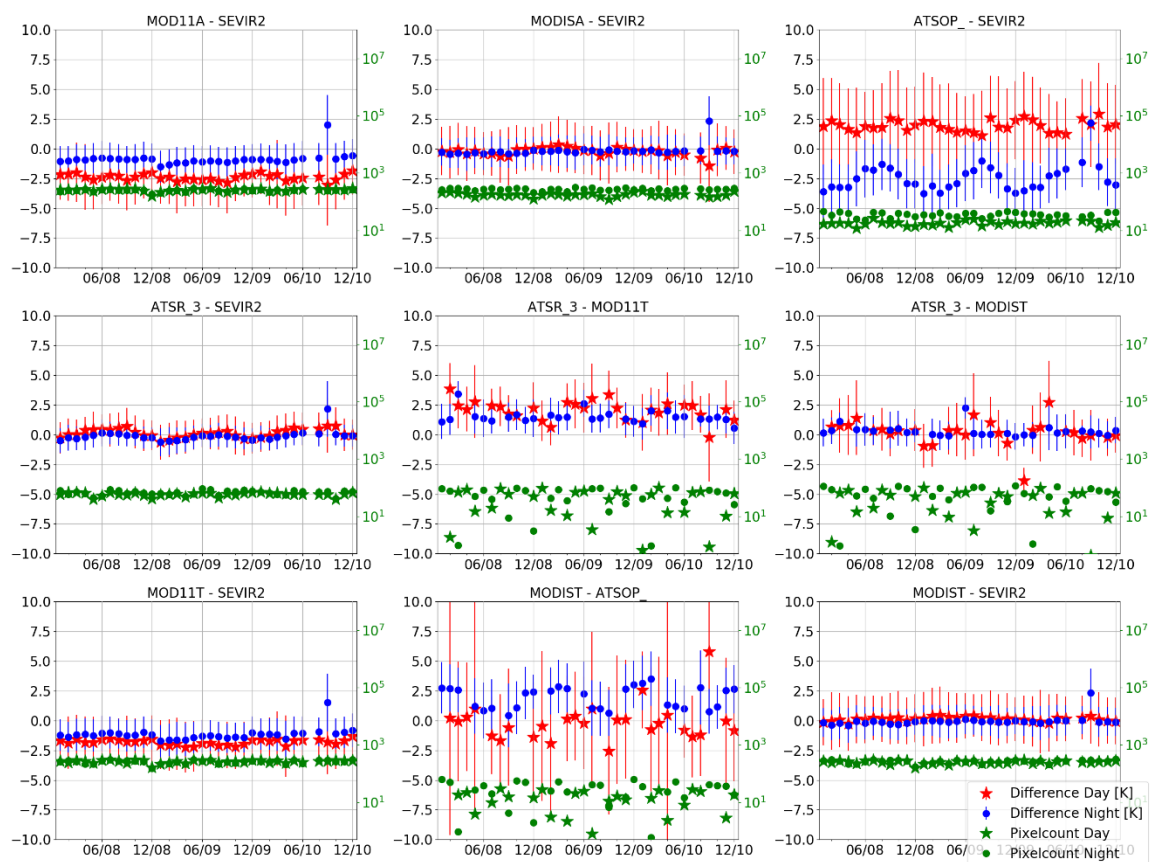


Figure 29: Monthly time series for all investigated satellite – satellite data sets over Africa for the time span 2008 - 2010. Red stars represent the daytime data, blue dots the night-time data, the green stars and dots on the right axis display the averaged pixel numbers for daytime and night-time, respectively.

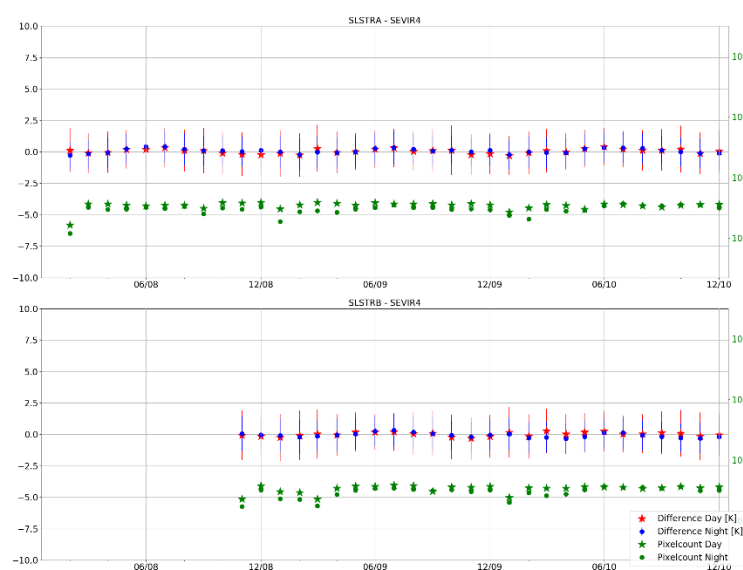


Figure 30: Monthly time series for the investigated satellite – satellite data sets over Africa for the time span 2018 - 2020. Red stars represent the daytime data, blue dots the night-time data, the green stars and dots on the right axis display the averaged pixel numbers for daytime and night-time, respectively.

When comparing the results of the different intercomparison pairs over such large areas as continents, it has to be considered that the number and distribution of the averaged pixels might vary substantially between different pairs. And thus, the analysis of different regions and land covers might influence the results. Therefore, the distribution of the averaged pixels was also investigated. The results show that for all satellite- satellite pairs, fewer data points were found in the centre of Africa. For the comparison of ATSR_3-SEVIR2, the available data points were distributed in “stripes” over the continent (see Figure 31 for the seasonal number of averaged night-time data points for ATSR_3-SEVIR2).

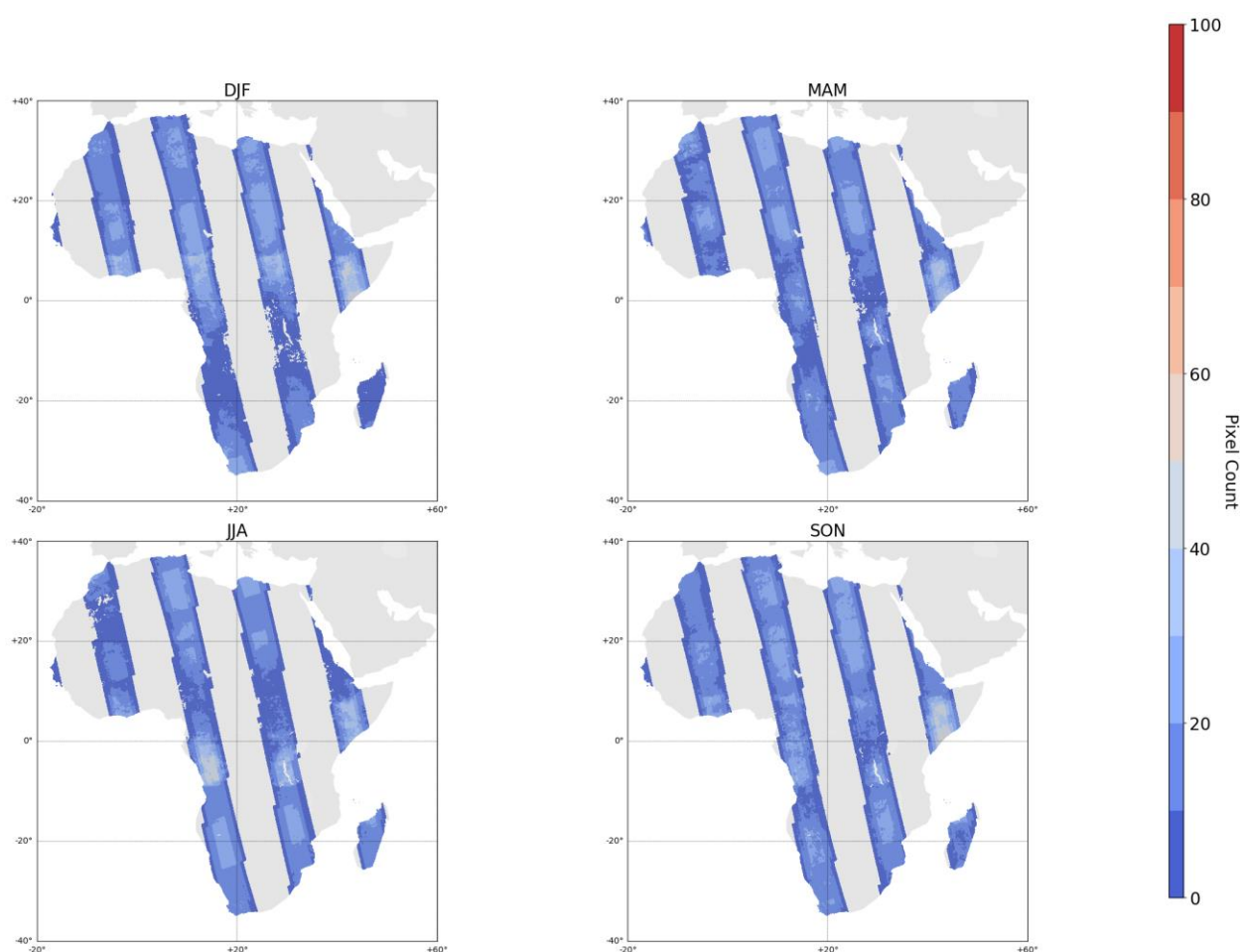


Figure 31: Number of seasonal night-time averaged data points per pixel for ATSR_3-SEVIR2 differences over Africa

The analysis of the differences for different elevation classes showed that most pixels have an elevation between 50– 200 m and between 200– 500 m. No significant differences between the different elevation classes were found.

The analysis of the land cover classes displayed that most pixels have a land cover of tree_broadleaved_deciduous_open (class 62 of the LCCS classification), shrubland (class 120), or

Bare_areas_of_soil_type_Entisols_Orthents (class 203). No significant differences between them could be seen.

The influence of the satellite angles on the results was investigated by calculating the differences for different ranges of the satellite zenith angle (satze) multiplied by the sign of the satellite azimuth angle (sataz). These results gave no large differences for all continents for ATSR_3 and ATSR_3 satellite angles, as the satze for these data sets ranges from -22° to $+22^\circ$ only (Figure 32 for ATSR_3-SEVIR2 differences). The intercomparisons of MODIS data sets against SEVIR2 showed an increase in the number of pixel counts for MODIS values of $\text{satze} \cdot \text{sign}(\text{sataz})$ between -65° to -55° and from 55° to 65° (Figure 33 for MODIS-SEVIR2 differences). The daytime differences increase substantially for larger MODIS satze values, due to an increased influence of sunlit and shadow areas. This increase has an asymmetric shape. It is stronger for MODIS and MOD11T for negative sataz values and stronger for positive sataz values for MODISA and MOD11A. This is caused by the local overflight time of the satellites. When the sataz is negative, it means that the satellite is viewing the scene from west to east, and vice-versa when the sataz is positive. As the local overpass time is in the morning for Terra-MODIS, the sun is shining from the east and casting more shadows to the west. It is the reverse for Aqua-MODIS, which has a local overpass time in the afternoon. For the intercomparisons of SLSTRA and SLSTRB against SEVIR4 (Figure 34 for SLSTRA against SEVIR4), few data points with $\text{satze} \cdot \text{sign}(\text{sataz})$ between -10° to 10° were found, which is likely due to the conical scan of the SLSTRs. Furthermore, above $+35^\circ$ $\text{satze} \cdot \text{sign}(\text{sataz})$ only daytime data points are found and below -35° only night-time data points, which is due to the asymmetric swath of the SLSTRs.

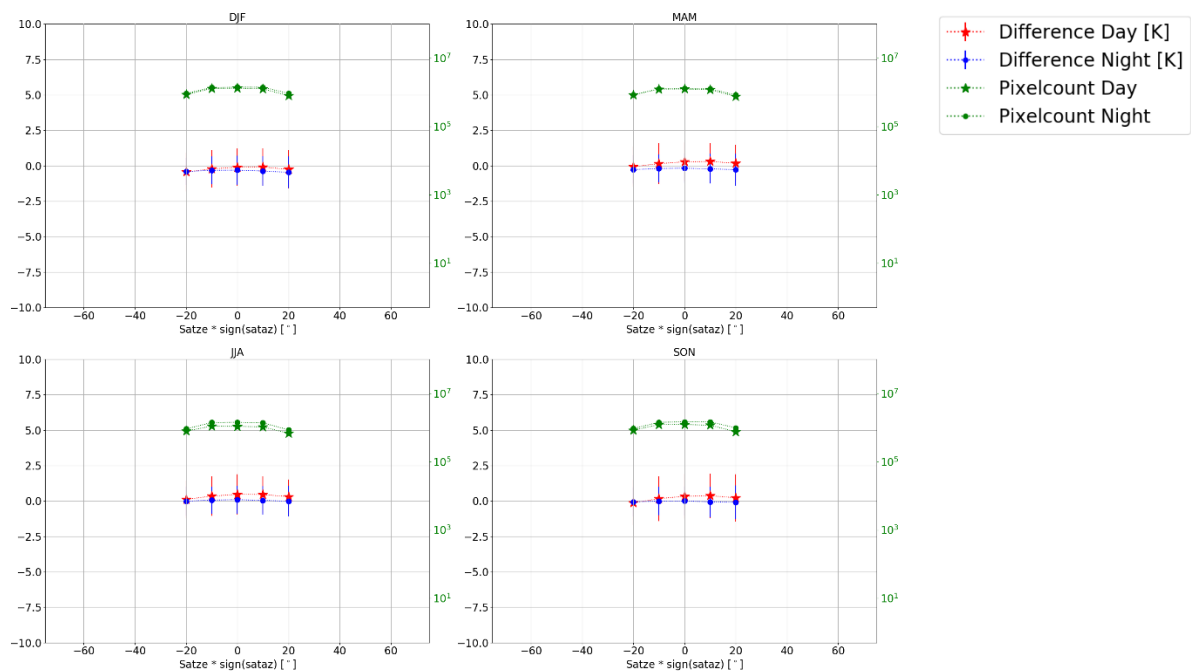


Figure 32: Seasonal differences between ATSR3-SEVIR2 LST data for different $\text{satze} \cdot \text{sign}(\text{sataz})$ values of ATSR_3; red stars represent the daytime data, blue dots the night-time data, and the green stars and dots on the right axis display the averaged pixel numbers for daytime and night-time data, respectively

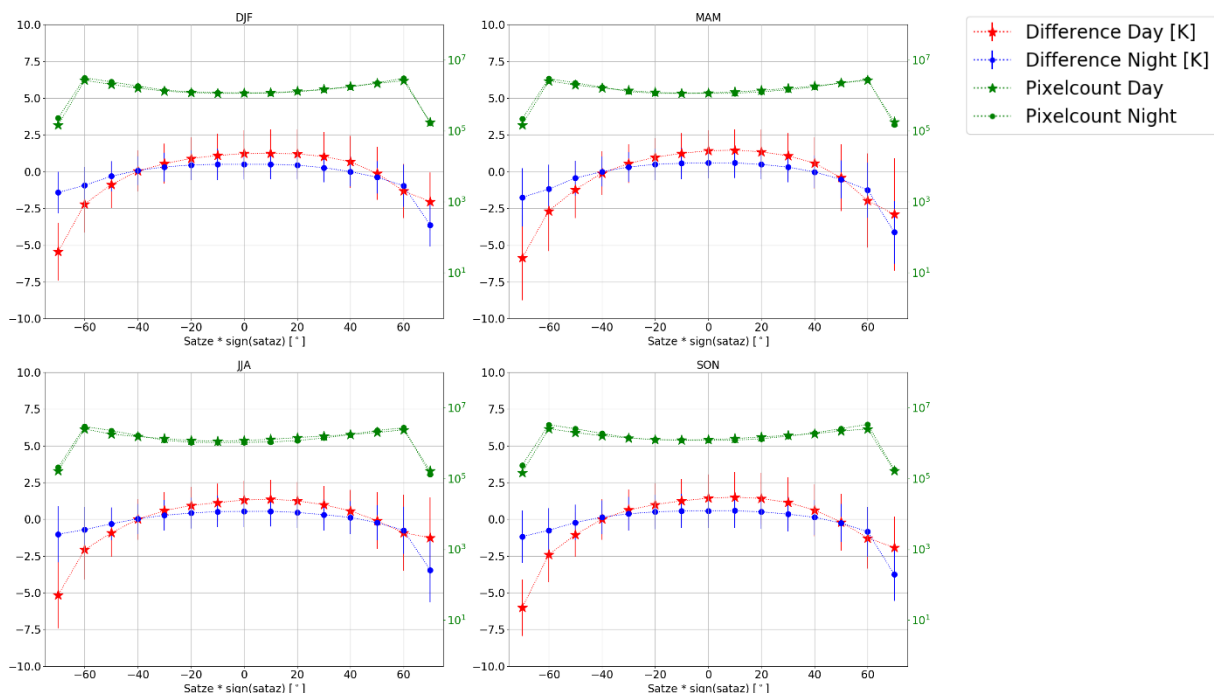


Figure 33: Seasonal differences between MODIST and SEVIR2 LST data for different $\text{satze} \cdot \text{sign}(\text{sataz})$ of MODIST; red stars represent the daytime data, blue dots the night-time data, and the green stars and dots on the right axis display the averaged pixel numbers for daytime and night-time data, respectively

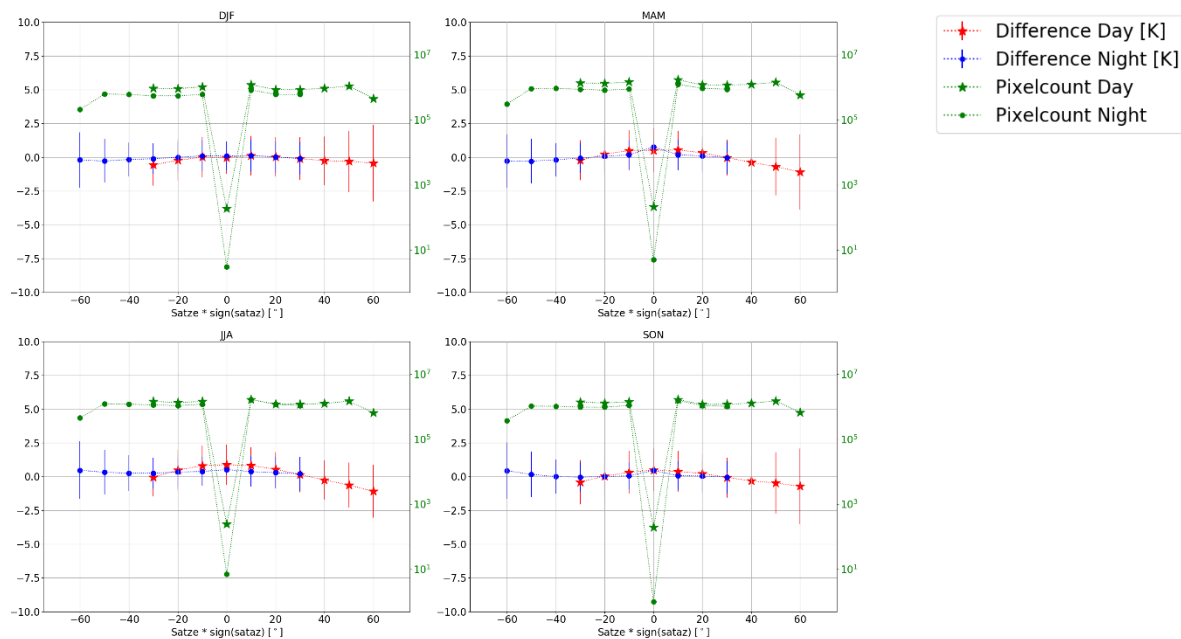


Figure 34: Seasonal differences between SLSTRA and SEVIR4 LST data for different $\text{satze} \cdot \text{sign}(\text{sataz})$ of SLSTRA; red stars represent the daytime data, blue dots the night-time data, and the green stars and dots on the right axis display the averaged pixel numbers for daytime and night-time data, respectively

4.2.2. Results over Antarctica

The time series of the three analysed satellite – satellite data sets (Figure 35) reveals that the differences are small over Antarctica, and mainly below 2 K for all three intercomparisons. ATSR_3-MOD11T and ATSR_3-MODIST have positive differences, whereas MODIST-ATSOP_ has more negative differences. For MODIST-ATSOP_, some positive daytime outliers are detected. The number of analysed pixels shows a seasonal cycle for daytime and night-time data due to the polar summer and winter.

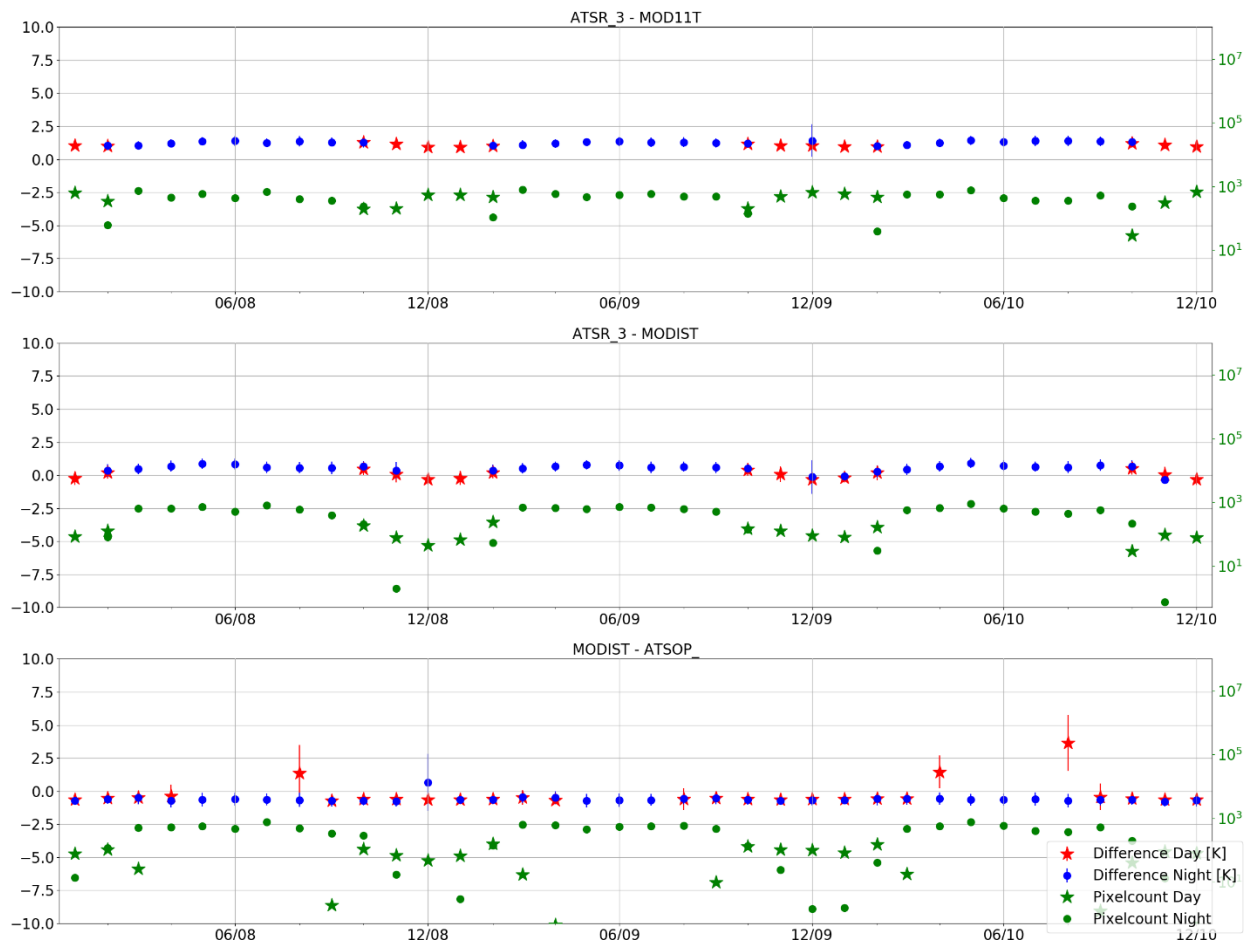


Figure 35: Monthly time series for all investigated satellite – satellite data sets over Antarctica. Red stars represent the daytime data, blue dots the night-time data, the green stars and dots on the right axis display the averaged pixel numbers for daytime and night-time, respectively.

The analysis of the distribution of averaged data points showed that most analysed pixels are in the south of Antarctica, where there are more overpasses due to the proximity of the pole. The distribution between daytime and night-time data shifts, as mentioned above, due to the polar seasons.

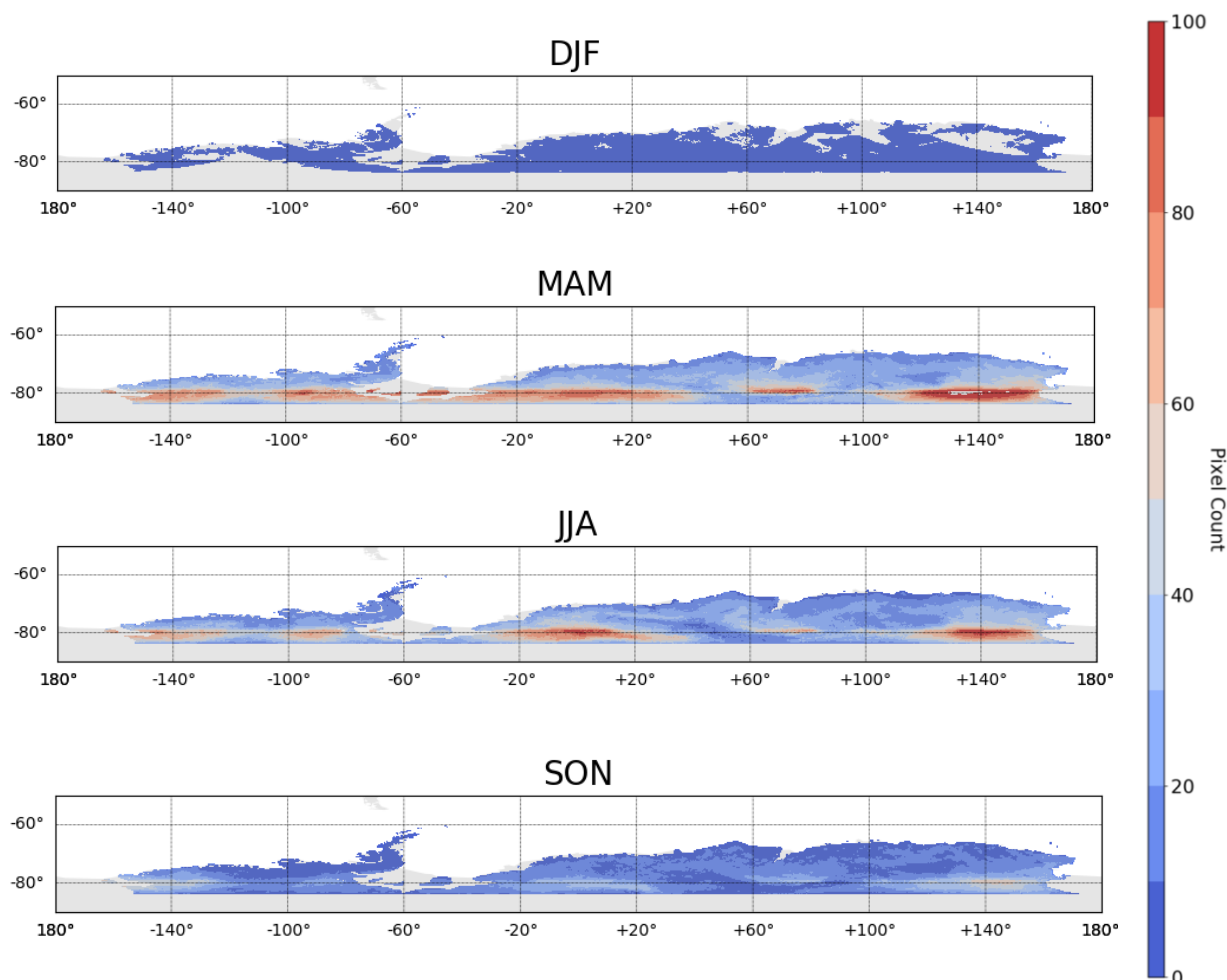


Figure 36: Number of seasonal night-time averaged data points per pixel for ATSR_3-MOD11T differences over Antarctica

The analysis of the different elevation classes revealed that most pixels are located in a height above 2000 m, but no significant differences were found between different classes.

Most pixels over Antarctica are classified in the land cover class “snow_and_ice” (class 220 of the LCCS classification) and the remaining pixels as “water” (class 210), but no significant difference between them was seen.

The influence of the satellite angles showed no significant differences for ATSR_3 (in the intercomparisons ATSR_3 against MODIST and MOD11T) satellite angles, for MODIST (MODIST against ASTOP_) it was found that most data points have a satellite zenith angle between 25° to 35°. The differences for different satellite angles is not significant, the differences only increase for MODIST satellite angles > 45° (Figure 37).

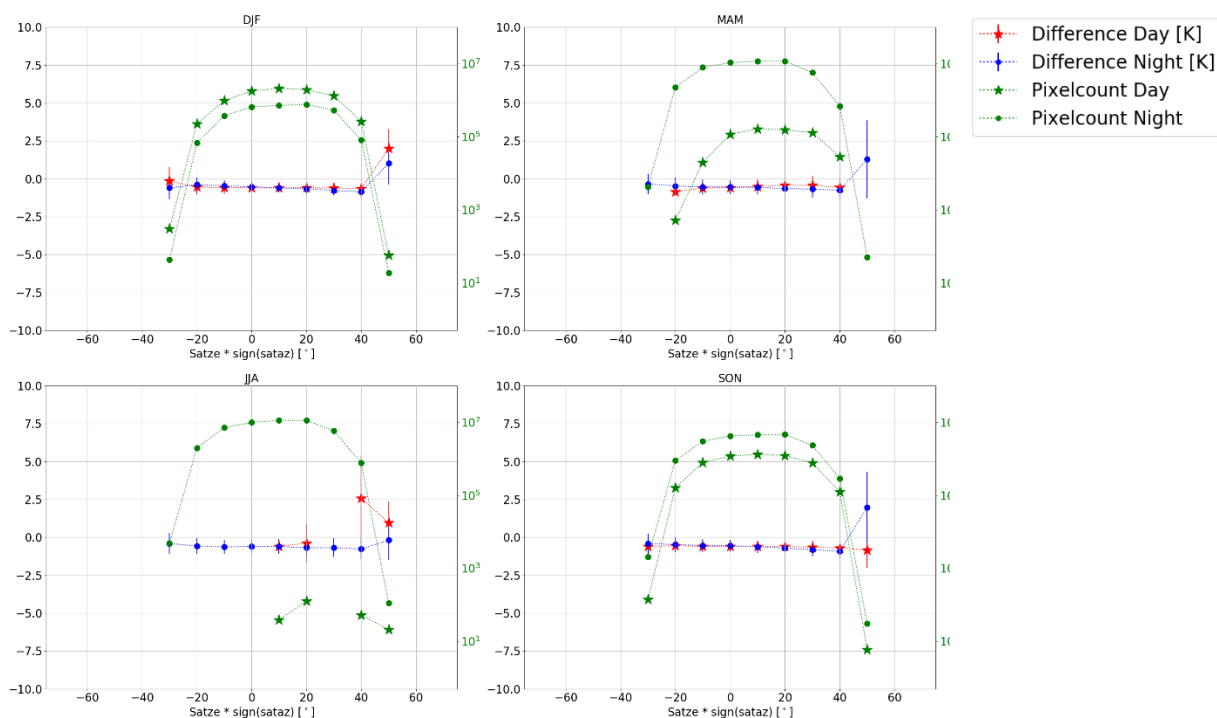


Figure 37: Seasonal LST differences between MODIST and ATSOP_ LST data for different $\text{satze} \cdot \text{sign}(\text{sataz})$ of MODIST; red stars represent the daytime data, blue dots the night-time data, and the green stars and dots on the right axis display the averaged pixel numbers for daytime and night-time data, respectively

4.2.3. Results over Asia

The time series of the three analysed satellite – satellite data sets over Asia can be seen in Figure 38. A minor yearly cycle is found in all data sets, which is most pronounced for the MODIST-ATSOP_ data set, with minimal difference between daytime and night-time. The most comparable matchups are for ATSR_3-MODIST.

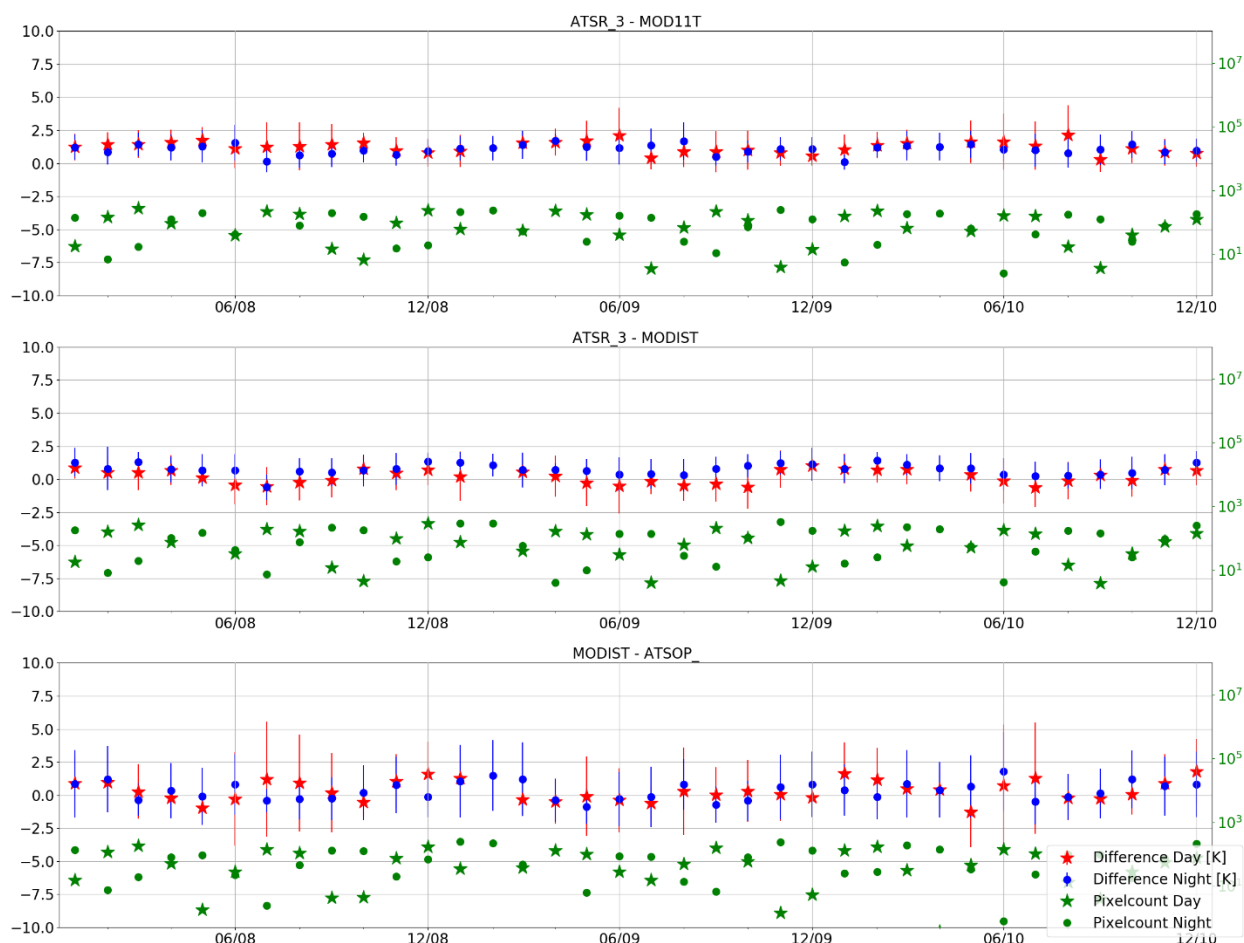


Figure 38: Monthly time series for all investigated satellite – satellite data sets over Asia. Red stars represent the daytime data, blue dots the night-time data, the green stars and dots on the right axis display the averaged pixel numbers for daytime and night-time, respectively.

The distribution of the pixel counts shows that the most of the continent is covered for all three data sets, with most data points in the north, whereas in the south, especially in JJA, there are less data points (see Figure 39 for ATSR_3-MOD11T daytime pixel counts) principally as a result of cloud clearing over these tropical regions.

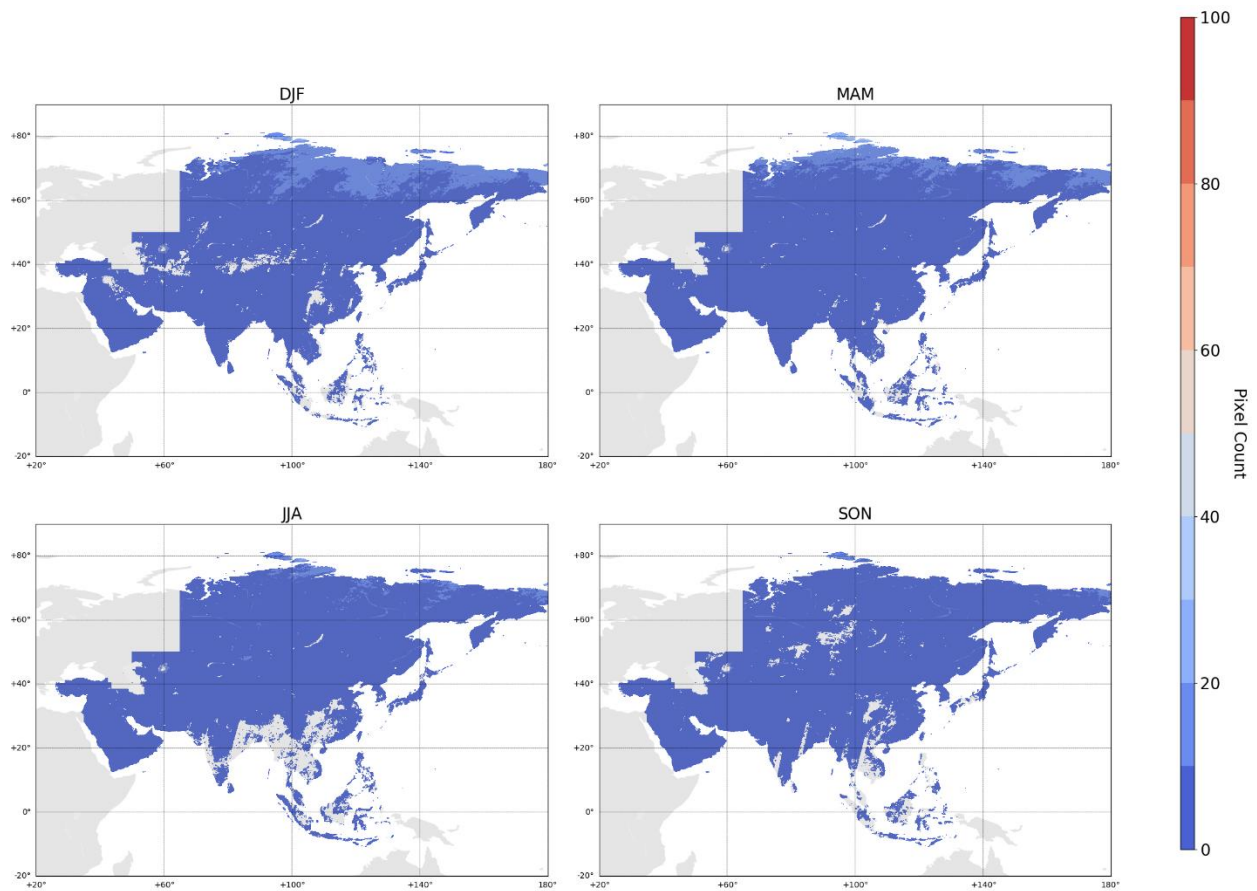


Figure 39: Number of seasonal daytime averaged data points per pixel for ATSR_3-MOD11T data over Asia

The analysis of the different elevation classes showed that most pixels are in the elevation classes between 0 m – 1000 m. No significant differences between the single classes were found. For all three data pairs, the RSTD increases for elevations > 2000 m during daytime. This is most significant for MODIST-ATSOP_.

The main land cover classes found for the intercomparisons over Asia are “tree_needleleaved_deciduous_closed_to_open” (class 80 of the LCCS classification), grassland (class 130) and “sparse_vegetation” (class 150). Class 130 and 150 are mainly located in the south of Asia, whereas class 80 is found in the north. No significant differences within the RSTDs were seen between these three classes (Figure 40 for MODIST-ATSR_3 daytime differences).

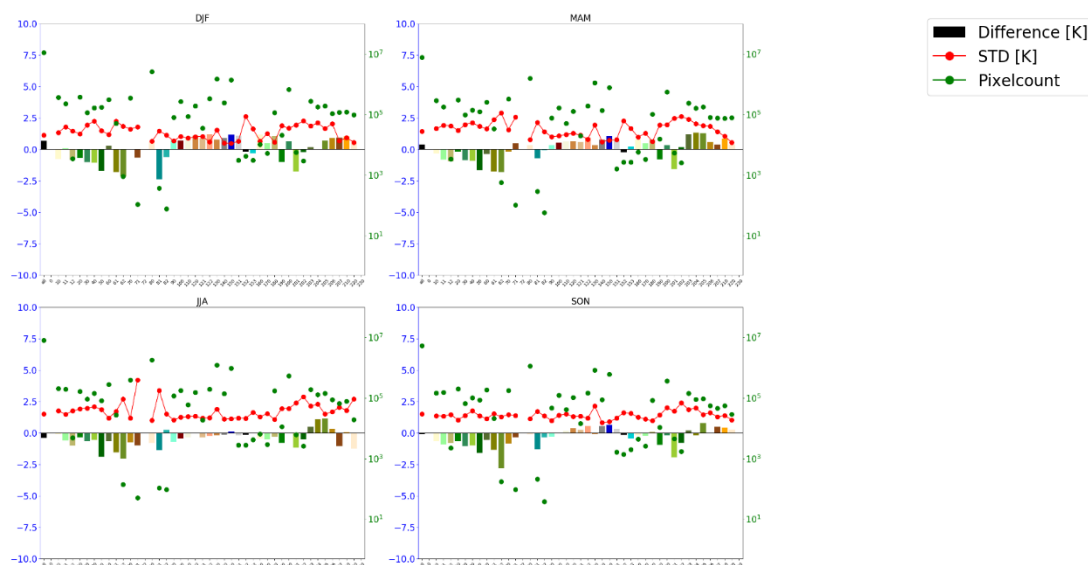


Figure 40: Seasonal daytime differences for different land cover classes for ATSR3-MODIST over Asia; the bars are the median differences, red points the RSTD and the green points on the right axis show the number of averaged data points

The analysis of the differences with respect to different satellite angles again showed no significant differences for the ATSR_3 intercomparisons, but for MODIST-ATSOP_ the value of MODIST $\text{satze} * \text{sign}(\text{sataz})$ increased significantly to large negative differences for satze values larger than 65° or smaller than -25° (see Figure 41).

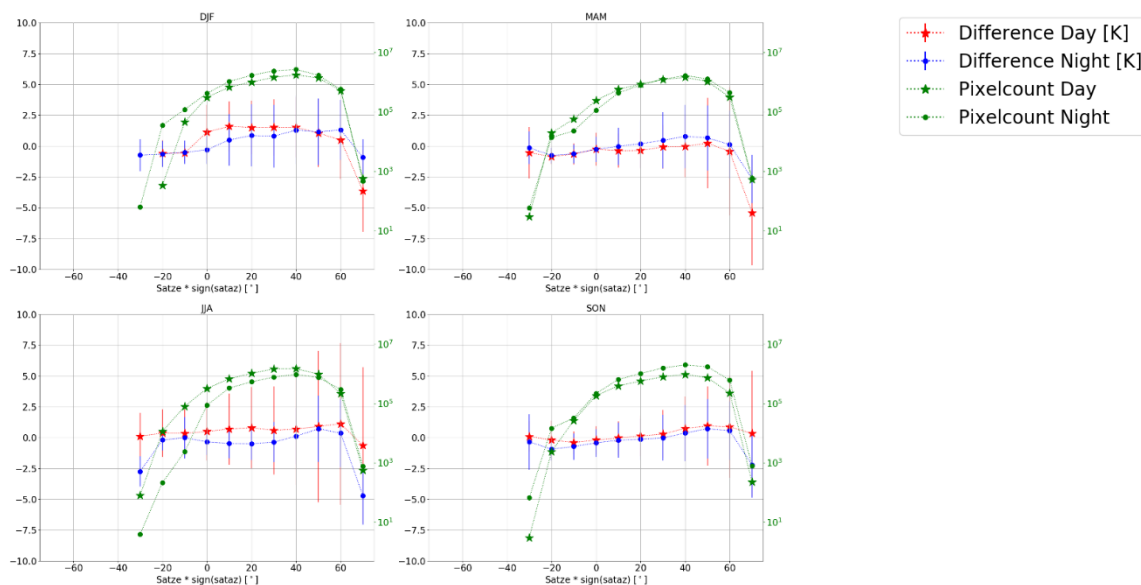


Figure 41: Seasonal LST differences between MODIST and ATSOP_ LST data for different $\text{satze} * \text{sign}(\text{sataz})$ of MODIST; red stars represent the daytime data, blue dots the night-time data, and the green stars and dots on the right axis display the averaged pixel numbers for daytime and night-time data, respectively

4.2.4. Results over Australia

The results of the time series analysis of the differences over Australia are shown in Figure 42. It can be seen that the differences are mainly positive for MODIST-ATSOP_ and for ATSR_3-MOD11T data pairs, whereas the differences fluctuate around 0 K for ATSR_3-MODIST. The higher daytime differences in SH summer months for ATSR_3-MOD11T might be caused by an increased influence of the solar radiation then, which increases the difference in temperature between sunlit and shadowy areas. ATSR_3-MOD11T has higher differences than ATSR_3-MODIST, a more pronounced seasonal cycle, and also higher robust standard deviations, as already seen before. The two LST_cci data sets ATSR_3 and MODIST have smaller differences.

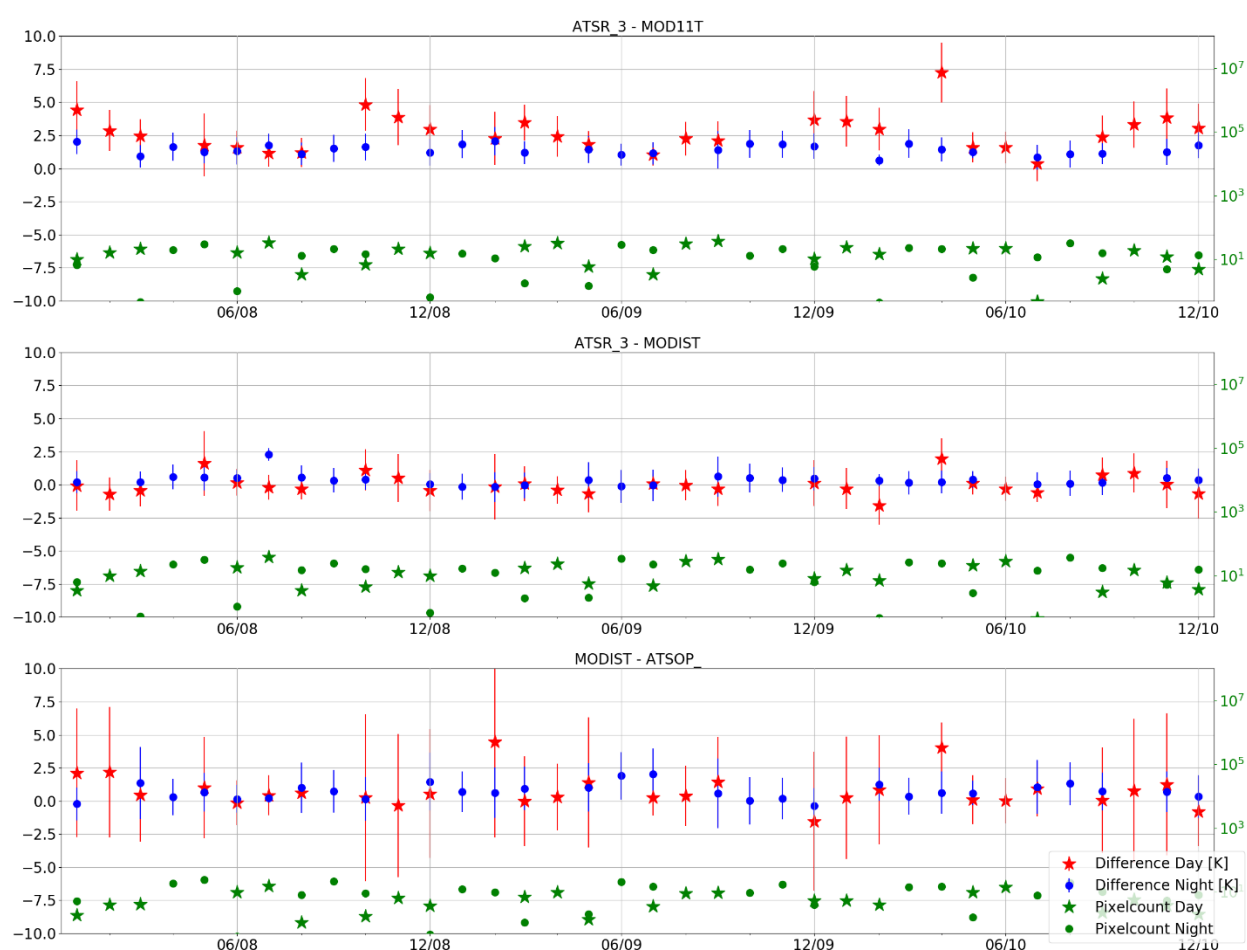


Figure 42: Monthly time series for all investigated satellite – satellite data sets over Australia. Red stars represent the daytime data, blue dots the night-time data, the green stars and dots on the right axis display the averaged pixel numbers for daytime and night-time, respectively.

The number of averaged data points per pixel is < 10 per pixel for all satellite – satellite intercomparisons. More data points are seen during day, and in general, the south has a better coverage than the north (Figure 43 for ATSR_3-MOD11T intercomparisons).

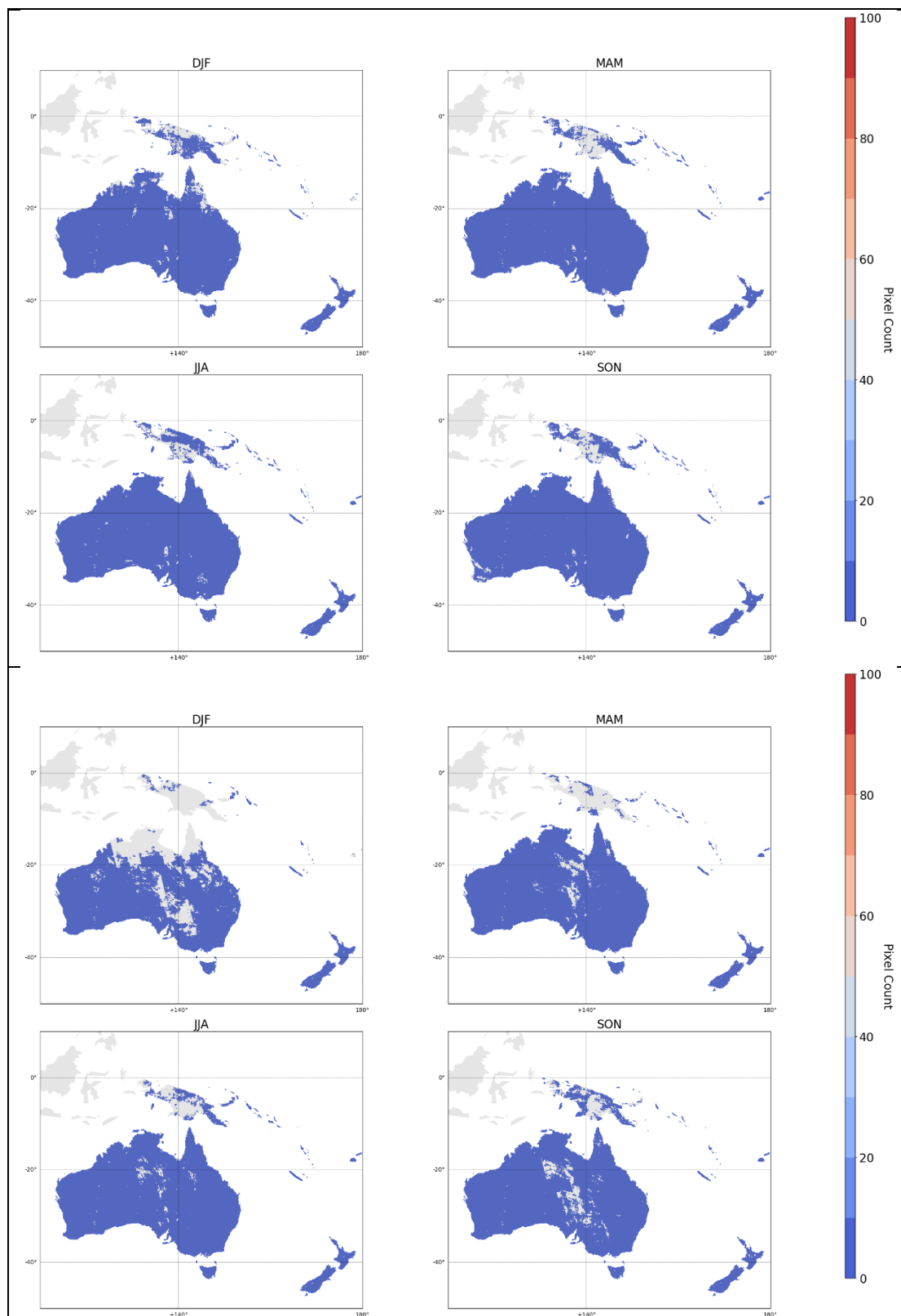


Figure 43: Seasonal distribution of the number of daytime (upper) and night-time (lower) averaged data points per pixel for ATSR_3-MOD11T data over Australia

The analysis of the differences for different elevation classes showed that most analysed pixels have an elevation between 200 m – 500 m, for ATSR3-MOD11T the largest absolute differences for this elevation class were found in Australian summer (Figure 44), in accordance with what the time series analysis showed. The absolute differences increase for the two highest elevation classes, where the influence of the orography is more pronounced. However, also the RSTD increases for higher classes, as the number of data points decreases rapidly.

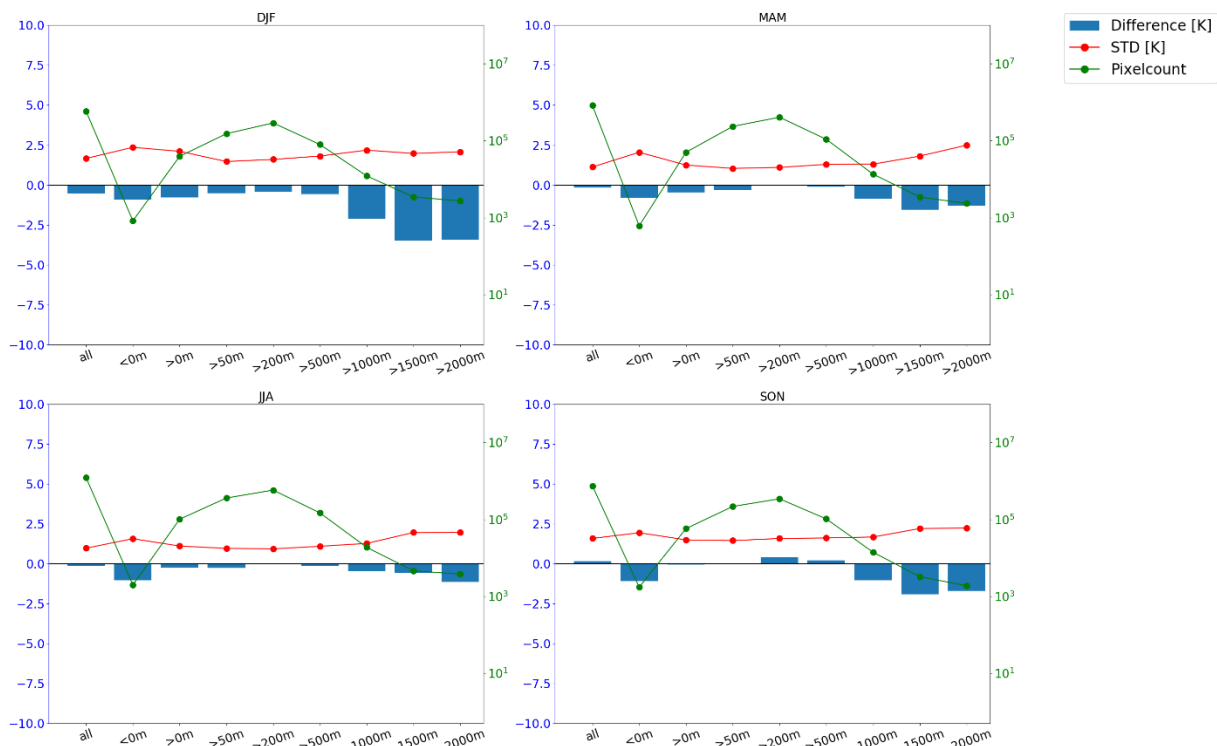


Figure 44: Seasonal daytime differences for different elevation classes for ATSR3-MODIST over Australia; blue bars are the median differences, red points the RSTD and the green points on the right axis show the number of averaged data points

The main land cover class found over Australia is “sparse_vegetation” (class 150 of the LCCS classification), which covers the centre of Australia (Figure 45 for daytime results of ATSR_3-MOD11T differences).

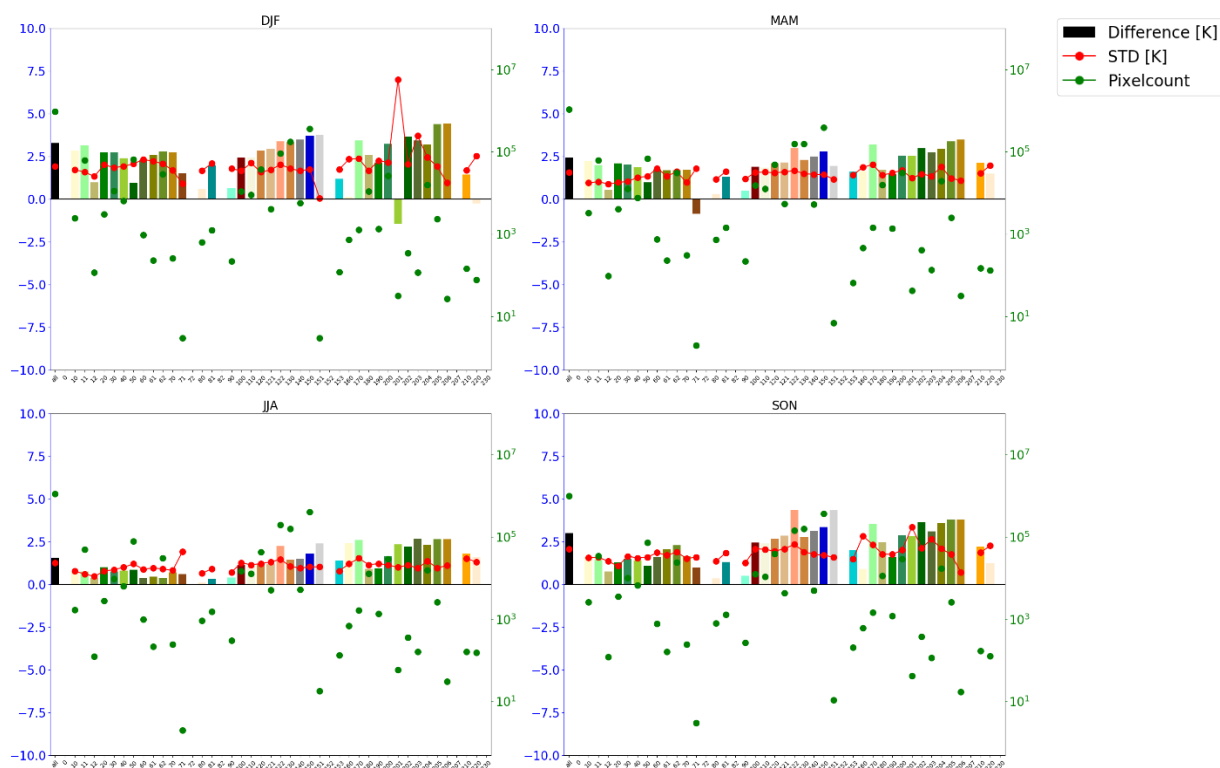


Figure 45: Seasonal daytime differences for different land cover classes for ATSR_3-MOD11T over Australia; the bars are the median differences, red points the RSTD and the green points on the right axis show the number of averaged data points

The comparison of the differences against the satellite angles showed that for the intercomparisons of ATSR_3-MOD11T and ATSR_3-MODIST the differences were lower for more negative values of $\text{satze} \cdot \text{sign}(\text{sataz})$ and increased for positive values of $\text{satze} \cdot \text{sign}(\text{sataz})$ (Figure 46 for ATSR_3-MODIST). This increase was more pronounced than found over the other continents. The local overpass time for the ATSR_3 satellite is in the morning, thus, when the ATSR_3 satellite azimuth angle is negative, it is looking on the scene from the West whereas the sun is shining from the east, which leads to a larger influence of shadows for these azimuth angles.

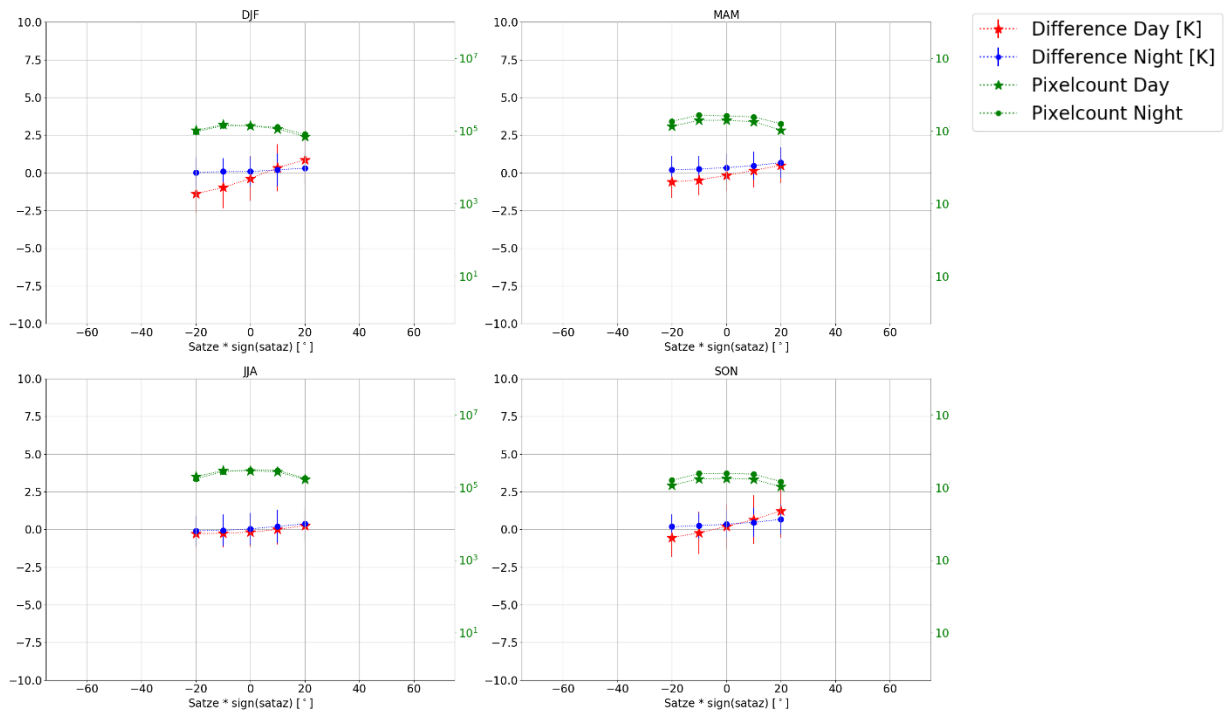


Figure 46: Seasonal LST differences between ATSR_3 and MODIST LST data for different $\text{satze} \cdot \text{sign}(\text{sataz})$ of ATSR_3; red stars represent the daytime data, blue dots the night-time data, and the green stars and dots on the right axis display the averaged pixel numbers for daytime and night-time data, respectively

4.2.5. Results over Europe

The time series for the nine analysed satellite – satellite intercomparisons over Europe in the time period from 2008 – 2010 are displayed in Figure 47, the time series for the two satellite pairs analysed from 2018 – 20 in Figure 48. A seasonal cycle for daytime data was found for all data pairs intercompared against SEVIR2 or SEVIR4, with increased differences in summer, which was most pronounced for ATSR_3-SEVIR2. This is in contrast to what was seen over Africa, where no strong seasonal cycle for the daytime data was detected. The intercomparison of LEO data sets vs SEVIR2 gave in general higher differences than the intercomparison of LEO vs LEO data sets. For the satellite intercomparisons against SEVIR2, there is again the strong positive outlier for night-time data in 2010/09 found, that was also seen over Africa. This will be investigated for the next reprocessing.

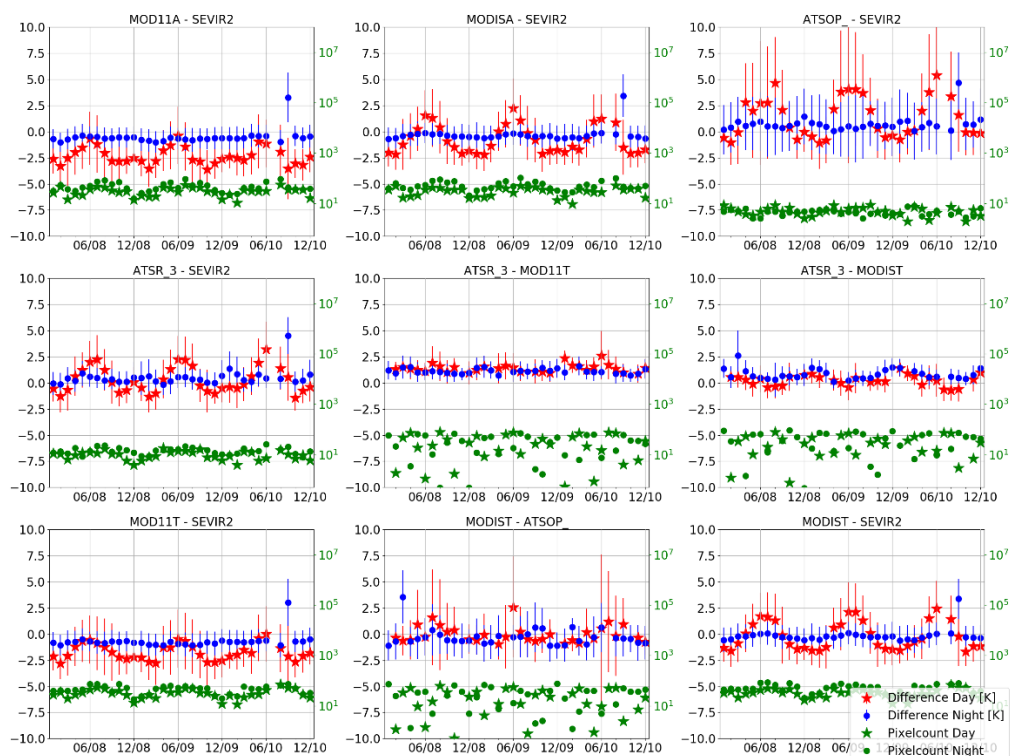


Figure 47: Monthly time series for all investigated satellite – satellite data sets over Europe from 2008 - 10. Red stars represent the daytime data, blue dots the night-time data, the green stars and dots on the right axis display the averaged pixel numbers for daytime and night-time, respectively.

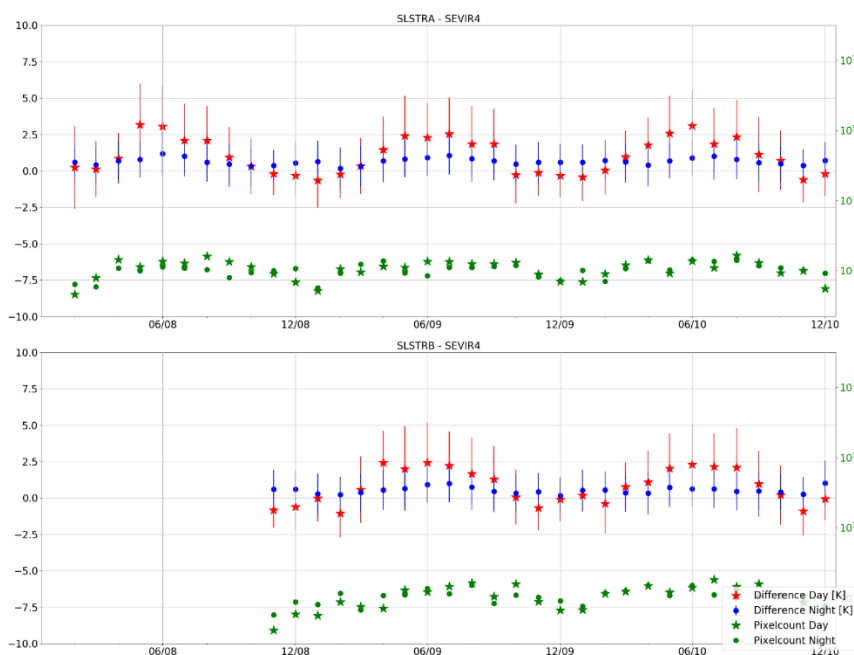


Figure 48: Monthly time series for the investigated satellite – satellite data sets over Europe from 2018 - 2020. Red stars represent the daytime data, blue dots the night-time data, the green stars and dots on the right axis display the averaged pixel numbers for daytime and night-time, respectively.

The number of the averaged data points per pixel is lowest for ATSOP_-SEVIR2, and the LEO against LEO data pair cover a larger area than the LEO against GEO data pairs, where the NE part of the continent is not covered (see Figure 49 for the analysis of MODIST-SEVIR2 and MODIST-ATSOP_ daytime data). This might be caused by large uncertainties for these extreme SEVIRI satellite angles. The intercomparisons of ATSR_3-SEVIR2 and ATSOP_-SEVIR2 covered the continent only partly in “stripes”.

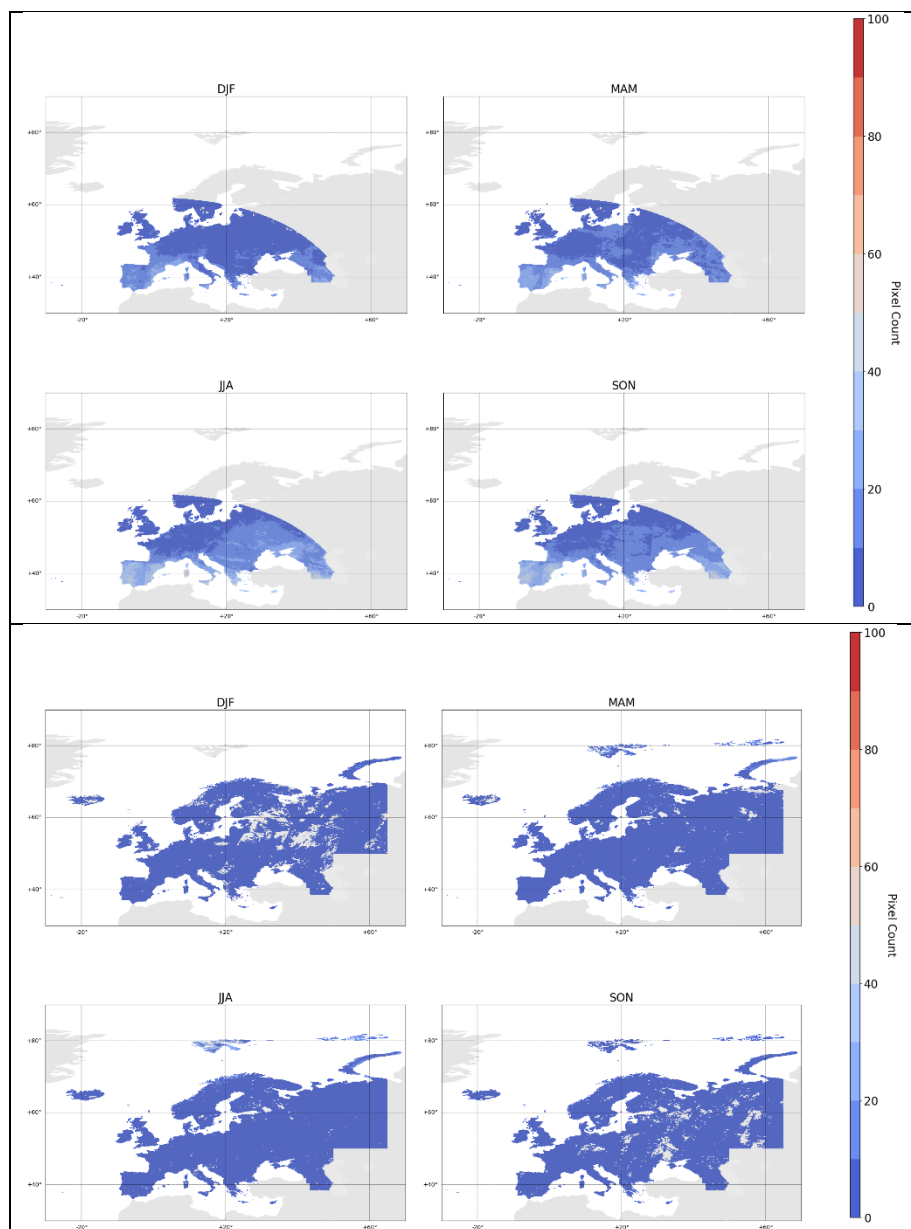



Figure 49: Number of seasonal daytime averaged data points per pixel for MODIST-SEVIR2 (upper plot) and MODIST-ATSOP_ (lower plot) data over Europe

	Product Validation Plan (PVP) <i>WP4 – DEL4.1</i>	Ref.: LST-CCI-D4.1-PVIR Version: 3.1 Date: 23-Jun-2023 Page: 77
---	---	--

The analysis of the differences for different elevation classes showed that most pixels fall into an elevation class of 50 m – 200 m. The differences and RSTD increased for elevations > 1500 m, no other significant differences between single elevation classes was found.

The main land cover classes found over Europe are “tree_needleleaved_evergreen_closed_to_open” (class 70 of the LCCS classification), “cropland_rainfed_herbaceous_cover ” (class 11) and “cropland_rainfed” (class 10). For the LEO-LEO data pairs, many data points fall also in the class “tree_broadleaved_deciduous_closed_to_open”. This LCC is mainly found in the northeastern part of the continent, which is not covered by the LEO-GEO data pairs, and is therefore less frequent in the LEO-GEO analysis. The land cover classes for MODISA-SEVIR2 daytime differences are shown in Figure 50. Class 70 is mainly found in the northern part of the continent, class 11 throughout it and class 10 in the east.

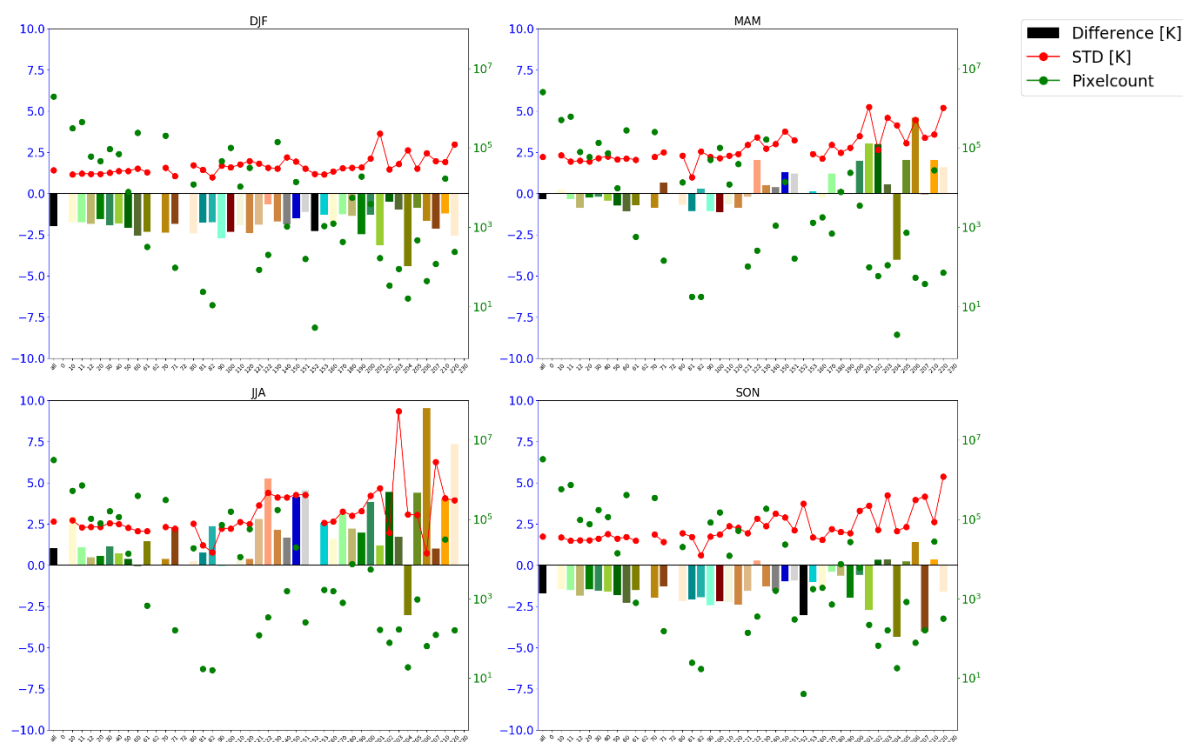


Figure 50: Seasonal daytime differences for different land cover classes for MODISA-SEVIR2 over Europe; the bars are the median differences, red points the RSTD and the green points on the right axis show the number of averaged data points

The analysis of the differences with respect to different classes of $\text{satze} * \text{sign}(\text{sataz})$ showed again the asymmetric distribution of data points for the MODIS data sets against SEVIR2, that were already found over Asia. This is less pronounced here for autumn and winter season (Figure 51 for MODISA-SEVIR2 differences), when the influence of the solar radiation is smaller.

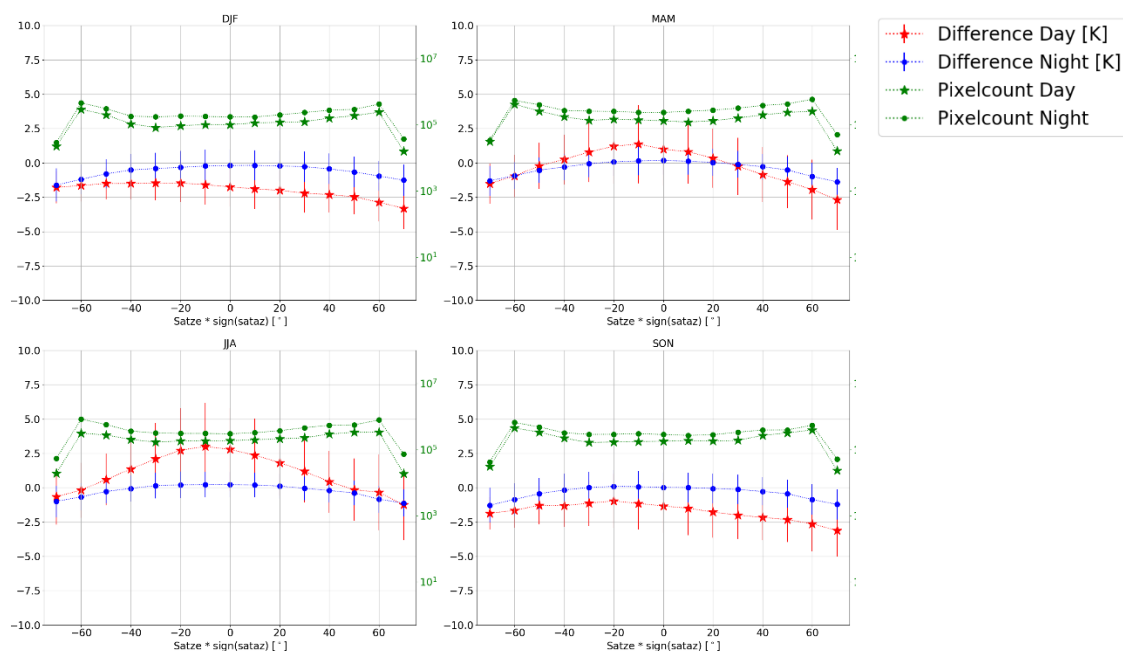


Figure 51: Seasonal LST differences between MODISA -SEVIR2 LST data for different $\text{satze} \cdot \text{sign}(\text{sataz})$ of MODISA; red stars represent the daytime data, blue dots the night-time data, and the green stars and dots on the right axis display the averaged pixel numbers for daytime and night-time data, respectively

4.2.6. Results over North America

The results of the time series analysis over North America is shown in Figure 52. The differences are positive for ATSR_3-MOD11T and ATSR_3-MODIST, and negative for MODIST-ATSOP_. They are mainly below 2 K for all data sets. A yearly cycle is seen in the monthly differences as well, but it is not very pronounced.

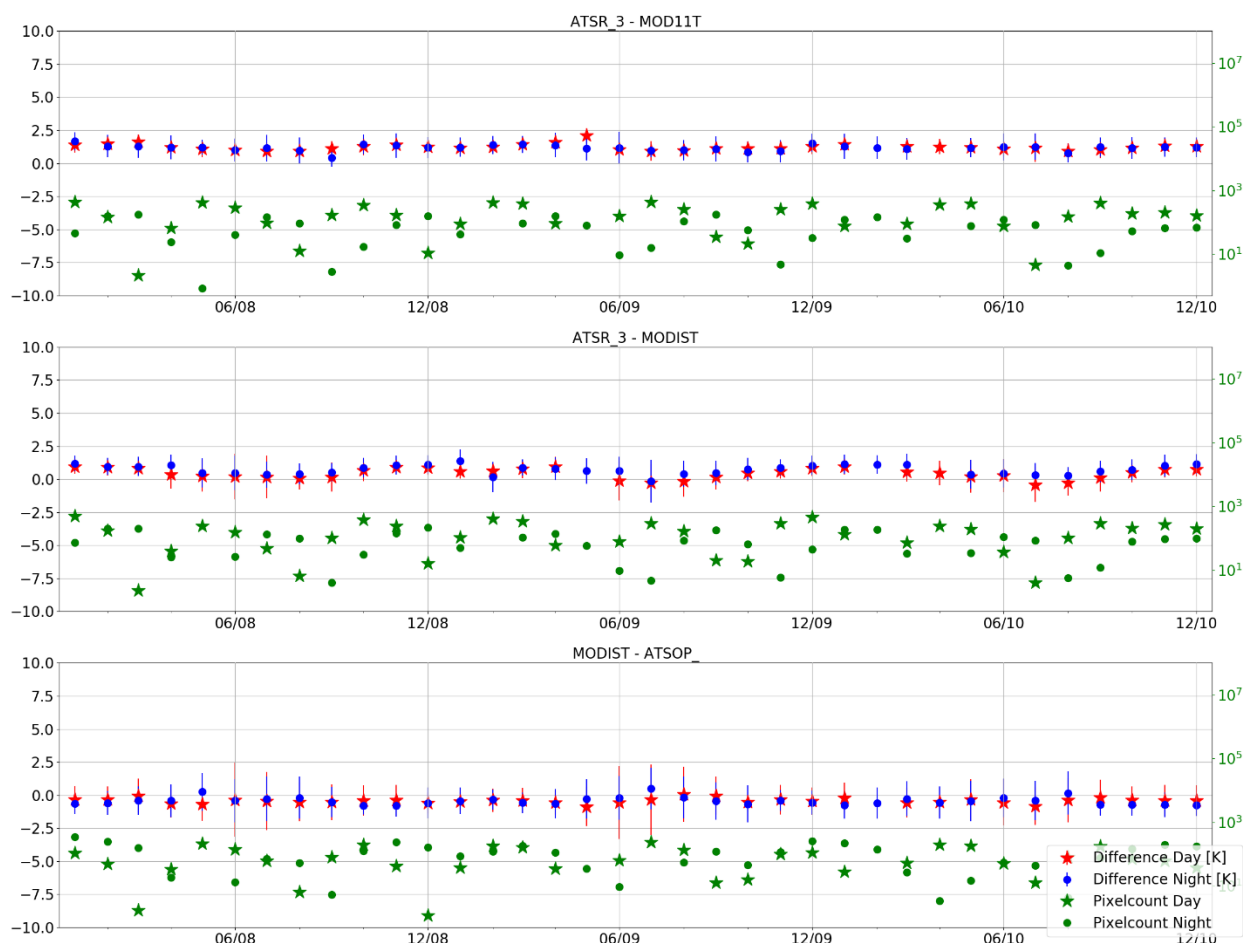


Figure 52: Monthly time series for all investigated satellite – satellite data sets over North America. Red stars represent the daytime data, blue dots the night-time data, the green stars and dots on the right axis display the averaged pixel numbers for daytime and night-time, respectively.

Over this continent, the number of averaged data points varied substantially between daytime and night-time data for all satellite pairs in the north of the continent. For ATSR_3-MOD11T and ATSR_3-MODIST, there were many data points (up to 100) during day, and the number was lower during night (<20), see Figure 53 for the data distribution for ATSR_3-MODIST data pair. It was opposite for MODIST-ATSOP_ with more data points during night in the north and less during day. This indicates the difference in the cloud masking between ATSR_3 and ATSOP_ is the cause. In the north, the number of overpasses increases due to the proximity of the pole.

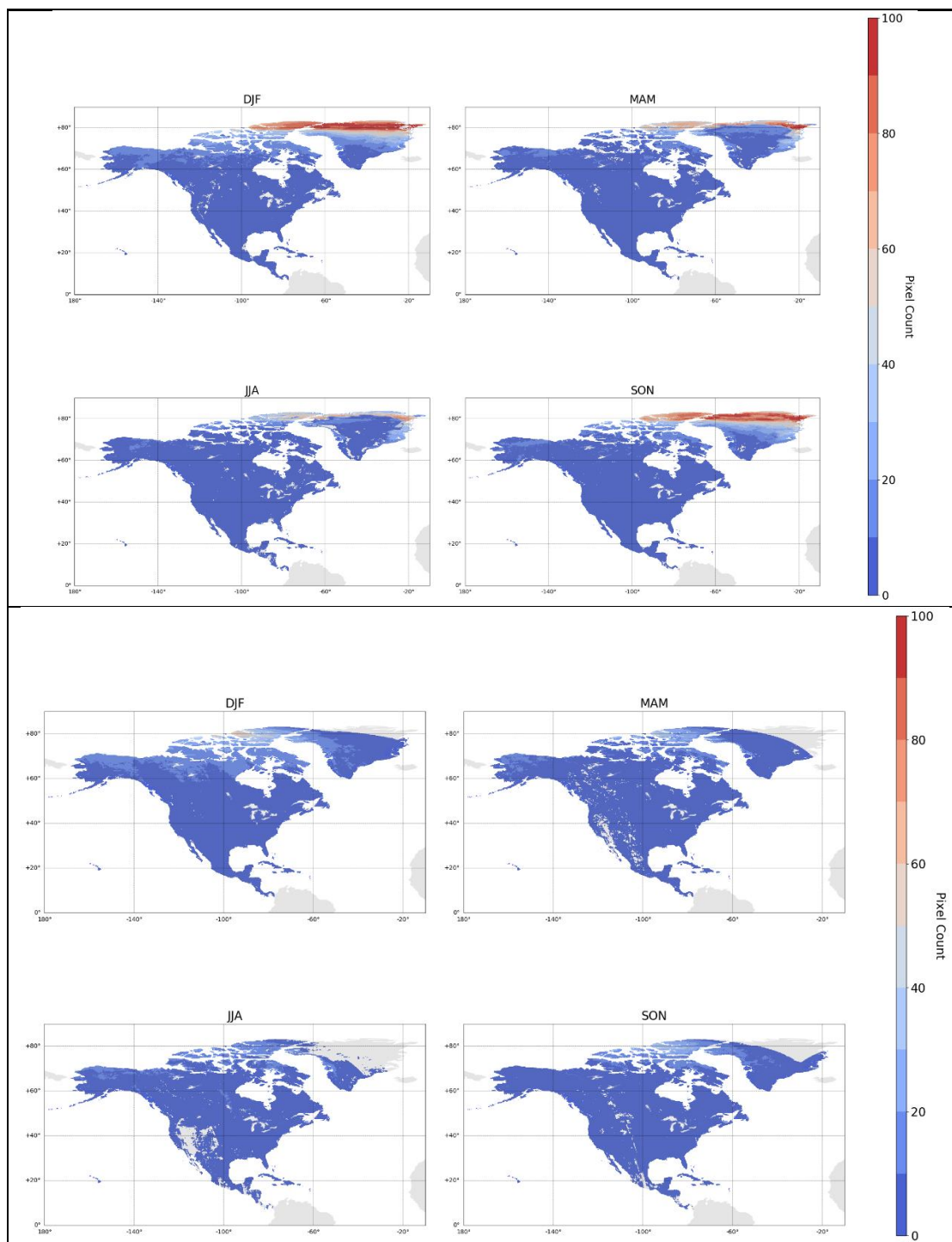


Figure 53: Number of seasonal daytime (upper) and night-time (lower) averaged data points per pixel for ATSR_3-MODIST data over North America

The analysis of the differences for different elevation classes showed that most analysed pixels have an elevation of 200 – 1000 m or larger than 2000 m. No significant differences between the single classes were found (see Figure 54 for daytime differences of ATSR_3-MODIST).

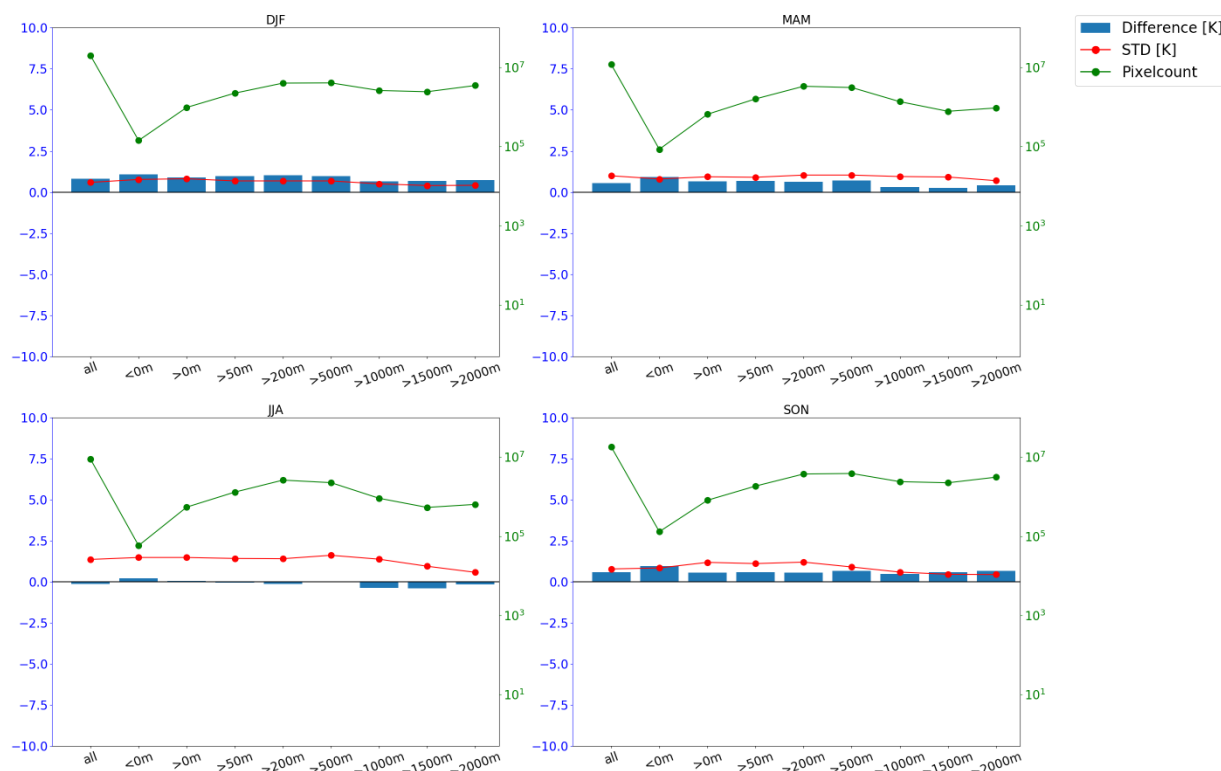


Figure 54: Seasonal daytime differences for different elevation classes for ATSR_3-MODIST over North America; blue bars are the median differences, red points the RSTD and the green points on the right axis show the number of averaged data points

The analysis of the different land cover classes showed that most data points fall in the land cover class of “snow_and_ice” (class 220 of the LCCS classification), class of “Bare_areas_of_soil_types_not_contained_in_biomes_21_to_25” (class 200), “sparse_vegetation” (class 150) and “lichens_and_mosses” (class 140). All of these classes are located in the north of the continent, where, as described above, most data points are located (Figure 55 for differences over different land cover classes for ATSR_3-MOD11T). Another frequent land cover class is “tree_needleleaved_evergreen_closed” (class 71), which is found throughout the continent.

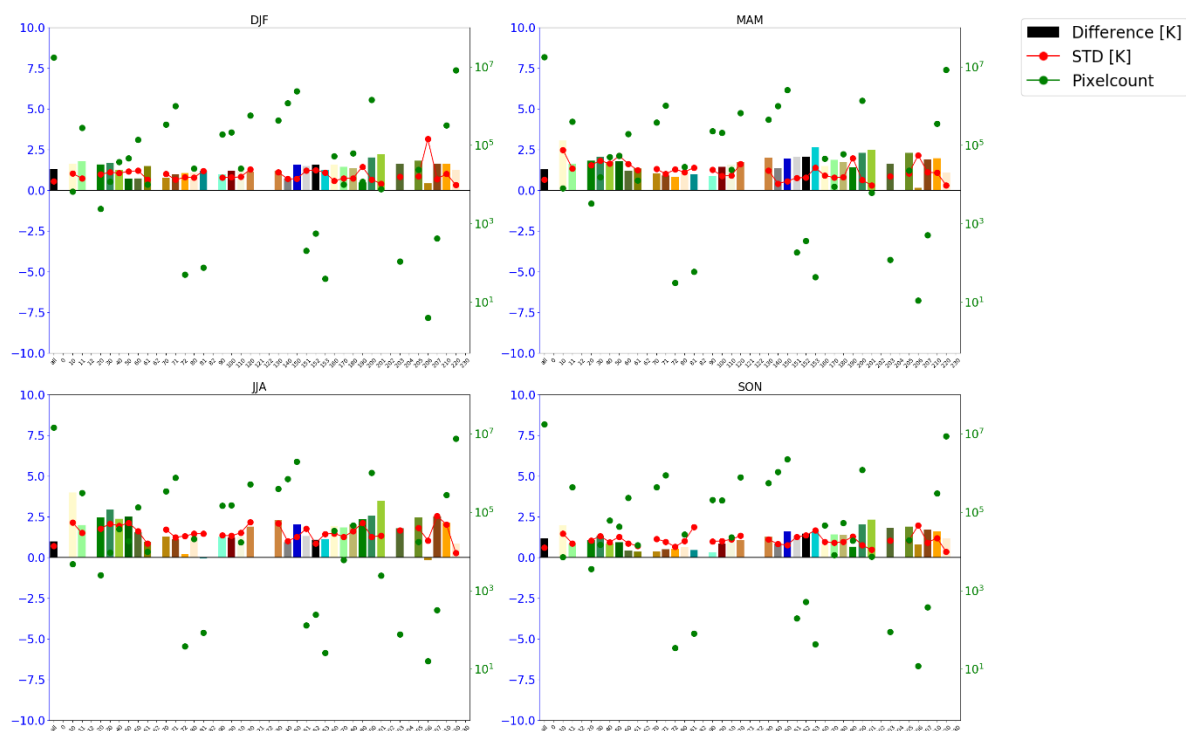


Figure 55: Seasonal daytime differences for different land cover classes for ATSR_3-MOD11T over North America; the bars are the median differences, red points the RSTD and the green points on the right axis show the number of averaged data points

The analysis of the satellite angles gave, as seen for the other continents described above, that for MODIST satellite angles, the differences and RSTD increase for larger zenith angles, and the number of data points decreases for increasing absolute zenith angles (see Figure 56 for ATSR_3 versus MODIST results).

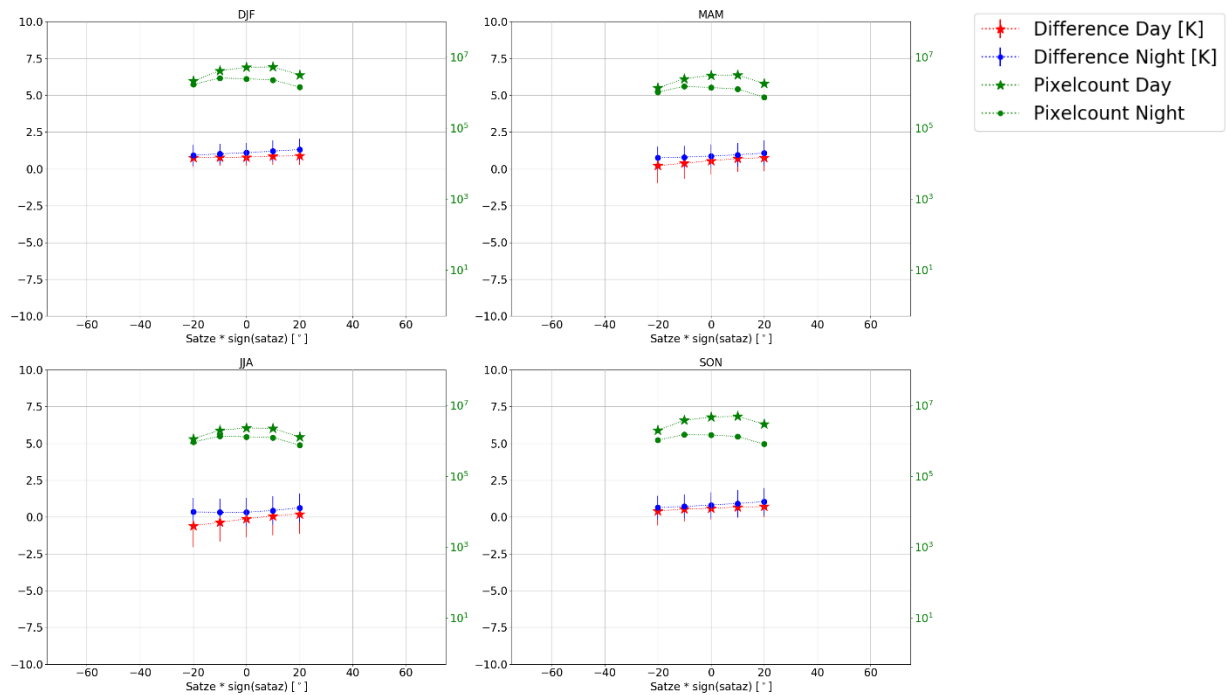


Figure 56: Seasonal LST differences between ATSR_3 and MODIST LST data for different $\text{satze} \cdot \text{sign}(\text{sataz})$ of MODIST; red stars represent the daytime data, blue dots the night-time data, and the green stars and dots on the right axis display the averaged pixel numbers for daytime and night-time data, respectively

4.2.7. Results over South America

The results of the time series analysis over South America is displayed in Figure 57. ATSR_3-MOD11T has more positive differences than ATSR_3-MODIST. The largest seasonal cycle is found for MODIST-ATSOP_.

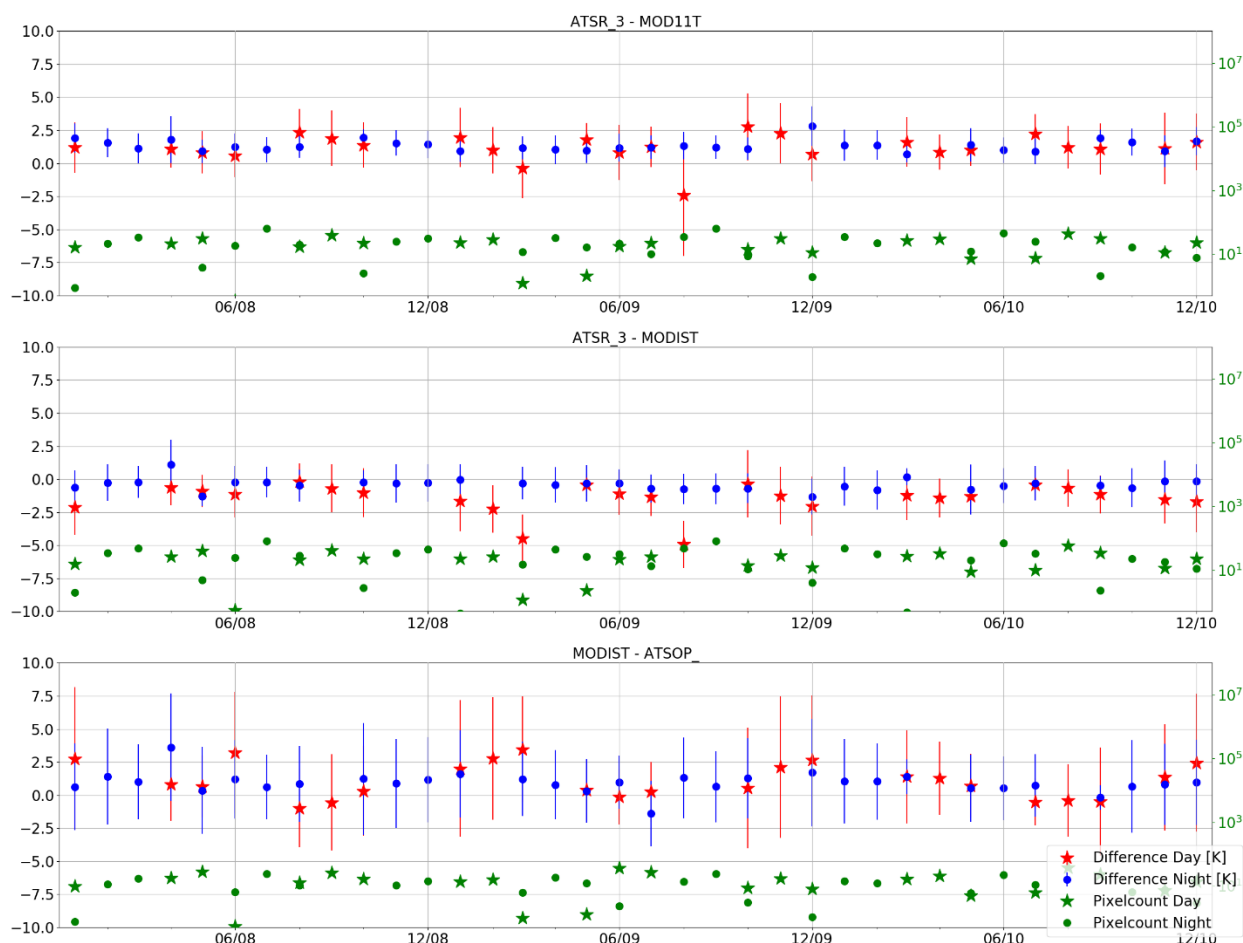


Figure 57: Monthly time series for all investigated satellite – satellite data sets over South America. Red stars represent the daytime data, blue dots the night-time data, the green stars and dots on the right axis display the averaged pixel numbers for daytime and night-time, respectively.

The number and distribution of the averaged data points per pixel showed that more data points lie in the south of the continent, whereas the north is not totally covered due to cloud clearing over the Amazon. Figure 58 displays the daytime pixel count for ATSR_3-MODIST data pair.

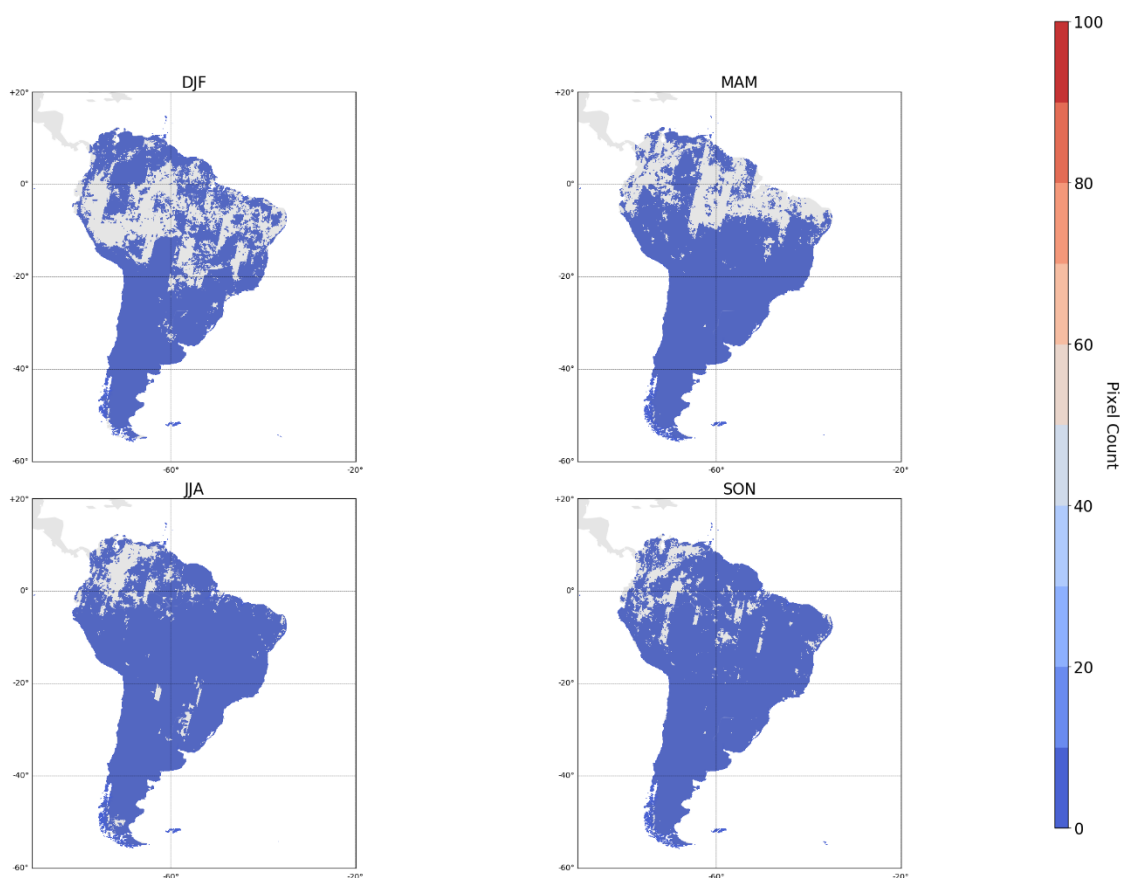


Figure 58: Number of seasonal daytime averaged data points per pixel for ATSR_3-MODIST data over South America

It was found with the analysis of the differences for different elevation classes that most pixels have an elevation between 50 to 500 m or above 2.000 m. These high elevations are mainly seen for the Andes in the west of the continent. There is a slope in the differences between the different elevation classes found for daytime data, for ATSR_3-MOD11T, the differences get smaller for larger classes, for ATSR_3-MODIST it gets more negative and for MODIST-ATSOP_ more positive. The increase is largest for MODIST-ATSOP_. The RSTD increases for all data pairs for larger elevation classes, which is most pronounced for the SH summer months, when the influence of sunlight and shadowy areas is largest. See Figure 59 for differences for different land cover classes for ATSR_3-MOD11T.

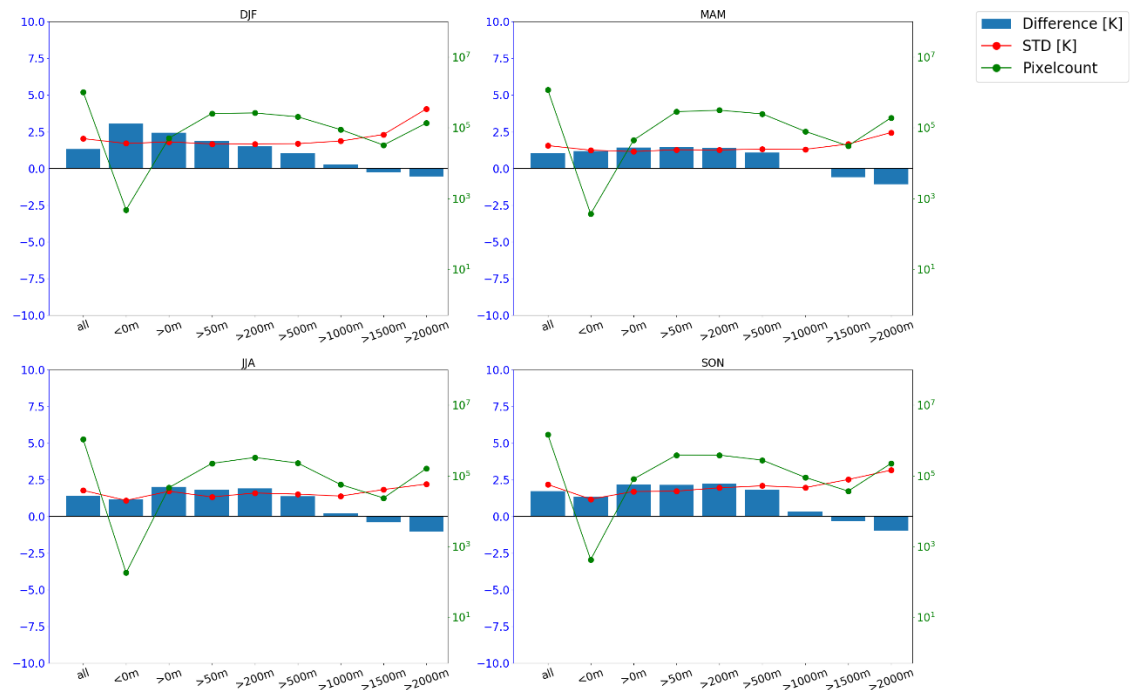


Figure 59: Seasonal daytime differences for different elevation classes for ATSR_3-MOD11T over South America; blue bars are the median differences, red points the RSTD and the green points on the right axis show the number of averaged data points

The main land cover classes found in the analysis over South America was “tree_broadleaved_evergreen_closed_to_open” (class 50 of the LCCS classification), followed by „shrubland” (class 120). Class 50 covers the north of the continent, whereas class 120 is found in the south. No significant differences between these two major classes could be found within the uncertainty range (see Figure 60 for daytime differences for ATSR_3-MODIST). For ATSR_3-MODIST, the daytime differences in DJF for class 50 are more negative than those for 120, for ATSR_3-MOD11T, the daytime differences in DJF are more positive for class 120. These results might be connected to the results of the elevation classes, as class 120 is found along the mountain ridge in the west, where also the elevation is highest.

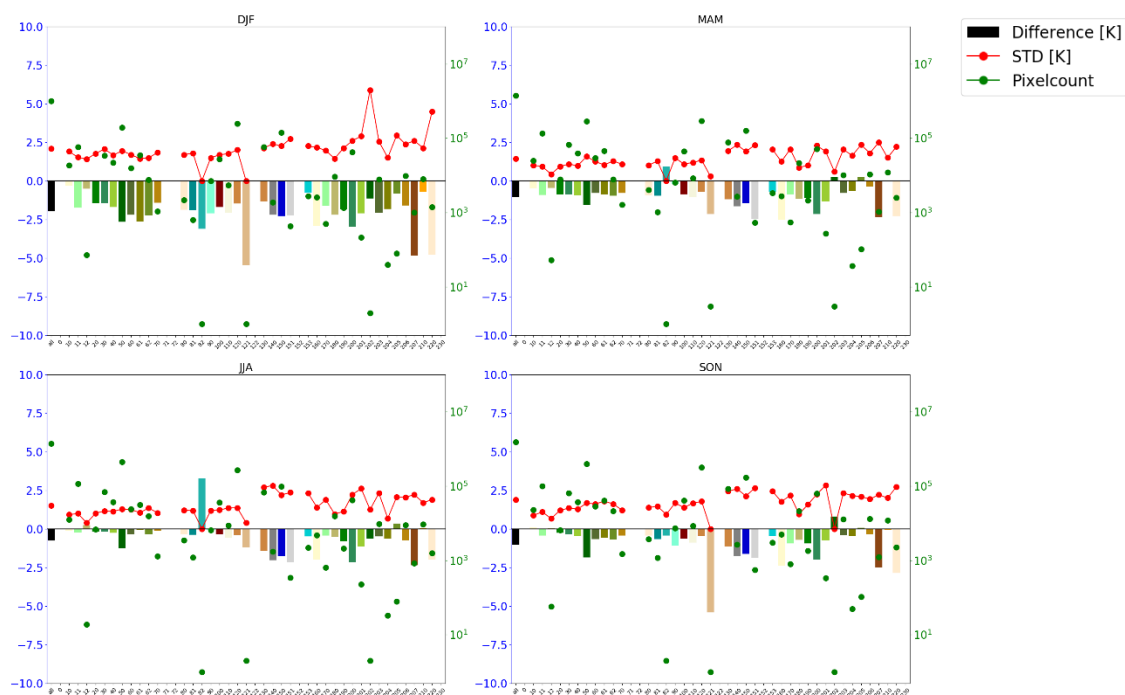


Figure 60: Seasonal daytime differences for different land cover classes for ATSR_3-MODIST over South America; the bars are the median differences, red points the RSTD and the green points on the right axis show the number of averaged data points

The analysis of the different satellite angles showed an asymmetric increase with increasing satellite zenith angles which is more pronounced during daytime as has been found for the other continents before (see Figure 61 for results of ATSR_3 versus MODIST).

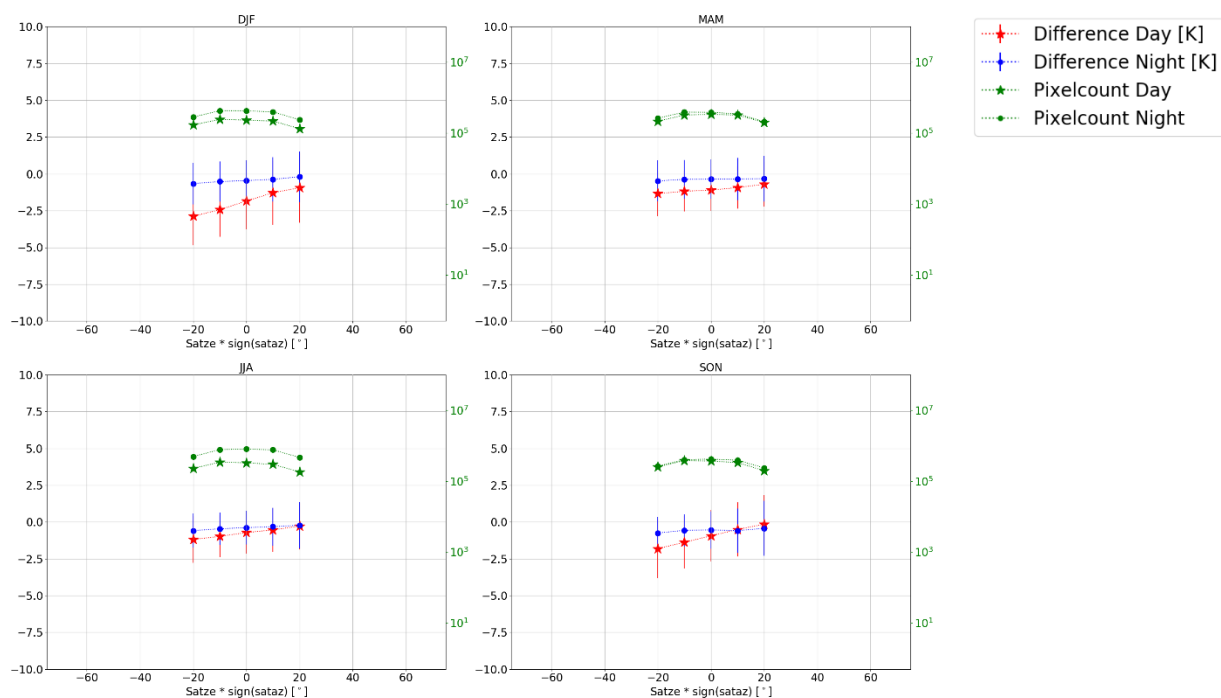



Figure 61: Seasonal LST differences between ATSR_3 and MODIST LST data for different $\text{satze} * \text{sign}(\text{sataz})$ of ATSR_3; red stars represent the daytime data, blue dots the night-time data, and the green stars and dots on the right axis display the averaged pixel numbers for daytime and night-time data, respectively

 land surface temperature cci	Product Validation Plan (PVP) <i>WP4 – DEL4.1</i>	Ref.: LST-CCI-D4.1-PVIR Version: 3.1 Date: 23-Jun-2023 Page: 89
--	---	--

5. Conclusions


In this work the results of the validation of the satellite LST data sets developed within the LST_cci project are presented. The validation is done in two parts, first is an in situ validation against point measurements at different, globally distributed stations. Second is the intercomparison of the LST_cci data sets with operational and reference data sets over different continents.

For the in situ validation, seven IR LEO satellite LST data sets (AVHRMA, ATSR_2, ATSR_3, MODISA, MODIST, SLSTRA, and SLSTRB), nine IR GEO satellite LST data sets (GOES12, GOES13, GOES16, HMWR_8, MTSAT2, SEVIR1, SEVIR2, SEVIR3, and SEVIR4) and two MW LST data sets (SSM13 and SSM17) have been validated. The in situ data consists of observations from 16 stations including stations from the KIT network, SURFRAD network, an ARM station, a Copernicus LAW station and Heihe stations over the time period from 1995 - 2020. The time period varied investigated depends on the data availability of the satellite as well as the in situ data. Stations from the Copernicus LAW network were added to the validation data base, however only one of them (KIT_F_) could be use since the others started in November 2021. These sites will be included in the next validation round, and the time of validation for all data sets will be extended.

The results are presented in terms of product accuracy and robust standard deviation (RSTD) for both validation types: i) in terms of bias (satellite LST – in situ LST) for the in situ validation; and ii) differences (satellite 1 LST – satellite 2 LST) for the intercomparisons.

The results of the in situ validation show that in general the accuracies of the LST_cci products are better at night than during the day, as the influence of sunlit and shadow areas during day can increase the point-to-area differences between the satellite scale LST and the in situ point measurements. The biases found for ATSR_2, ATSR_3, MODISA, and MODIST are in general good, and MODISA and MODIST often have similar results over the same station. For those four data sets, the biases during daytime were larger for V1.00 of the data sets over certain stations than for the latest V3.00 data. The validation of the V1.00 AVHRMA data set was included in this validation round. High RSTDs were observed at some stations due to unmasked cloud pixels. The AVHRMA cloud mask is at an early maturity level and is expected to improve in future versions of the AVHRMA data set. The biases of GOES12, GOES13 and GOES16 are also acceptable. For the V1.00 SLSTRA data set a simple cloud mask was used, which led to more negative biases due to missed clouds. This has improved with V3.00 of the data set, as the cloud mask was enhanced. The V1.00 HMWR_8 data set included in this validation cycle showed similar biases to MTSAT2 dataset at Heihe sites, but had lower RSTDs. The four SEVIRI data sets (SEVIR1 – SEVIR4) are analysed over the KIT stations only due to the spatial coverage of the data sets. They show low biases compared to the in situ data, with the exception of DAH_T_ station, which has a large spread in bias for all analysed data sets due to a strong seasonal cycle observed over that station. High positive biases were found for the two MW data sets over some stations, however, these data sets also view a larger area than the IR satellite sensors, with greater heterogeneity leading to larger biases. Furthermore, for the MW data sets the differences between daytime and night-time biases are smaller, as the local overflight time is close to sunset and sunrise.

It was also found that the biases as well as the RSTD varies significantly between the stations, which indicates that the satellite algorithms perform differently over different land covers, elevations and regions. For example, high RSTD are found over stations DAH_T and EVO___. These differences were further investigated by analysing the time series of biases over each station individually.


 land surface temperature cci	Product Validation Plan (PVP) <i>WP4 – DEL4.1</i>	Ref.: LST-CCI-D4.1-PVIR Version: 3.1 Date: 23-Jun-2023 Page: 90
--	---	--

For the validation of the in situ uncertainties, the total uncertainty of the validation is compared to the robust standard deviation of the bias for the same time period as the in situ validation. The results fit well over several stations, however, there are some stations located in a more heterogeneous surrounding (like TBL____) or with a larger influence of shadows (EVO____ station) or rainy seasons (DAH_T_ station) that showed larger differences between total uncertainty and RSTD. Concerning the satellite data sets, the CAMEL emissivity uncertainty might not be estimated well in all regions, and for the GEO data sets the assessment of the spatial uncertainty should be further investigated. For the MW data, the spatial uncertainty could not be determined due to the coarse spatial resolution of the data sets, which needs to be determined in the next phase of the LST_cci project.

For the second part of the presented validation, eleven satellite vs. satellite pairs were intercompared, being MOD11A-SEVIR2, MODISA-SEVIR2, ATSOP_-SEVIR2, ATSR_3-SEVIR2, MOD11T-SEVIR2, and MODIST-SEVIR2, ATSR_3-MOD11T, ATSR_3-MODIST, MODIST-ATSOP_, SLSTRA-SEVIR4, and SLSTRB-SEVIR4. They were matched globally, and the analysis was performed for each continent. The intercomparisons against SEVIR2 and SEVIR4 were carried out over Africa and Europe, as the SEVIRI instrument is flown on a geostationary satellite, and the data sets are not available globally. For the three other data pairs, intercomparisons over Antarctica, Asia, Australia, North America and South America were also analysed. All intercomparisons were carried out for a time period of 2008 – 2010 to coincide with the SEVIR2 data availability, with the exception of the SLSTRA-SEVIR4 and SLSTRB-SEVIR4, which were analysed for 2018 – 2020, due to the data availability of the SLSTR data sets. Monthly time series of differences are analysed, and additional metrics were obtained from investigating further the dependence of the differences on the elevation, land cover classes, satellite angles, and number of averaged data points.

It was found that for daytime data, ATSR_3-MODIST performed better than ATSR_3-MOD11T, also the differences for ATSR_3-MOD11T decreased for V3.00 of ATSR_3. During night-time, high differences were often found for MODIST-ATSOP_. MOD11A-SEVIR2 and MOD11T-SEVIR2 have more negative differences than MODISA-SEVIR2 and MODIST-SEVIR2, which indicates that MOD11T has in general lower LST values than MODIST. ATSR_3-SEVIR2 tends to have more positive differences, with MODIST-ATSOP_ showing more negative and absolute higher differences during day and a stronger seasonal cycle. The differences for SLSTRA-SEVIR4 and SLSTRB-SEVIR4 are mainly within a ± 2 K range. Over Africa, the differences between the results were larger during night, whereas over Europe, they were larger during day. For the three data sets analysed over all continents, larger differences were found over Asia and South America. The results over the single continents showed that the additional analysis for elevation angles, land cover classes and satellite angles can give valuable further insights into the differences.

Overall, from the in situ validation it can be concluded that in the third round of validation within LST_cci, that the data sets perform well, especially during night. Same results were provided for the data-sets validated in the second round of validation, since only one year more of data are available. Thus, in comparison with the first round of validation, an improvement was found for ATSR_2, ATSR_3, MODISA, MODIST and SLSTRA. Two new data sets were added to the analysis: AVHRMA and HMWR_8, which showed a good agreement with in situ data at night-time. Furthermore, ATSR_3 and MODIST seem to be well correlated even though their retrieval algorithms are different. The additional intercomparisons revealed that the LEO IR LST_cci products are more comparable with the SEVIRI LST_cci products than the corresponding operational products, with differences generally < 2 K, which is within the corresponding uncertainty range of the SEVIRx products.

 land surface temperature cci	Product Validation Plan (PVP) <i>WP4 – DEL4.1</i>	Ref.: LST-CCI-D4.1-PVIR Version: 3.1 Date: 23-Jun-2023 Page: 91
--	---	--

6. Recommendations for the next Processing Cycle

In this section, important points that should be considered when developing a LST data set are summarized for producers of LST data sets. They are drawn from the validation work within LST_cci presented in this report, where the comparisons of several LST data sets with in situ data sets as well as with other operational satellite data sets are presented.

First of all, it is very helpful if all important information on the data set is presented with the data set itself in form of comprehensive metadata, which can easily be done using the netCDF data format.

In this work, we found that different LST data set perform differently over different land cover classes, over different regions, elevation heights or in different climatic zones. Thus, it is best to validate the developed data sets over many different stations or in different regions to better understand their performance. Results of the validation analysis should be presented in a statistical meaningful way, i.e. using the median instead of the mean and robust standard deviation instead of standard deviation so as to provide more representative results without single, large outliers having undue influence.

It is also advisable to validate the produced data sets for different time periods or over a long time period dependent on data availability to see if there are drifts or step changes in the LST data over time.

Comparisons of the LST_cci data sets with other data sets, either in direct intercomparisons, or by comparing differences from different satellite data sets with the same in situ data, can give further insights in the performance of the data set. One can distinguish where the differences to other data sets are large, and where they give similar results, and investigate this further.

It is also helpful to compare the LST_cci data sets with other LST data sets that are derived from the same satellite instrument but with a different algorithm. This analysis can show how large the influence of algorithm formulation is on the resulting LST product.

Additional analysis of biases or differences and RSTD with respect to different viewing angles, topography and land covers can further help to understand the LST_cci data sets over special regions.

Finally, if large negative biases between the satellite and in situ LST data are found in the validation, this might be due to missed clouds in the satellite data set and should be investigated further by the data providers.

7. Appendix

7.1. Africa

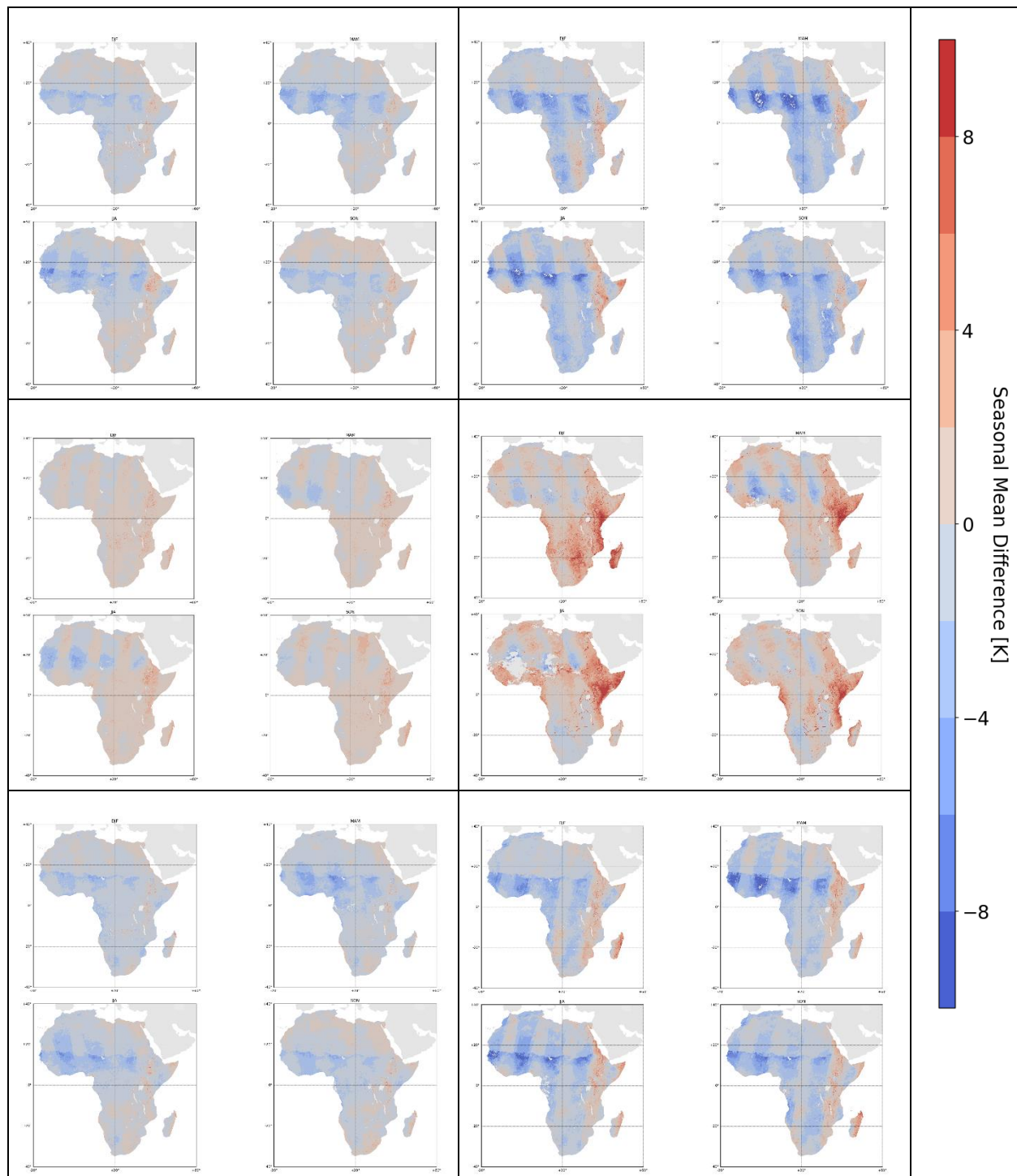


Figure 62: Seasonal mean differences of LST_{satellite 1} – LST_{satellite 2} in K; left row displays night-time and right row daytime data. Upper plots are for MOD11A-SEVIR2, middle plots for MODISA-SEVIR2, and lower plots for MOD11T-SEVIR2.

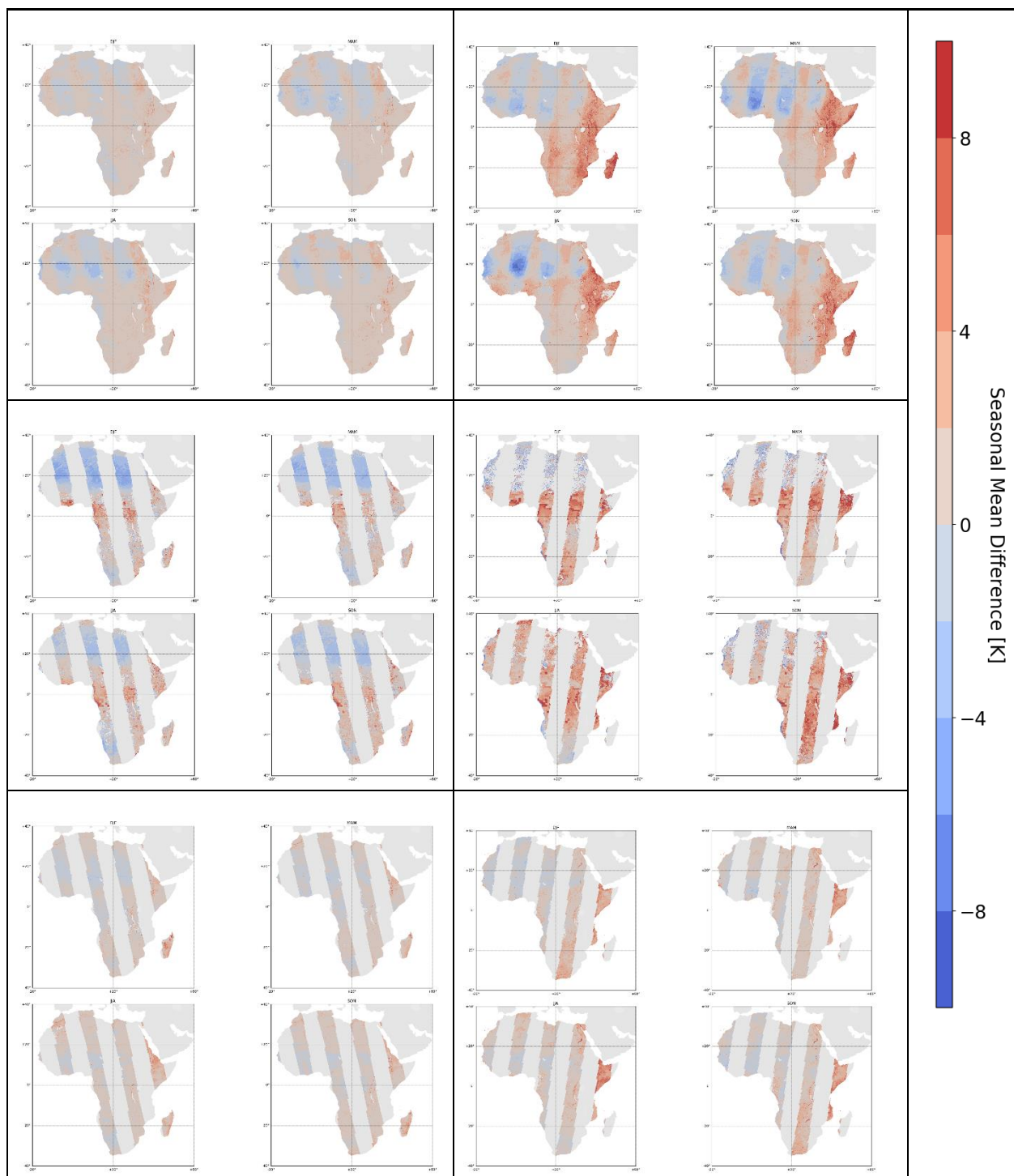


Figure 63: Seasonal mean differences of LST_satellite 1 – LST_satellite 2 in K; left row displays night-time and right row daytime data. Upper plots are for MODIST-SEVIR2, middle plots for ATSOP-SEVIR2, and lower plots for ATSR_3-SEVIR2.

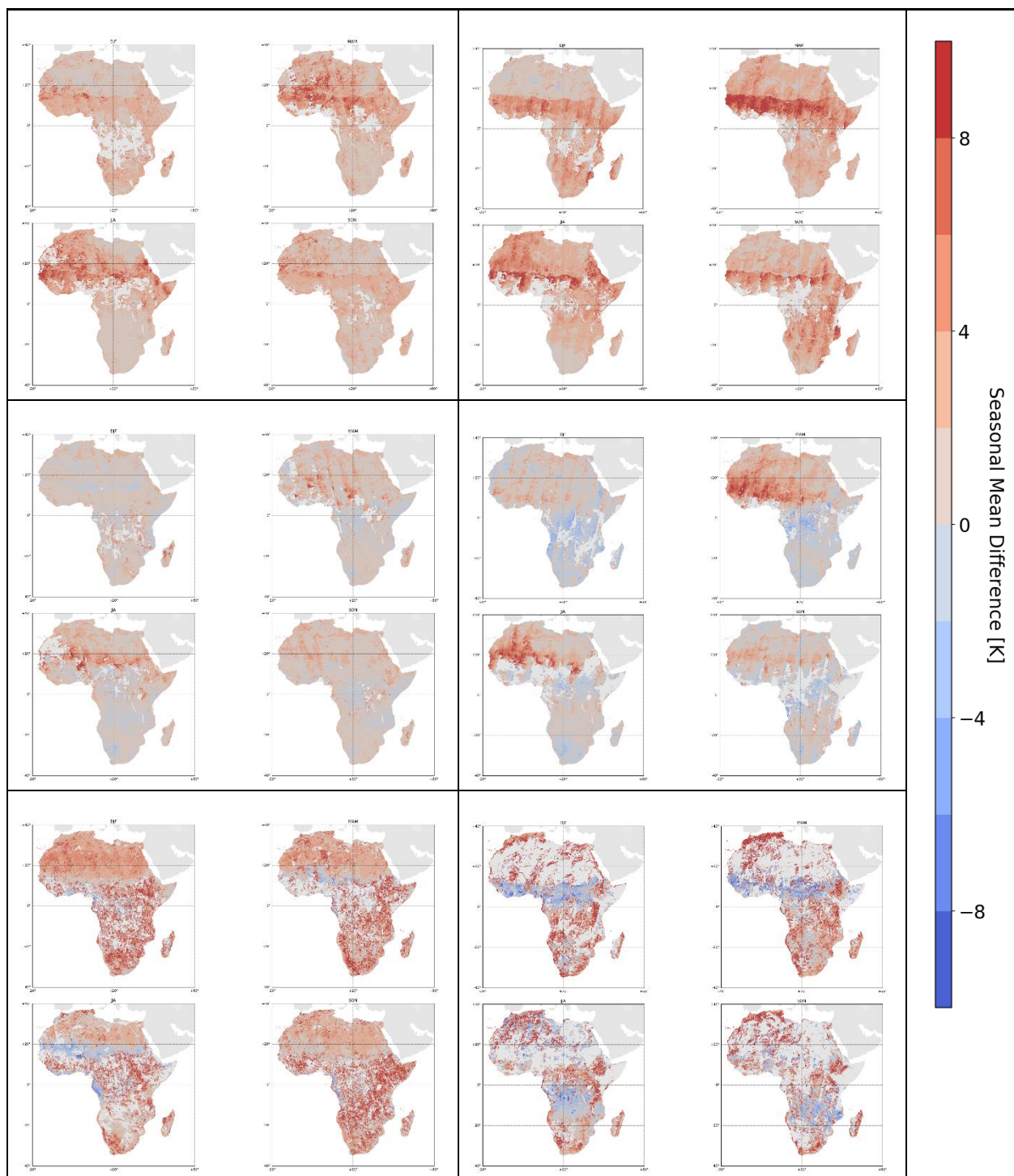


Figure 64: Seasonal mean differences of LST_satellite 1 – LST_satellite 2 in K; left row displays night-time and right row daytime data. Upper plots are for ATSR_3-MOD11T, middle plots for ATSR_3-MODIST, and lower plots for MODIST-ATSOP_.

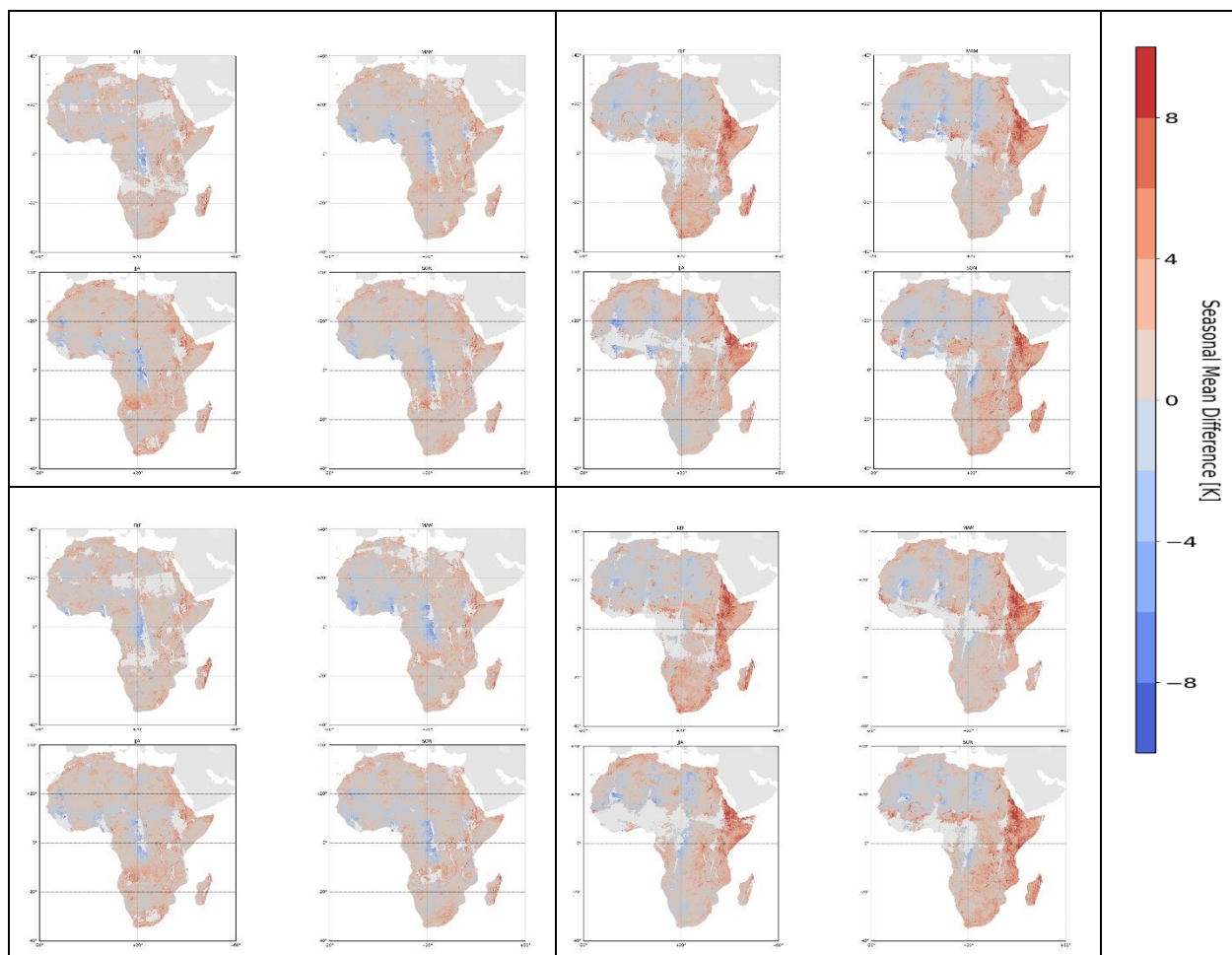


Figure 65: Seasonal mean differences of LST_satellite 1 – LST_satellite 2 in K; left row displays night-time and right row daytime data. Upper plots are for SLSTRA-SEVIR4, middle plots for SLSTRB-SEVIR4, for the years 2018 - 2020.

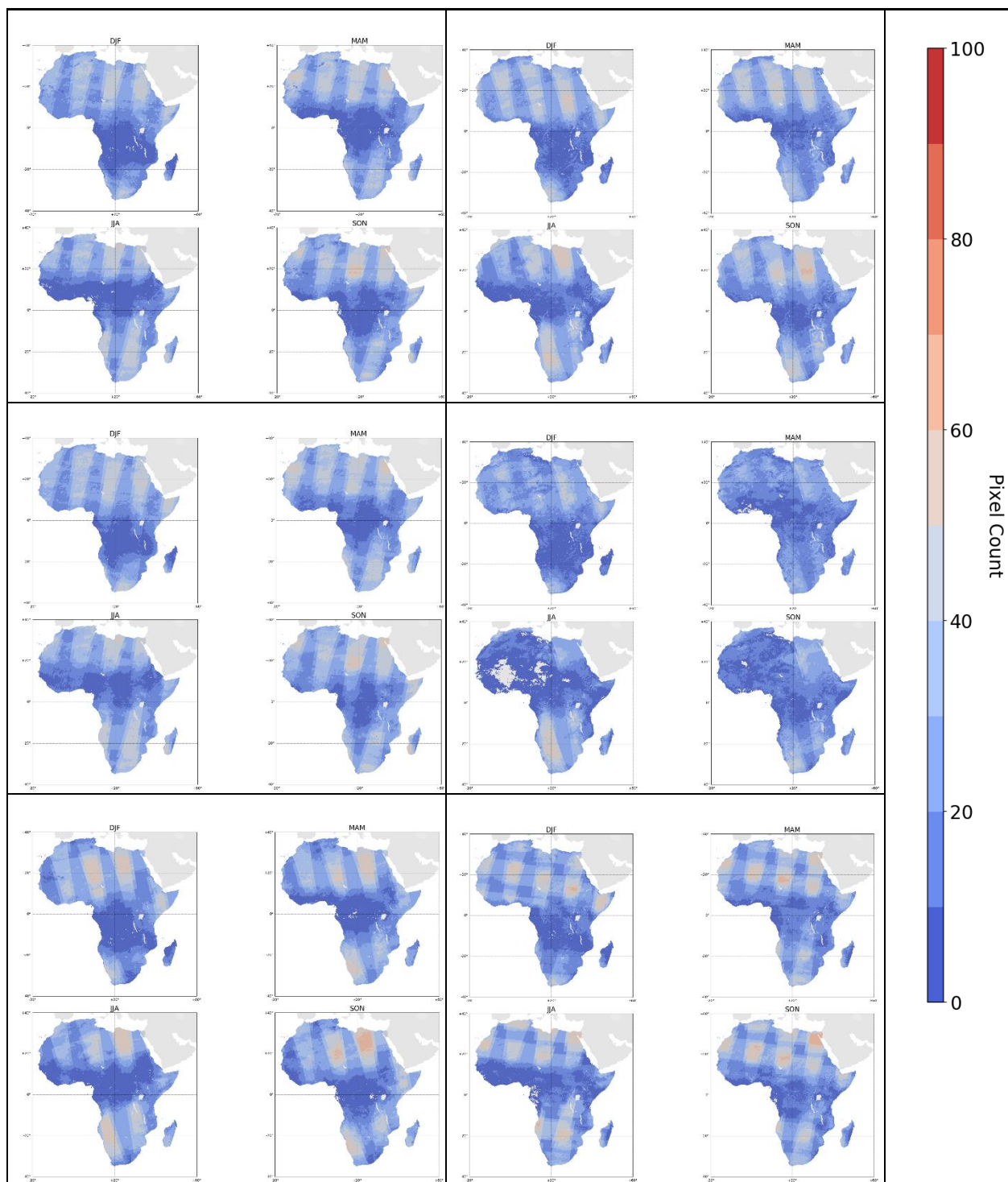


Figure 66: Number of seasonal averaged data points per pixel; left row displays night-time and right row daytime data. Upper plots are for MOD11A-SEVIR2, middle plots for MODISA-SEVIR2, and lower plots for MOD11T-SEVIR2.

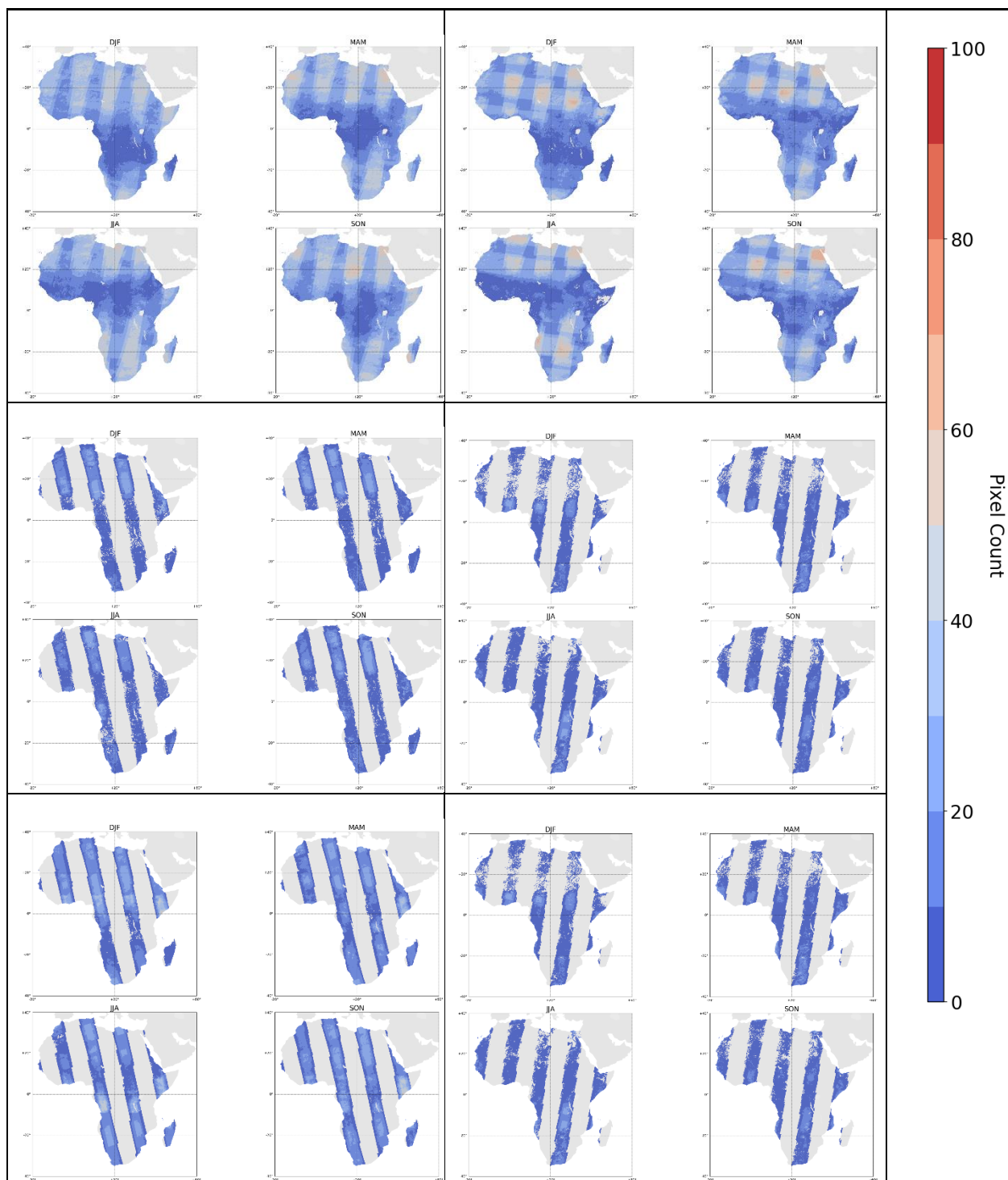


Figure 67: Number of seasonal averaged data points per pixel; left row displays night-time and right row daytime data. Upper plots are for MODIST-SEVIR2, middle plots for ATSOP-SEVIR2, and lower plots for ATSR_3-SEVIR2.

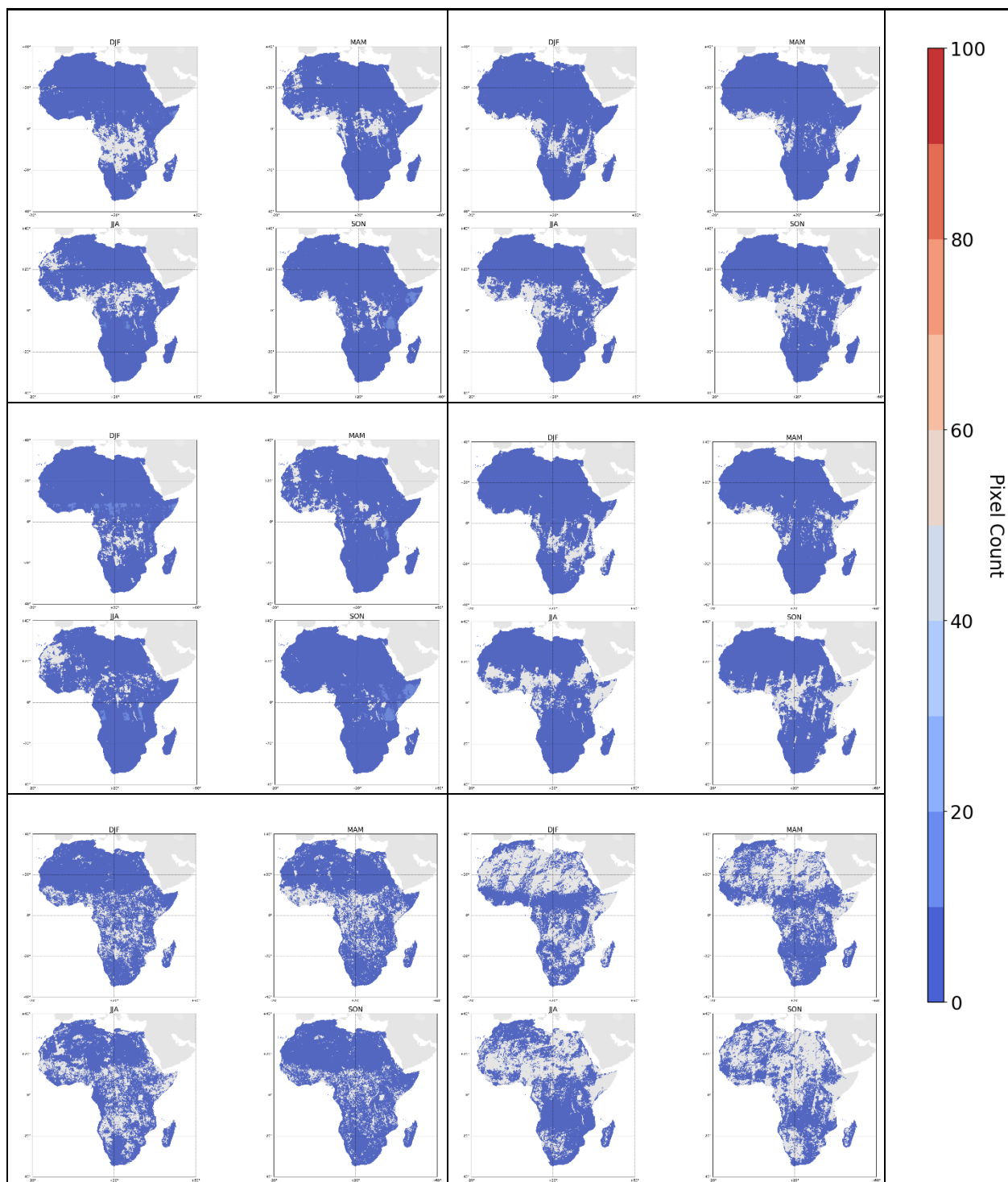


Figure 68: Number of seasonal averaged data points per pixel; left row displays night-time and right row daytime data. Upper plots are for ATSR_3-MOD11T, middle plots for ATSR_3-MODIST, and lower plots for MODIST-ATSOP_.

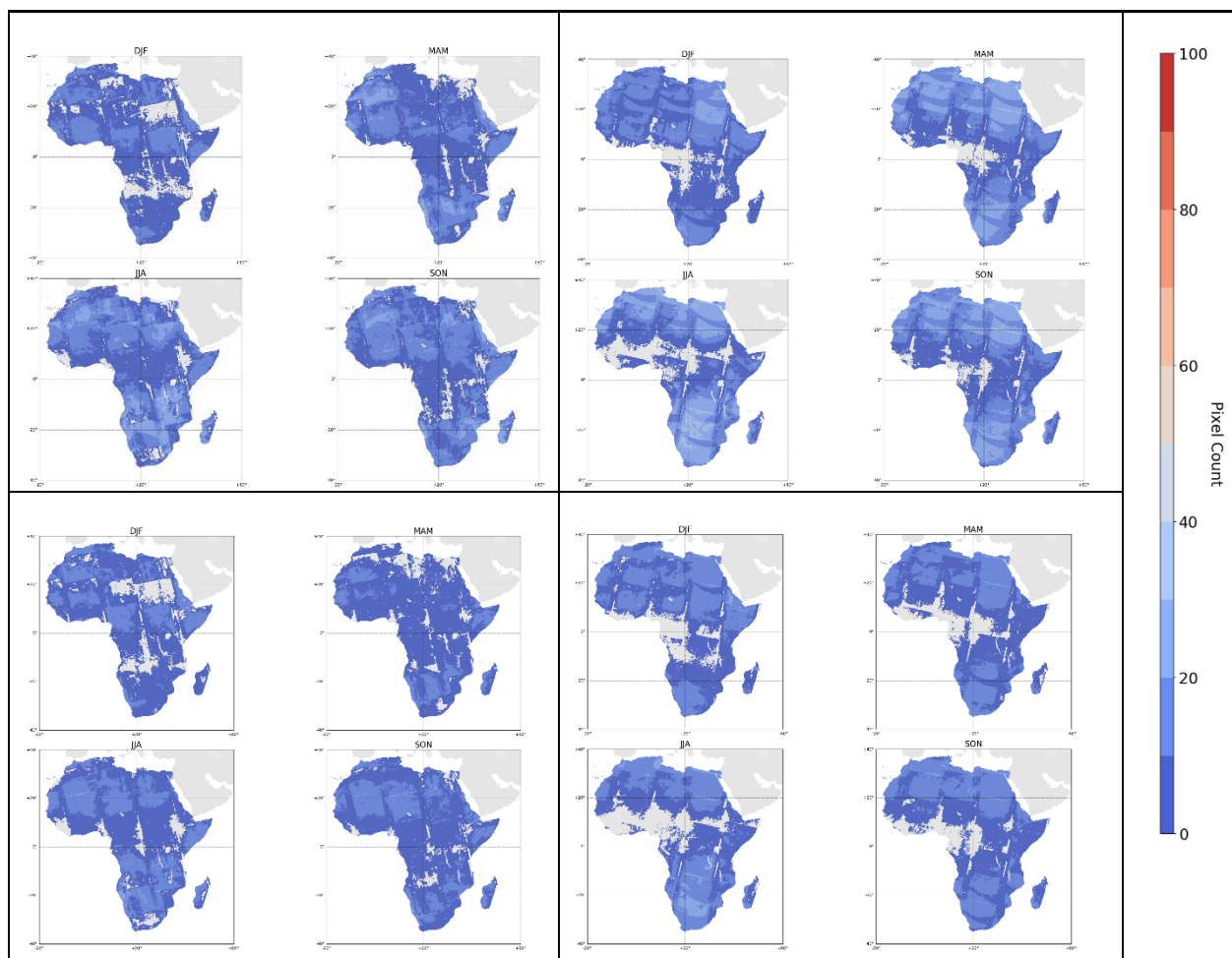


Figure 69: Number of seasonal averaged data points per pixel; left row displays night-time and right row daytime data. Upper plots are for SLSTRA-SEVIR4, middle plots for SLSTRB-SEVIR4, for the years 2018 - 2020.

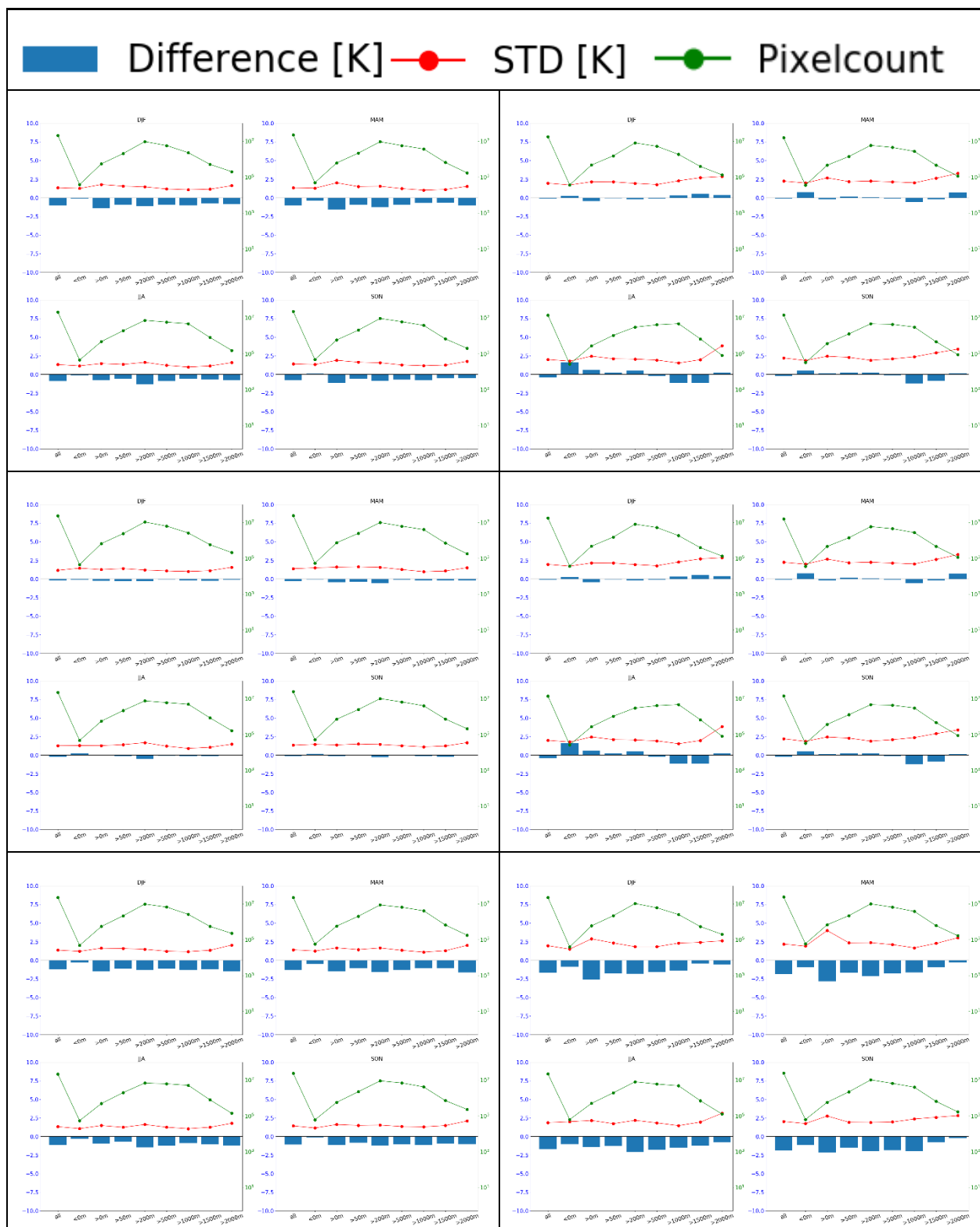


Figure 70: Seasonal differences for different elevation classes; blue bars are the median differences, red points the RSTD and the green points on the right axis show the number of averaged data points Left row displays night-time and right row daytime data. Upper plots are for MOD11A-SEVIR2, middle plots for MODISA-SEVIR2, and lower plots for MOD11T-SEVIR2.

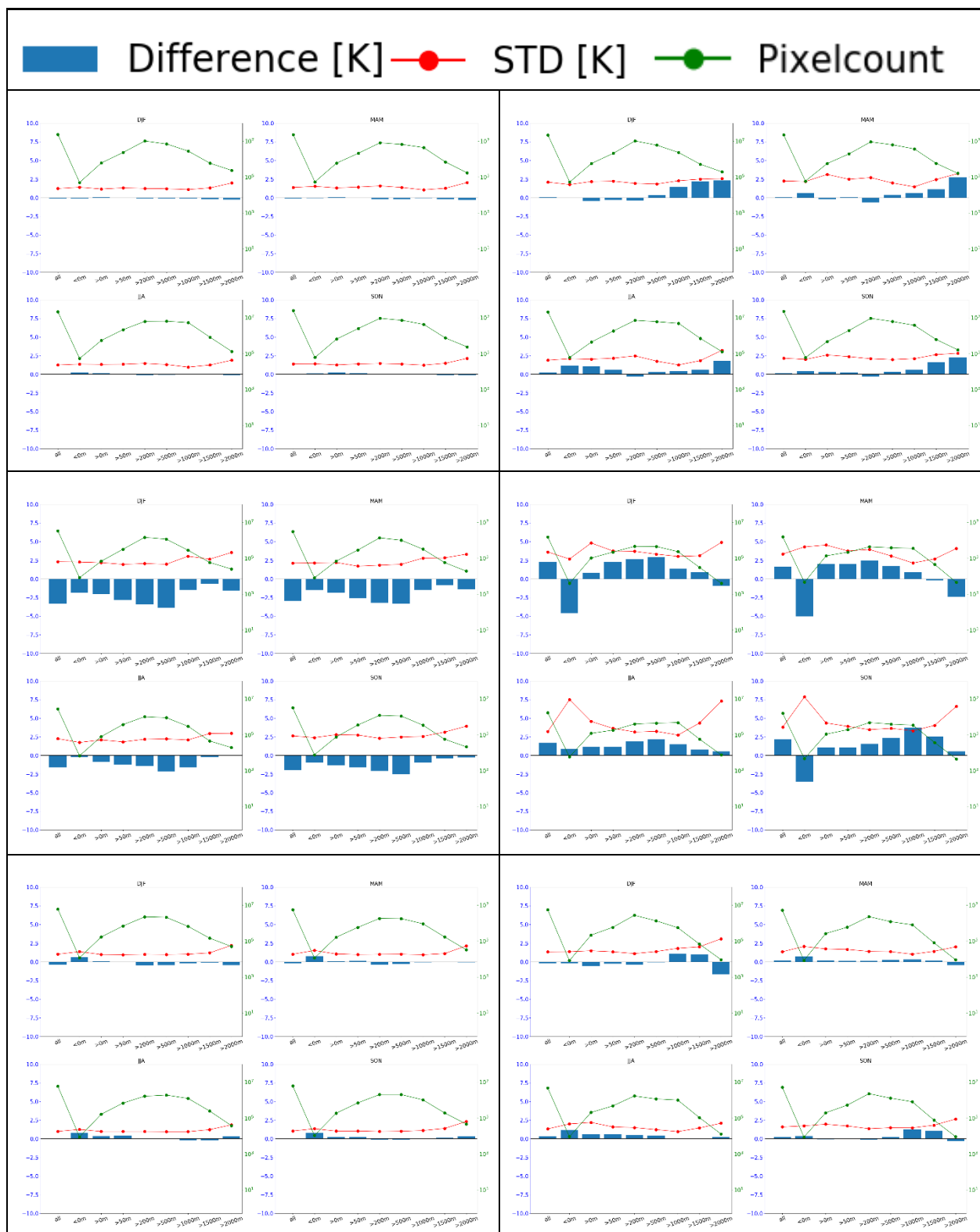


Figure 71: Seasonal differences for different elevation classes; blue bars are the median differences, red points the RSTD and the green points on the right axis show the number of averaged data points Left row displays night-time and right row daytime data. Upper plots are for MODIST-SEVIR2, middle plots for ATSOP-SEVIR2, and lower plots for ATSR_3-SEVIR2.

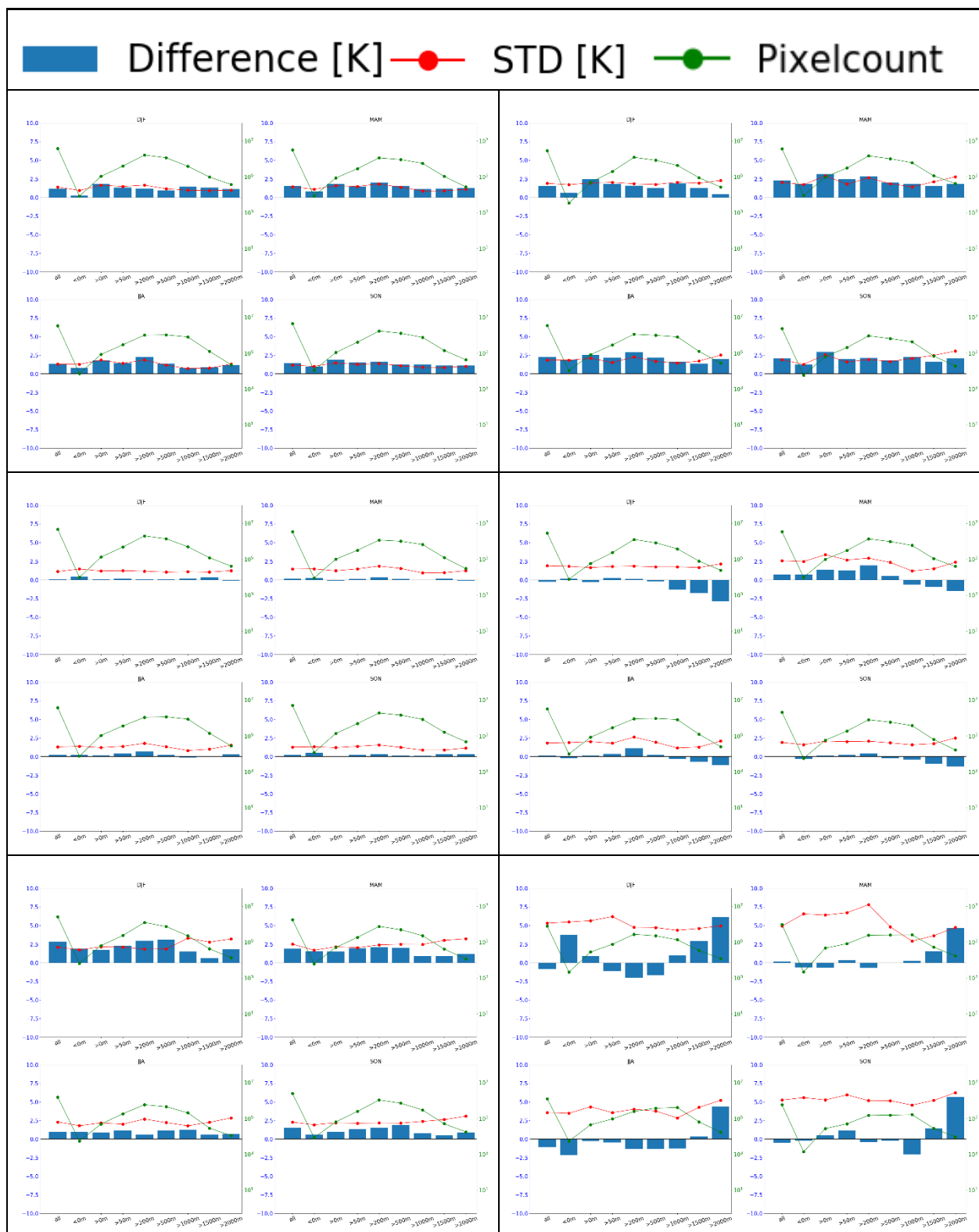


Figure 72: Seasonal differences for different elevation classes; blue bars are the median differences, red points the RSTD and the green points on the right axis show the number of averaged data points Left row displays night-time and right row daytime data. Upper plots are for ATSR_3-MOD11T, middle plots for ATSR_3-MODIST, and lower plots for MODIST-ATRSOP_.

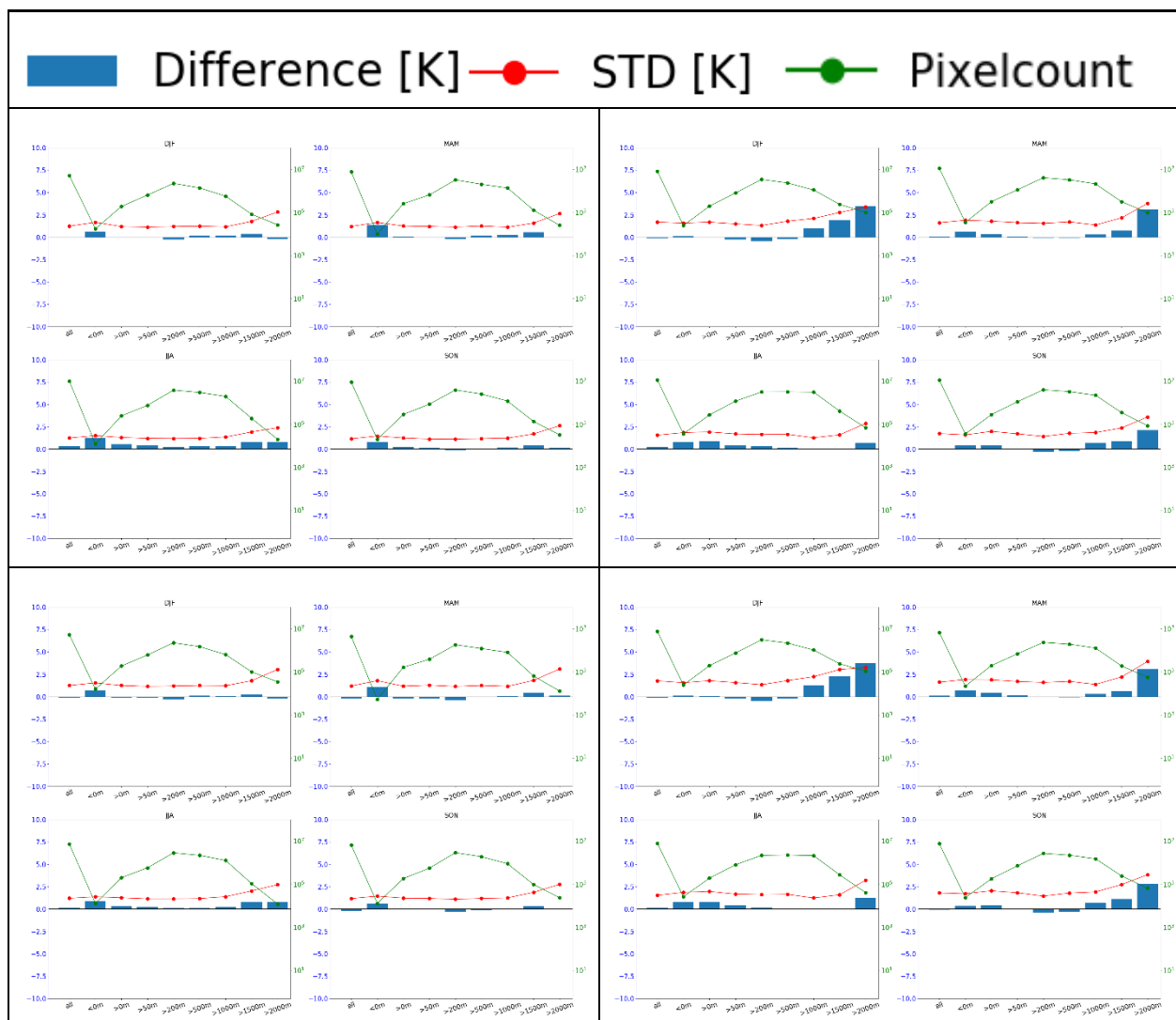


Figure 73: Seasonal differences for different elevation classes; blue bars are the median differences, red points the RSTD and the green points on the right axis show the number of averaged data points Left row displays night-time and right row daytime data. Upper plots are for SLSTRA-SEVIR4, middle plots for SLSTRB-SEVIR4, for the years 2018 - 2020.

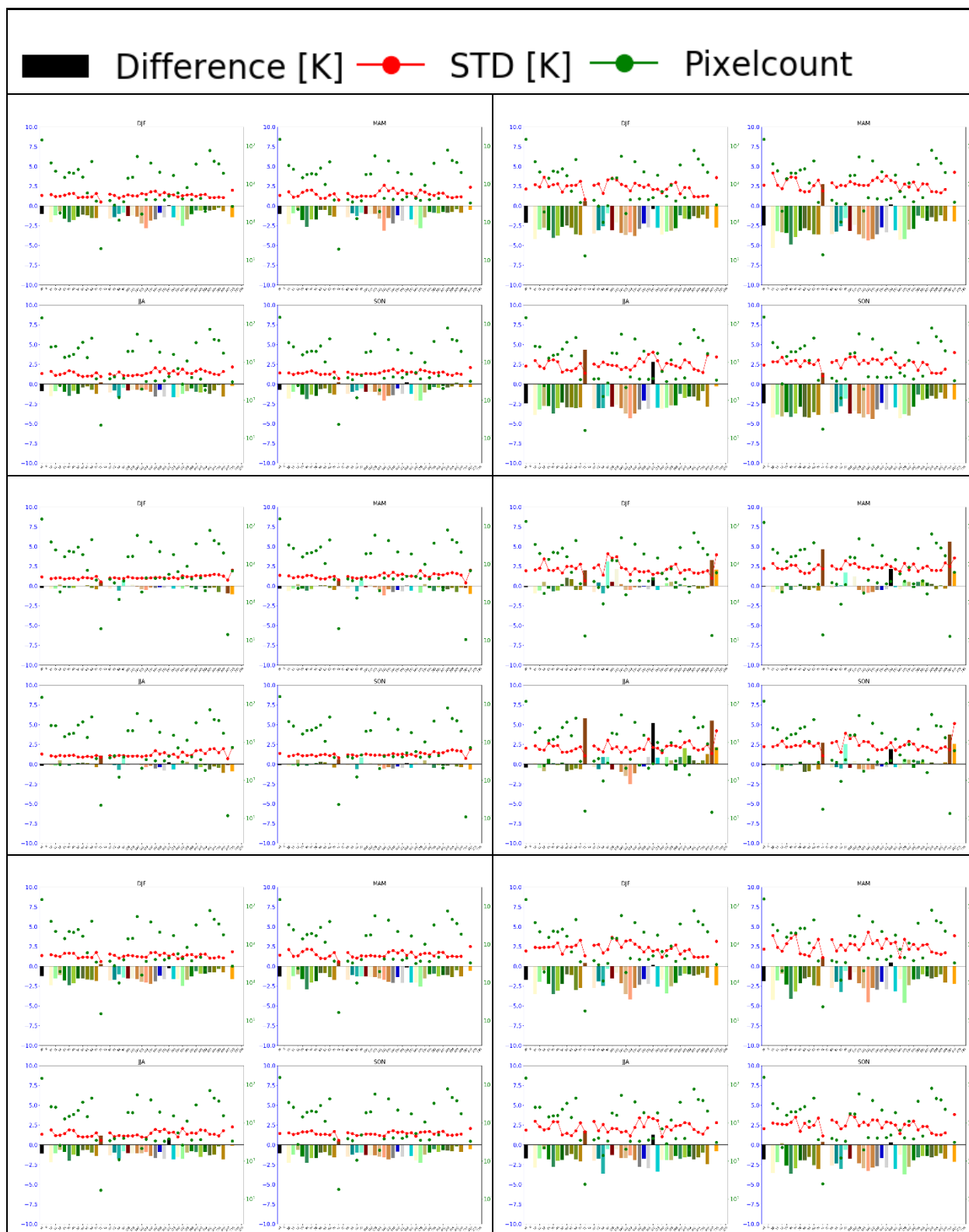


Figure 74: Seasonal differences for different land cover classes; coloured bars are the differences, red points the RSTD and the green points on the right axis show the number of averaged data points. Left row displays night-time and right row daytime data. Upper plots are for MOD11A-SEVIR2, middle plots for MODISA-SEVIR2, and lower plots for MOD11T-SEVIR2.



Figure 75: Seasonal differences for different land cover classes; coloured bars are the differences, red points the RSTD and the green points on the right axis show the number of averaged data points. Left row displays night-time and right row daytime data. Upper plots are for MODIST-SEVIR2, middle plots for ATSR_3-SEVIR2, and lower plots for ATSR_3-SEVIR2.



Figure 76: Seasonal differences for different land cover classes; coloured bars are the differences, red points the RSTD and the green points on the right axis show the number of averaged data points. Left row displays night-time and right row daytime data. Upper plots are for ATSR_3-MOD11T, middle plots for ATSR_3-MODIST, and lower plots for MODIST-ATSOP_.

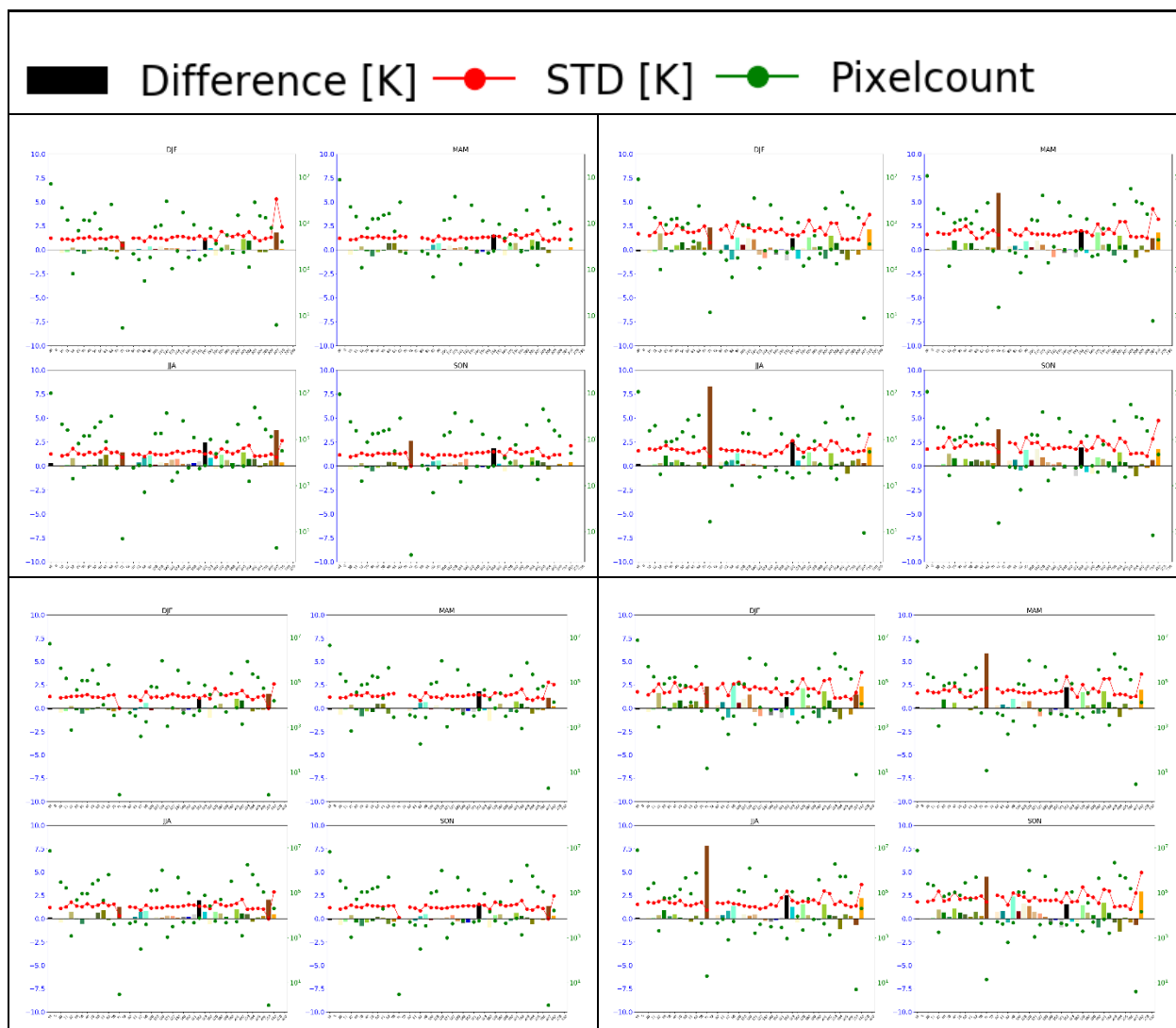


Figure 77: Seasonal differences for different land cover classes; coloured bars are the differences, red points the RSTD and the green points on the right axis show the number of averaged data points. Left row displays night-time and right row daytime data. Upper plots are for SLSTRA-SEVIR4, middle plots for SLSTB-SEVIR4, for the years 2018 – 2020.

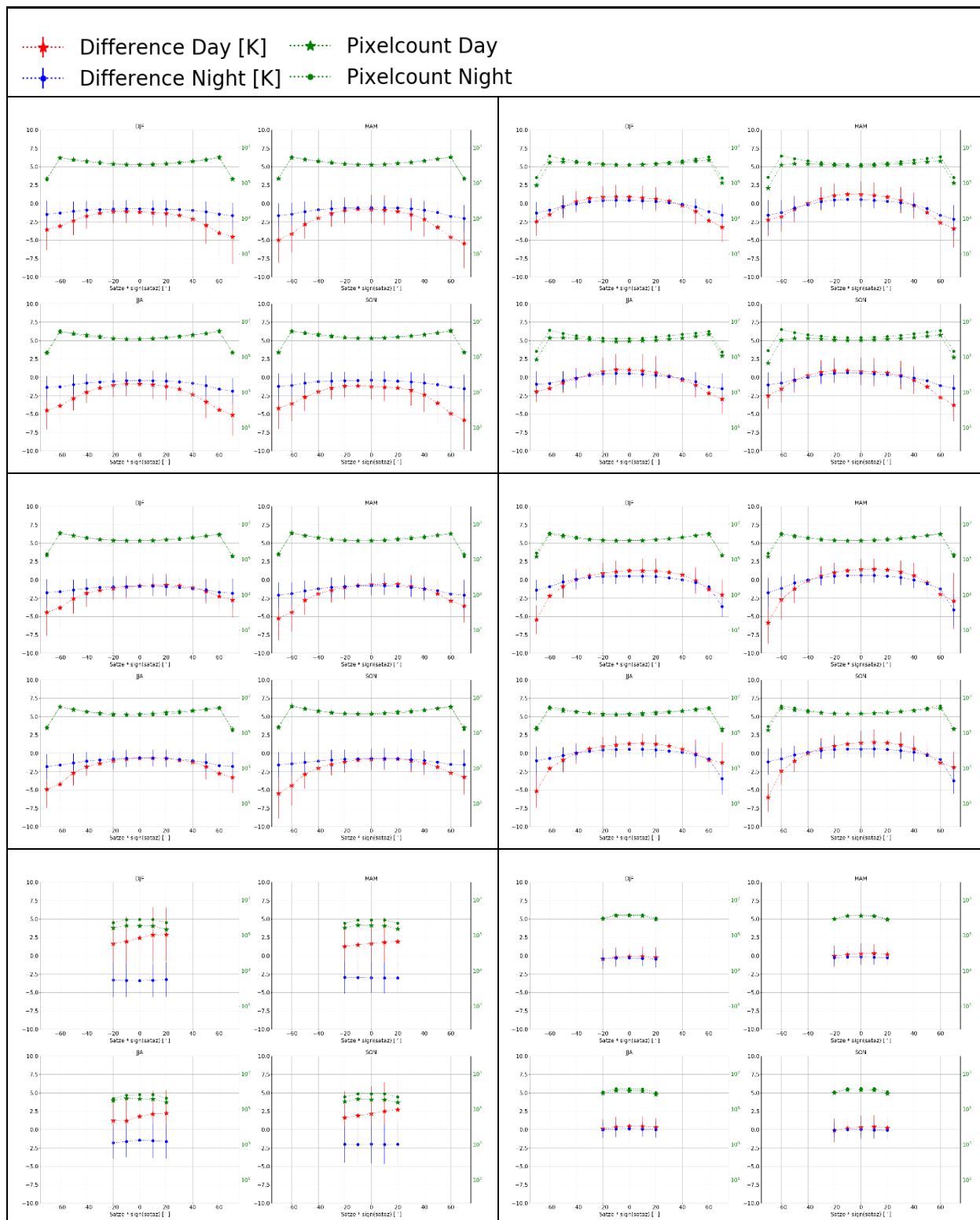


Figure 78: Seasonal differences versus $\text{satze} \cdot \text{sign}(\text{sataz})$ of satellite_1 ; red stars represent the daytime data, blue dots the night-time data, and the green stars and dots on the right axis display the averaged pixel numbers for daytime and night-time data. Upper left plot displays MOD11A-SEVIR2, upper right MODISA-SEVIR2, middle left MOD11T-SEVIR2, middle right MODIST-SEVIR2, lower left ATSOP_-SEVIR2, and lower right ATSR_3-SEVIR2.

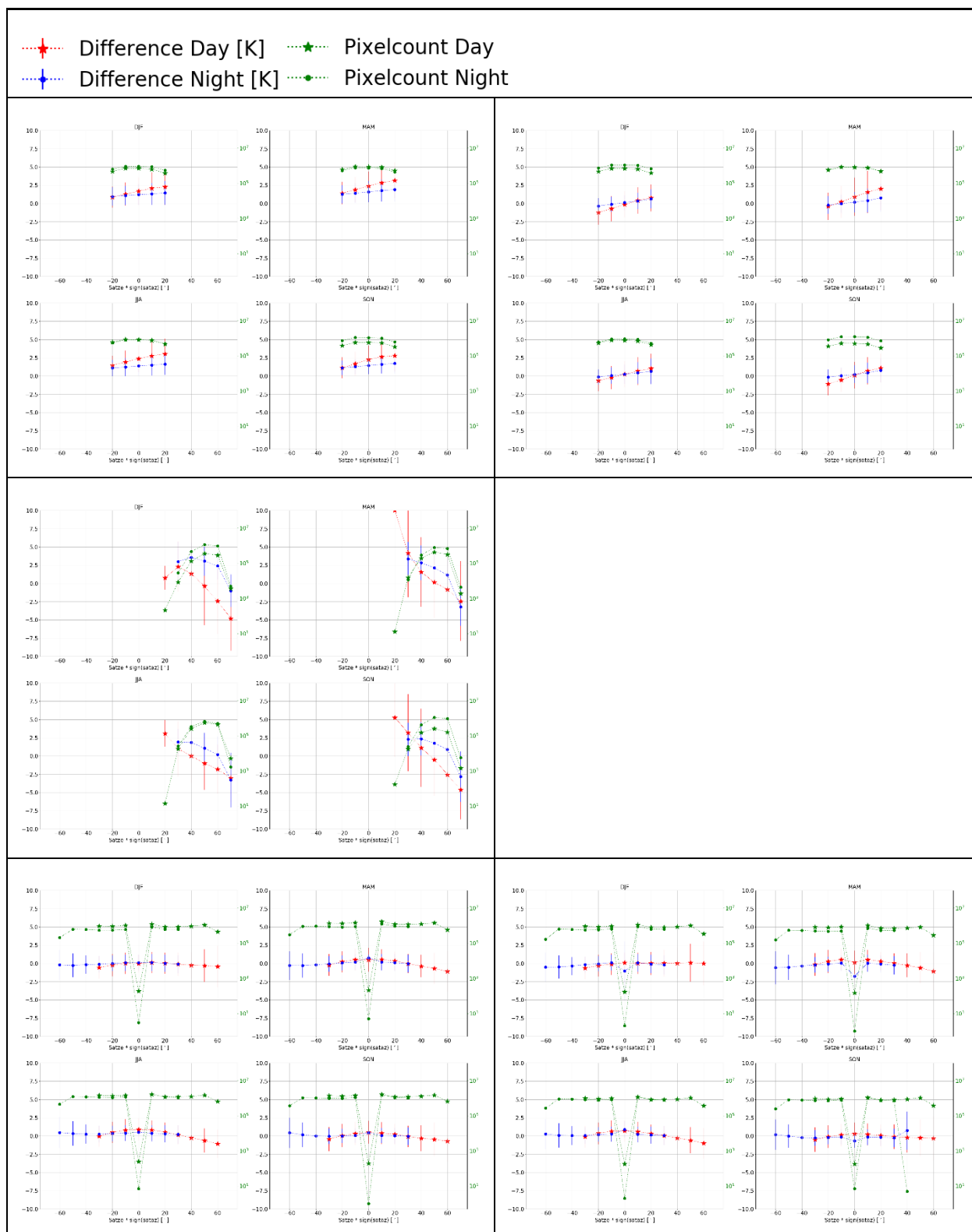


Figure 79: Seasonal differences versus $\text{satze} \cdot \text{sign}(\text{sataz})$ of satellite_1 ; red stars represent the daytime data, blue dots the night-time data, and the green stars and dots on the right axis display the averaged pixel numbers for daytime and night-time data. Upper left plot displays ATSR_3-MOD11T, upper right ATSR_3-MODIST, middle left MODIST-ATSOP_, lower left SLSTRA-SEVIR4, lower right SLSTRB-SEVIR4.

7.2. Antarctica

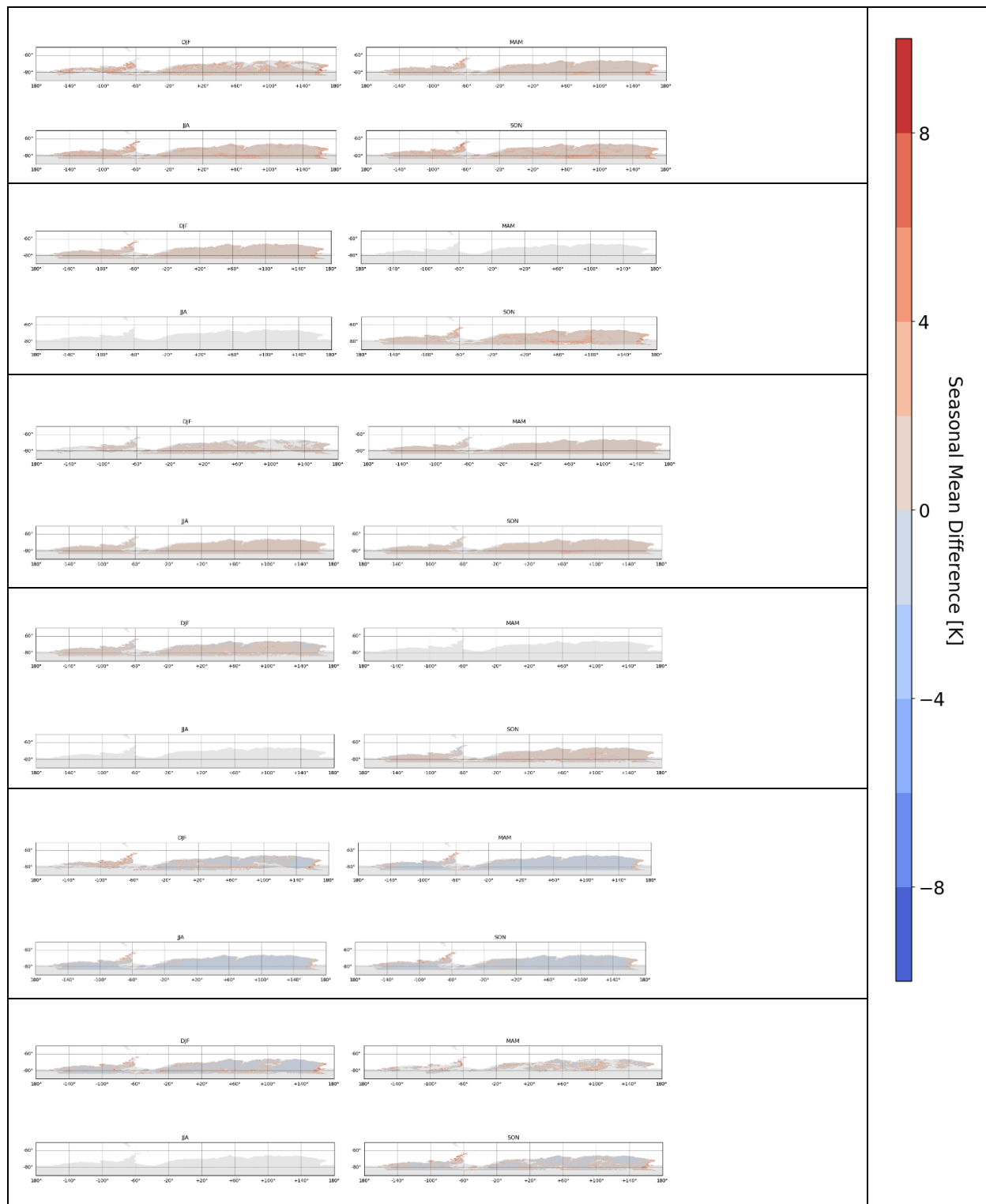


Figure 80: Seasonal mean differences of LST_satellite 1 – LST_satellite 2 in K; two upmost plots are for ATSR_3-MOD11T, two middle plots for ATSR_3-MODIST, and two lowest plots for MODIST-ATSOP_, each time for night-time and daytime data, respectively.

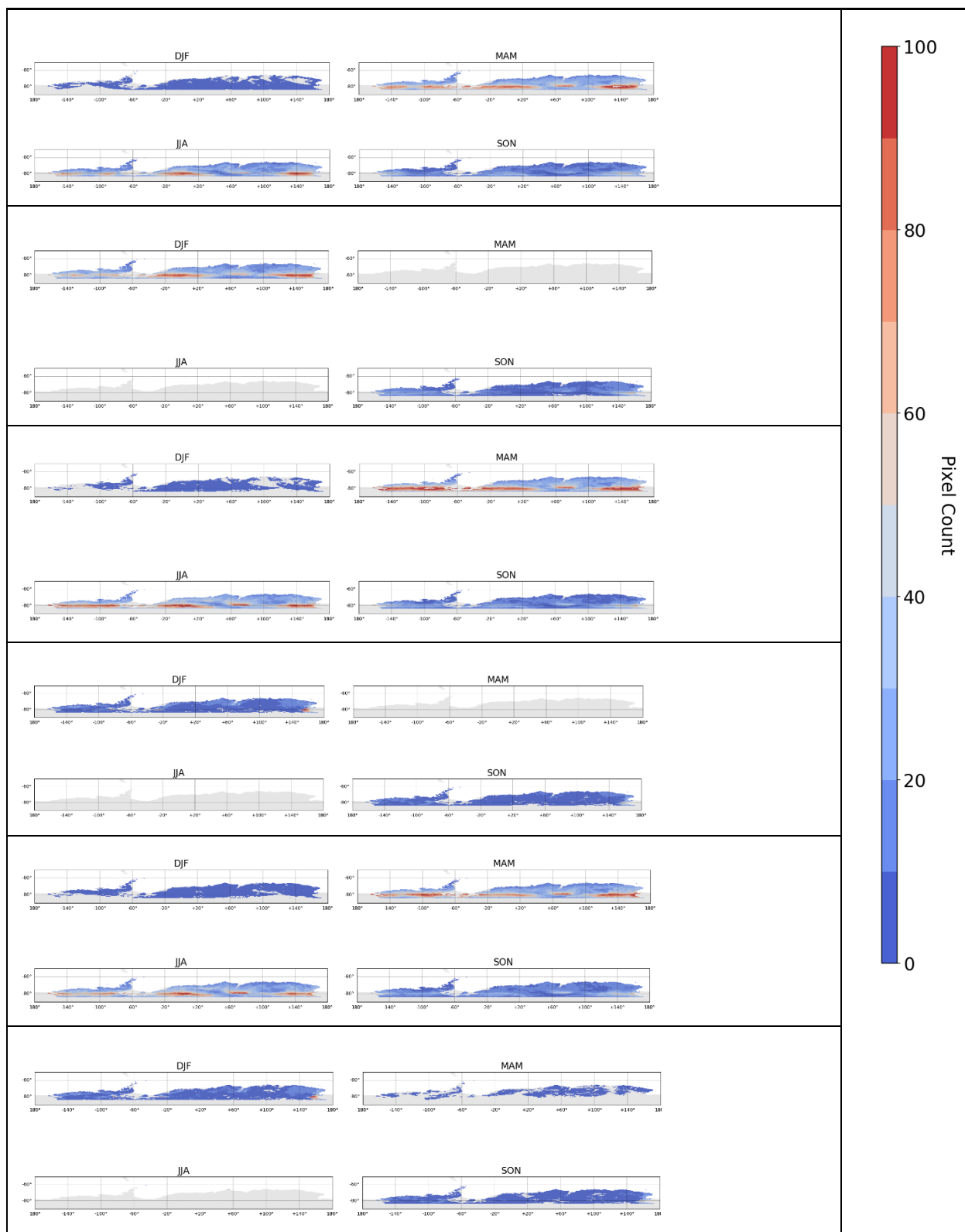


Figure 81: Number of seasonal averaged data points per pixel; two upmost plots are for ATSR_3-MOD11T, two middle plots for ATSR_3-MODIST, and two lowest plots for MODIST-ATSOP_. Each time for night-time and daytime data, respectively.

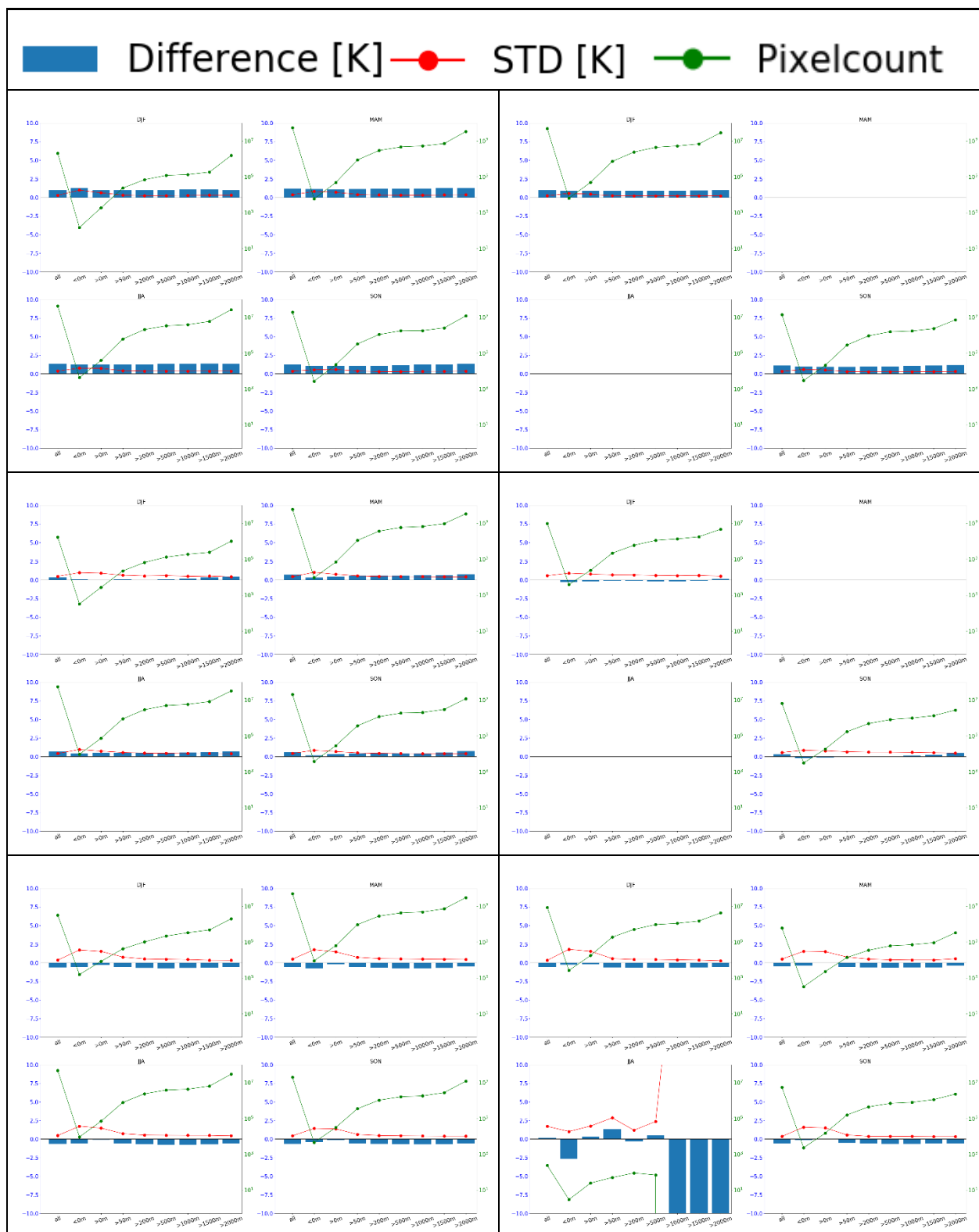


Figure 82: Seasonal differences for different elevation classes; blue bars are the median differences, red points the RSTD and the green points on the right axis show the number of averaged data points Left row displays night-time and right row daytime data. Upper plots are for ATSR_3-MOD11T, middle plots for ATSR_3-MODIST, and lower plots for MODIST-ATSOP_.

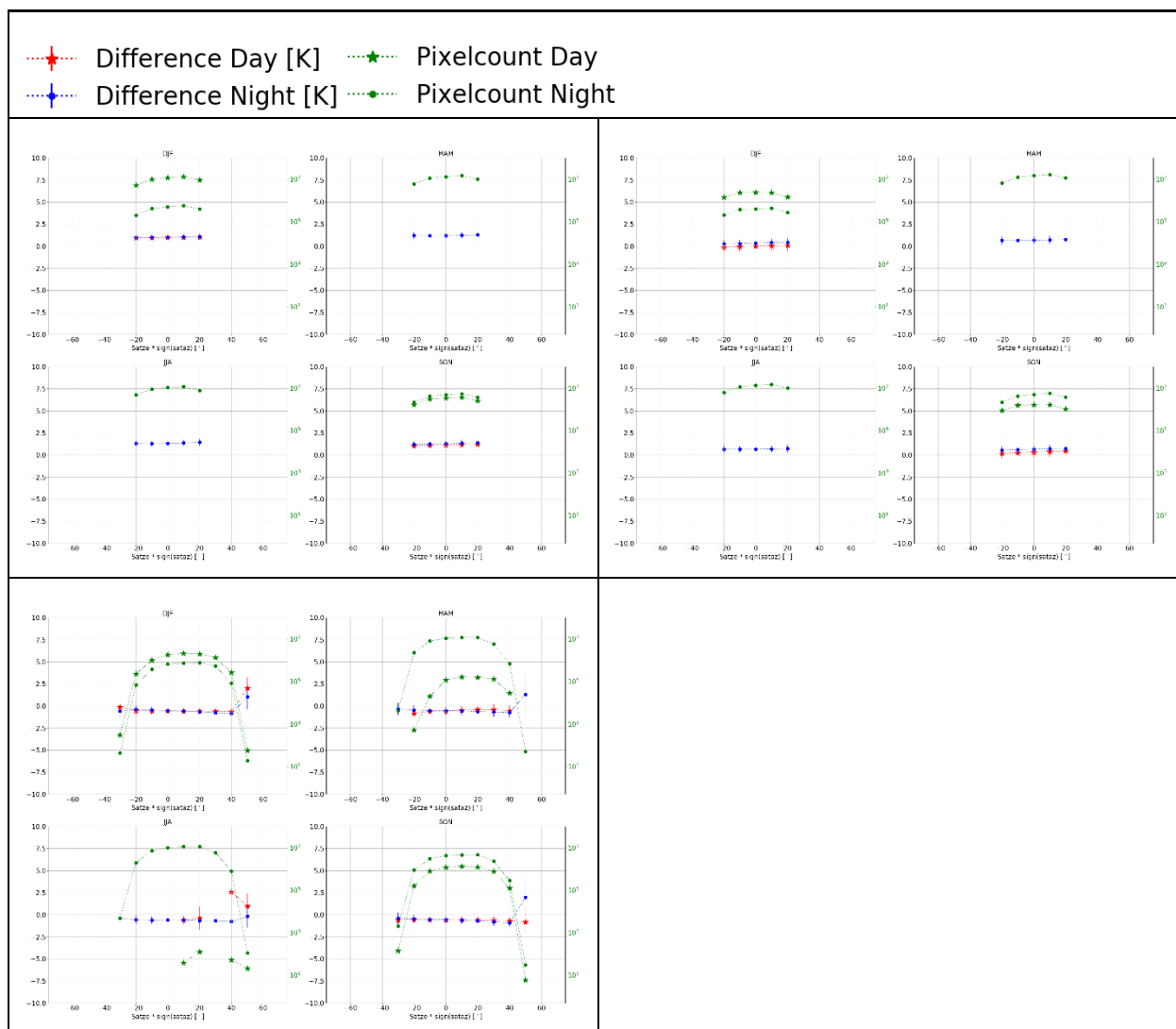


Figure 83: Seasonal differences versus $\text{satze} \cdot \text{sign}(\text{sataz})$ of satellite_1 ; red stars represent the daytime data, blue dots the night-time data, and the green stars and dots on the right axis display the averaged pixel numbers for daytime and night-time data. Upper left plot displays ATSR_3-MOD11T, upper right ATSR_3-MODIST, lower left MODIST-ATSOP_.

7.3. Asia

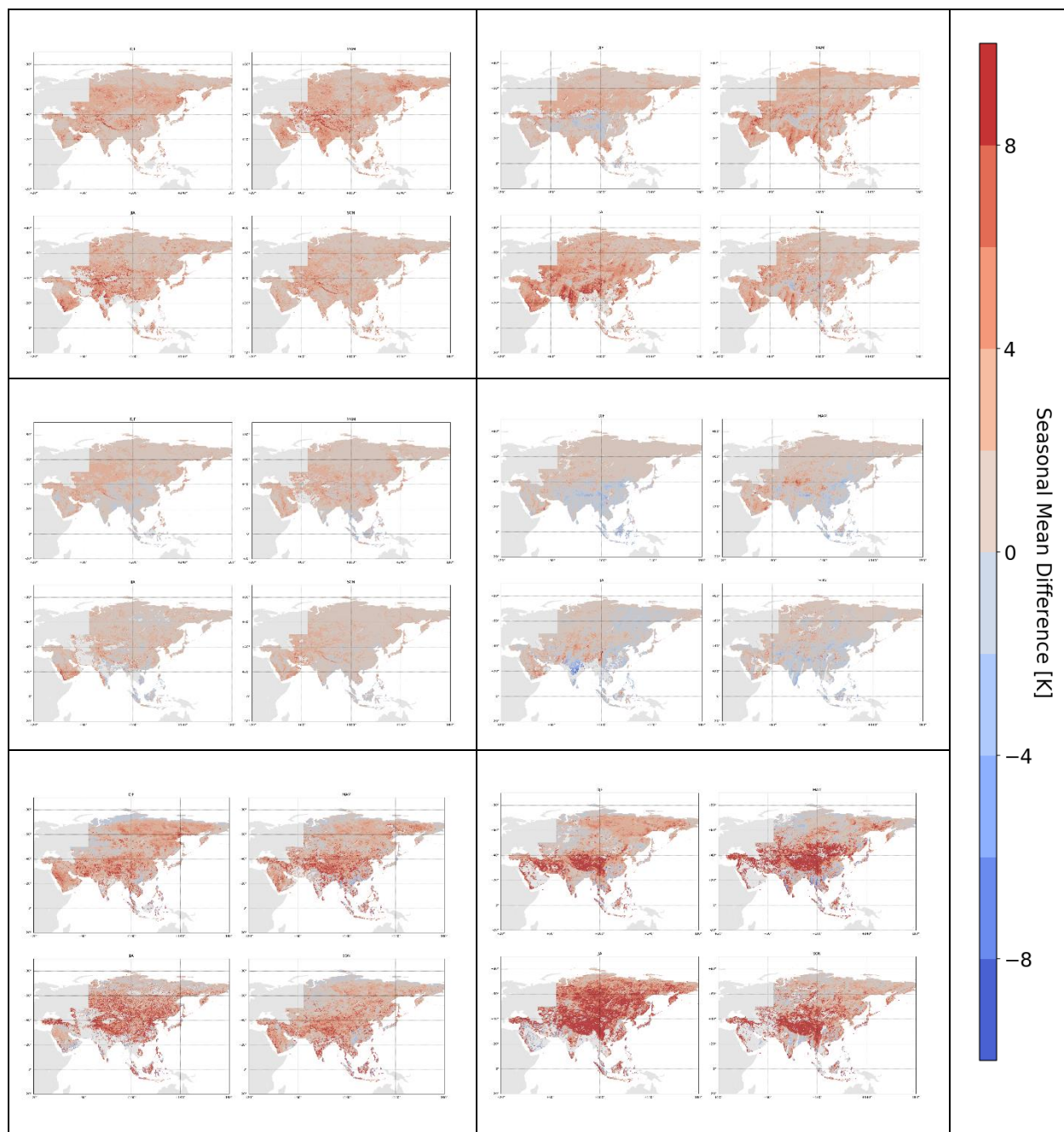


Figure 84: Seasonal mean differences of LST_satellite 1 – LST_satellite 2 in K; left row displays night-time and right row daytime data. Upper plots are for ATSR_3-MOD11T, middle plots for ATSR_3-MODIST, and lower plots for MODIST-ATSOP_.

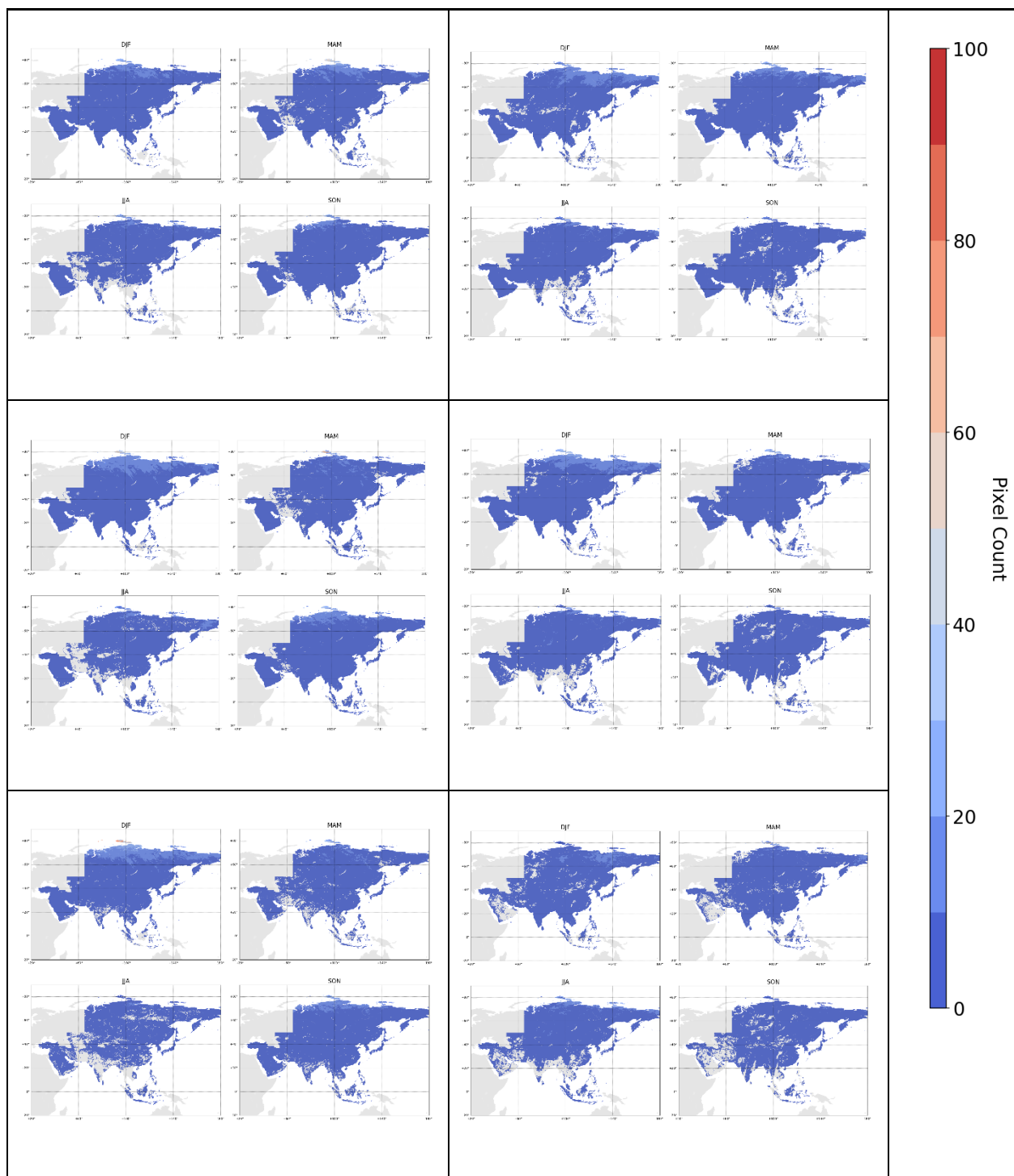


Figure 85: Number of seasonal averaged data points per pixel; left row displays night-time and right row daytime data. Upper plots are for ATSR_3-MOD11T, middle plots for ATSR_3-MODIST, and lower plots for MODIST-ATSOP_.

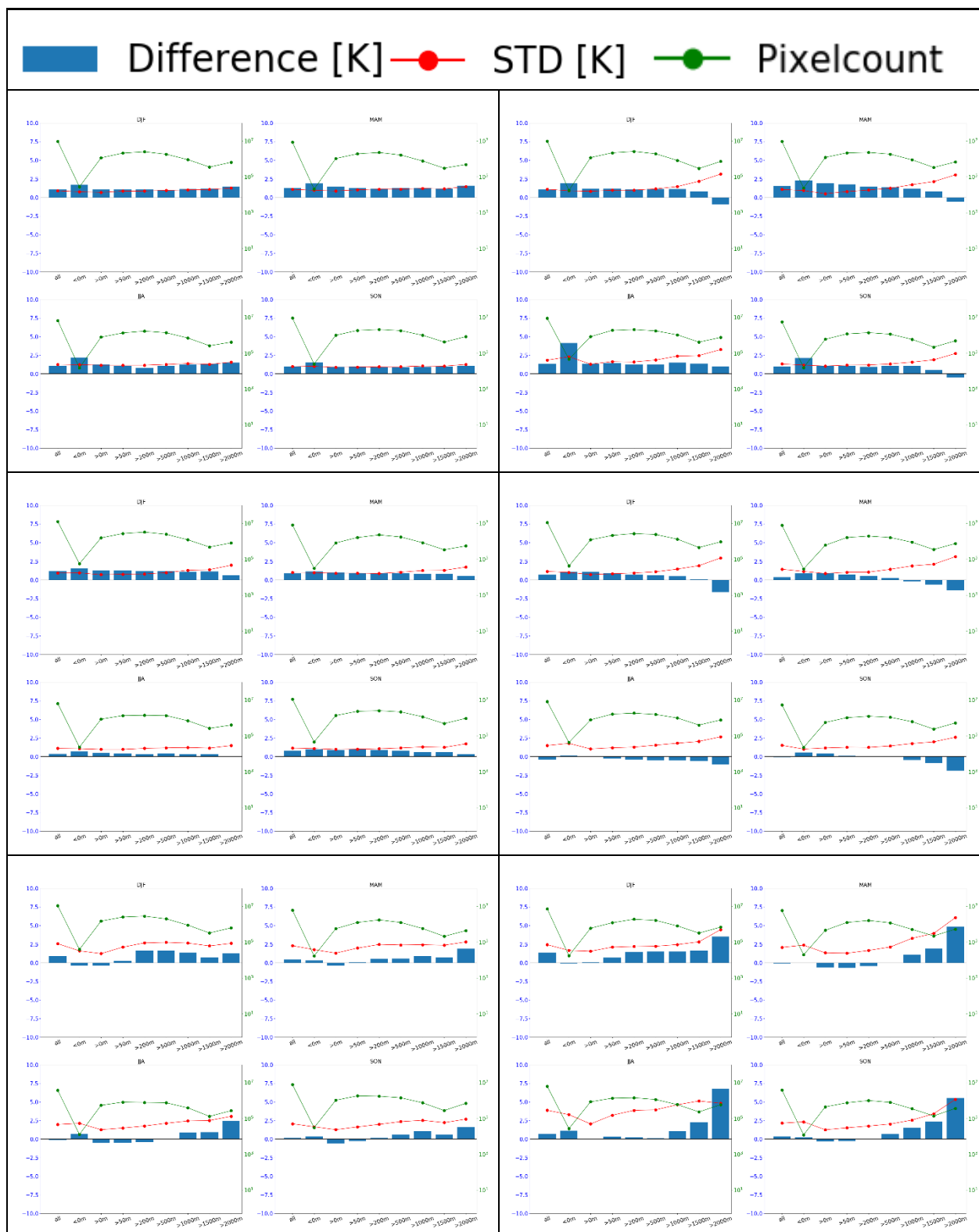


Figure 86: Seasonal differences for different elevation classes; blue bars are the median differences, red points the RSTD and the green points on the right axis show the number of averaged data points Left row displays night-time and right row daytime data. Upper plots are for ATSR_3-MOD11T, middle plots for ATSR_3-MODIST, and lower plots for MODIST-ATSOP_.



Figure 87: Seasonal differences for different land cover classes; coloured bars are the differences, red points the RSTD and the green points on the right axis show the number of averaged data points. Left row displays night-time and right row daytime data. Upper plots are for ATSR_3-MOD11T, middle plots for ATSR_3-MODIST, and lower plots for MODIST-ATSOP_.

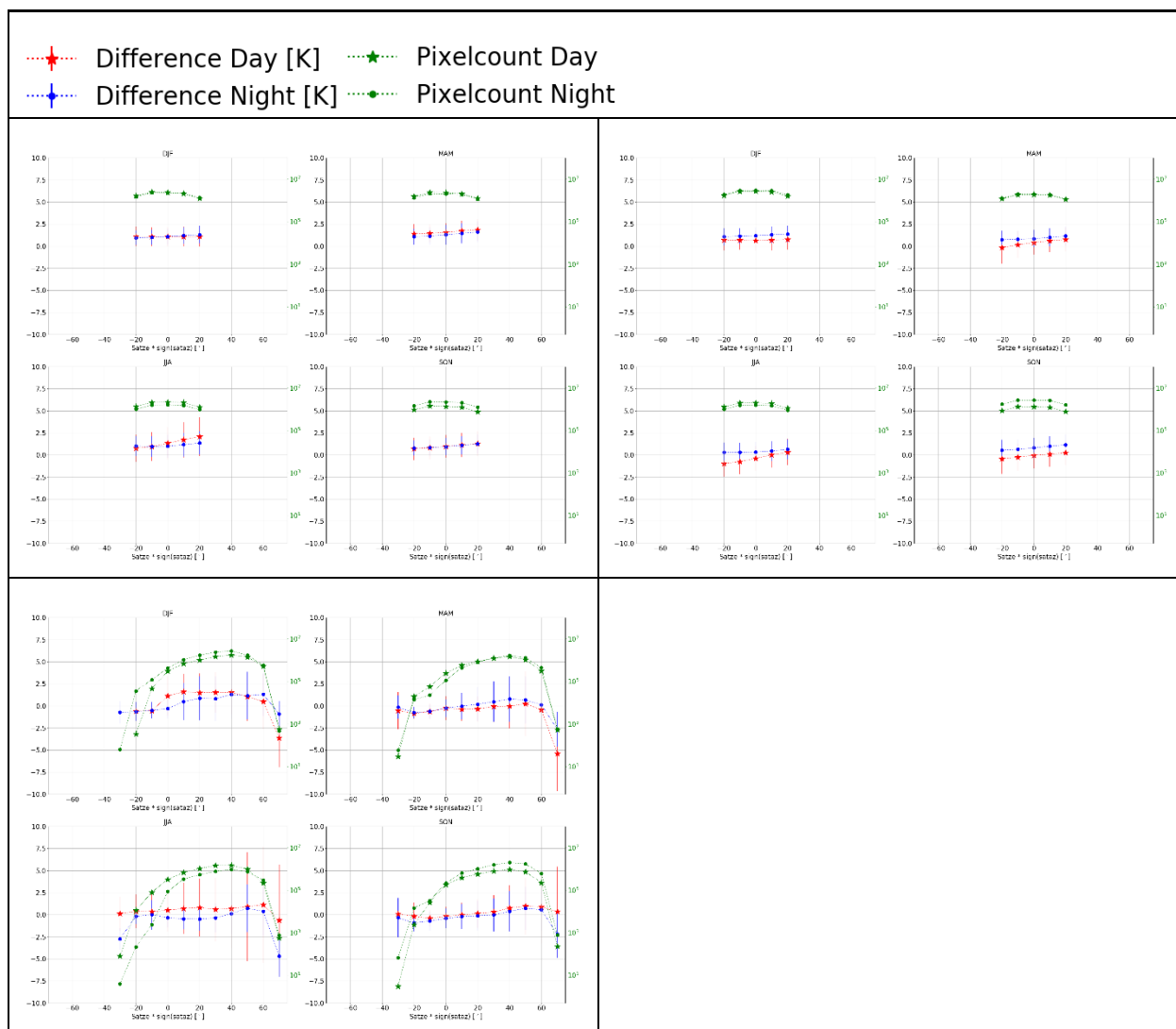


Figure 88: Seasonal differences versus $\text{satze} \cdot \text{sign}(\text{sataz})$ of satellite_1 ; red stars represent the daytime data, blue dots the night-time data, and the green stars and dots on the right axis display the averaged pixel numbers for daytime and night-time data. Upper left plot displays ATSR_3-MOD11T, upper right ATSR_3-MODIST, lower left MODIST-ATSOP_.

7.4. Australia

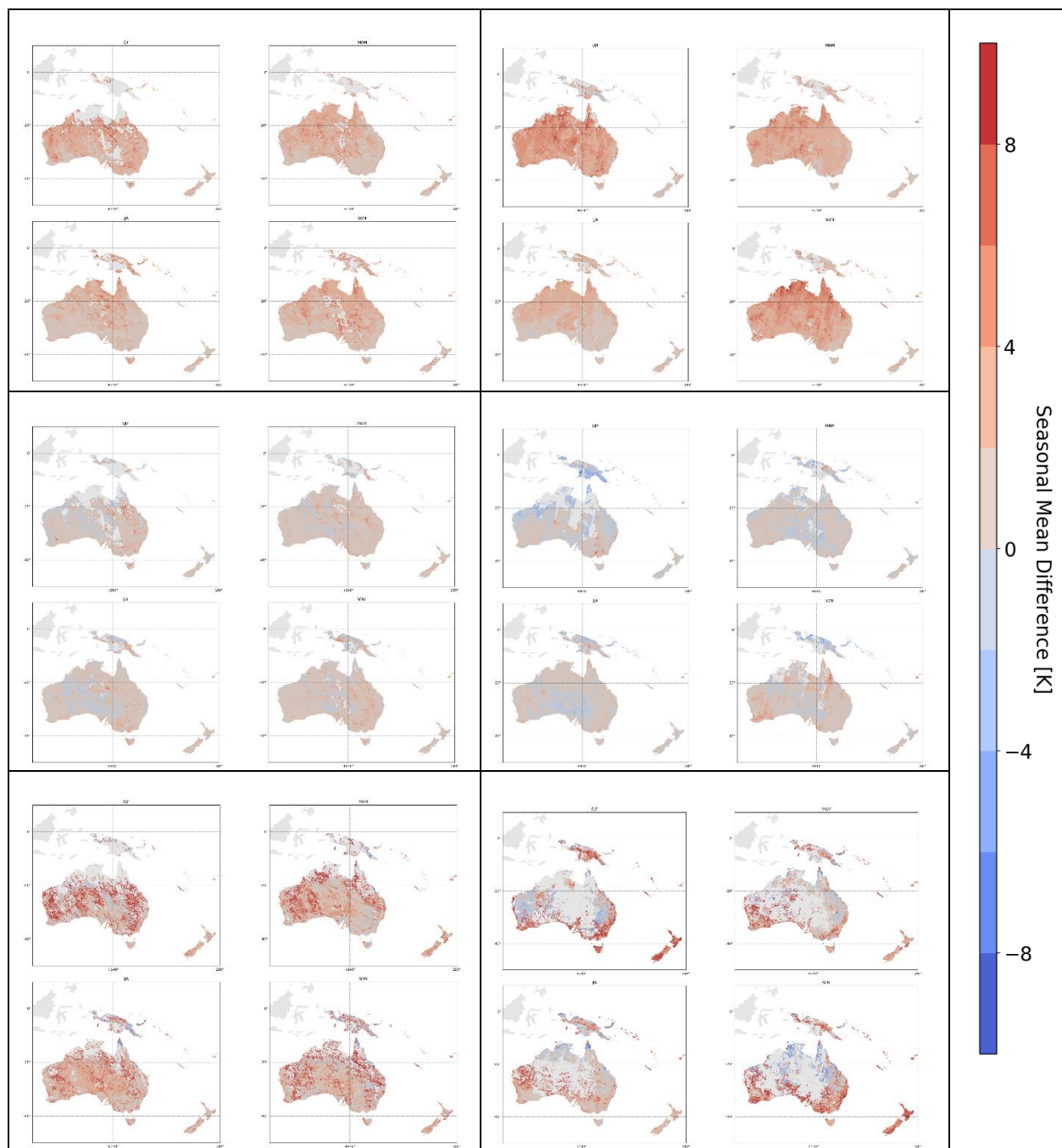


Figure 89: Seasonal mean differences of LST_satellite 1 – LST_satellite 2 in K; left row displays night-time and right row daytime data. Upper plots are for ATSR_3-MOD11T, middle plots for ATSR_3-MODIST, and lower plots for MODIST-ATSOP_.

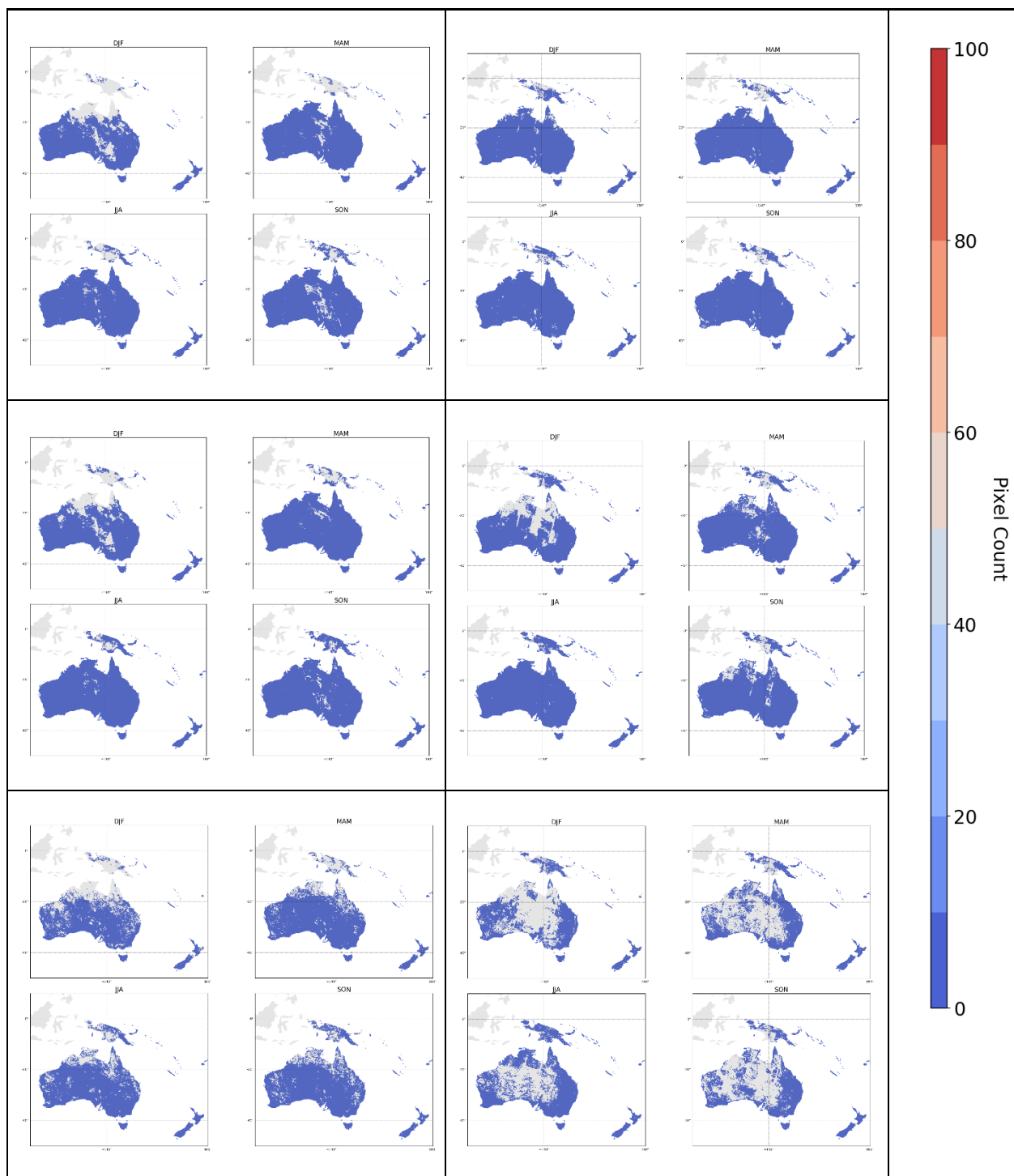


Figure 90: Number of seasonal averaged data points per pixel; left row displays night-time and right row daytime data. Upper plots are for ATSR_3-MOD11T, middle plots for ATSR_3-MODIST, and lower plots for MODIST-ATSOP_.

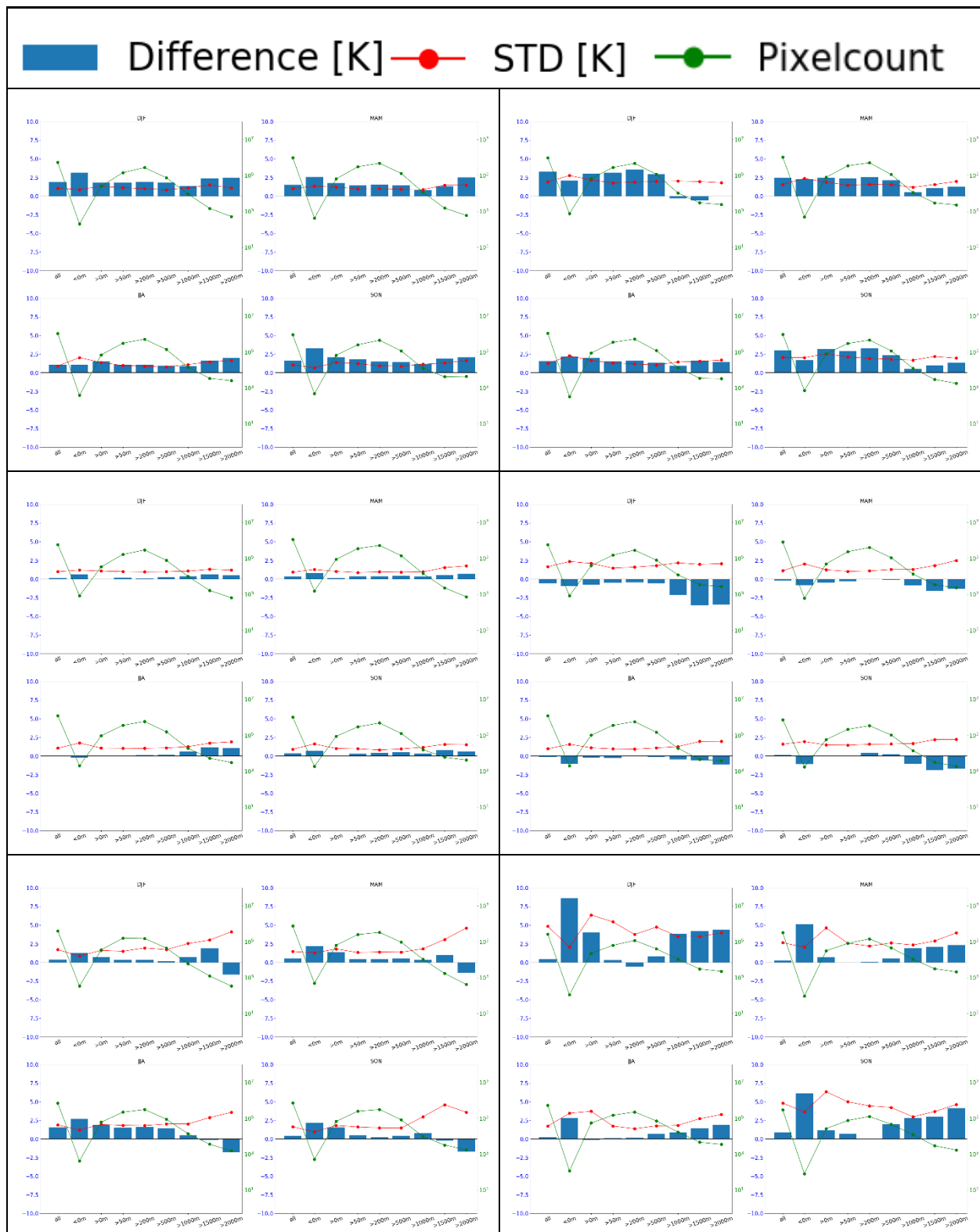


Figure 91: Seasonal differences for different elevation classes; blue bars are the median differences, red points the RSTD and the green points on the right axis show the number of averaged data points Left row displays night-time and right row daytime data. Upper plots are for ATSR_3-MOD11T, middle plots for ATSR_3-MODIST, and lower plots for MODIST-ATSOP_.



Figure 92: Seasonal differences for different land cover classes; coloured bars are the differences, red points the RSTD and the green points on the right axis show the number of averaged data points. Left row displays night-time and right row daytime data. Upper plots are for ATSR_3-MOD11T, middle plots for ATSR_3-MODIST, and lower plots for MODIST-ATSOP_.

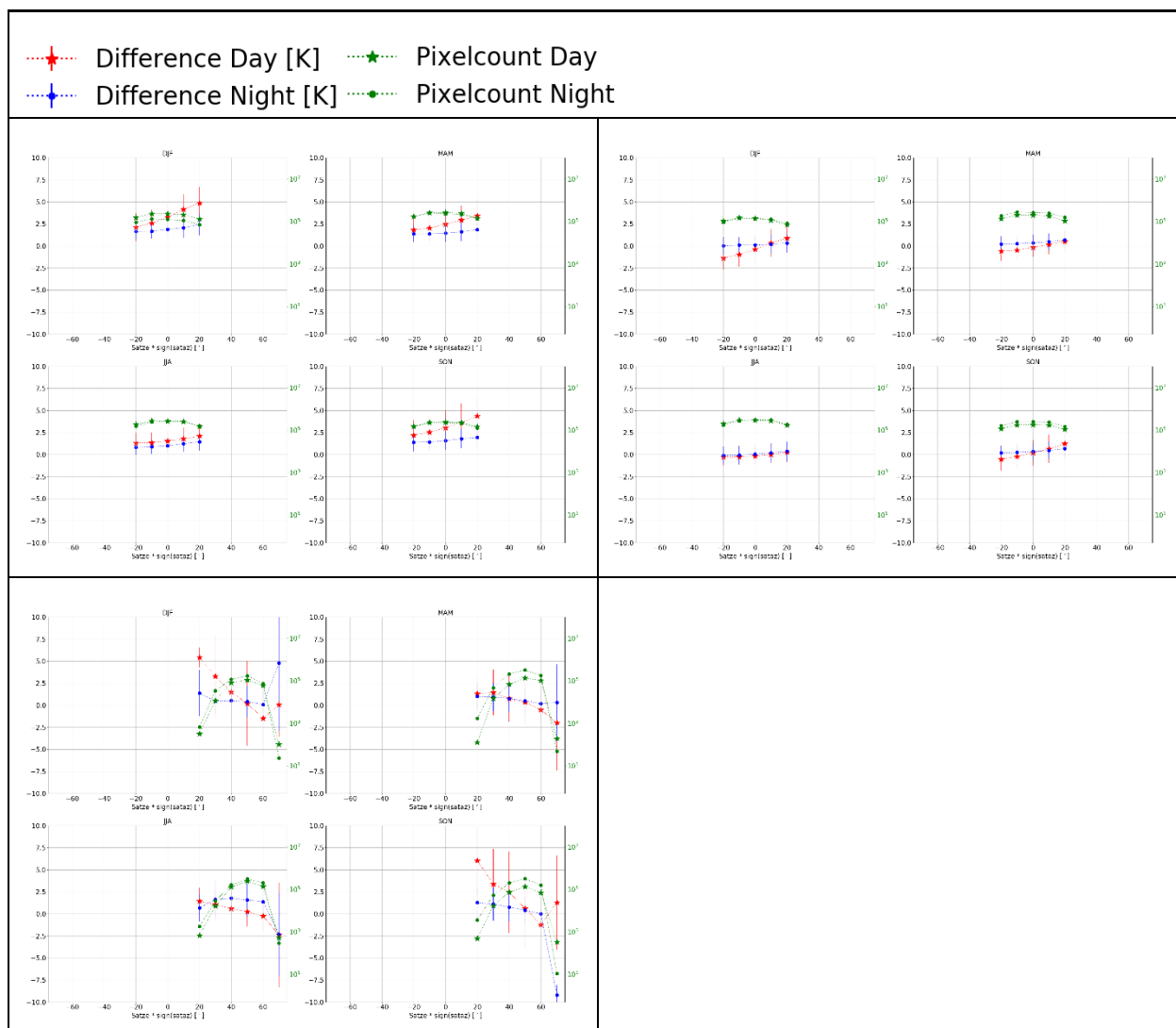


Figure 93: Seasonal differences versus $\text{satze} \cdot \text{sign}(\text{sataz})$ of satellite_1 ; red stars represent the daytime data, blue dots the night-time data, and the green stars and dots on the right axis display the averaged pixel numbers for daytime and night-time data. Upper left plot displays ATSR_3-MOD11T, upper right ATSR_3-MODIST, lower left MODIST-ATSOP_.

7.5. Europe

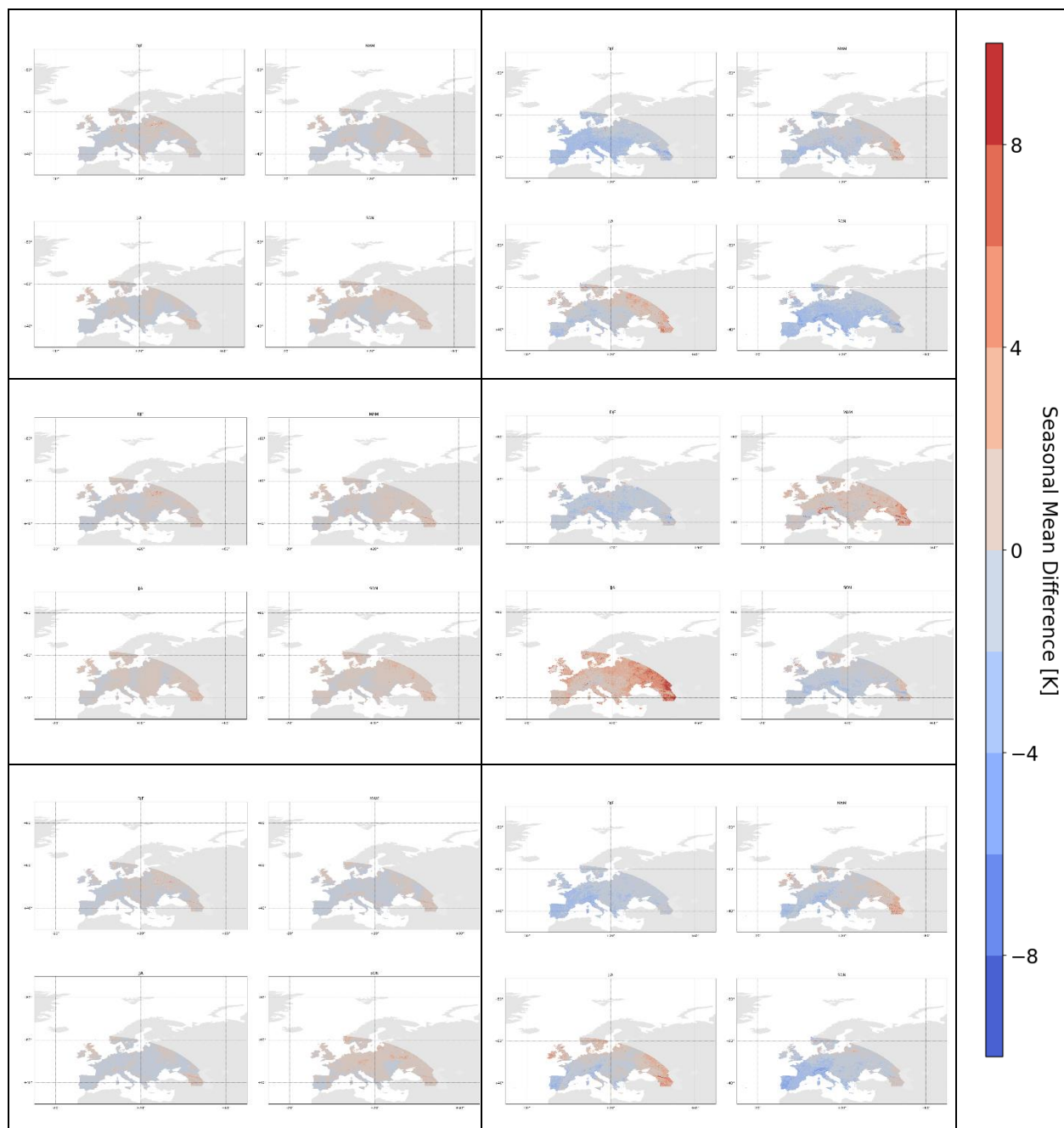


Figure 94: Seasonal mean differences of LST_satellite 1 – LST_satellite 2 in K; left row displays night-time and right row daytime data. Upper plots are for MOD11A-SEVIR2, middle plots for MODISA-SEVIR2, and lower plots for MOD11T-SEVIR2.

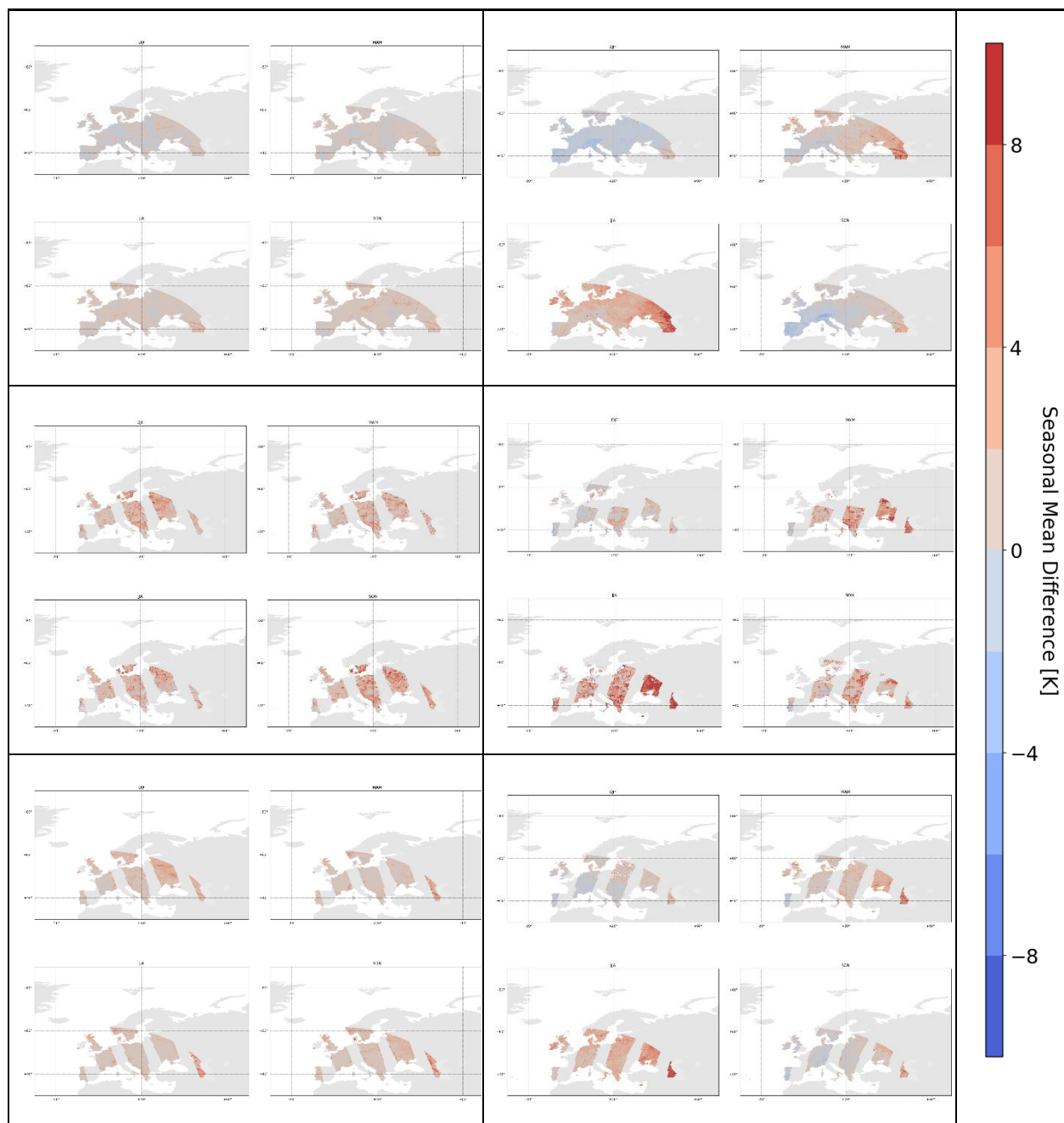


Figure 95: Seasonal mean differences of LST_satellite 1 – LST_satellite 2 in K; left row displays night-time and right row daytime data. Upper plots are for MODIST-SEVIR2, middle plots for ATSOP-SEVIR2, and lower plots for ATSR_3-SEVIR2.

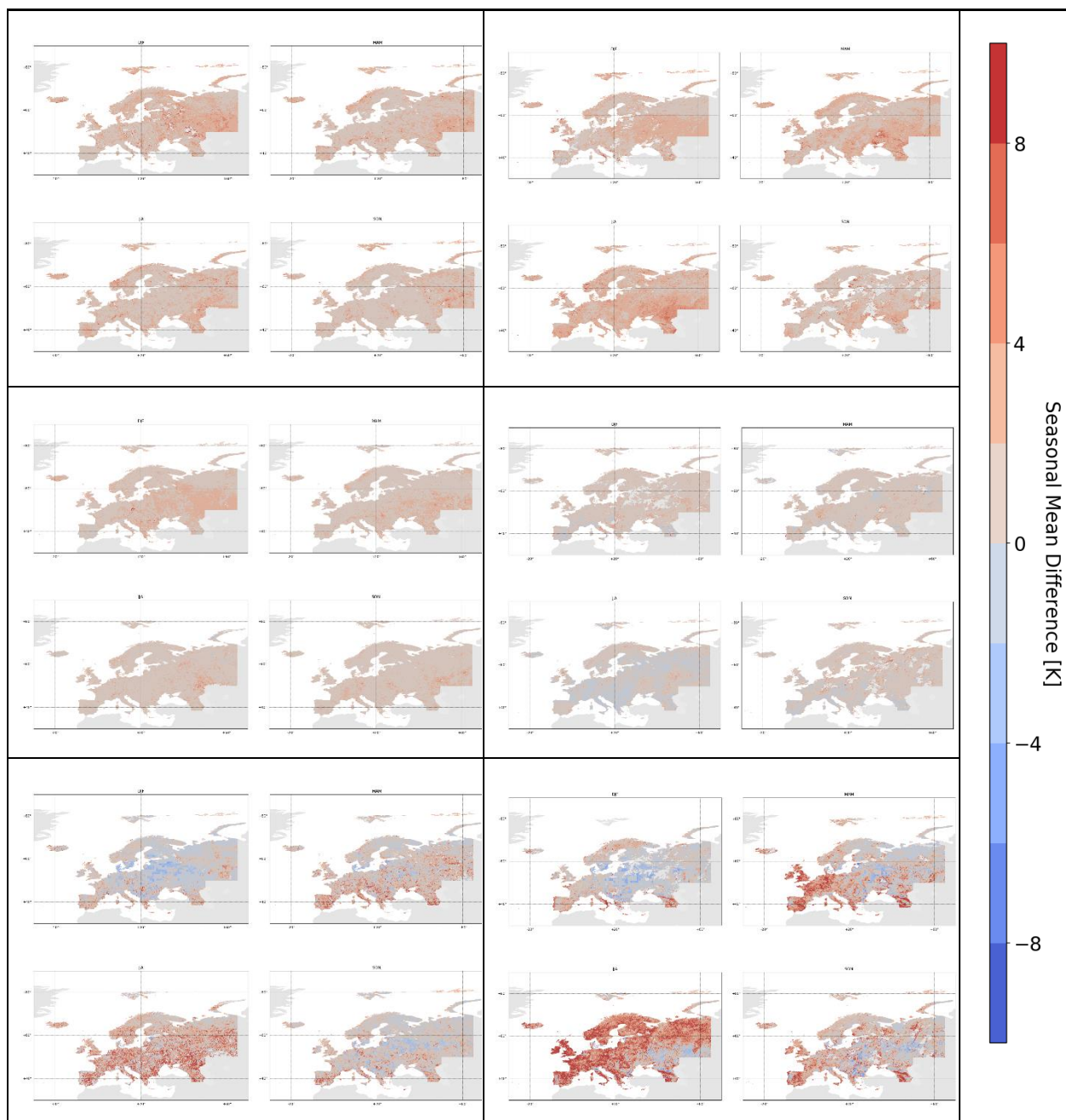


Figure 96: Seasonal mean differences of LST_satellite 1 – LST_satellite 2 in K; left row displays night-time and right row daytime data. Upper plots are for ATSR_3-MOD11T, middle plots for ATSR_3-MODIST, and lower plots for MODIST-ATSOP_.

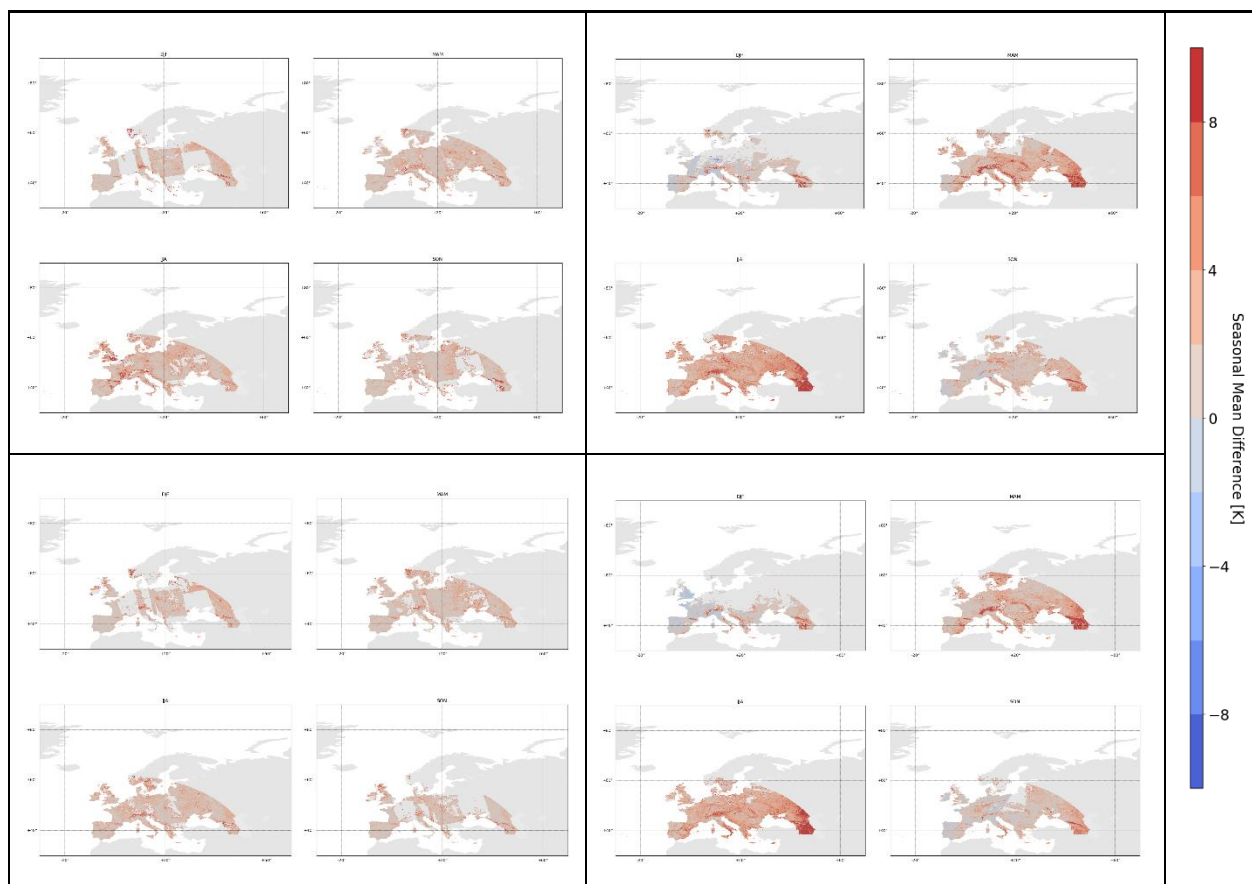


Figure 97: Seasonal mean differences of LST_satellite 1 – LST_satellite 2 in K; left row displays night-time and right row daytime data. Upper plots are for SLSTRA-SEVIR4, middle plots for SLSTB-SEVIR4, for the years 2018 - 2020.

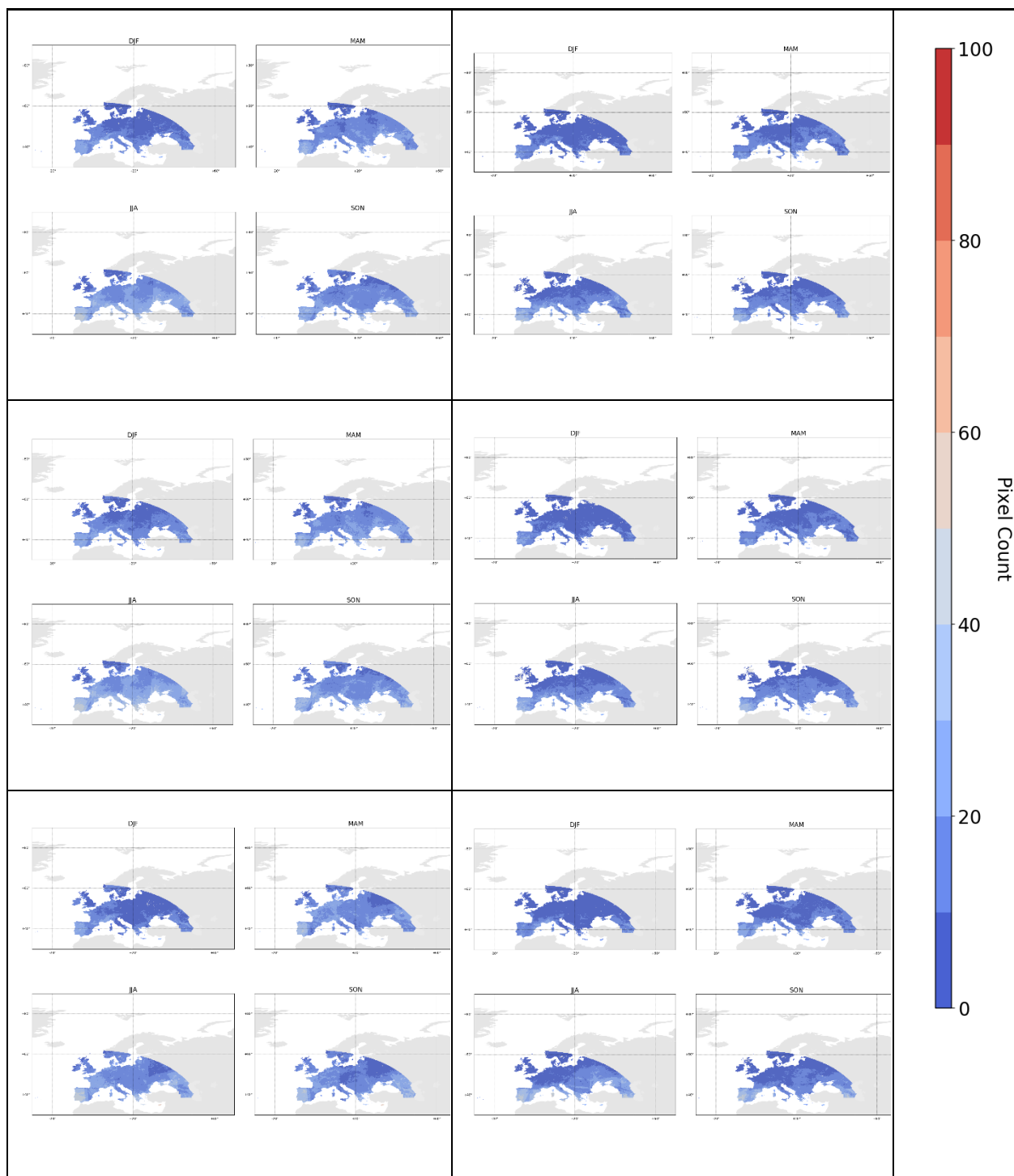


Figure 98: Number of seasonal averaged data points per pixel; left row displays night-time and right row daytime data. Upper plots are for MOD11A-SEVIR2, middle plots for MODISA-SEVIR2, and lower plots for MOD11T-SEVIR2.

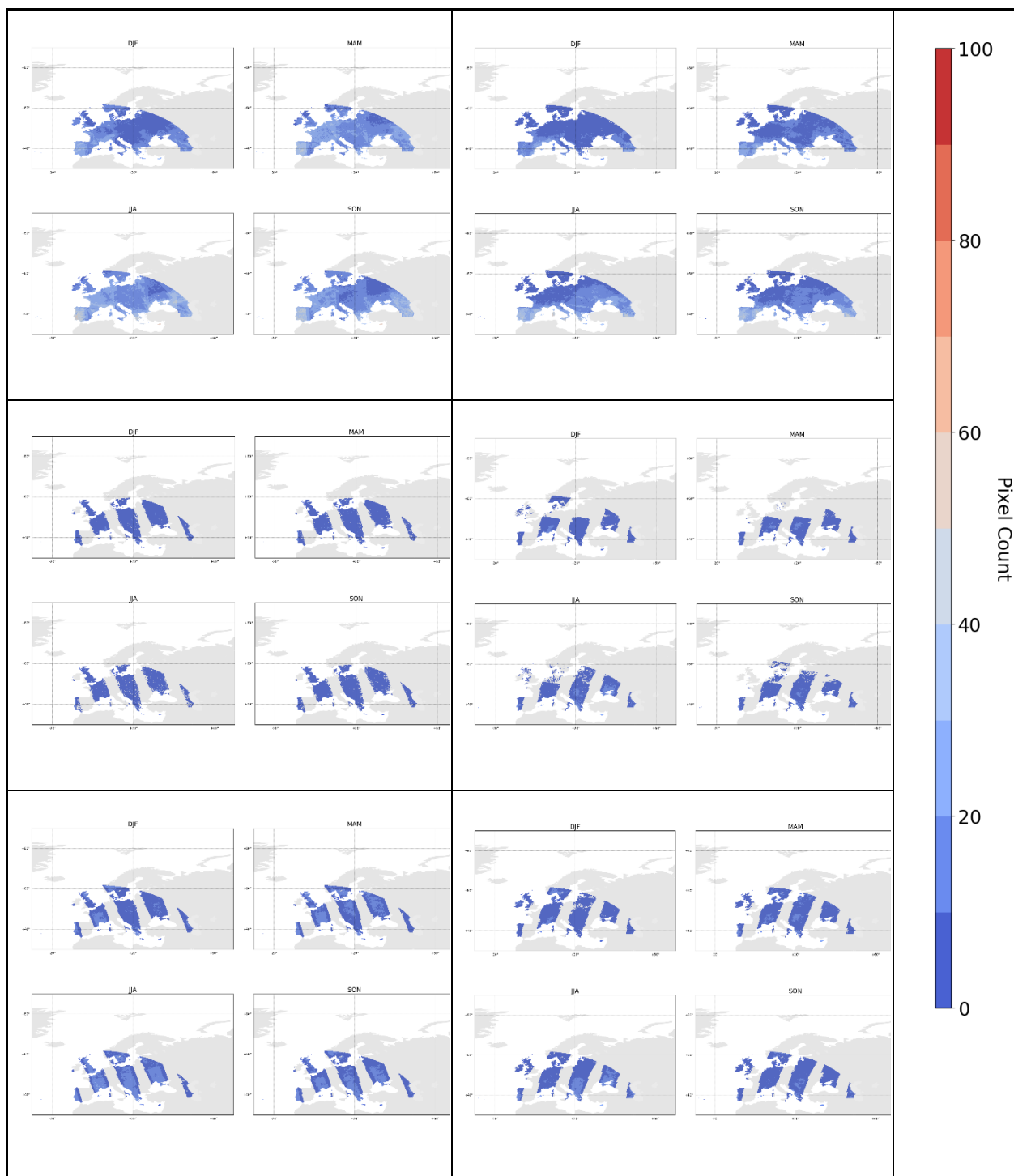


Figure 99: Number of seasonal averaged data points per pixel; left row displays night-time and right row daytime data. Upper plots are for MODIST-SEVIR2, middle plots for ATSOP-SEVIR2, and lower plots for ATSR_3-SEVIR2.

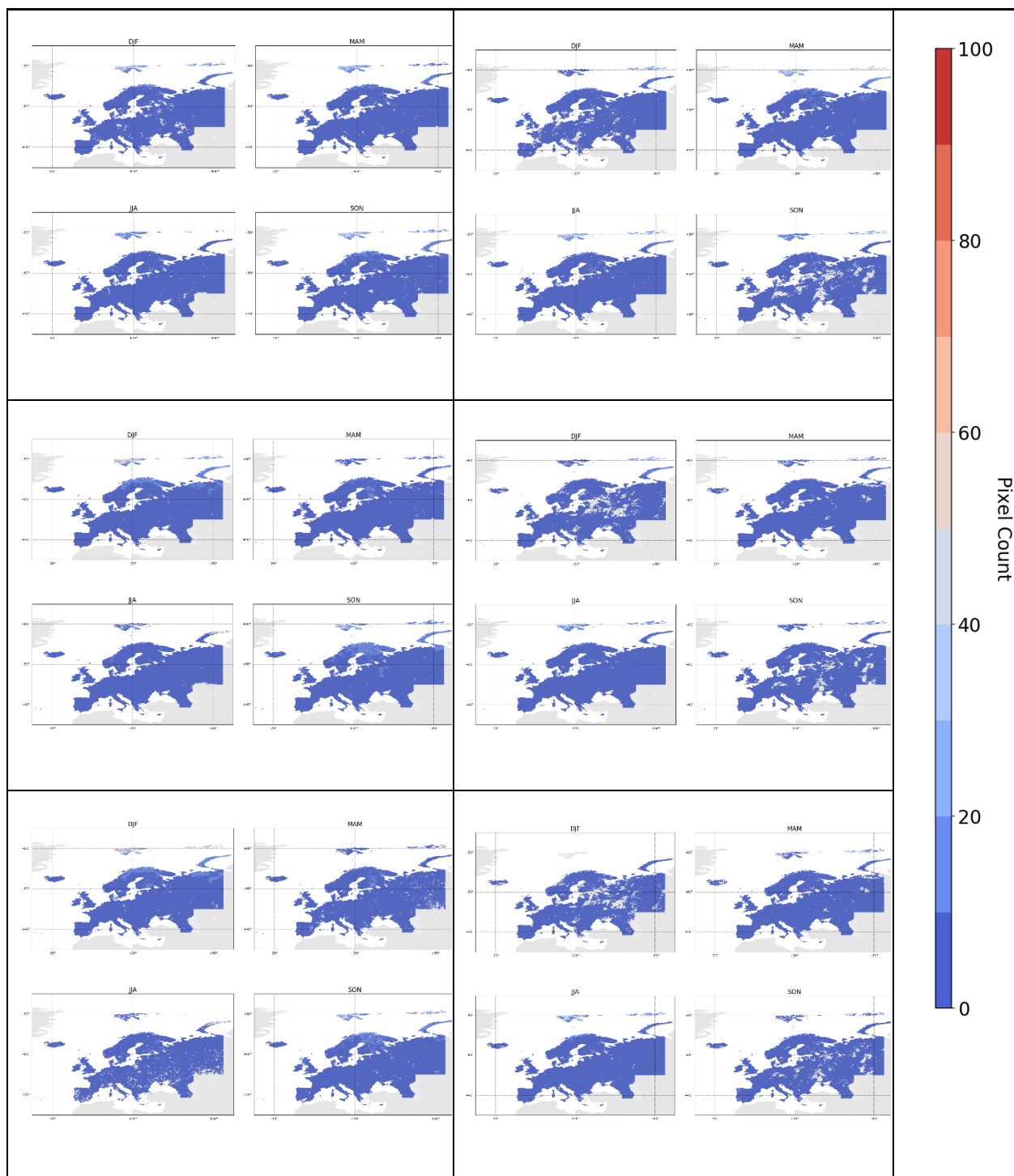


Figure 100: Number of seasonal averaged data points per pixel; left row displays night-time and right row daytime data. Upper plots are for ATSR_3-MOD11T, middle plots for ATSR_3-MODIST, and lower plots for MODIST-ATSOP_.

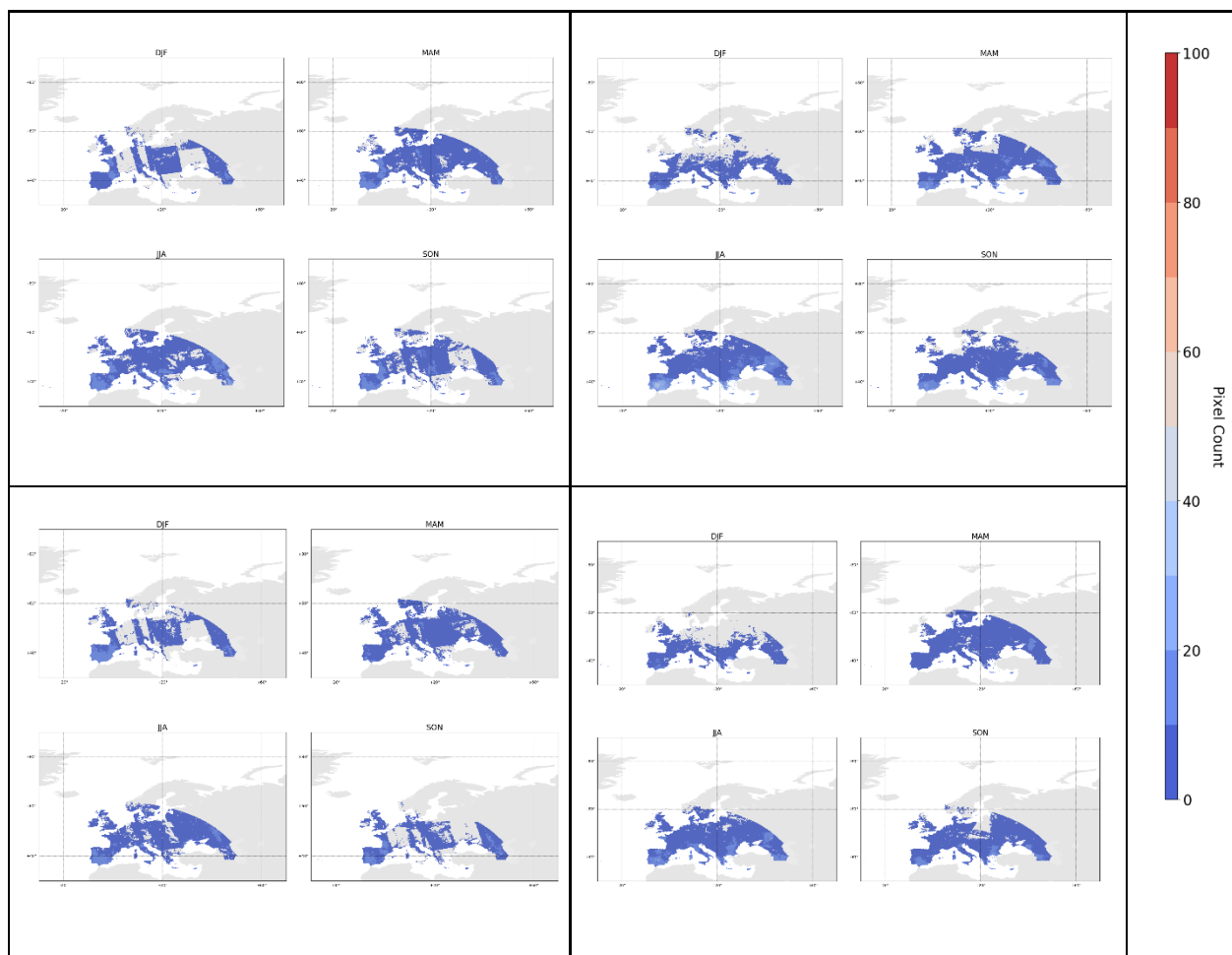


Figure 101: Number of seasonal averaged data points per pixel; left row displays night-time and right row daytime data. Upper plots are for SLSTRA-SEVIR4, middle plots for SLSTRB-SEVIR4, for the years 2018 - 2020.

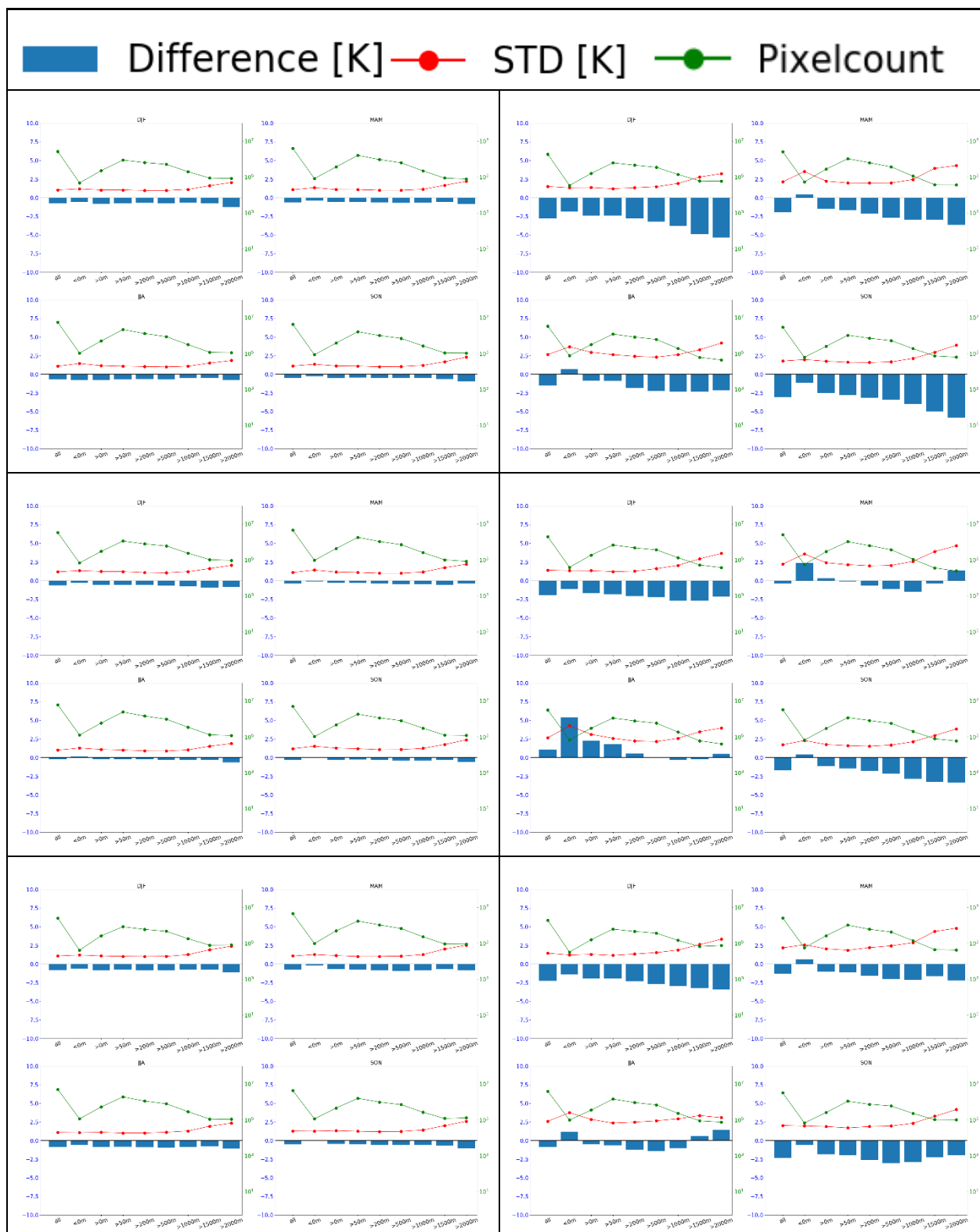


Figure 102: Seasonal differences for different elevation classes; blue bars are the median differences, red points the RSTD and the green points on the right axis show the number of averaged data points Left row displays night-time and right row daytime data. Upper plots are for MOD11A-SEVIR2, middle plots for MODISA-SEVIR2, and lower plots for MOD11T-SEVIR2.

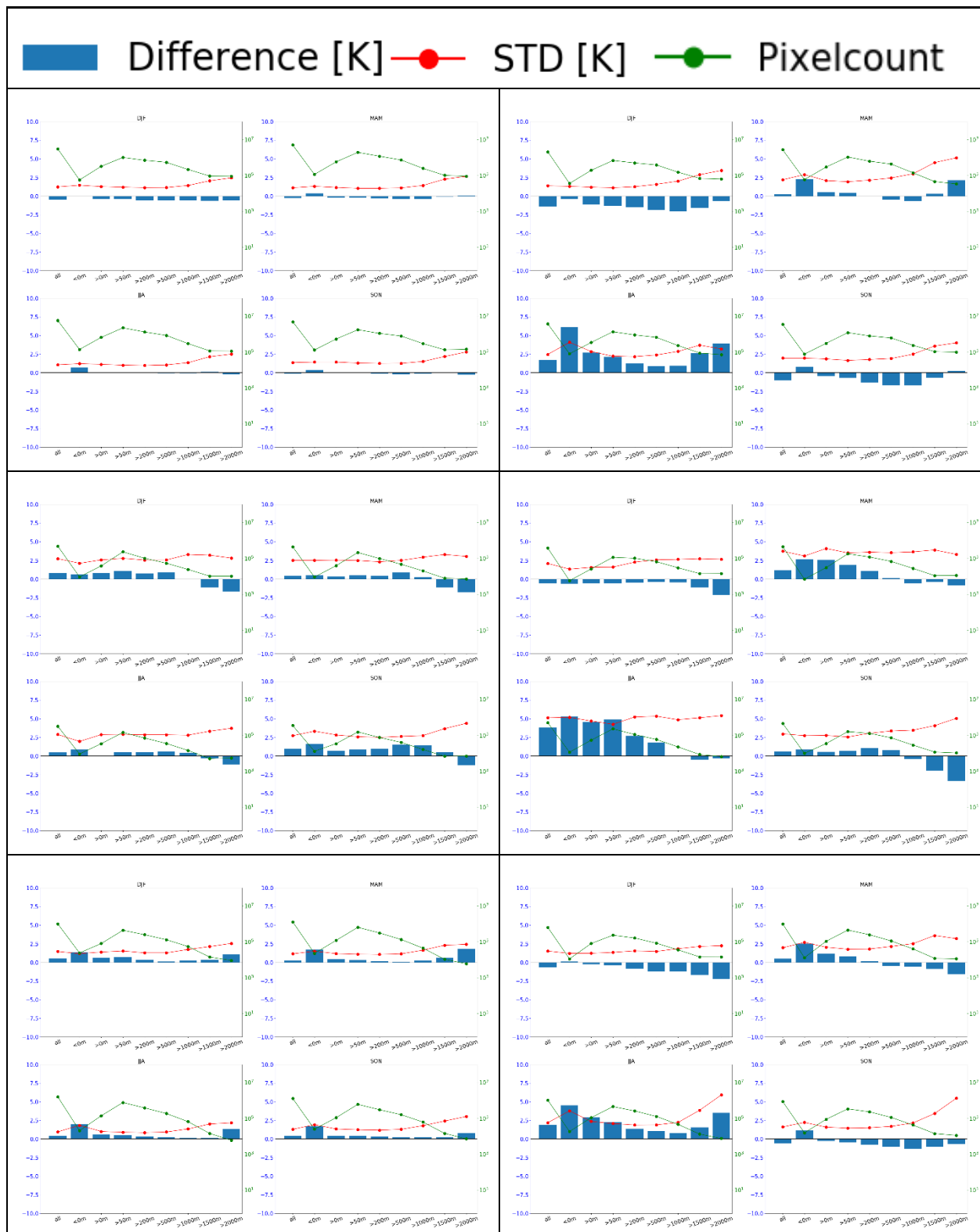


Figure 103: Seasonal differences for different elevation classes; blue bars are the median differences, red points the RSTD and the green points on the right axis show the number of averaged data points Left row displays night-time and right row daytime data. Upper plots are for MODIST-SEVIR2, middle plots for ATSOP-SEVIR2, and lower plots for ATSR_3-SEVIR2.

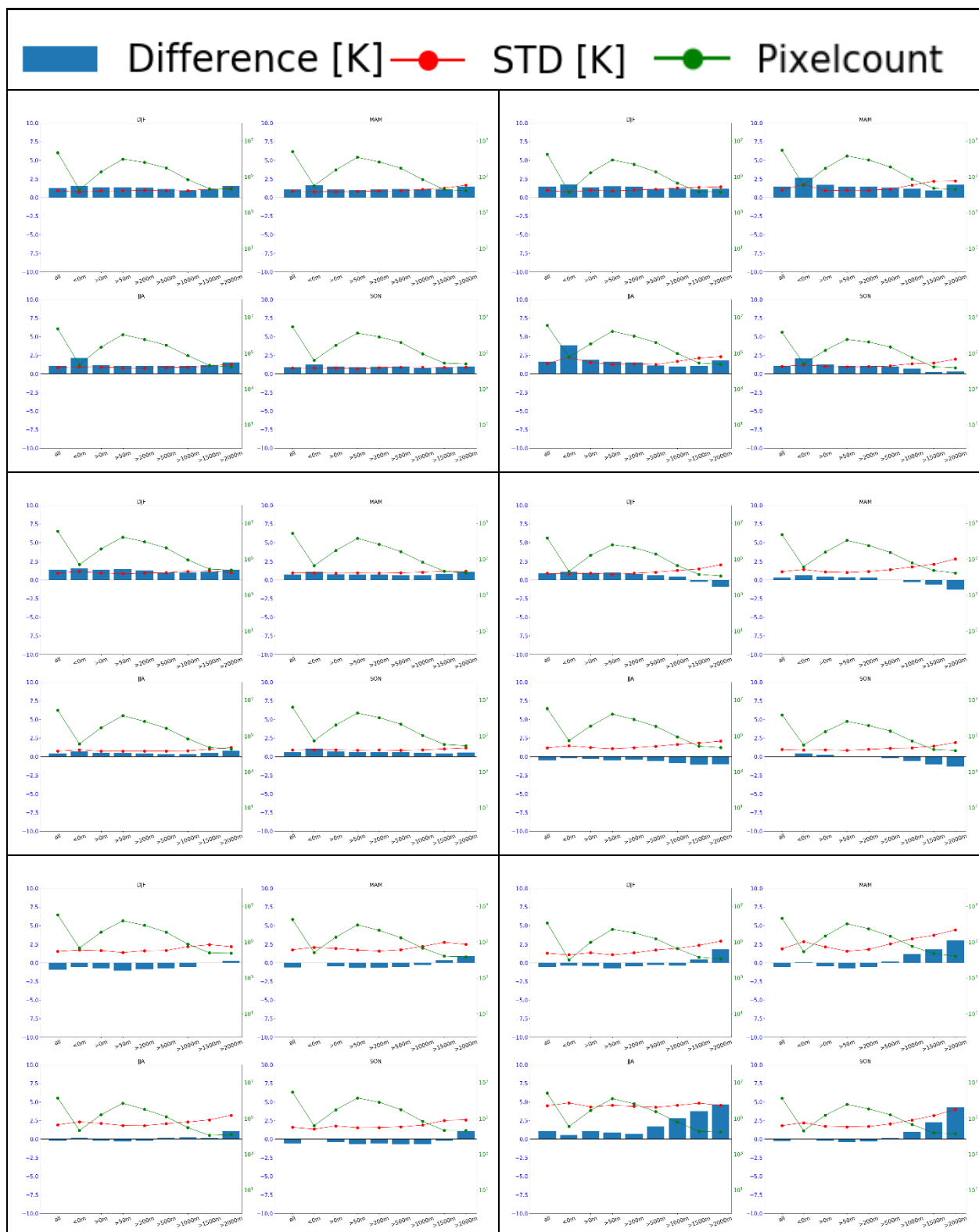


Figure 104: Seasonal differences for different elevation classes; blue bars are the median differences, red points the RSTD and the green points on the right axis show the number of averaged data points Left row displays night-time and right row daytime data. Upper plots are for ATSR_3-MOD11T, middle plots for ATSR_3-MODIST, and lower plots for MODIST-ATSOP_.

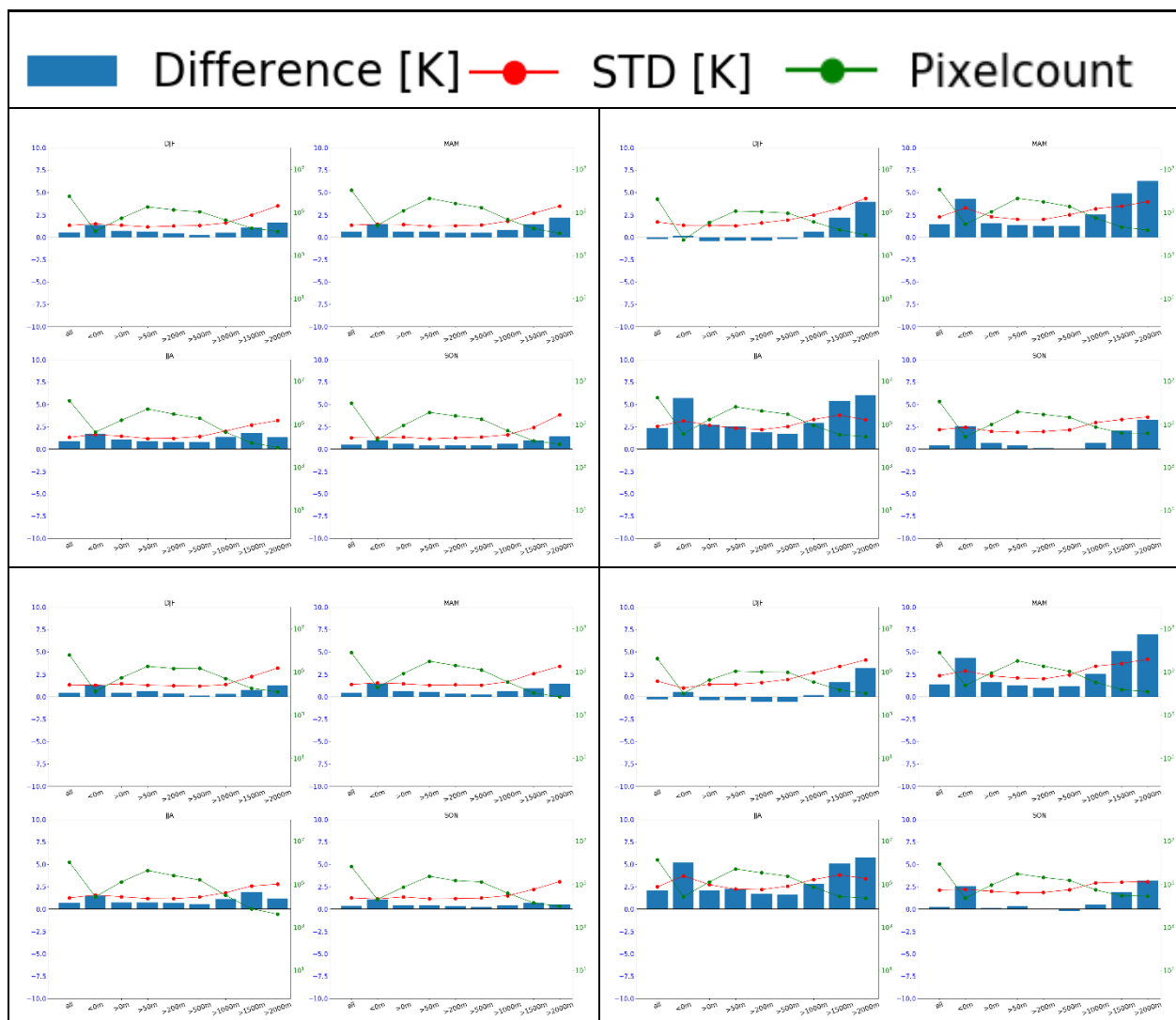


Figure 105: Seasonal differences for different elevation classes; blue bars are the median differences, red points the RSTD and the green points on the right axis show the number of averaged data points Left row displays night-time and right row daytime data. Upper plots are for SLSTRA-SEVIR4, middle plots for SLSTRB-SEVIR4, for the years 2018 - 2020.

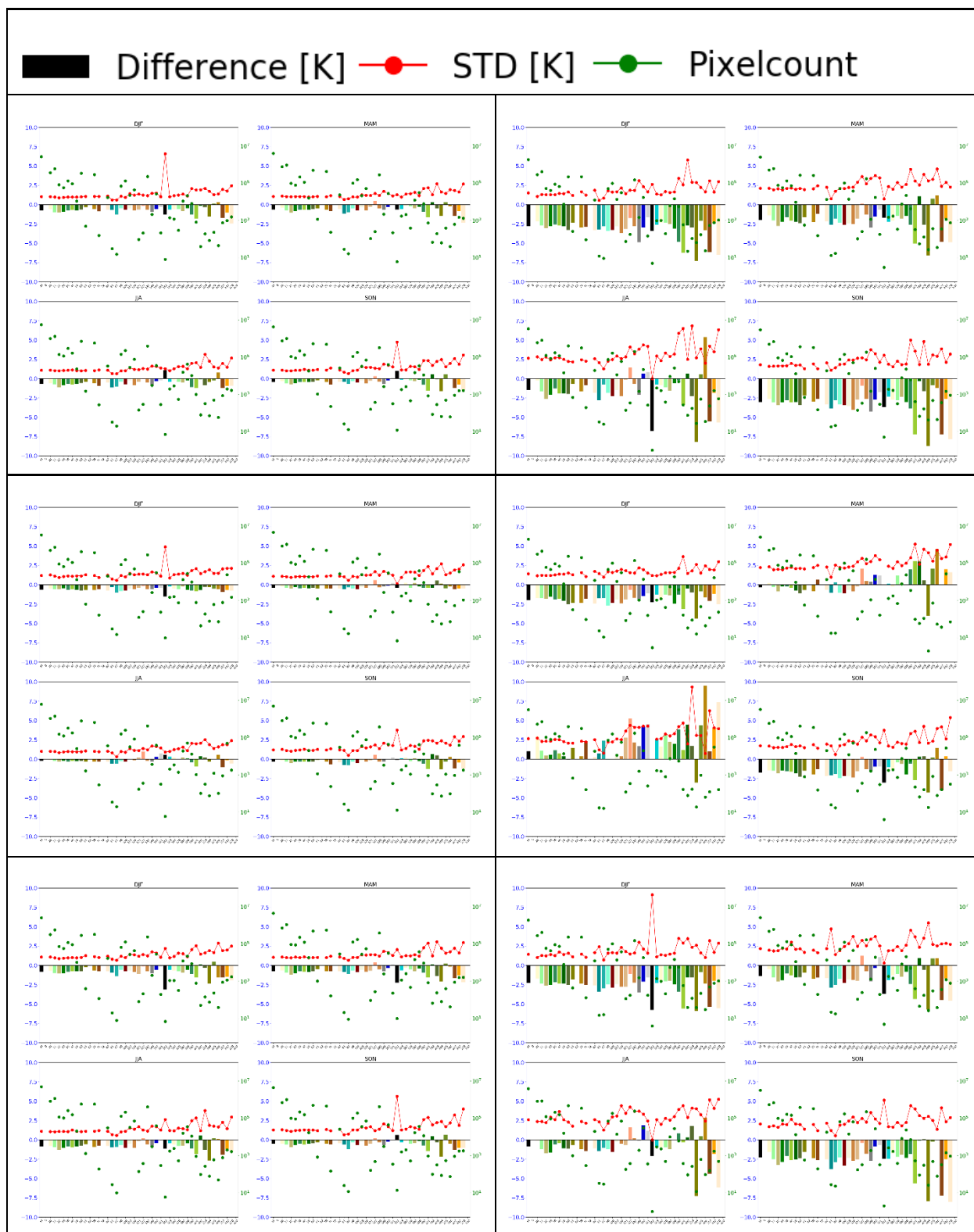


Figure 106: Seasonal differences for different land cover classes; coloured bars are the differences, red points the RSTD and the green points on the right axis show the number of averaged data points. Left row displays night-time and right row daytime data. Upper plots are for MOD11A-SEVIR2, middle plots for MODISA-SEVIR2, and lower plots for MOD11T-SEVIR2.

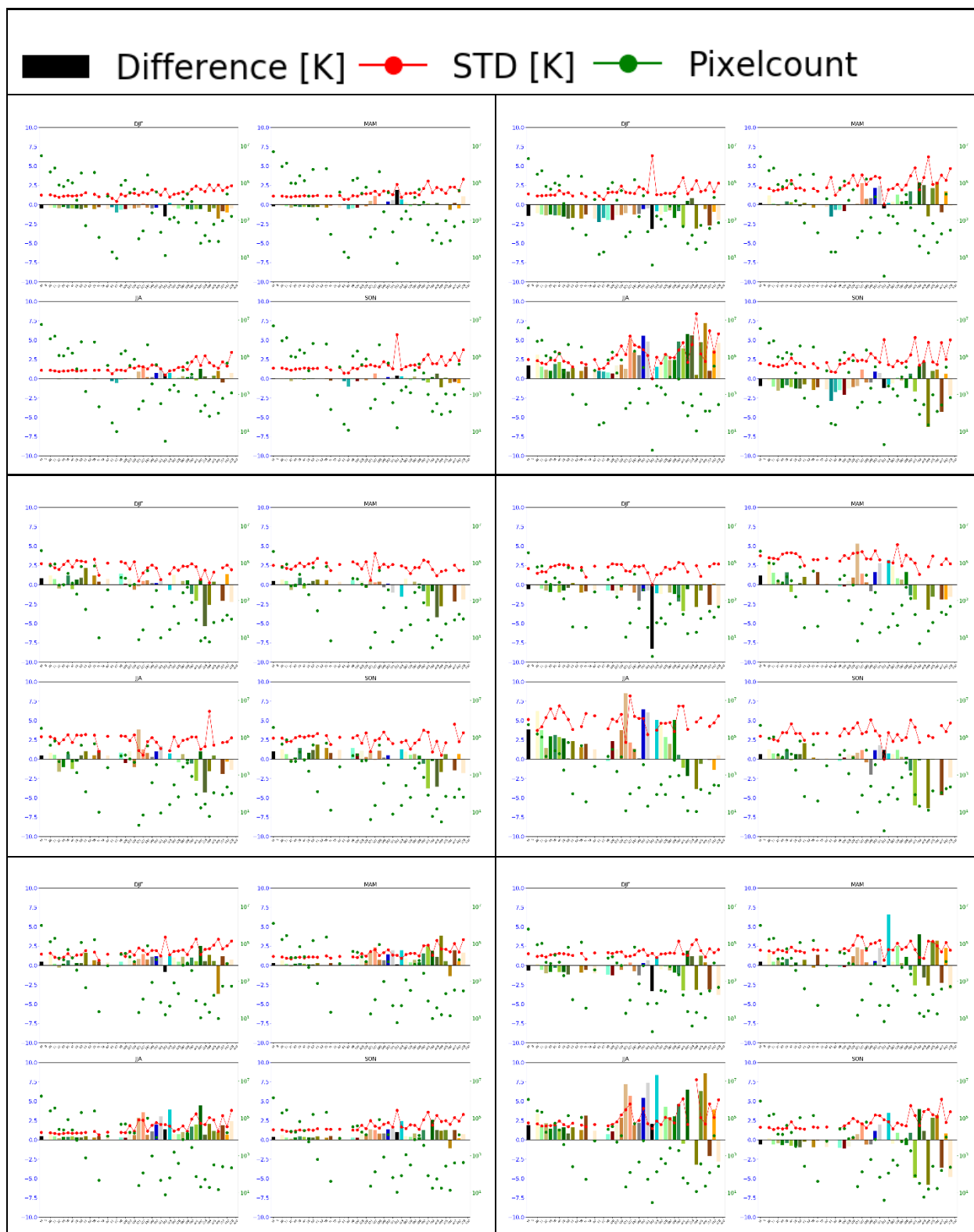


Figure 107: Seasonal differences for different land cover classes; coloured bars are the differences, red points the RSTD and the green points on the right axis show the number of averaged data points. Left row displays night-time and right row daytime data. Upper plots are for MODIST-SEVIR2, middle plots for ATSR-SEVIR2, and lower plots for ATSR_3-SEVIR2.



Figure 108: Seasonal differences for different land cover classes; coloured bars are the differences, red points the RSTD and the green points on the right axis show the number of averaged data points. Left row displays night-time and right row daytime data. Upper plots are for ATSR_3-MOD11T, middle plots for ATSR_3-MODIST, and lower plots for MODIST-ATSOP_.

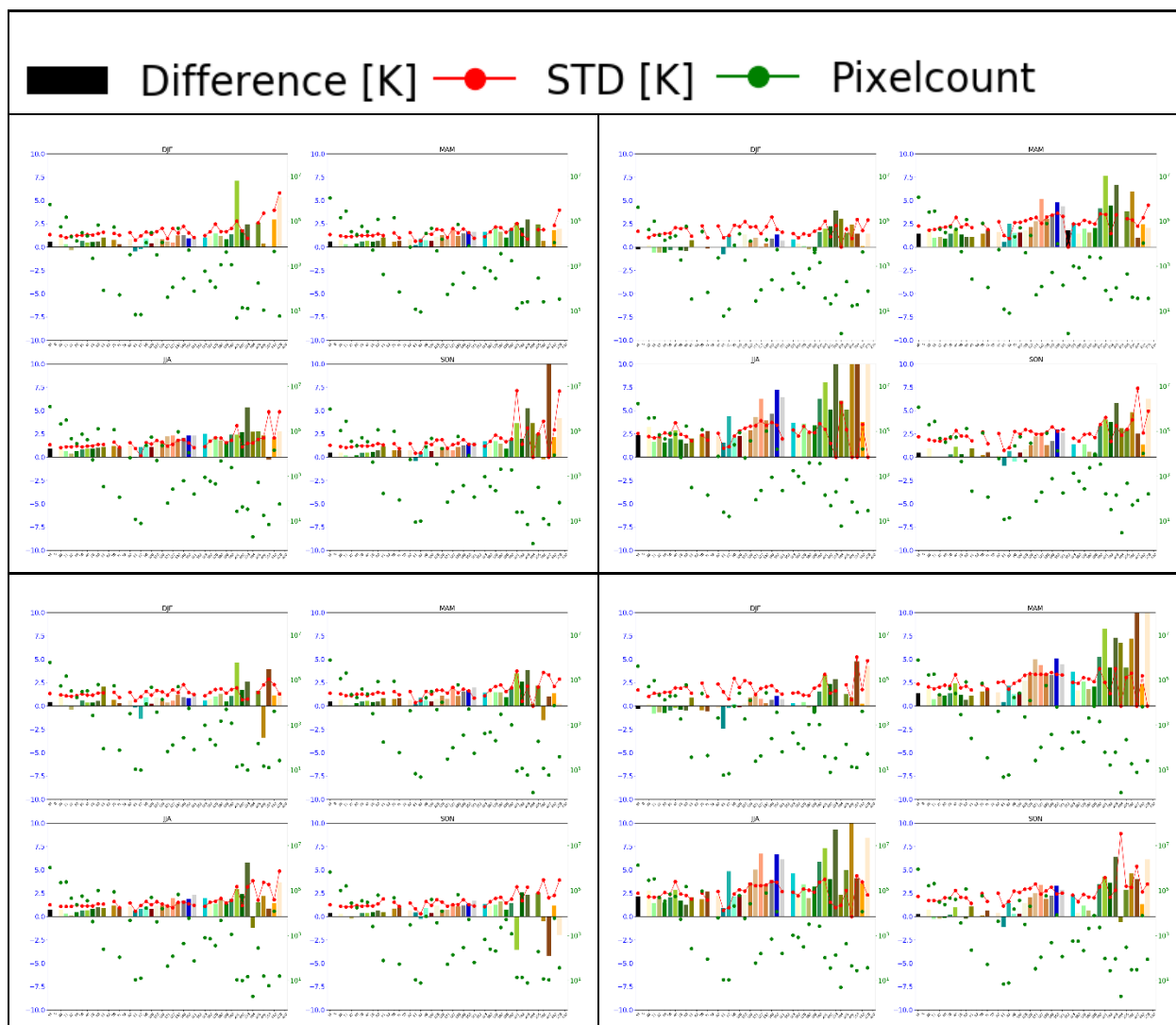


Figure 109: Seasonal differences for different land cover classes; coloured bars are the differences, red points the RSTD and the green points on the right axis show the number of averaged data points. Left row displays night-time and right row daytime data. Upper plots are for SLSTRA-SEVIR4, middle plots for SLSTRB-SEVIR4, for the years 2018 - 2020.

★ Difference Day [K] ★ Pixelcount Day
★ Difference Night [K] ★ Pixelcount Night

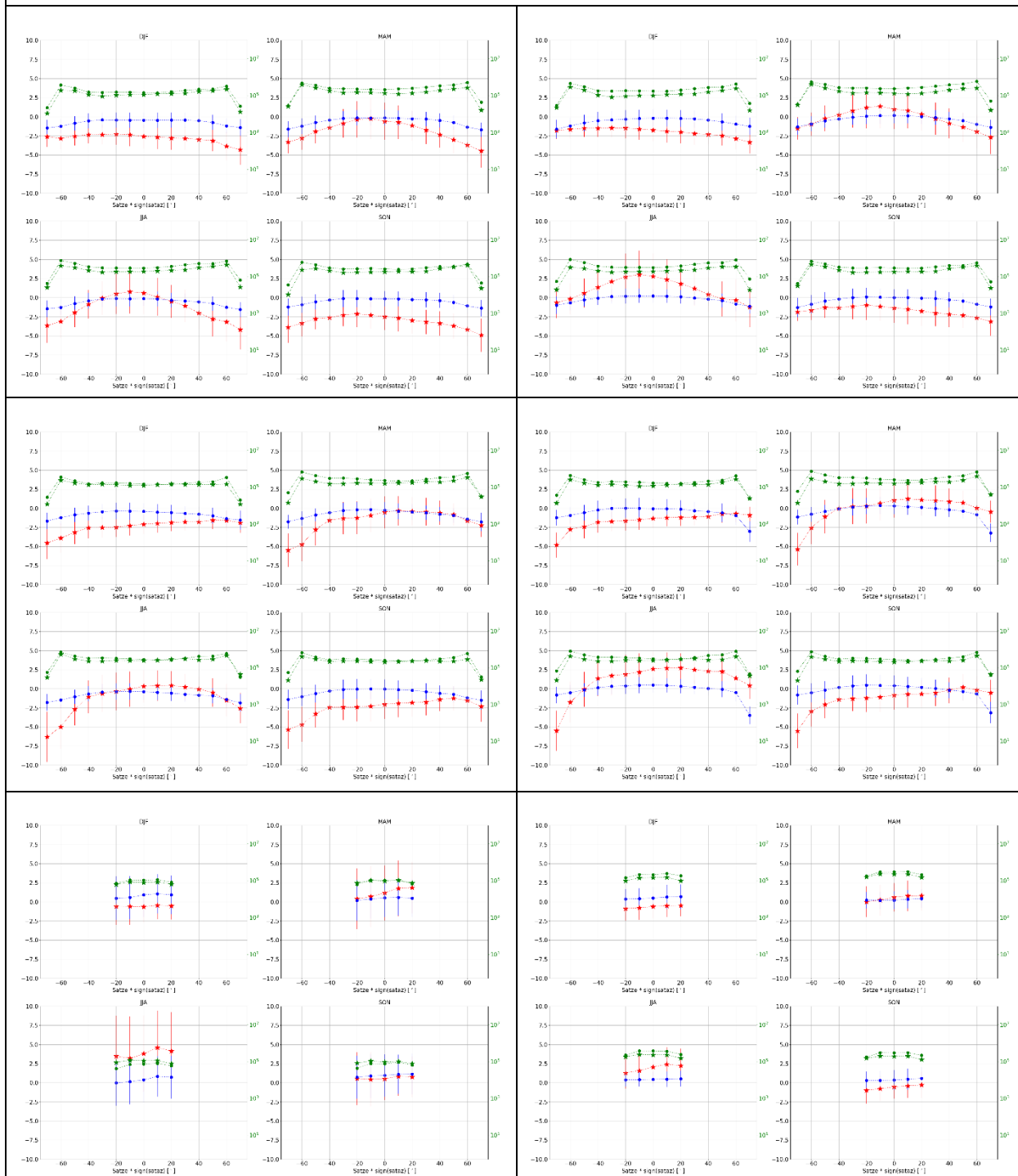


Figure 110: Seasonal differences versus $\text{satze} \cdot \text{sign}(\text{sataz})$ of satellite₁; red stars represent the daytime data, blue dots the night-time data, and the green stars and dots on the right axis display the averaged pixel numbers for daytime and night-time data. Upper left plot displays MOD11A-SEVIR2, upper right MOD11A-SEVIR2, middle left MOD11T-SEVIR2, middle right MOD11T-SEVIR2, lower left ATSR_3-SEVIR2, and lower right ATSR_3-SEVIR2.

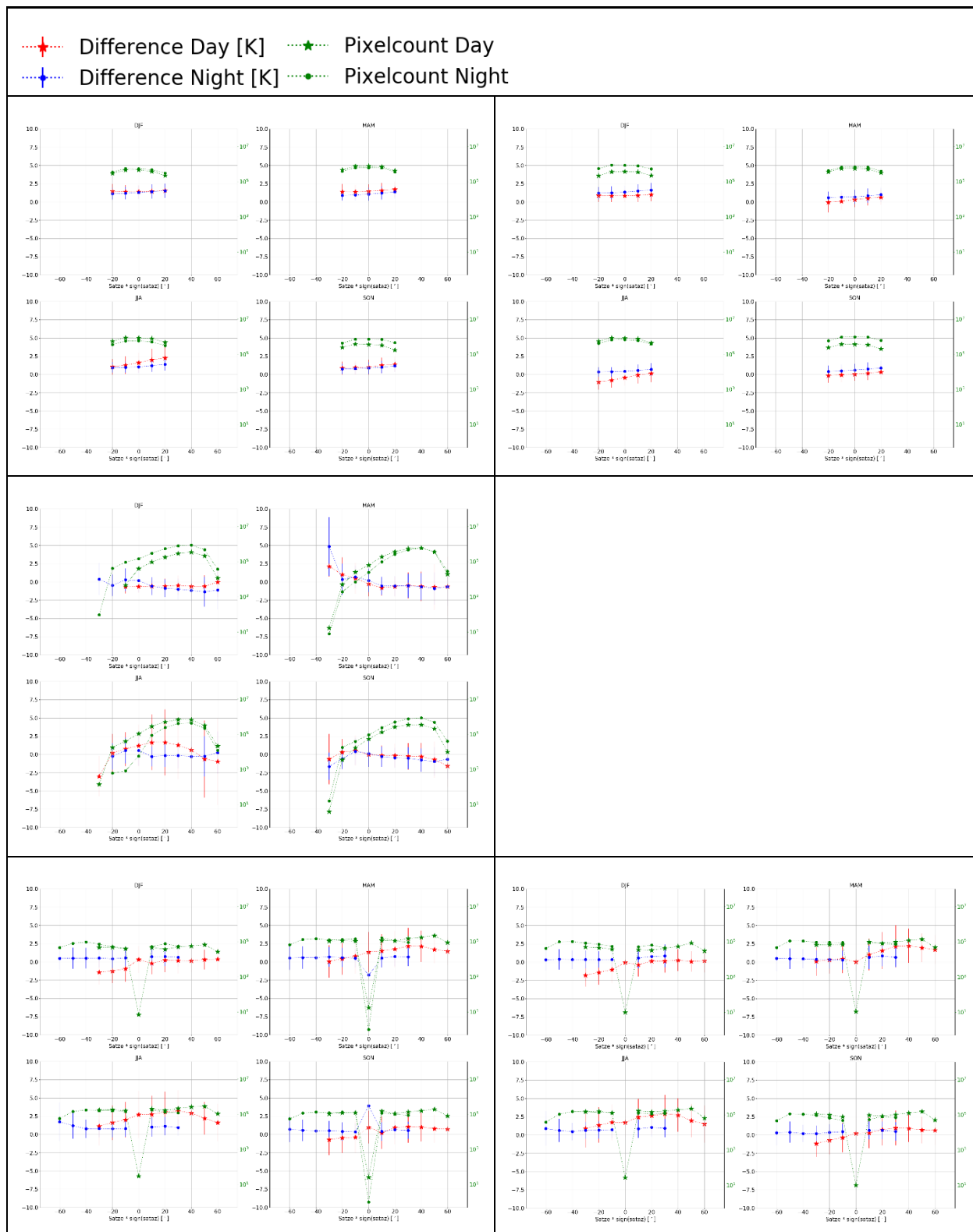


Figure 111: Seasonal differences versus $\text{satze} \cdot \text{sign}(\text{satze})$ of satellite_1 ; red stars represent the daytime data, blue dots the night-time data, and the green stars and dots on the right axis display the averaged pixel numbers for daytime and night-time data. Upper left plot displays ATSR_3-MOD11T, upper right ATSR_3-MODIST, lower left MODIST-ATRSOP_, lower left SLSTRA-SEVIR4, lower right SLSTRB-SEVIR4.

7.6. North America

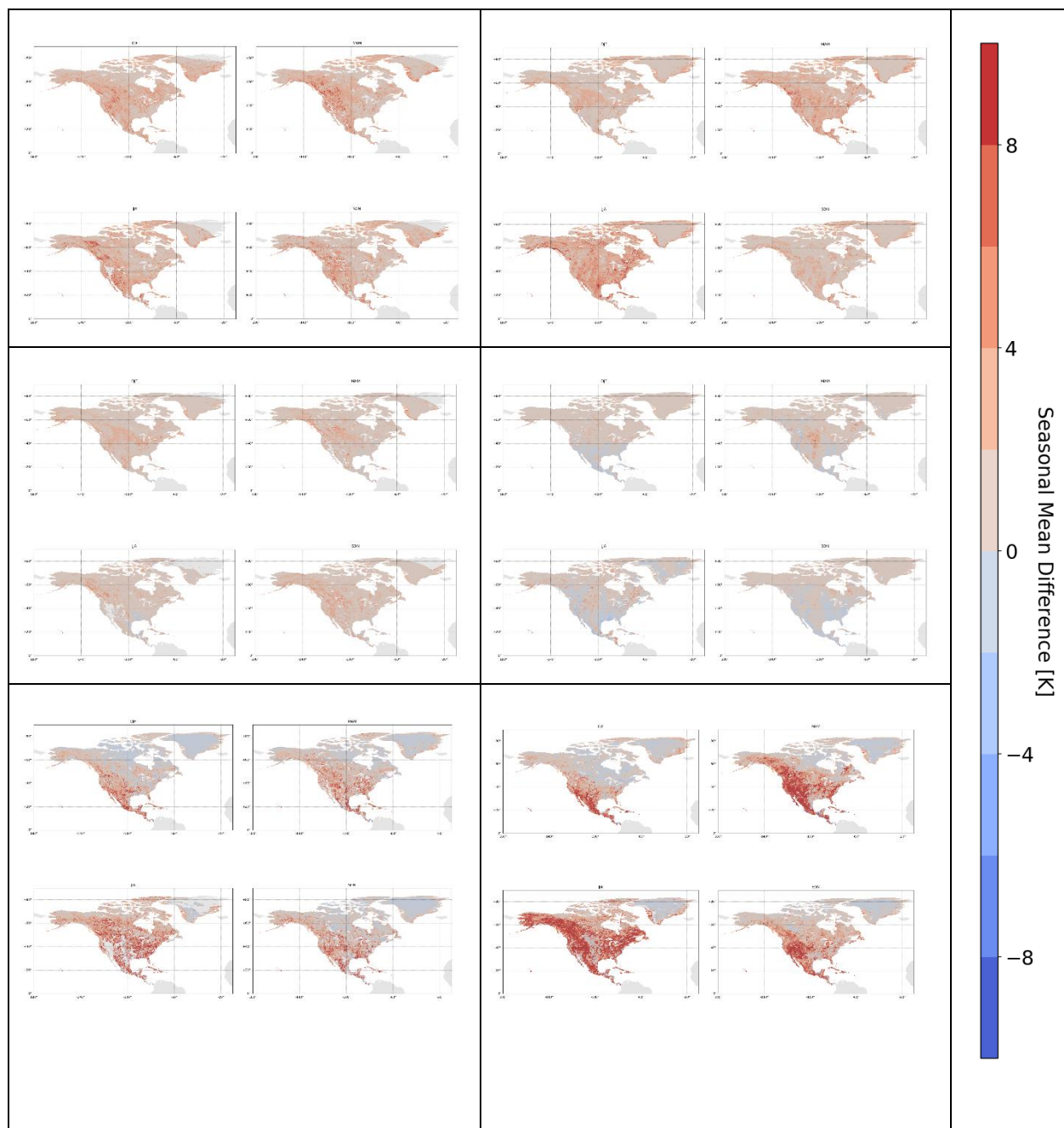


Figure 112: Seasonal mean differences of LST_satellite 1 – LST_satellite 2 in K; left row displays night-time and right row daytime data. Upper plots are for ATSR_3-MOD11T, middle plots for ATSR_3-MODIST, and lower plots for MODIST-ATSOP_.

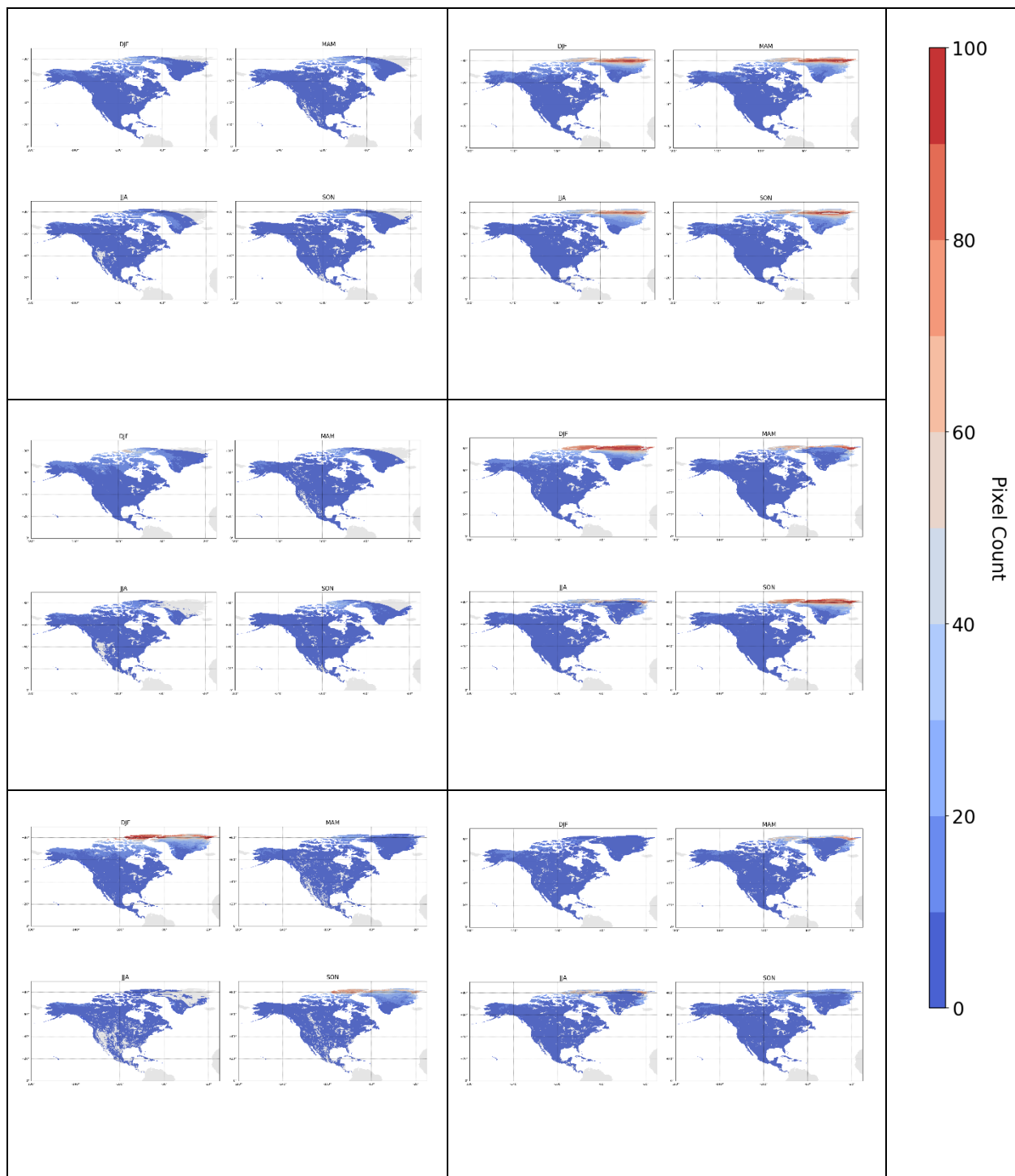


Figure 113: Number of seasonal averaged data points per pixel; left row displays night-time and right row daytime data. Upper plots are for ATSR_3-MOD11T, middle plots for ATSR_3-MODIST, and lower plots for MODIST-ATSOP.

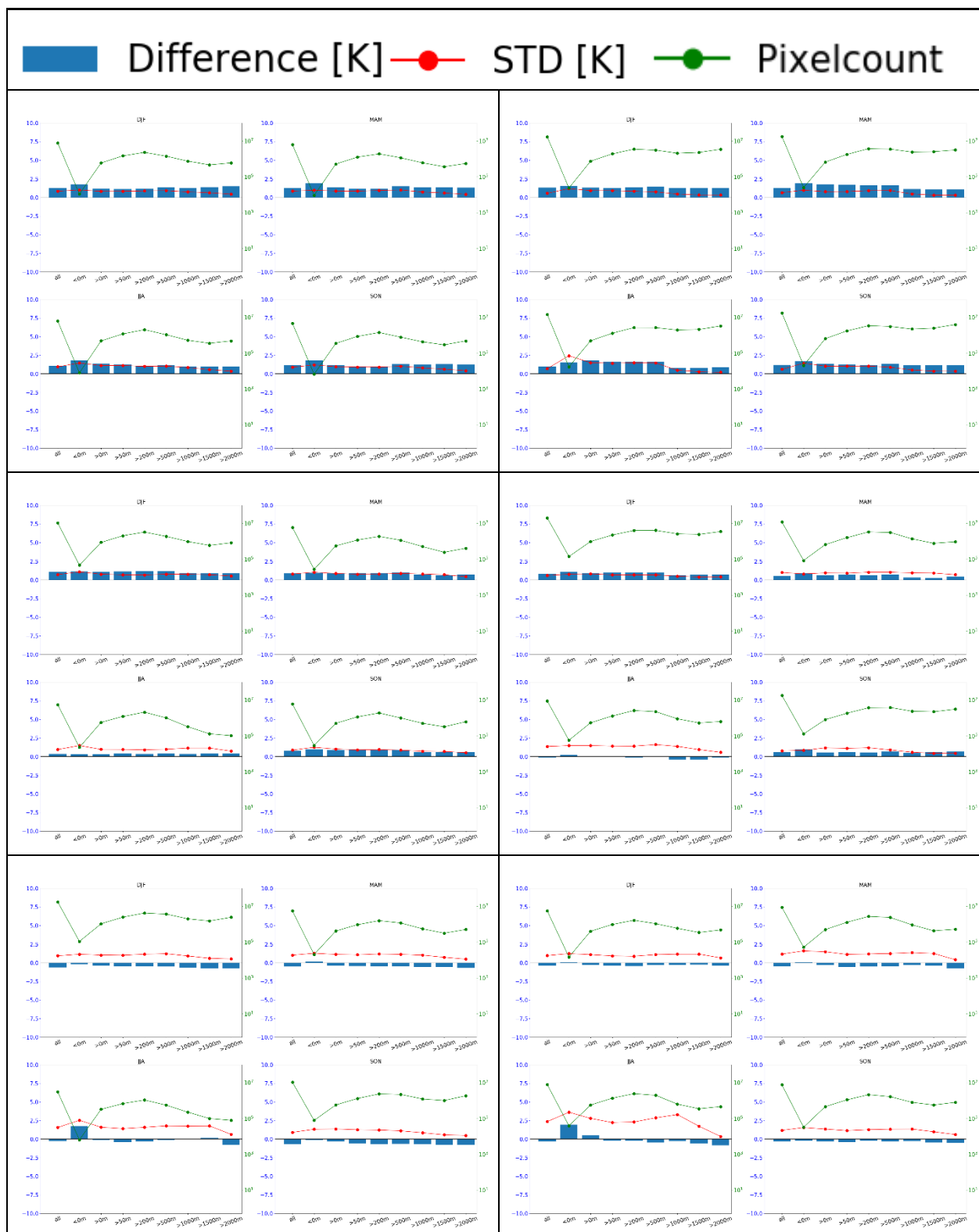


Figure 114: Seasonal differences for different elevation classes; blue bars are the median differences, red points the RSTD and the green points on the right axis show the number of averaged data points Left row displays night-time and right row daytime data. Upper plots are for ATSR_3-MOD11T, middle plots for ATSR_3-MODIST, and lower plots for MODIST-ATSOP_.



Figure 115: Seasonal differences for different land cover classes; coloured bars are the differences, red points the RSTD and the green points on the right axis show the number of averaged data points. Left row displays night-time and right row daytime data. Upper plots are for ATSR_3-MOD11T, middle plots for ATSR_3-MODIST, and lower plots for MODIST-ATSOP_.

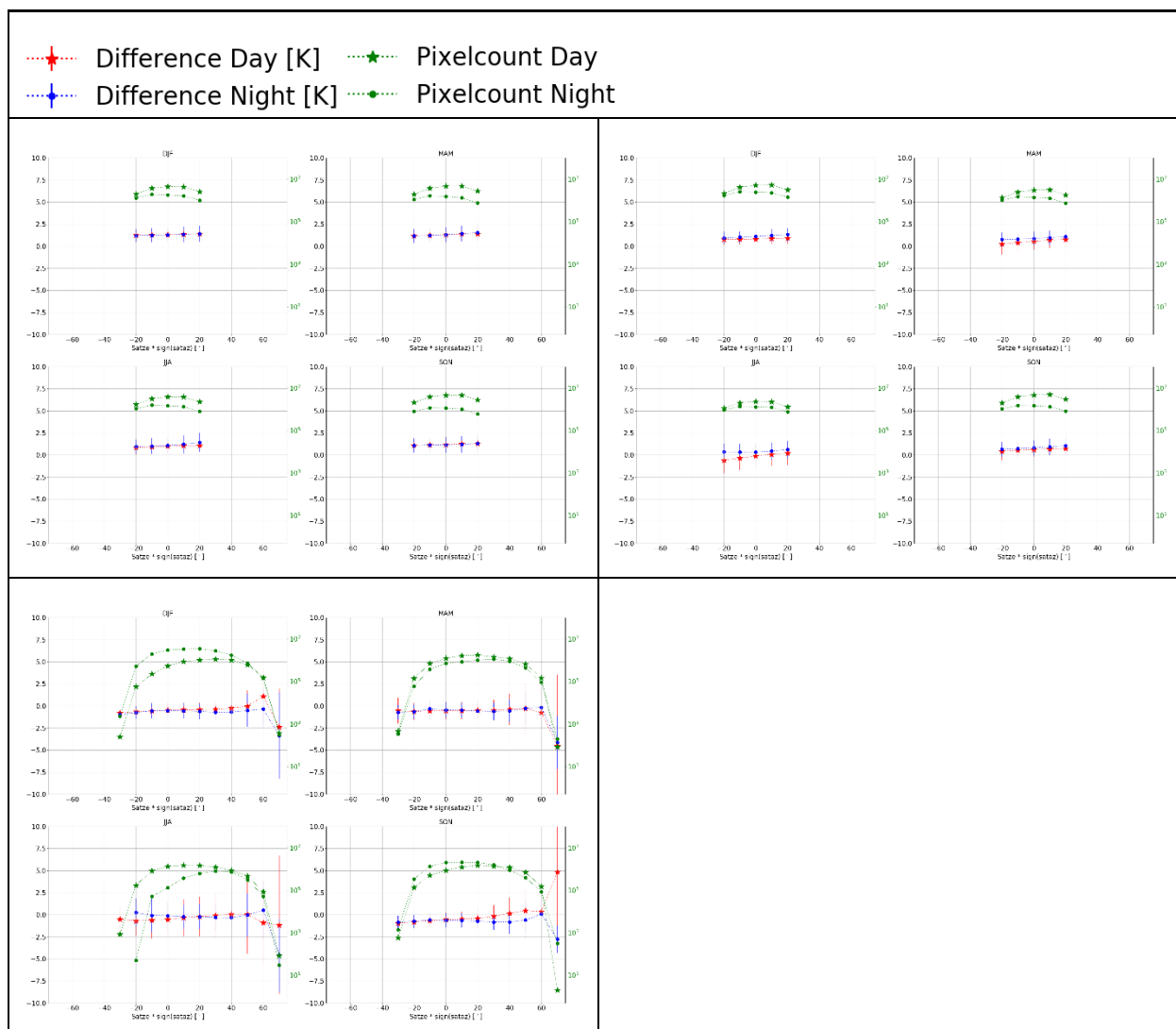


Figure 116: Seasonal differences versus $\text{satze} \cdot \text{sign}(\text{sataz})$ of satellite_1 ; red stars represent the daytime data, blue dots the night-time data, and the green stars and dots on the right axis display the averaged pixel numbers for daytime and night-time data. Upper left plot displays ATSR_3-MOD11T, upper right ATSR_3-MODIST, lower left MODIST-ATSOP_.

7.7. South America

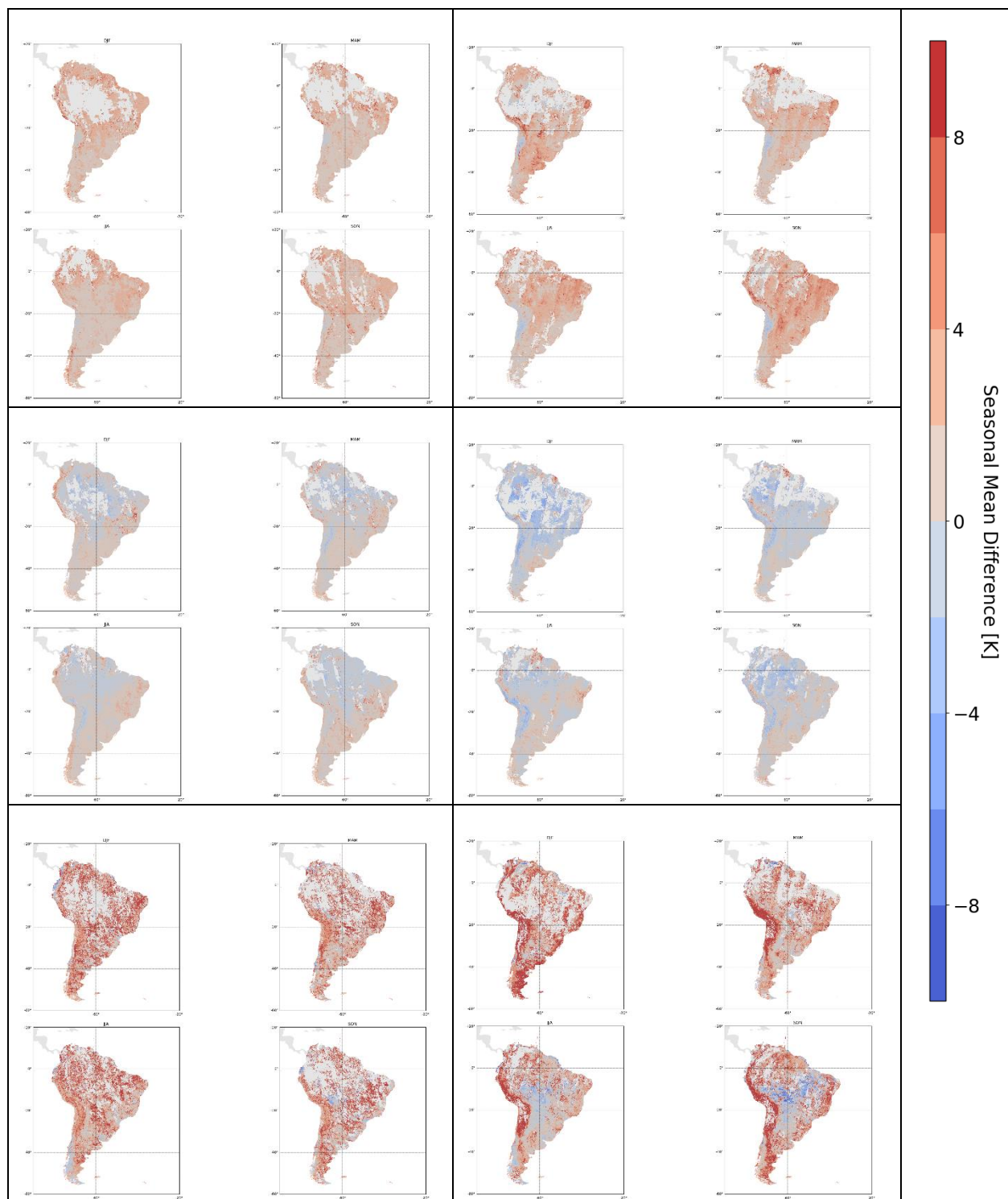


Figure 117: Seasonal mean differences of LST_satellite 1 – LST_satellite 2 in K; left row displays night-time and right row daytime data. Upper plots are for ATSR_3-MOD11T, middle plots for ATSR_3-MODIST, and lower plots for MODIST-ATSOP_-.

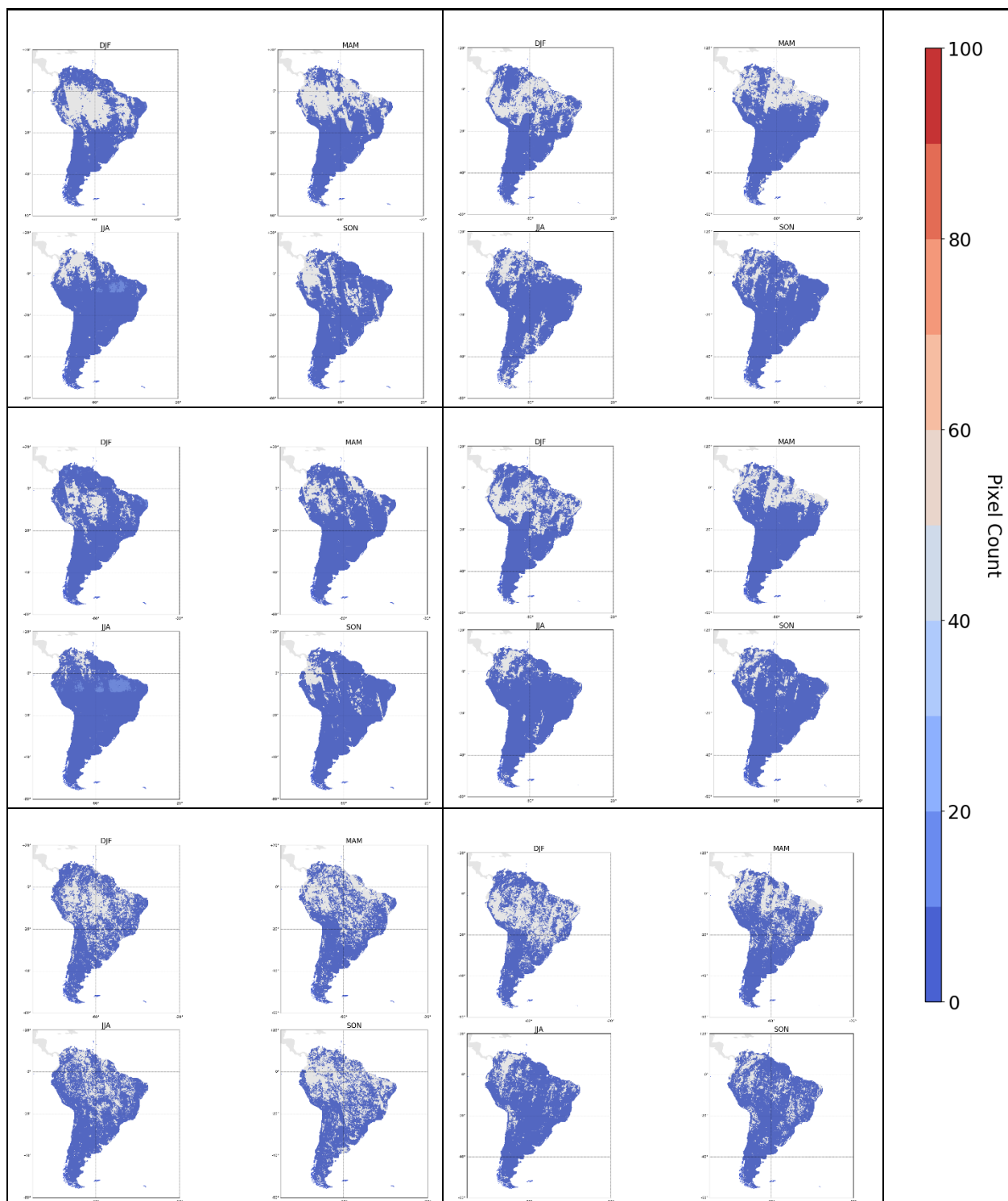


Figure 118: Number of seasonal averaged data points per pixel; left row displays night-time and right row daytime data. Upper plots are for ATSR_3-MOD11T, middle plots for ATSR_3-MODIST, and lower plots for MODIST-ATSOP_.

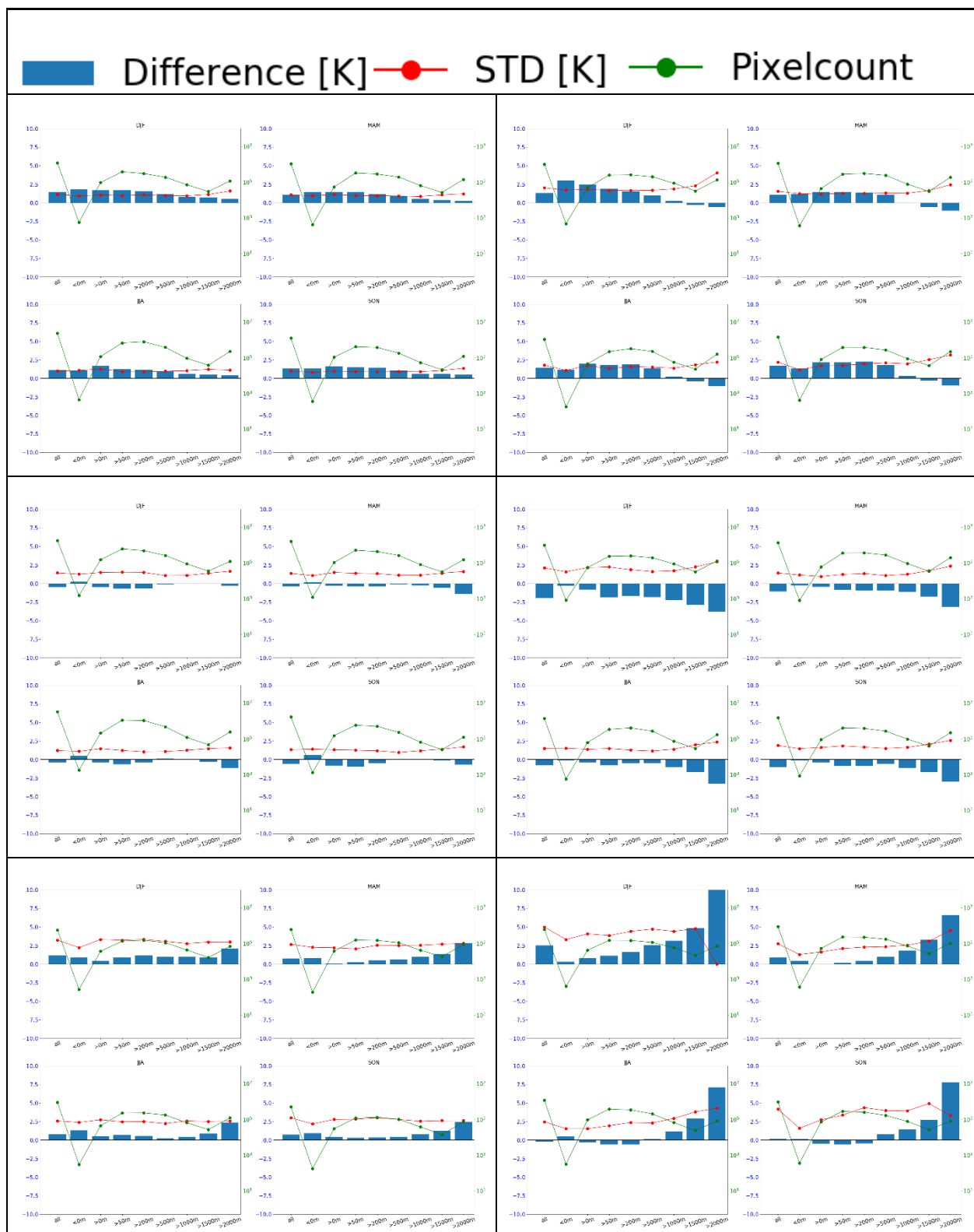


Figure 119: Seasonal differences for different elevation classes; blue bars are the median differences, red points the RSTD and the green points on the right axis show the number of averaged data points Left row displays night-time and right row daytime data. Upper plots are for ATSR_3-MOD11T, middle plots for ATSR_3-MODIST, and lower plots for MODIST-ATSOP_.



Figure 120: Seasonal differences for different land cover classes; coloured bars are the differences, red points the RSTD and the green points on the right axis show the number of averaged data points. Left row displays night-time and right row daytime data. Upper plots are for ATSR_3-MOD11T, middle plots for ATSR_3-MODIST, and lower plots for MODIST-ATSOP_.

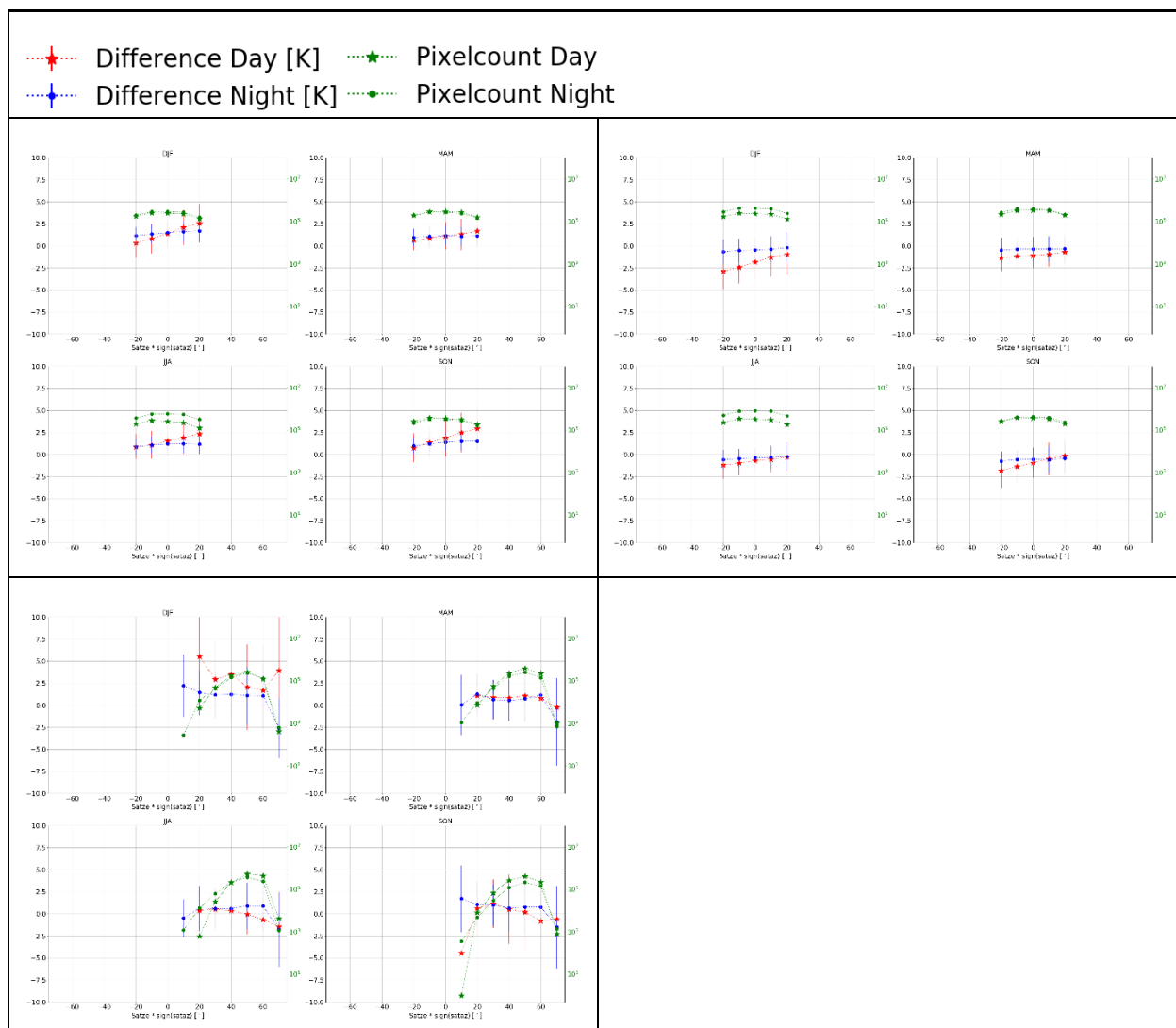


Figure 121: Seasonal differences versus $\text{satze} \cdot \text{sign}(\text{sataz})$ of satellite_1 ; red stars represent the daytime data, blue dots the night-time data, and the green stars and dots on the right axis display the averaged pixel numbers for daytime and night-time data. Upper left plot displays ATSR_3-MOD11T, upper right ATSR_3-MODIST, lower left MODIST-ATSOP_.